UNIVERSITY OF NAPLES FEDERICO II

PH.D. PROGRAMME IN SEISMIC RISK

XXIV CYCLE

Flavia De Luca

RECORDS, CAPACITY CURVE FITS AND REINFORCED CONCRETE DAMAGE STATES WITHIN A PERFORMANCE BASED EARTHQUAKE ENGINEERING FRAMEWORK

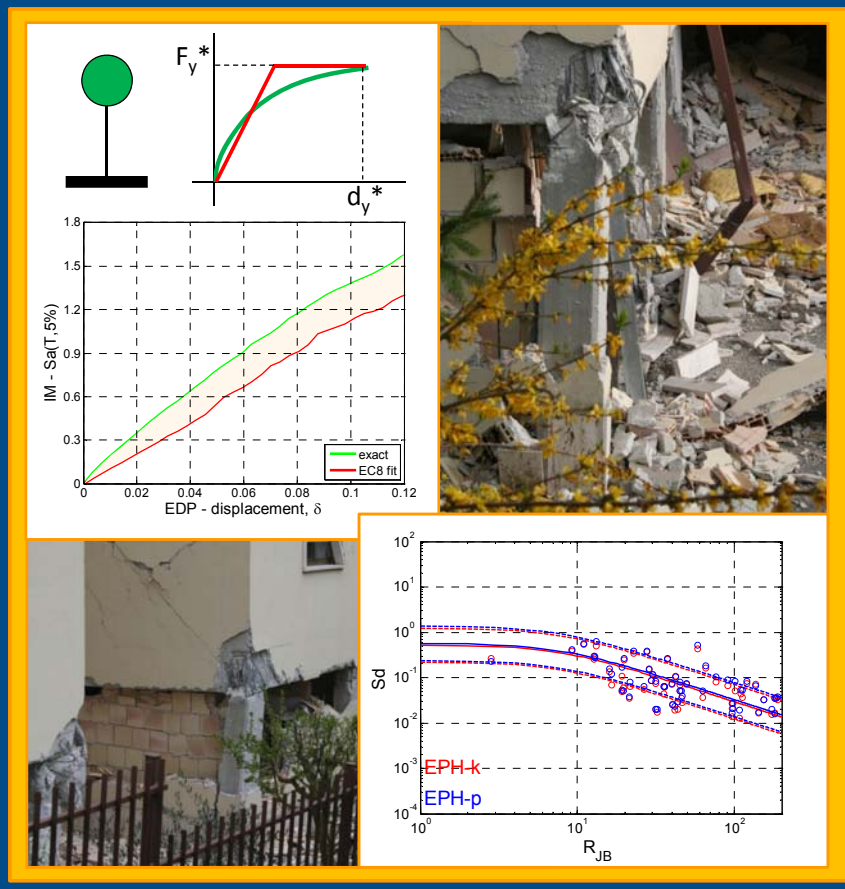

2011

UNIVERSITY OF NAPLES FEDERICO II

Dipartimento di Ingegneria STtrutturale

PH.D. PROGRAMME IN SEISMIC RISK

COORDINATOR PROF. ALDO ZOLLO

XXIV CYCLE

FLAVIA DE LUCA

PH.D. THESIS

RECORDS, CAPACITY CURVE FITS AND REINFORCED CONCRETE DAMAGE STATES WITHIN A PERFORMANCE BASED EARTHQUAKE ENGINEERING FRAMEWORK

TUTOR PROF. GAETANO MANFREDI

CO-TUTORS PROF. IUNIO IERVOLINO, PROF. GERARDO M. VERDERAME

2011

To Momy,
the marvelous surprise
of the last three years

Acknowledgements

It is quite hard finding the right words at the end of an important experience. The last three years have been full of surprises, difficulties and, above all, they made me grow up. Today I am a different person. The opportunity to be a researcher is an invaluable experience, it allows you to play a game while you are dealing with important issues; it is a continuous challenge.

First of all I would like to thank Professor Edoardo Cosenza and Professor Gaetano Manfredi that gave me the chance to join their research group. A special thank goes to two persons that belong to this research group, my two co-tutors: Prof. Iunio Iervolino and Prof. Gerardo Verderame, two enthusiast researchers that, in different ways, helped me during this experience. Thanks to their guidance, during these three years, I had important opportunities and improved my knowledge.

All my gratitude goes to Prof. Dimitrios Vamvatsikos, for his help, his friendship and, most of all, for his example: the six months I spent in Cyprus collaborating with him have been one of the greatest experiences of my life.

A big thank you goes to all my colleagues: we shared enjoyable time together, such as the "DIST dinners" but mostly because they always made me feel their respect and high esteem.

I cannot forget my special friends, Roberta, Luna and Bianca; they followed me closely during this hard crossing, even when being far away.

The last huge thank you goes to my family, the treasure I can enjoy every day. Above all, I have to thank my father, the closest example of honesty and intellectual value I have had in my life.

These few lines by John Donne are for all the special persons I came across during these three years but especially for those I did not mentioned above.

"No man is an island, entire of itself; every man is a piece of the continent, a part of the main. If a clod be washed away by the sea, Europe is the less..."

Naples, November 2011,

Flavia

Abstract

Earthquake engineering aims at the goal of controlling the seismic risk to socio-economically acceptable problems, encompassing multidisciplinary efforts from various branches of science and engineering. Such efforts in the last decades allowed structural engineering progressing towards an approach that can fit the general framework of the assessment and the control of seismic risk: performance based earthquake engineering (PBEE).

PBEE represents a common platform for researchers and engineers. It is the frame in which the topics of this research have grown up.

The first step of PBEE, *hazard* and *ground motion*, is discussed in the first part of this research. The employment of advanced intensity measures (IM) in Probabilistic Seismic Hazard Analysis (PSHA) is investigated. New prediction equations for inelastic displacement and equivalent number of cycles based on the ITalian ACcelerometric Archive are provided as IMs for both peak and cyclic inelastic response of structures. This tool goes towards further enhancements of PSHA. Moreover it can be a tool for the validation of simulated scenario for a robust employment in the assessment of critical facilities and finally for it can play a role in future perspective of large scale risk assessment.

Issues regarding ground motion selection for nonlinear dynamic analyses are then examined: the reliability of artificial records, wavelet adjusted and linearly scaled records is investigated within a code-based framework. The inelastic displacement of such records was shown to be statistically equivalent to the one of unscaled real records, given the same spectral constraint suggested by codes; on the other hand, regarding cyclic response artificial records showed their statistically significant overestimation that can cause problem when employed for specific facilities in which cyclic response has a significant role in the assessment of the seismic performances.

The second step discussed is the aspect of seismic *demand prediction* and estimation. Analysis methodologies are described and their level of accuracy is discussed, focusing on specific code prescriptions concerning structural analysis. Some critical issues of the recent Italian Code regarding choice and applicability conditions of analysis methods are emphasized. Special attention is given to the static pushover analysis, a methodology nowadays in the between of research and practice. A review of the approximations implicit in this methodology is provided, focusing the attention on the piecewise linear approximation of the capacity curve. A methodology for the systematical investigation of this aspect is presented and then employed for the definition of an optimized fit for capacity curves allowing a reduction and, above all, a quantification of the error introduced by this step when performing nonlinear static analysis.

The third step within the PBEE framework, and the final one of this research, deals with *modeling of damage states*. The damage measures for reinforced concrete (RC) structures are investigated. Limit states for reinforced concrete structures are considered, focusing on the aspects of brittle failures in existing reinforced concrete structures. The latter represents one of the most critical issues for existing reinforced concrete structures, given the absence of capacity design. Brittle failures in reinforced concrete (RC) elements are analyzed according to code provisions, considering different code approaches and the analytical models are finally compared with experimental data. Non conventional brittle modes of failures such as the sliding shear mechanism are reviewed, with special attention to the structural details that allow the development of sufficient capacity against this failure mode. Finally the influence of masonry infill on the whole structural behavior of RC structures is investigated. The whole aspect of damage measures in reinforced concrete structures is further examined by means of the result of a reconnaissance post earthquake campaign. 6th April 2009 L'Aquila event is considered, and performances of existing reinforced concrete buildings during the earthquake are reviewed. Finally the results of the in-field campaign allowed the analytical study of a soft storey collapse. The back analysis of the case study structure selected emphasized the critical aspects regarding brittle mode of failure and singles out the likely causes of the structural collapse.

The whole research, through the above three step path, aims to focus on some critical issues providing some tools, suggesting enhancements in methodologies and procedures and finally outlining possible future perspectives for the PBEE framework. In fact, this consolidated spine for earthquake engineering, allows a separate focus on issues that can then be recombined in the multidisciplinary context of assessment and control of the seismic risk.

Keywords: *advanced IMs for PSHA, artificial records, static pushover, incremental dynamic analysis, existing Reinforced Concrete buildings, brittle failures.*

Tables of contents

PART III: MODELING OF DAMAGE STATES

List of figures

List of tables

Chapter 1
INTRODUCTION

"Earthquake engineering encompasses multidisciplinary efforts from various branches of science and engineering with the goal of controlling the seismic risk to socio-economically acceptable problems", (Bertero and Bozorgnia, 2004). This definition provides a general idea of the wide impact that earthquake engineering can have on communities and clearly recognizes its multidisciplinary character. On the other hand such a comprehensive definition represents a relatively recent achievement (since 1960s) while birth and growth of earthquake engineering can be dated at the end of the 19th century when some European engineers suggested designing structures with a few percent of the weight of the structures as the horizontal load, (Hu et al., 1996). Most of the experience regarding the early earthquake engineering was collected after disastrous earthquakes in seismically prone areas in the world such as Japan (Edo, 1855), California (San Francisco, 1906) and Italy (Messina, 1908). Thus, reducing seismic risk to acceptable levels is the main object of earthquake engineering.

Got to this point it is worth to ask *what is seismic risk?* and more in general *how risk can be quantified?*; according to the glossary of Earthquake Engineering Research Institute (EERI) Committee on Seismic Risk (1984), seismic risk is "the probability that social or economic consequences of earthquakes will equal or exceed specified values at a site, at various sites or in an area during a specified exposure time". Such a probability can be evaluated according to the *total probability theorem* evaluating *Risk* as a combination of *Hazard* (*H*), *Vulnerability* (*V*) and *Exposure* (*E*).

As summarized in Bertero and Bozorgnia (2004), assessing and controlling seismic risk at any given site requires at least the following:

- Estimating the seismic activity at the site. This requires identification of all seismic sources.
- Predicting earthquake ground motions (preferably all six components) that could significantly contribute to the seismic risk.
- Evaluating whether the earthquake ground motions could induce (besides direct significant vibratory motions to the entire facility system) any of the following potential hazards at the site or the surrounding region: surface fault ruptures, tsunamis, seiches, landslides and floods.
- Predicting whether the predicted earthquake ground motions could induce ground failure, that is, liquefaction, settlement, subsidence, differential compaction, loss of bearing and shearing strength and lateral spreading.
- Assessing the performance of the facility system under the direct and indirect effects of the predicted earthquake ground motions and estimating the degree of damage and losses. This includes evaluating the serviceability, operability, life safety, near-collapse and collapse performance levels under different levels of earthquake hazards that the facility could undergo during its expected service life and economic consequences and other socio-economical impacts on the community.
- Evaluating the possibility of the following incidents: fire, flood, release of hazardous materials, environmental impact and other consequences that could affect the built environment.
- Conducting a cost–benefit analysis of seismic upgrading and replacing existing hazardous facilities.

The above requirements, which can be interpreted as a generalized definition of *H*, *V* and *E*, clarify the complexities of the problems of assessing and controlling seismic risks and the wide range of knowledge involved in such assessment and control (geophysics, geology, seismology, vibration theory, structural dynamics, material dynamics, structural engineering,…).

1.1 Motivation

The general framework outlined above emphasizes earthquake engineering issues in general. In particular, structural engineering has progressed in the years towards an approach that can fit the general framework of the assessment and the control of seismic risk also known as performance based earthquake engineering (PBEE).

"PBEE implies design, evaluation, construction, monitoring the function and the maintenance of engineered facilities whose performance under common and extreme loads respond to the diverse needs and objectives of owners-users and society. It is based on the premise that performance can be predicted and evaluated with quantifiable confidence to make, together with the client, intelligent and informed trade-offs based on life cycle considerations rather than construction costs alone"; (Krawinkler and Miranda, 2004).

Guidelines and codes, since 90' have partially implemented, in their general framework, the basic concepts of PBEE in various forms, resulting in the attempt to tie design criteria to a performance level, usually that of collapse prevention (SEAOC, 1995; FEMA 273, 1996; FEMA 274, 1996; ATC-40, 1996).

The Pacific Earthquake Engineering Research (PEER) Center has focused for several years on the development of procedures, knowledge and tools for a comprehensive seismic performance assessment of buildings and bridges. The efforts made have resulted in a general framework that is now shared by the earthquake engineering community all over the world.

Sharing a common vision and approach allows placing further enhancements and progresses in this PBEE consolidated framework, thus aiming at the final challenge to contribute effectively to the reduction of losses and the improvement of safety, (Cornell and Krawinkler, 2000).

The basis of performance assessment, according to PEER, can be summarized in a single equation (see Eq. 1). This equation suggests a generic structure for coordinating, combining and assessing the many considerations implicit in performance-based seismic assessment. The variables in equation

(1.1) are summarized in Table 1-1.

$$\lambda(DV) = \iiint \left| G\langle DV \mid DM \rangle dG\langle DM \mid EDP \rangle dG\langle EDP \mid IM \rangle d\lambda(IM) \right| \quad (1.1)$$

Inspection of equation (1.1) reveals that it "de-constructs" the assessment problem into the four basic elements of hazard analysis, demand prediction, modeling of damage states and failure or loss estimation, by introducing the three intermediate variables, IM, EDP and DM. Then it recouples the elements via integration over all levels of the selected intermediate variables. This integration implies that, in principle, one must assess the conditional probabilities G(EDP|IM), G(DM|EDP) and G(DV|DM) parametrically over a suitable range of DM, EDP and IM levels.

Table 1-1. Components and variables in performance assessment approach (Krawinkler and Miranda, 2004).

Performance Targets	Decision Variables	Damage Measures	Engineering Demands	Seismic Hazard
	DV	DM	EDP	IM
• Colapse & Life safety Pf<y • Losses<x • Downtime<z	• Colapse • Number of casualities • € losses • Length of downtime	• Fragilities for failure states • Structural • Nonstructural • - Content	• Engrg. Analysis (stoy drift, floor acc.) • - Soil-foundation-structure system	• Hazard analysis • Ground motions
$\lambda(DV)$	$G(DV \mid DM)$	$G(DM \mid EDP)$	$G(EDP \mid IM)$	$\lambda(IM)$

In the written form, the assumption is that appropriate intermittent variables (EDPs and DMs) are chosen such that the conditioning information need not be carried forward (e.g., given EDP, the DMs and DVs) and are conditionally independent of IM; otherwise IM should appear after the EDP in the first factor. So, for example, the EDPs should be selected so that the DMs (and DVs) do not also vary with intensity, once the EDP is specified. Similarly one should choose the intensity measures (IM) so that, once it is given, the dynamic response (EDP) is also not further influenced by magnitude or

distance (which have already been integrated into the determination of λ(IM)).

1.2 Objectives

The primary general objective of this research is to contribute to the development of methods and tools towards enhancements and progresses in the consolidated PEER framework of PBEE. This general challenging objective can be pursued focusing separately on specific issues, given the "de-construction" of the assessment problem into the four basic elements (hazard analysis, demand prediction, modeling of damage states and failure or loss estimation). More specifically, the sub-objectives of this study are as follows; they are referred to three of the basic elements of the assessment problem, and the contributions of this thesis to the specific issues investigated obviously enjoys the previous work of many other researchers.

The first sub-objective of this research is to provide additional data and tools for *hazard analysis and ground motion selection* with a specific reference to Italy. Two issues are investigated: the development of prediction equations of peak and cyclic inelastic response as an effort to improve accuracy in definition of structural design targets and the suitability of artificial and simulated records as seismic input for structural analysis.

The second sub-objective is focused on *demand prediction*, in particular on nonlinear analysis methods, providing an improvement to nonlinear static analysis procedure by means of the development of a benchmarking methodology aimed at isolating the specific approximation introduced by piecewise linear fitting of capacity curves.

The third sub-objective lies at the core of *modeling of damage states*. It is focused on the specific problem of the evaluation of the capacity of reinforced concrete elements; focusing on brittle failures, and on the role played by nonstructural elements in causing brittle failures in existing reinforced concrete buildings. Then data from an infield campaign made after the 2009 L'Aquila earthquake are collected. Damage observation is also supported by

information on the characteristics of the building stock and by a study on the design criteria in the last decades in the area considered for the reconnaissance.

1.3 Organization and outline

This thesis is divided in three parts and it is mostly based on a compilation of research papers. Each part represents one of the three sub-objectives above and focuses on a specific element of the PBEE framework. All the papers are coauthored, so the first section of each chapter gives credit for the contributions of each author. Each Chapter's topic is represented in Figure 1.1 providing the outline of the research in the PBEE framework.

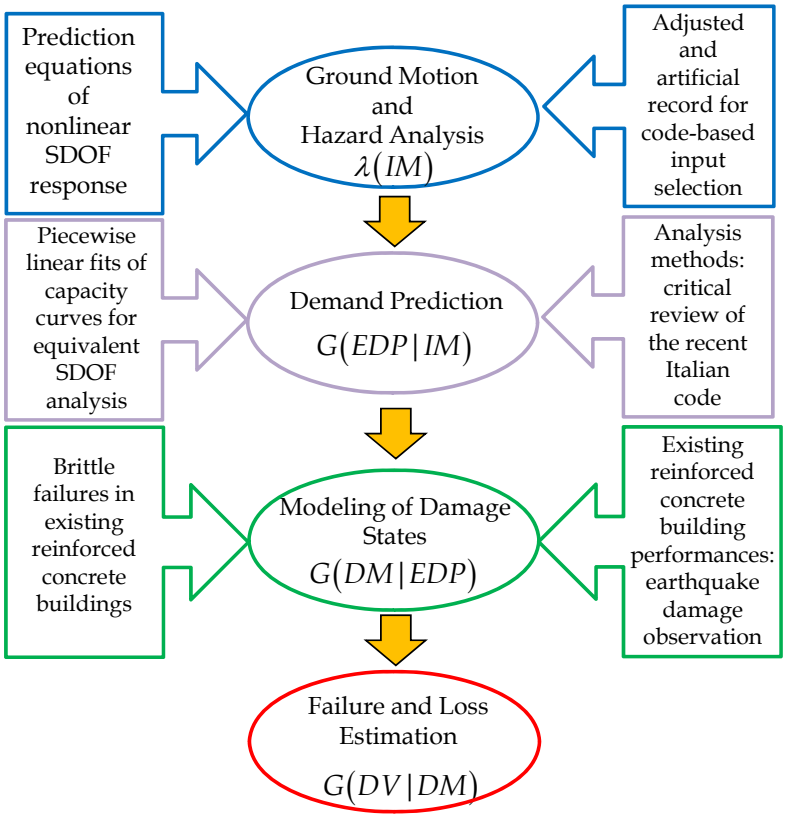

Figure 1.1. Outline of the research in the PBEE framework: flow-chart.

Part I, based on the characterization of earthquake hazards and ground motion selection, is made of two chapters. In **Chapter 2** the possibility to develop prediction equations for peak and cyclic EDPs is investigated with reference to the Italian ACcelerometric Archive. Finally **Chapter 3** focuses on the employment of scaled, adjusted and artificial records in a code-based seismic input selection framework.

Part II, focused on demand prediction, provides in **Chapter 4** an overview of the structural analysis methodologies and their implementation in codes and guidelines with a critical overview of the new Italian seismic code prescriptions; then, in **Chapter 5** the piecewise linear approximation of capacity curves in nonlinear static analysis procedures is investigated.

Part III is refereed to modeling of damage states and in particular it focuses on brittle failures in existing reinforced concrete (RC) buildings. **Chapter 6** introduces the issue of existing reinforced concrete buildings, their typical weaknesses and the modes of failure of RC elements, focusing on brittle failure modes; firstly conventional and non-conventional brittle failure modes are investigated, then a practice-oriented approach for the assessment of shear-flexure hierarchy in existing RC elements is presented and finally the role of masonry infills in existing reinforced concrete structures is analyzed.

Chapter 7 is the final step of this way through the PBEE. It shows the results of a reconnaissance campaign on the observed performance of RC buildings during the recent 2009 L'Aquila earthquake focusing on seismic design criteria in Italy in the last decades and working as in-field benchmark for the aspects described in the previous chapter. The chapter ends with a back analysis of an RC building in which non-conventional brittle failures are the likely cause of the observed soft storey mechanism registered during L'Aquila earthquake.

Chapter 8 presents the general conclusions of this research, as well as its limitations, and perspectives.

References

ATC-40, 1996. Seismic evaluation and retrofit of existing concrete buildings. Applied Technology Council, Redwood City, CA.

Bertero V.V. and Bozorgnia Y. , 2004. The early years of earthquake engineering and its modern goal. In: Bozorgnia Y. and Bertero V.V. Editors *Earthquake Engineering: From engineering seismology to performance-based engineering*, CRC Press, chapter 1.

Cornell, A. and Krawinkler, H. , 2000. Progress and challenges in seismic performance assessment. PEER News, April 2000.

FEMA 273, 1996. NEHRP guidelines for the seismic rehabilitation of buildings. U.S. Federal Emergency Management Agency.

FEMA 274, 1996. NEHRP commentary on the guidelines for the seismic rehabilitation of buildings. U.S. Federal Emergency Management Agency.

Hu Y.-X., Liu S.-C., Dong W., 1996. Earthquake Engineering. E &FN Spon, London.

Krawinkler H. and Miranda E., 2004. Performance-Based Earthquake Engneering. In: Bozorgnia Y. and Bertero V.V. Editors *Earthquake Engineering: From engineering seismology to performance-based engineering*, CRC Press, chapter 9.

SEAOC, 1995. Vision 2000 — Performance based seismic engineering of buildings. Structural Engineers Association of California, Sacramento, California, USA.

PART I

HAZARD ANALYSIS AND GROUND MOTION

Chapter 2
PREDICTION EQUATIONS OF NONLINEAR SDOF RESPONSE

De Luca F., Iervolino I., Ameri G., Pacor F., Bindi D. *Prediction equations for nonlinear SDOF response from the ITalian ACcelerometric Archive: preliminary results*. XIV Convegno ANIDIS 2011, Bari 18-22 Settembre, 2011.

De Luca F.,Iervolino I., Ameri G., Pacor F., Bindi D. *Prediction equations of nonlinear SDOF response: towards an enhanchment of hazard analysis*. 30° Convegno Nazionale GNGTS, 14-17 Novembre, 2011.

2.1 Authorship of Chapter

This general idea of this chapter is based on two publications (cited above) and shows further enhancements respect to them. The whole study, shown herein, resulted from a collaboration with Istituto Nazionale di Geofisica e Vulcanologia (INGV) within the activities of the Rete dei Laboratori Universitari di Ingegneria Sismica – ReLUIS for the research program funded by the Dipartimento di Protezione Civile 2010-2013. It covers some the aspects of the project dealing *engineering issues regarding seismic input*, (Task RS1). The study resulted from the main purpose to provide an unbiased benchmark aimed at systematical validation of techniques for the generation of synthetic records.

2.2 Introduction

It is easy to recognize that seismic design would benefit of hazard expressed in terms of nonlinear structural performance. In fact, currently, the conversion of common ground motion intensity measures (IMs), such as elastic spectral ordinates for which hazard is available, to inelastic deformations is essential for most of the design procedures based on static or modal response

analyses. This is carried out via strength, ductility, and oscillation period relationships, *R-μ-T*, or simply based on the *equal displacement rule* (e.g., Veletsos and Newmark, 1960).

Available relations, for generality purposes, were calibrated in the past via regression of data from relatively limited ground motion sets (see also Vidic et al., 1994; Miranda and Bertero, 1994). These refer to single degree of freedom (SDOF) systems, typically with an elastic-plastic backbone[1], to which the structure of interest is somehow rendered equivalent during design.

The relationships between elastic and inelastic response, for practicality and manageability, are only taken in approximate format within codes, which often means to neglect significant associated uncertainty. In fact, recent attempts aim at performing probabilistic seismic hazard analysis, PSHA, (McGuire, 2004) directly in terms of inelastic response. This would provide the seismic threat at a site by means of a parameter more informative for engineering practitioners.

In previous studies (Tothong and Cornell, 2007; Tothong and Luco, 2007) it has been shown that the inelastic displacement of SDOF systems can be a reliable solution as an advanced intensity measure (IM) to perform hazard analyses for first mode dominated structures, for both ordinary and pulse-like ground motions. Inelastic displacement as an advanced IM was shown to be *efficient*, *sufficient* and *robust to scaling* when seismic risk assessment of first mode dominated structures is of concern.

An IM can be defined as *efficient* if it produces small variability of structural response for a given IM level ($\sigma_{\ln EDP|IM}$); such a property is desirable because the standard error of the sample mean of *lnEDP* for a specified IM level is proportional to $\sigma_{\ln EDP|IM}$. Analogously an IM is *sufficient* when the conditional probability distribution of EDP given IM ($G_{EDP|IM}$, the first integrand of equation 1.1) is independent of the other parameters involved in computing the seismic hazard, mainly magnitude (M_w), distance (R_{JB}) and

[1] This is also because it has been found that the role of hysteresis shape may be minor.

epsilon (ε); the latter is a desirable property since it implies that any set of ground motions selected for nonlinear dynamic analyses of the structure will result in approximately the same $G_{EDP|IM}$. Finally, *robustness to scaling* implies that scaling records to a value of the IM results in unbiased structural response compared to the analogous responses obtained from unscaled ground motions; this property is desirable since scaled records are often employed in nonlinear structural analyses according to codes, see chapter 3, (Tothong and Cornell, 2007). Spectral acceleration at the fundamental period of a structure is an example of IM that does not exhibit robustness to scaling (Luco and Bazzurro, 2004). The three mentioned properties, when held by an IM, allow a reliable seismic risk assessment according to the PBEE methodology by PEER Center.

Once it has been assessed that inelastic displacement is characterized by all the desirable properties for IMs it can be attractive and useful to develop prediction equations for such an IM considering a specific area oriented approach, so providing a prediction equation characteristic of a specific area, in the specific case of this study for Italy.

Two are the possible approaches to incorporate nonlinear structural response in seismic hazard: (1) to analytically model the inelastic to elastic response ratio (e.g., Tothong and Cornell, 2006); or (2) to develop prediction equations (or *attenuation models*) in terms of nonlinear response (e.g., Buratti et al., 2009; Bozorgnia et al., 2010a and 2010b). The latter approach is pursued herein where relationships are developed for two nonlinear SDOF backbones, based on a set of ground motion data contained in the ITalian ACcelerometric Archive or ITACA (Luzi at al. 2008; Pacor et al., 2011).

Estimating directly inelastic structural response rather than converting the elastic one, although equivalent in principle, allows reducing the consequences of semi-empirical estimation issues propagating when predicting nonlinear behavior, has shown by Tothong and Luco (2007) for first mode dominated structures.

The two considered SDOF systems include bilinear with hardening backbone with and without stiffness' degrading hysteretic behavior.

While inelastic displacement (Sd_i) represents an advanced IM for peak structural response, in this study it is provided for the same SDOFs a prediction equation for an advanced IM to be used when cyclic response is of any concern, the equivalent number of cycles, N_e, (Manfredi, 2011). The employment of such a duration related advanced IM in the PBEE framework still requires studies but at the same time it can have an immediate employment for the validation of simulated scenario earthquake with synthetic accelerograms, representing a reliable benchmark for cyclic structural response.

Elastic periods of SDOFs range in a broad interval sampled by 20 values. Level of nonlinearity is accounted for by considering four different *strength reduction factors* (R_s) that ranges from mildly to highly inelastic response.

The functional forms relating the two IMs considered to source, site, and path characteristics are derived starting from those employed to compute the elastic IMs' attenuation relationships of Bindi et al. (2011). The results refer to the geometric mean of the two horizontal components of ground motion.

In the following, details of the considered simple structural systems and response measures are given first. Then, the main features of the ground motion dataset are illustrated. Finally, the obtained equations for different nonlinear responses, and their dependency on the earthquake covariates, are discussed highlighting the use in the next generation of seismic hazard analysis, and as a benchmark for engineering validation of other types of ground motions obtained, for example, by means of physics-based simulations.

2.3 Structural cases and advanced intensity measures

The structural cases considered were selected to emphasize both peak and cyclic response issues; thus two classes of hysteretic behaviors were selected. For each class of SDOFs, 20 elastic periods varying from 0.04s to 2s were considered, assuming the same sampling values selected in Bindi et al. (2011). The first structural behavior is represented by an elastic hardening backbone with the post-yielding stiffness assumed as 0.05 of the initial stiffness

(k_{el}). These systems are characterized by a standard kinematic strain hardening hysteretic model (EPH-k), without any cyclic degradation, see Figure 2.1a. This SDOF family is the same considered in the study by Tothong and Cornell (2006). The second structural behavior (EPH-p) features cyclic stiffness degradation, characterized by pinching hysteresis (Ibarra et al., 2005) and by the same elastic hardening backbone of the previous family of SDOFs; see Figure 2.b.

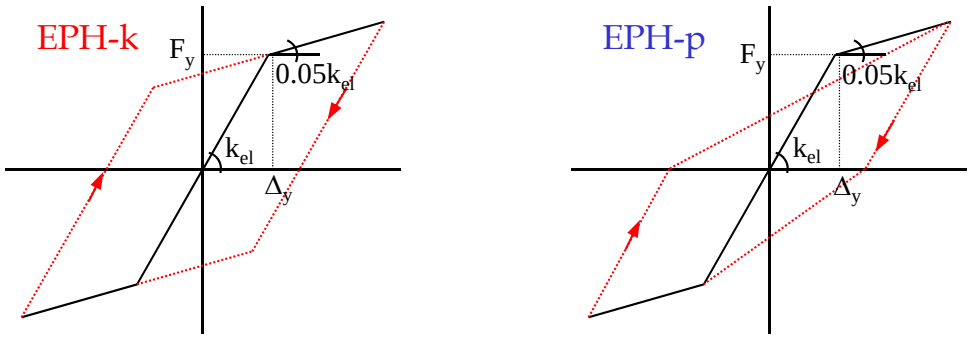

Figure 2.1. Elastic hardening monotonic backbone with standard kinematic strain hardening hysteretic model, (EPH-k), and with pinching hysteresis featuring cyclic stiffness degradation, (EPH-p).

Four different strength reduction factors R_s were considered, equal to 2, 4, 6, 8, respectively; being representative of a mildly to significant inelastic structural behavior. It has to be noted that it is possible to achieve the same value of R_s either for each record in a dataset (*constant R approach*) or on an average sense (*constant strength approach*), keeping constant the yielding strength. The former was adopted in this case, allowing every single record to show inelastic behavior in the SDOF. Therefore, the value of the yield strength (F_y) at a given oscillation period T is a record-specific quantity.

Two response parameters, in the following referred to as advanced IMs, were selected to investigate both peak and cyclic seismic response. The displacement-based parameter is the peak inelastic displacement (Sd_i). The cyclic response-related parameter is the equivalent number of cycles (N_e). This latter is given by the cumulative hysteretic energy (E_H), evaluated as the sum of the areas of the hysteretic cycles (not considering contribution of viscous

damping), normalized with respect to the largest cycle, evaluated as the area underneath the monotonic backbone curve from the yielding displacement to the peak inelastic displacement ($A_{plastic}$), see Equation (2.1). This allows separating peak demand, already considered in Sd_i, from cyclic demand (Manfredi, 2001).

$$N_e = \frac{E_H}{A_{plastic}} \tag{2.1}$$

Once the peak and cyclic inelastic response to each single horizontal component of the record selected is evaluated according to the EDPs defined above, the geometric mean of the EDPs is considered for regression.

2.4 Ground motion data

To compute peak and cyclic response parameters, the accelerograms corresponding to the strong ground-motion dataset used to develop the Italian Ground Motion Prediction Equations (ITA10, Bindi et al., 2011), were selected. The dataset is comprised of 747 records (three-components), with hypocentral depth within 30 km, and 150 stations over the magnitude range $4.1 \leq M_w \leq 6.9$ and distance, R_{JB}, range from 0 to 200 km (Figure 2.2). This dataset is extracted by the new Italian strong motion data base, ITACA (http//itaca.mi.ingv.it/) and includes all Italian events with $M_w > 4$ recorded from 1972 up to 2007 and the most relevant data from recent moderate earthquakes (M_w = 6.3, 2009 L'Aquila and M_w = 5.4, 2008 Parma) and aftershocks. The dataset considered is not exactly equal to the one employed in ITA10; 22 records form stations TLM1, VLB, SMT and SPC were excluded since the records were found to be affected by the structure in which the stations are located.

The development of ITA10 was feasible, thanks to the improvements in the quality and quantity of data and metadata in the new release of the ITACA database. In the selected dataset, distances larger than 10 km are well sampled over the entire magnitude range, while the recordings for distances shorter than 5 km are relevant in number for earthquakes with $M_w < 6$. All stations are

classified following the Eurocode 8 or EC8 (CEN, 2004) scheme. The local site conditions values were obtained either from measurements or inferred by geological and geophysical data. Classes D and E (soft soils according to EC8) are poorly sampled, while the other classes are well represented with about 200 records in each class.

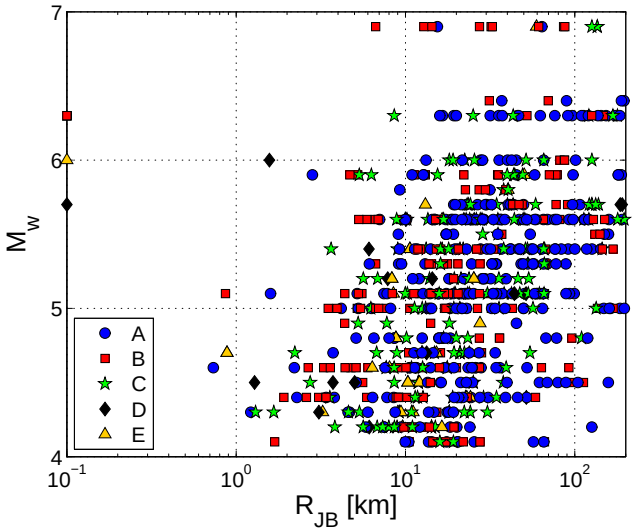

Figure 2.2. Magnitude versus distance plot of the dataset, grouped according to the EC8 site classification .

The accelerometric waveforms were downloaded from ITACA in the processed version form. The procedure for processing the data, consists in (Paolucci et al., 2011; Pacor et al., 2011): 1) baseline correction; 2) application of a cosine taper, based on the visual inspection of the record (typically between 2% and 5% of the total record length); records identified as late-triggered are not tapered; 3) visual inspection of the Fourier spectrum to select the band-pass frequency range; 4) application of a 2nd order a-causal time-domain Butterworth filter to the acceleration time-series padded with zeros; 5) double-integration to obtain displacement time series; 6) linear de-trending of displacement; 7) double-differentiation to get the corrected acceleration. The applied procedure ensures the compatibility among acceleration, velocity and

displacement time series.

A check on the displacement waveform resulting from the double-integration of the corrected accelerograms supported the choice of the high-pass corner frequency, f_h. Digital records are generally filtered with $f_h \leq 0.5$ Hz, down to values < 0.1 Hz (for the L'Aquila seismic sequence). On the other hand, analogue data, due to their lower quality, are generally high-pass filtered at frequencies higher than 0.2 Hz, with few exceptions, especially for large magnitude earthquakes.

2.5 Results and discussion

The equation used for the regression is similar to the model considered by Bindi et al. (2011) except for the exclusion of the style-of-faulting term and of a term linearly decreasing with distance (accounting for *anelastic attenuation*). equation (2.2) and equation (2.3) shows the functional form considered in this study for both the two advanced IMs; e_1 is the constant term, $F_{Di}(R,M)$, $F_{Mi}(M)$, F_s and F_{Rs} represent the distance (R) function, the magnitude (M) scaling and the site amplification correction, respectively. Magnitude measure is the moment magnitude (M_w), distance is the *Joyner-Boore distance* (R_{JB}), or the epicentral distance (in km), when the fault geometry is unknown (generally when M_w <5.5).

$$\log_{10} \mathrm{Sd}_i = e_1 + F_{D1}(R,M) + F_{M1}(M) + F_S + F_{R_S} \tag{2.2}$$

$$\log_{10} \mathrm{N}_e = e_1 + F_{D2}(R,M) + F_{M2}(M) + F_S + F_{R_S} \tag{2.3}$$

The proposed equation for the distance functions (F_{Di}) is shown in equation (2.4) and (2.5), while the magnitude function (F_{Mi}) is shown in equation (2.6) and (2.7), where M_{ref}, M_h, R_{ref} are coefficients to be determined through the analysis. It has to be noted that a different functional form was assumed for peak displacement and equivalent number of cycles, given the observed different trends of these IMs with the magnitude that will be shown in the following.

$$F_{D1}(R,M)=\left[c_1+c_2\left(M-M_{ref}\right)\right]\log_{10}\left(\sqrt{R_{JB}^2+h^2}\,/R_{ref}\right) \tag{2.4}$$

$$F_{D2}(R,M)=c_1\cdot\log_{10}\left(\sqrt{R_{JB}^2+h^2}\,/R_{ref}\right) \tag{2.5}$$

$$F_{M1}(M)=\begin{cases}b_1\left(M-M_h\right)+b_2\left(M-M_h\right)^2 & for\ M\le M_h\\ b_3\left(M-M_h\right) & otherwise\end{cases} \tag{2.6}$$

$$F_{M2}(M)=\begin{cases}b_1\left(M-M_h\right) & for\ M\le M_h\\ b_3\left(M-M_h\right) & otherwise\end{cases} \tag{2.7}$$

The term F_S in equations (2.2) and (2.3) represents the site amplification and it is given by $F_S = s_jC_j$, for j=1,...5, where s_j are the coefficients to be determined through the regression analysis, while C_j are dummy variables used to denote the five different EC8 site classes (A to E). The term F_{Rs} in equations (2.2) and (2.3) represents the strength reduction factor effect and it is given by $F_{Rs} = r_kC_k$, for k=2, 4, 6, 8, where r_k are the coefficients to be determined through the regression analysis, while C_k are dummy variables used to denote the four different strength reduction factors considered.

The regressions are performed by applying a random effect approach (Abrahamson and Youngs, 1992) to the geometrical mean of the horizontal components. After some trial regressions and after Bindi et al. (2011) the following variables have been fixed: R_{ref}=1 km; M_{ref}=5;M_h=6.75; b_3=0. Overall, the model for Sd_i was calibrated over 15 period dependent parameters (e_1, c_1, c_2, h, b_1, b_2, s_1, s_2, s_3, s_4, s_5, r_2, r_4, r_6, r_8), while the model for N_e was calibrated over 13 period dependent parameters (e_1, c_1, h, b_1, s_1, s_2, s_3, s_4, s_5, r_2, r_4, r_6, r_8). In equation (2.2) and (2.3), F_s = 0 for A site class and F_{Rs} = 0 for Rs equal to 2.

As a side result and employing the same functional form in equation (2.2), also a prediction equation for elastic displacements (Sd_{el}) has been obtained. The regression coefficients for elastic displacement, Sd_{el}, are reported in Table A-1, for inelastic displacement Sd_i for the EPH-k and EPH-p systems are reported in Table A-2 and Table A-3 respectively. Finally equivalent number of cycles, N_e, regression coefficients for EPH-k and EPH-p are reported

in Table A-4 and Table A-5.

2.5.1. Residuals

In Figure 2.3 to Figure 2.11 the residual distribution as function of the earthquake magnitude (M_w) and of the distance (R_{JB}) from the source are shown. Residuals are presented for Sd_{el}, Sd_i and N_e at two different periods, 0.2 and 1.0 seconds. The distributions confirm that the derived models produce residuals independent on the explanatory variables.

Residuals are characterized by very similar trends if EPH-k and EPH-p residuals are compared. N_e residuals, for both EPH-k and EPH-p systems, are characterized by a lower dispersion if compared to Sd_{el} and Sd_i.

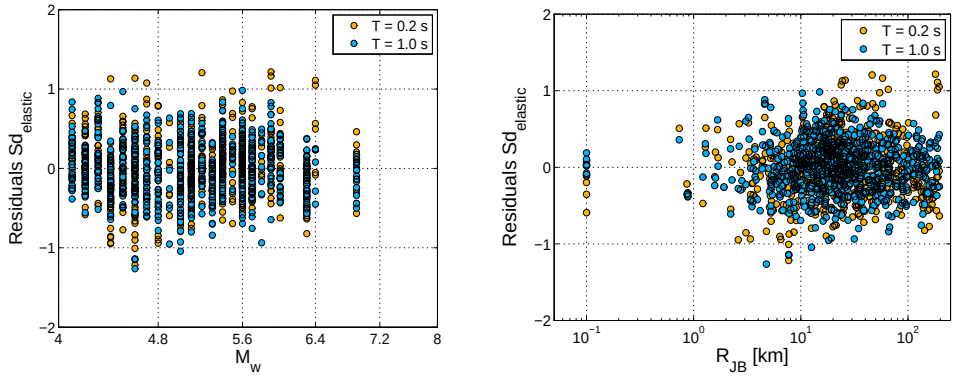

Figure 2.3. Residual distributions for Sdelastic as function of Mw and RJB.

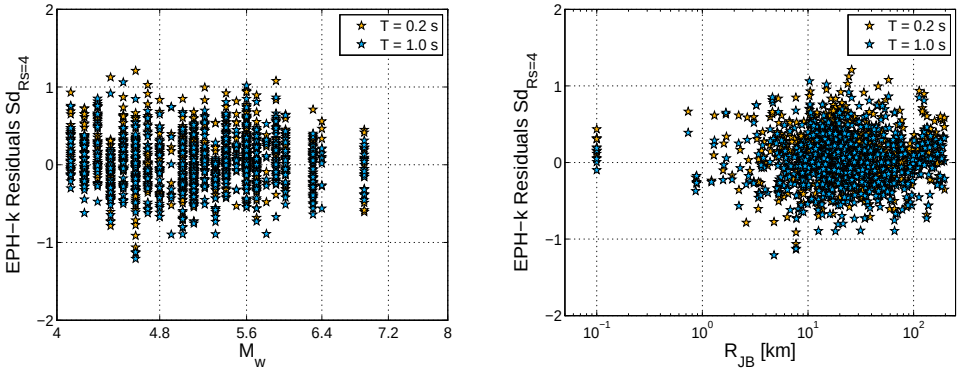

Figure 2.4. Residual distributions for EPH-k SDOFs at Rs equal to 4 as function of M_w and R_{JB} of the two EDPs considered: Sd_i for peak response.

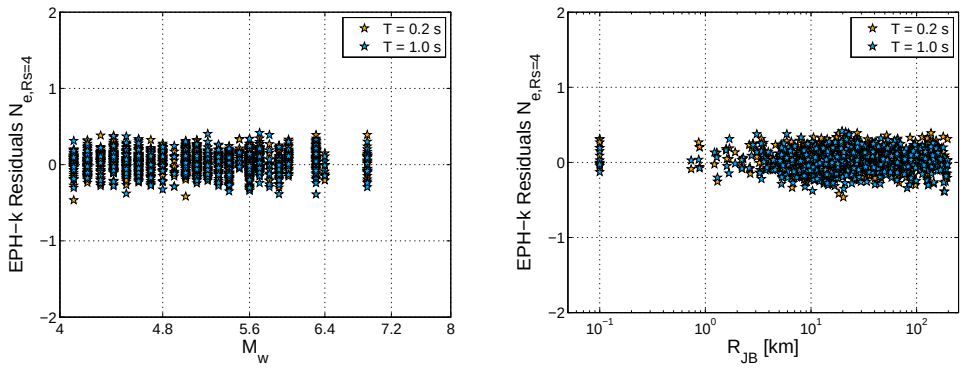

Figure 2.5. Residual distributions for EPH-k SDOFs at Rs equal to 4 as function of M_w and R_{JB} of the two EDPs considered: N_e for cyclic response.

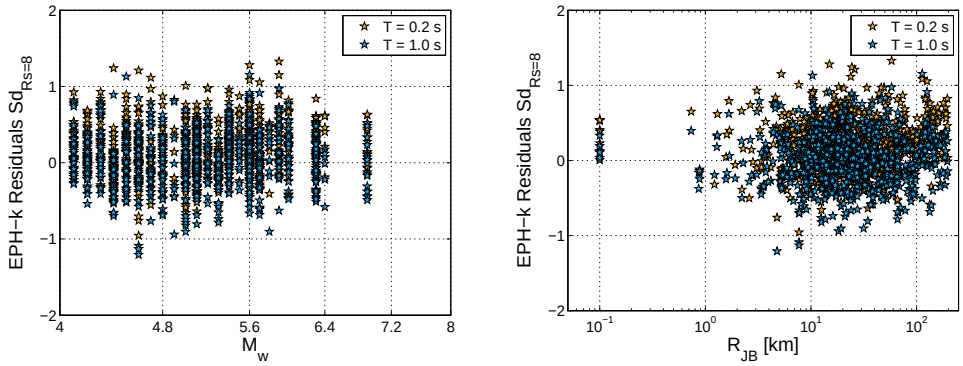

Figure 2.6. Residual distributions for EPH-k SDOFs at Rs equal to 8 as function of M_w)and R_{JB} of the two EDPs considered in this study: Sd_i for peak response .

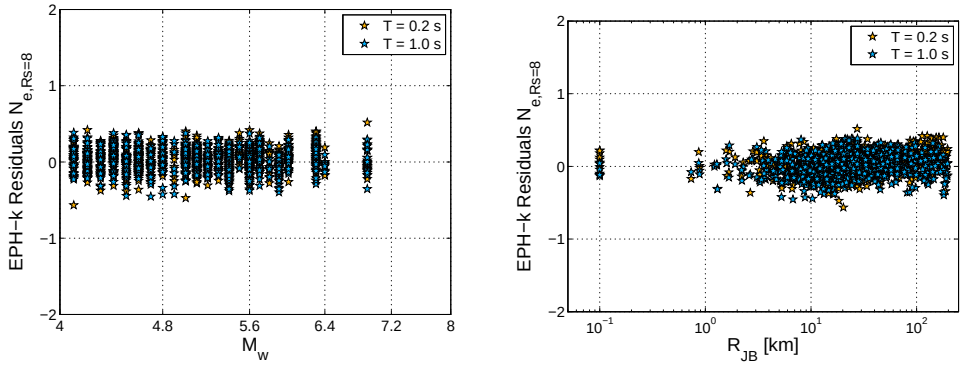

Figure 2.7. Residual distributions for EPH-k SDOFs at Rs equal to 8 as function of M_w and R_{JB} of the two EDPs considered in this study: N_e for cyclic response.

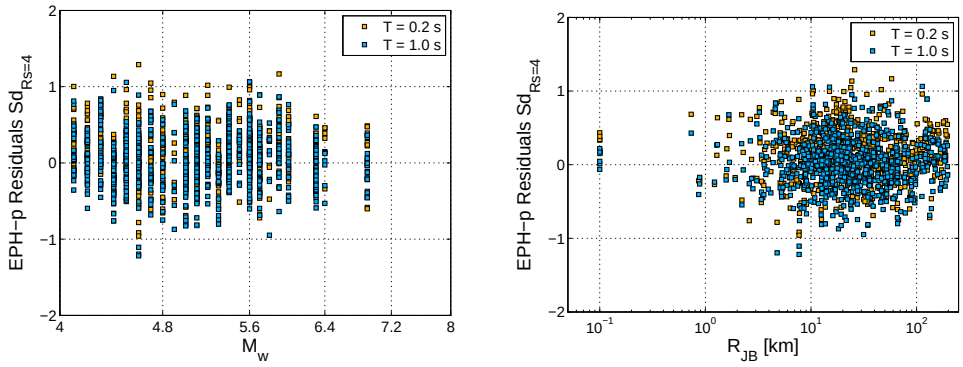

Figure 2.8. Residual distributions for EPH-p SDOFs at Rs equal to 4 as function of M_w and R_{JB} of the two EDPs considered in this study: Sd_i for peak response.

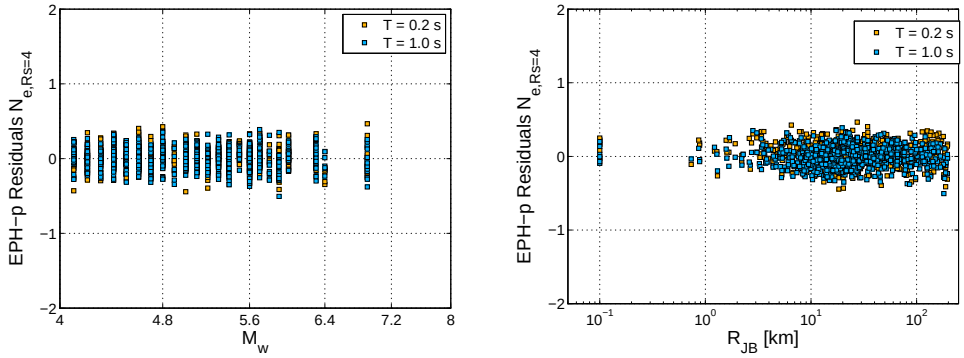

Figure 2.9. Residual distributions for EPH-p SDOFs at Rs equal to 4 as function of M_w and R_{JB} of the two EDPs considered in this study: N_e for cyclic response.

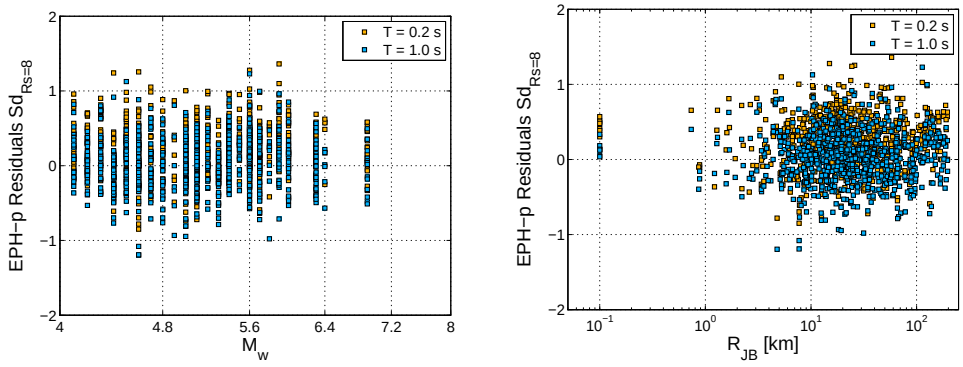

Figure 2.10. Residual distributions for EPH-p SDOFs at Rs equal to 8 as function of M_w and R_{JB} of the two EDPs considered in this study: Sd_i for peak response.

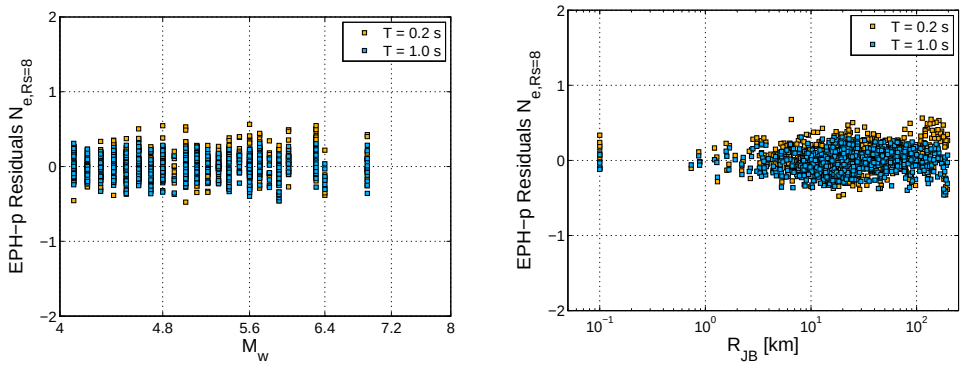

Figure 2.11. Residual distributions for EPH-p SDOFs at Rs equal to 8 as function of M_w and R_{JB} of the two EDPs considered in this study: N_e for cyclic response.

2.5.2. *Comparison with observed data*

The good performance of the predictive models is confirmed by Figure 2.12 and Figure 2.13 where the estimates for a magnitude 6.0 earthquake at two periods (T equal to 0.2 and 1.0 seconds), considering A soil type and two Rs values (equal to 4 in Figure 2.12 and equal to 8 Figure 2.13) are plotted as a function of distance, R_{JB}. The median estimate and the estimate plus and minus one standard deviation are reported for both the considered systems (EPH-k and EPH-p) and compared with Sd_i and N_e data for a magnitude interval of 6.0±0.3.

The difference between the Sd_i estimates for EPH-k and EPH-p systems emphasizes how influence of the hysteretic behavior, in the case of stiffness degradation only, can be neglected. On the other hand the hysteretic behavior of the SDOFs influences N_e estimates. The latter was an expected result, since N_e is a non dimensional measure of the cyclic response and it accounts specifically the way in which the whole energy of the record is dissipated (Manfredi, 2001).

It is evident, from the comparison of the panels in Figure 2.12 and Figure 2.13 referring to different periods (0.2 seconds versus 1.0 seconds), that while inelastic displacement tend to increase from low to medium period range, the equivalent number of cycles shows the opposite trend.

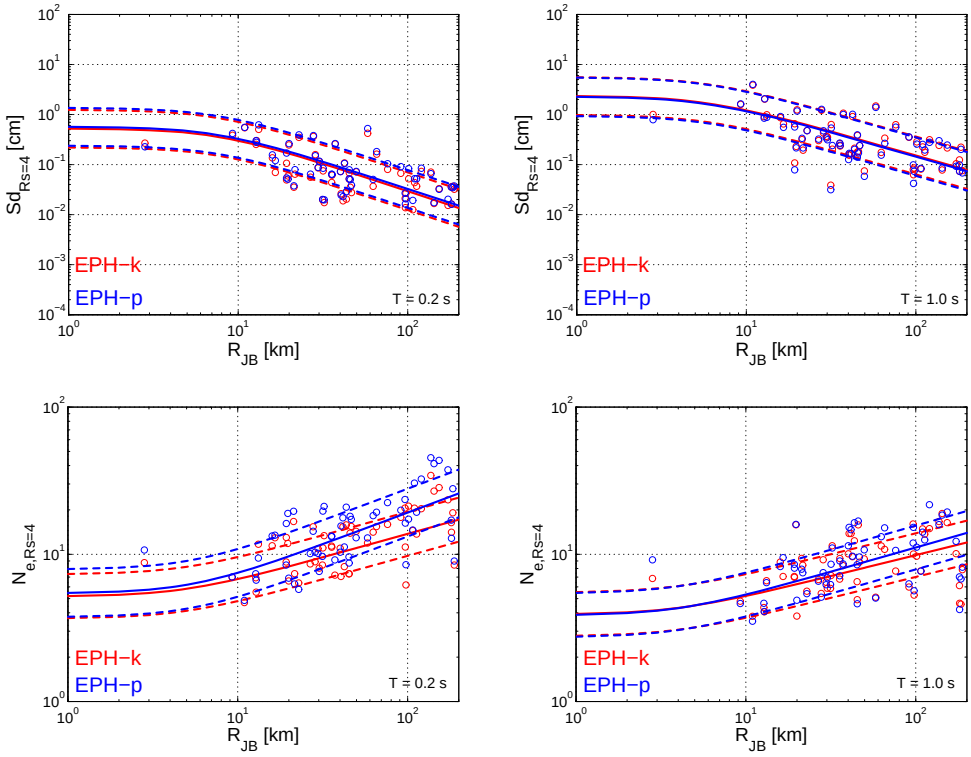

Figure 2.12. Estimates for a magnitude 6.0 earthquake, soil type A and Rs equal to 4 at two natural periods (T=0.2s and 1.0s) for both EPH-k and EPH-p systems, plotted as a function of R_{JB} and compared with Sd_i and N_e data for a magnitude interval of 6.0±0.3.

2.5.3. *Scaling with magnitude*

The scaling with magnitude of the predictions for Sd_i and N_e is shown in Figure 2.14 for the EPH-k systems and Figure 2.15 for the EPH-p. The estimates are plotted for soil type A and Rs equal to 6 at two different periods. The Sd_i curves are also compared with the predictions for elastic spectral displacement (dashed lines) derived using the same functional form and the same magnitude-distance distribution of records, see Equation (2.2).

The difference between elastic and inelastic displacement is more evident at short periods (e.g., 0.2s) and moderate to large magnitudes (M_w > 6), where larger values are predicted for the latter. At longer periods (e.g., 1.0s) elastic and inelastic spectral ordinates are comparable and for the largest magnitudes

slightly larger elastic response is predicted, this result confirms the equal displacement rule and the general trend of strength reduction factor, ductility and period (R-μ-T) relationships employed in Codes.

N_e regression is characterized by a dependence on magnitude almost negligible. The decreasing trend with increasing period of the cyclic response (recognizable from the comparison of the N_e panels for different periods in Figure 2.14 and Figure 2.15) is typical of parameters referring to cyclic response.

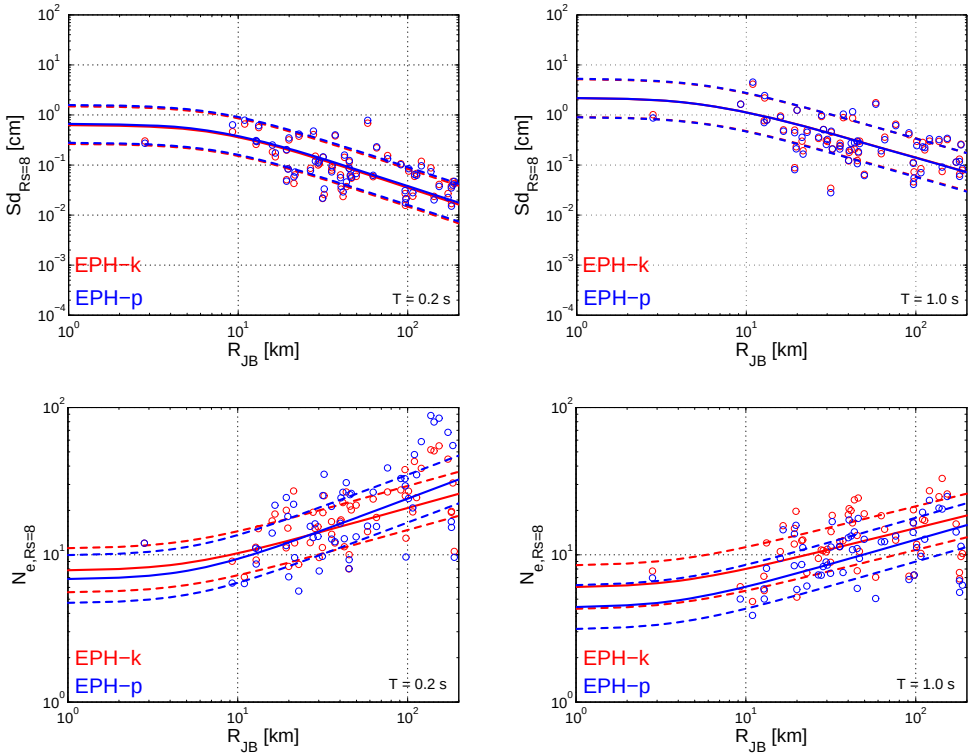

Figure 2.13. Estimates for a magnitude 6.0 earthquake, soil type A and Rs equal to 8 at two natural periods (T=0.2s and 1.0s) for both EPH-k and EPH-p systems, plotted as a function of R_{JB} and compared with Sd_i and N_e data for a magnitude interval of 6.0±0.3.

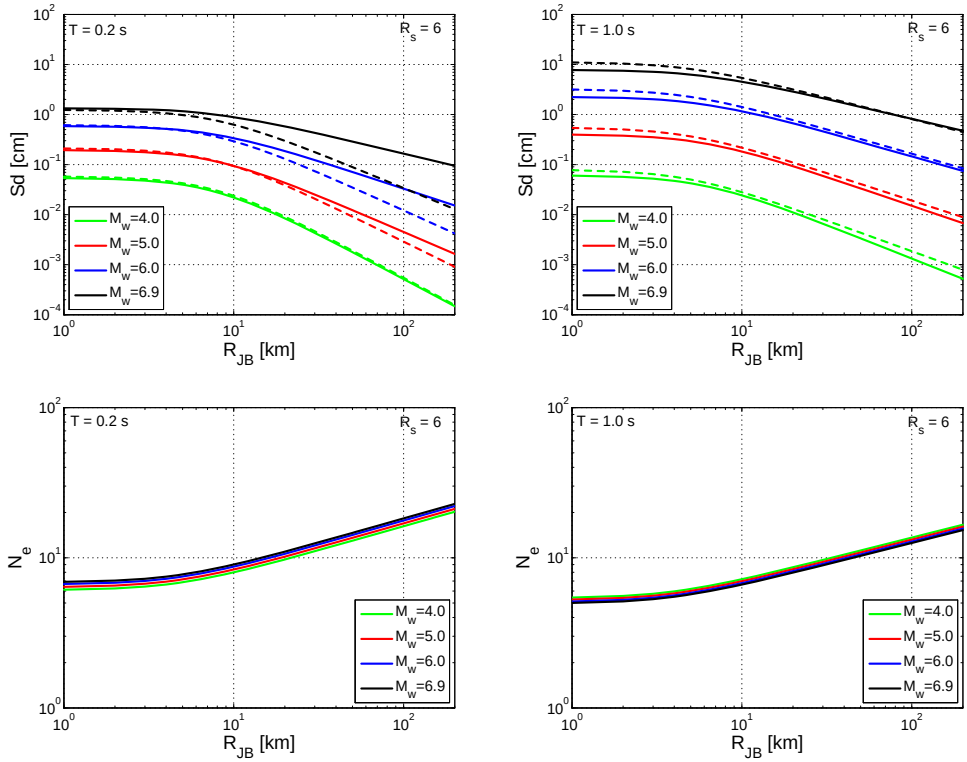

Figure 2.14. Scaling with magnitude of the predictions for Sd_i and N_e for EPH-k SDOF systems for A soil class, Rs equal to 6 for T = 0.2 s and 1.0 s.

The good correlation of N_e with intensity measures related to ground motion duration, such as the so called Cosenza and Manfredi index (I_D), (Iervolino et al., 2010a), provides a support to the increasing trend of N_e with the distance observed, (see Iervolino et al. 2010b).

The magnitude dependency is negligible; these results are, again, in accordance with the findings of the I_D attenuation relationship where magnitude coefficient is close to zero (Iervolino et al. 2010b). On the other hand M_w effect on N_e appears larger, even if slightly, for small oscillation periods. The negligible trend found with magnitude for N_e is the reason why it was necessary to consider a different functional form for this parameter, as it can be observed from the comparison of equations (2.4) and (2.5) and equations (2.6) and (2.7), respectively.

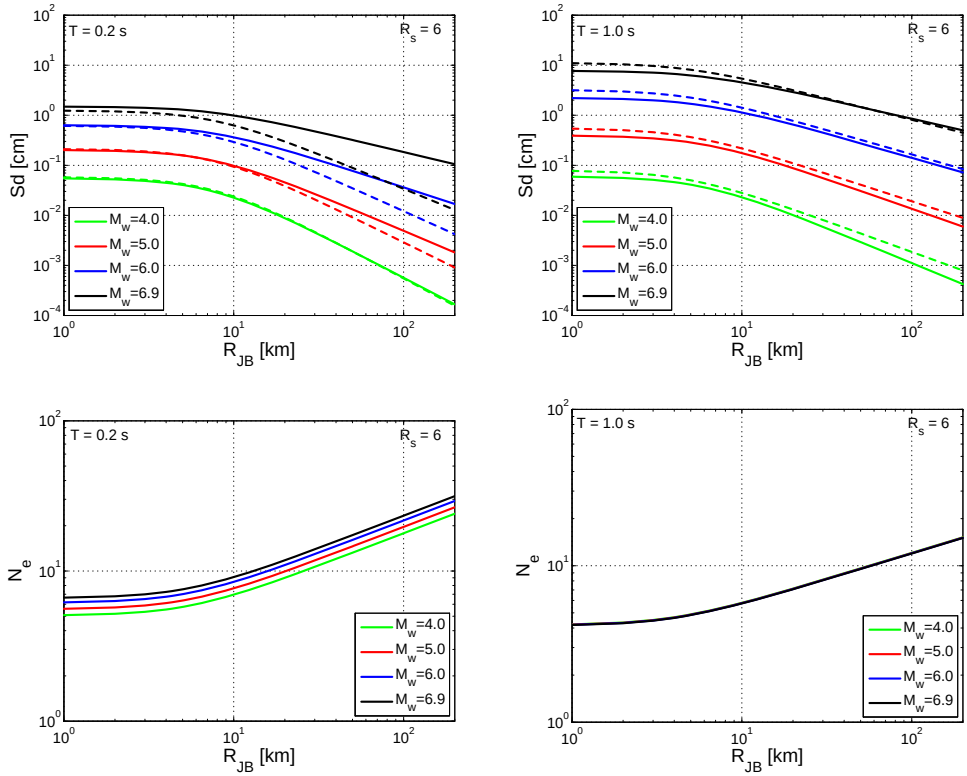

Figure 2.15. Scaling with magnitude of the predictions for Sd_i and N_e for EPH-p SDOF systems for A soil class, Rs equal to 6 for T = 0.2 s and 1.0 s.

2.5.4. *Soil class effect*

Soil class has a significant effect on the prediction of both inelastic displacements and equivalent number of cycles. It has to be noted that the number of records for each soil class is not equal represented in the dataset and in particular D and E soil classes are relatively poor. Soil class A is the larger one in the dataset, consisting in 325 records, followed by the 193 records for class B and 175 for class C. D and E class are composed respectively of 17 and 37 records and represent the soil conditions for which the maximum amplification is expected.

Figure 2.16 and Figure 2.17 show the effect of the soil classification on inelastic displacements and equivalent number of cycles for EPH-k and EPH-p SDOF systems as a function of the distance, respectively.

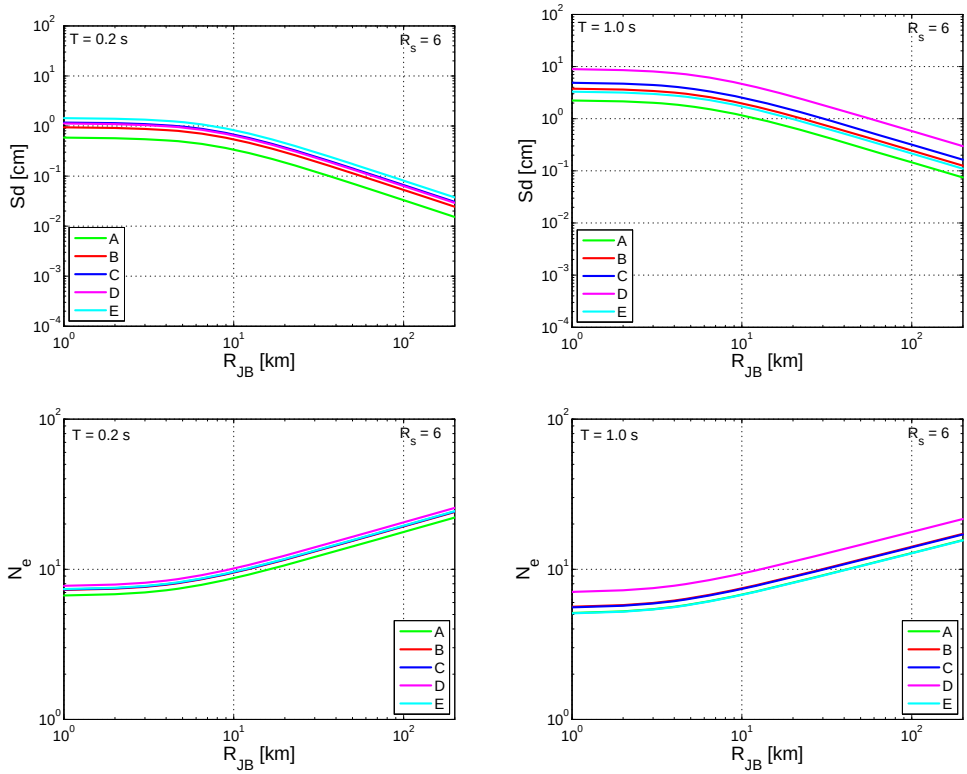

Figure 2.16. Scaling with soil class of the predictions for Sd_i and N_e for EPH-k SDOF systems, for M_w equal to 6.0 and Rs equal to 6 for T = 0.2 s and 1.0 s.

The estimates in Figure 2.16 and Figure 2.17 are made in the case of magnitude 6 and strength reduction factor equal to 6 at two different periods (0.2 and 1.0 seconds). Differences in the trends with soil classes between EPH-k and EPH-p SDOFs are negligible. Soil effect is amplified at medium periods for both inelastic displacements and equivalent number of cycles. D class is characterized by the highest amplification for both the considered IMs (Sd_i and N_e), the only exception is the inelastic displacement at 0.2 seconds for which E soil class show the larger amplification.

The amplification due to soil class is more evident for Sd_i; N_e, in fact, is a non dimensional parameter normalized by the hysteretic energy dissipated in the largest cycle. The value of this energy is affected by the soil class, thus leading to an attenuation of soil amplification on N_e.

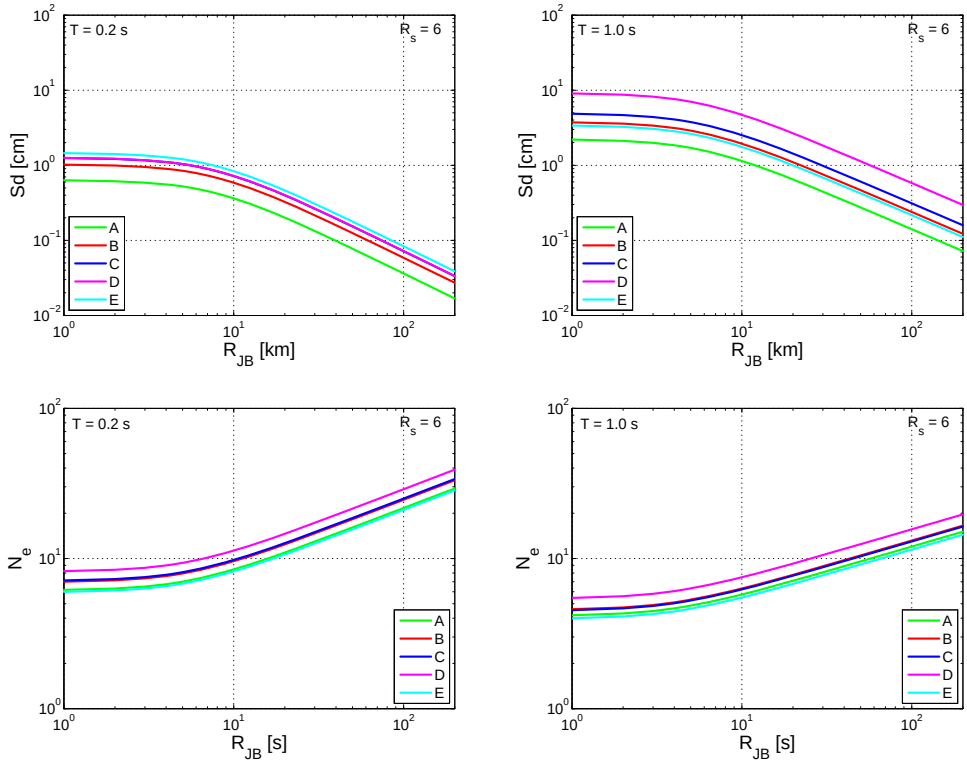

Figure 2.17. Scaling with soil class of the predictions for Sd_i and N_e for EPH-p SDOF systems, for M_w equal to 6.0 and Rs equal to 6 for T = 0.2 s and 1.0 s.

2.5.5. *Strength reduction factor effect*

The strength reduction factor, Rs, characterizes the specific value of yielding strength, F_y, for the SDOF considered; as it was emphasized before F_y is a specific record and period quantity in the *constant R* approach. In Figure 2.18 and Figure 2.19 is shown, for EPH-k and EPH-p SDOFs respectively, the effect of Rs parameter on the inelastic displacements and the equivalent number of cycles plotted as function of the distance at two different periods (0.2 and 1.0 seconds), for A soil class and magnitude equal to 6. Inelastic displacements at different Rs values are also compared with the estimate of the prediction equation for the elastic displacement. The trend shown by EPH-k and EPH-p systems are similar, so the following considerations are referred to both the SDOFs considered.

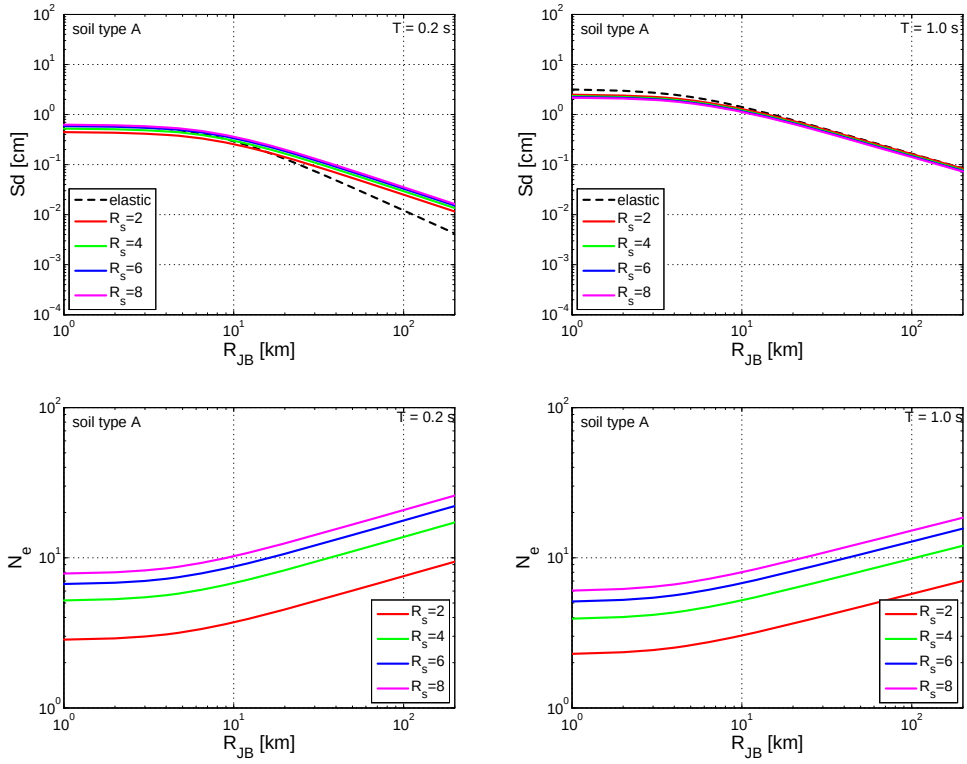

Figure 2.18. Predictions of Sdi and N_e for EPH-k SDOF systems at the different Rs values, M_w equal to 6.0 and soil class A, for T = 0.2 s and 1.0 s.

In medium period range (e.g. 1.0 seconds) elastic and inelastic displacement at the different Rs values tend to be the same, the latter, again, is a confirmation of equal displacement rule and the fact that its range of validity is independent from the specific Rs value considered; for low distances the elastic and peak response is even higher than the inelastic. At low periods (e.g. 0.2) the inelastic displacements at different Rs are similar to each other but show a significant difference with the peak elastic response. The results observed for inelastic displacement emphasize a significant difference between elastic and inelastic response. The above considerations find a confirmation in the trend of prediction equation of the ratio between inelastic and elastic displacement by Tothong and Cornell (2006).

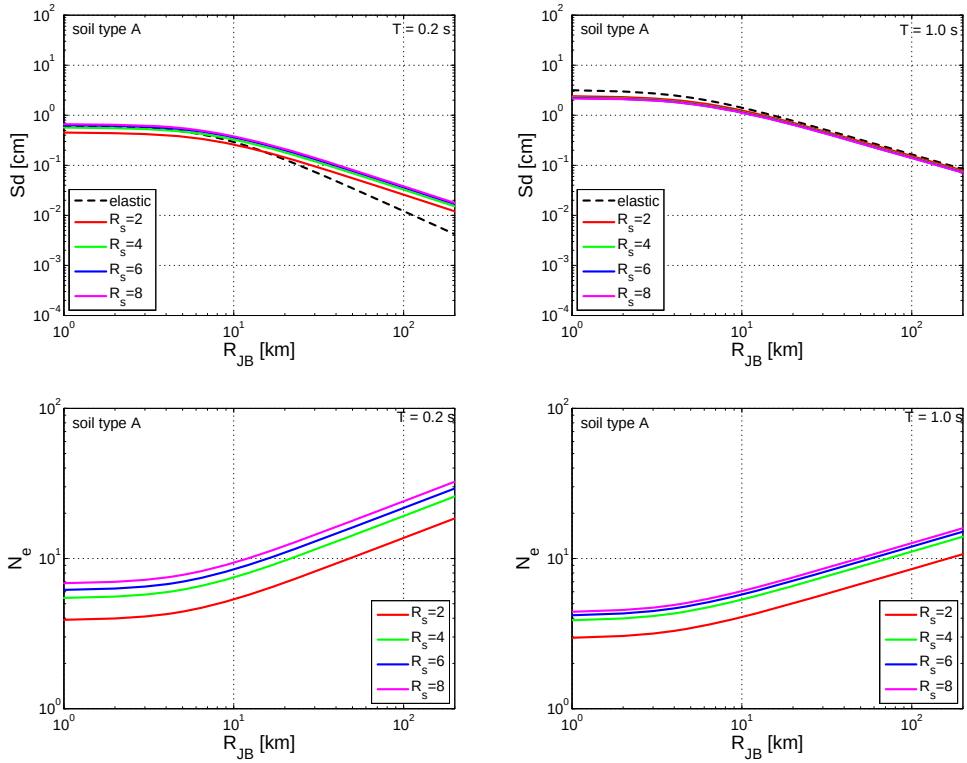

Figure 2.19. Predictions of Sdi and N_e for EPH-k SDOF systems at the different Rs values, M_w equal to 6.0 and soil class A, for T = 0.2 s and 1.0 s.

The strength reduction factor has, on the contrary, a significant effect on the equivalent number of cycles. This result is a consequence of the decreasing yielding strength with increasing of Rs that finally lead to an increase of N_e. The increasing trend of Ne with Rs tend to attenuate gradually form low (Rs equal to 2) to high (Rs equal to 8) inelastic behavior of the SDOF. The effect of Rs on Ne is so significant that difference between EPH-p and EPH-k become negligible if compared to it

The standard deviation of residuals (σ_{logY}) associated to the mean predictions of the models presented in equation (2.2) for the elastic and inelastic displacements and presented in equation (2.3) for the equivalent number of cycles is shown in Figure 2.20, as a function of period for both EPH-k and EPH-p systems. Such standard deviations are also compared to the σ_{logY}

of the ground motion prediction equation ITA10 for the spectral acceleration.

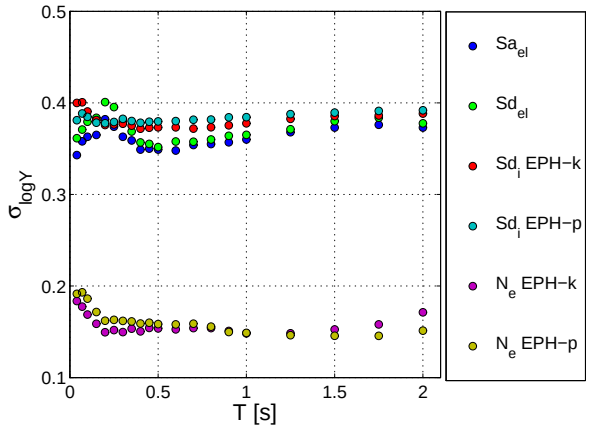

Figure 2.20. Standard deviation as function of periods of inelastic and elastic displacements, elastic acceleration (from Bindi et al., 2011) and equivalent number of cycles.

The σ_{logY} for elastic spectral displacement (derived in this study) and for elastic spectral acceleration (from Bindi et al., 2011) are shown as benchmark for the performance of the prediction equations in term of peak and cyclic inelastic response. The Sd_i standard deviations vary from about 0.37 to 0.40 for EPH-k and from 0.37 to 0.39 for EPH-p (see Table A-2 and Table A-3). The values do not increase significantly with respect to those derived for elastic displacement spectra that range from 0.35 to 0.40 and neither with respect to those derived for spectral acceleration in ITA10 that ranges from 0.33 to 0.38.

N_e standard deviation is smaller if compared to the standard deviation of the prediction equations for peak response and varies from about 0.14 to 0.18 for EPH-k and from 0.14 to 0.19 for EPH-p. Such results in term of σ_{logY} emphasize how it can be useful for PSHA to employ as IM the inelastic displacement rather than spectral acceleration, not only because of the robustness to scaling (see section 2.1), but also because the uncertainty introduced by such a prediction equation is comparable to that introduced by GMPEs in term of Sa with the final enhancement of an IM closer to the inelastic EDPs to be evaluated in the risk assessment.

2.5.6. *Spectra*

Figure 2.21 and Figure 2.22 show the mean spectra and their variability for the two systems, EPH-k and EPH-p, at two different strength reduction factors (Rs equal to 4 in Figure 2.21 and Rs equal to 8 in Figure 2.21) for the same scenario: A soil class, magnitude 6.3 and distance10 km. From the spectra it is possible to see that for the scenario selected and for both EPH-k and EPH-p systems for T > 0.5 the inelastic displacement is lower than the elastic, this result is similar to the trend shown by Tothong and Cornell (2006).

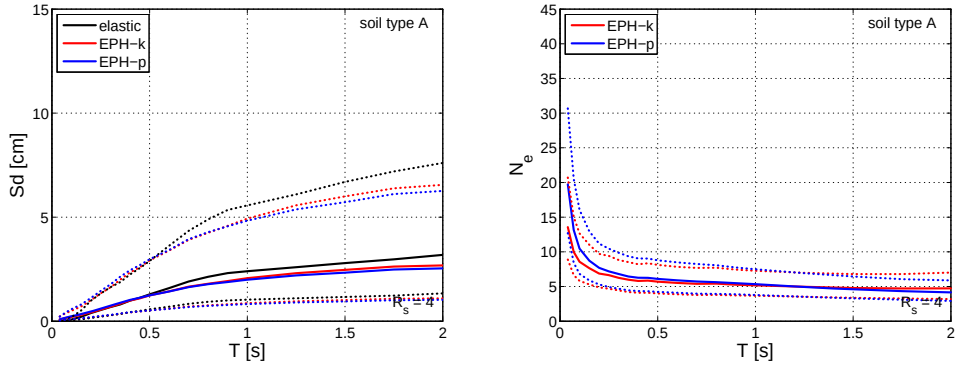

Figure 2.21. Mean Sd spectra and N_e spectra and their one standard deviation bands for EPH-k and EPH-p SDOFs, for Rs equal to 4, evaluated for an A soil class, Mw = 6.3 and RJB = 10 km scenario.

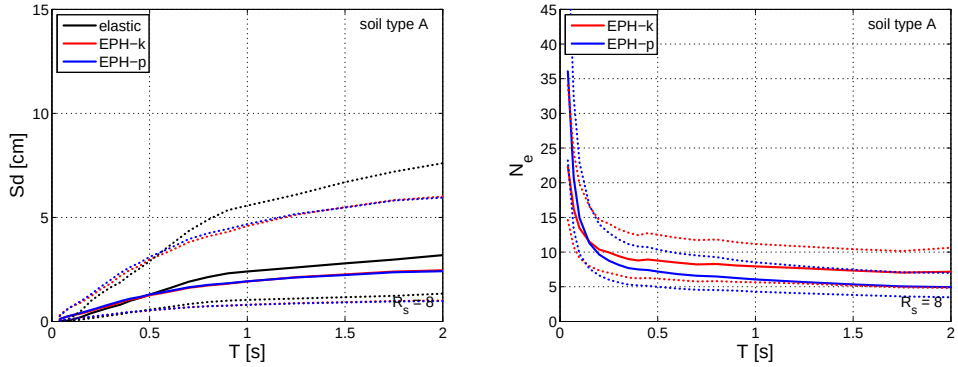

Figure 2.22. Mean displacement spectra and N_e spectra and their one standard deviation bands for EPH-k and EPH-p SDOFs, for Rs equal to 8, evaluated for an A soil class, Mw = 6.3 and RJB = 10 km scenario.

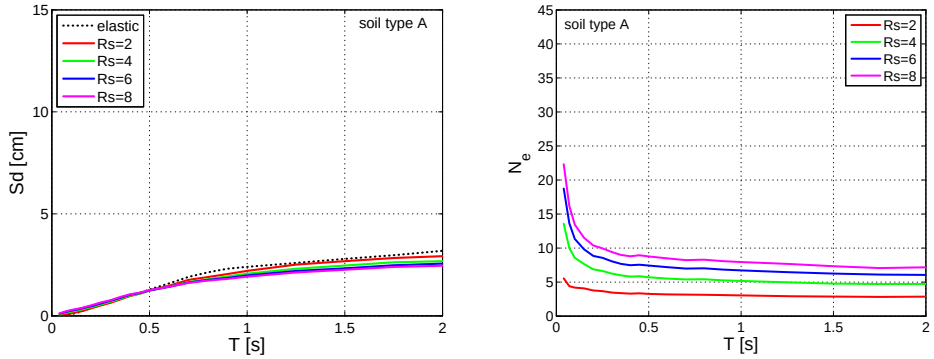

Figure 2.23. Mean displacement and N_e for EPH-k SDOFs, evaluated for A soil class, Mw = 6.3 and RJB = 10 km scenario.

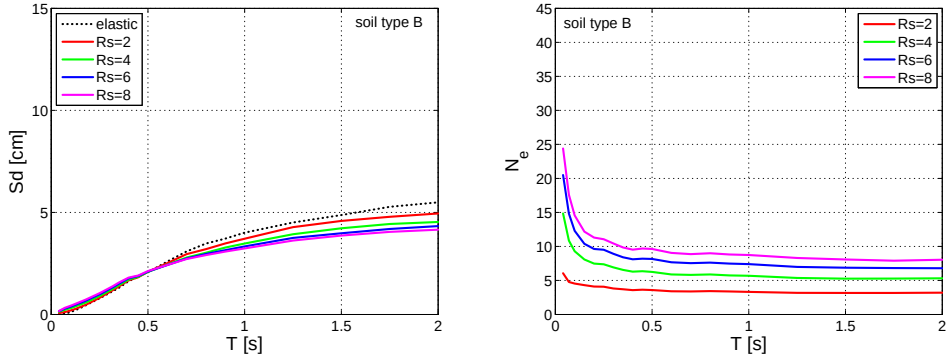

Figure 2.24. Mean displacement and N_e for EPH-k SDOFs, evaluated for B soil class, Mw = 6.3 and RJB = 10 km scenario.

Considering cyclic response, N_e spectra are slightly dependent from the hysteretic model; the curves for EPH-k and EPH-p are similar for T > 0.25s, whereas at shorter periods the EPH-p model predicts larger values.

The only stiffness degrading behavior (EPH-p) does not emphasize differences on cyclic response if compared to non-degrading hysteretic behavior (EPH-k), on the other hand when strength degradation is of concern the cyclic response dependence on hysteretic behavior can play a significant role in structural response (see Iervolino et al. 2010a).

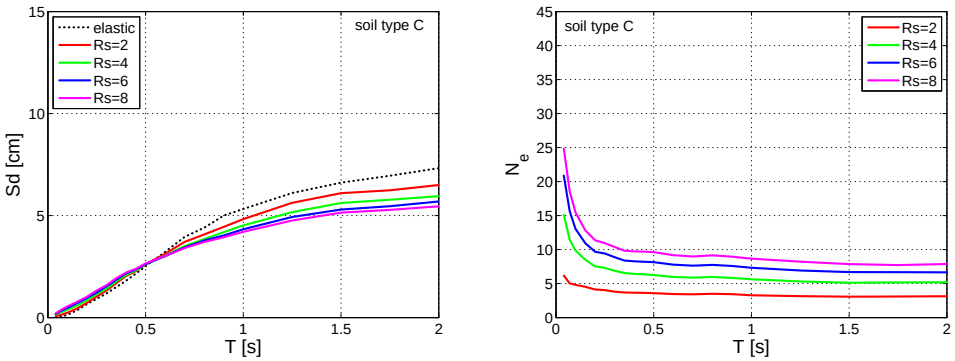

Figure 2.25. Mean displacement and N_e for EPH-k SDOFs, evaluated for C soil class, Mw = 6.3 and RJB = 10 km scenario.

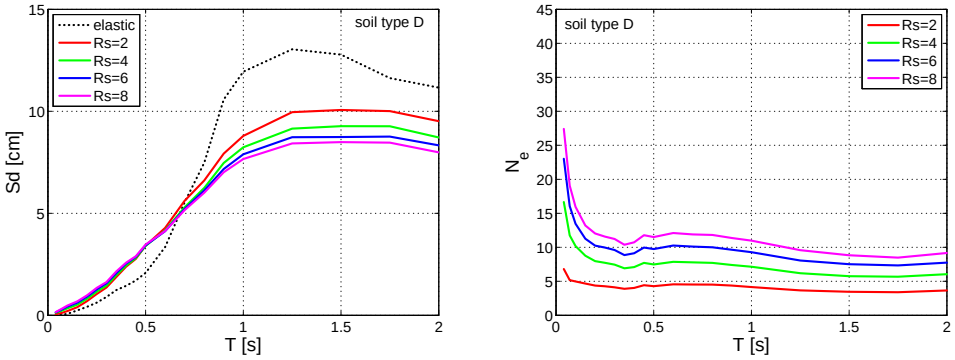

Figure 2.26. Mean displacement and N_e for EPH-k SDOFs, evaluated for D soil class, Mw = 6.3 and RJB = 10 km scenario.

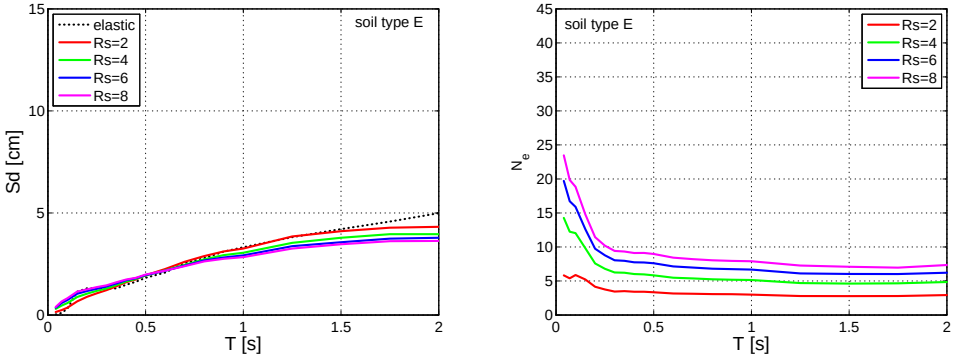

Figure 2.27. Mean displacement and N_e for EPH-k SDOFs, evaluated for E soil class, Mw = 6.3 and RJB = 10 km scenario.

This latter issue highlights the necessity to consider further SDOF models characterized by strength degradation (softening in the monotonic backbone) to allow a more fulfilling characterization of predictive equations for cyclic response parameters.

In Figure 2.23 to Figure 2.27 the spectra for magnitude 6.3 and distance 10 km are evaluated on different soil conditions and for all the Rs values considered in this study. Spectra on D soil class show the highest amplification, for both displacements and equivalent number of cycles.

2.6 Conclusions and perspectives

The possibility to develop prediction equations for nonlinear Single Degree of Freedom (SDOF) systems' peak and cyclic responses based on the Italian Accelerometric Archive (ITACA) was explored. Peak and cyclic inelastic structural response parameters were evaluated for the development of such attenuation models, useful for either design or assessment of structures. Two families of SDOF backbones were considered: first a non-degrading behavior with a slight hardening in the backbone, and second a stiffness degrading behavior with the same hardening backbone of the first family.

The preliminary results indicate that the standard deviations of the regressions are very similar to the dispersion of GMPEs based on elastic parameters. This result may lead to a more accurate estimation of nonlinear response with respect to what done in current practice where estimates of inelastic structural demand (and associated uncertainty) are applied on top of elastic prediction equations. Cyclic response evaluated in term of equivalent number of cycles showed similar trends with respect to those of duration-related measures. This result was expected according to the fair correlation found between those intensity measures and structural cyclic response.

The prediction equations obtained in this study, other than furnishing two advanced IMs for probabilistic seismic hazard analysis for the specific case of Italy, can allow a systematical validation for the peak and cyclic response of synthetic accelerograms, providing an unbiased benchmark to check the

performances of different techniques for the generation of accelerograms.

References

Abrahamson N.A., Youngs R.R., (1992). A stable algorithm for regression analyses using the random effects model. *Bulletin Seismological Society of America*, **82**, 505–510.

Bindi D., Pacor F., Luzi L., Puglia R., Massa M., Ameri G., Paolucci R., 2011. Ground motion prediction equations derived from the Italian strong motion database, Bulletin of Earthquake Engineering (DOI:10.1007/s10518-011-9313-z)

Bozorgnia Y., Hachem M.M., Campbell K.W., 2010a. Ground motion prediction equation ("attenuation relationship") for inelastic response spectra. *Earthquake Spectra* **26**(1), 1-23.

Bozorgnia Y., Hachem M.M., Campbell K.W., 2010b. Deterministic and probabilistic predictions of yield strength and inelastic displacement spectra. *Earthquake Spectra* **26**(1), 25-40.

Buratti N., Savoia M., 2009. Using non-stationary artificial accelerograms for estimating maximum drift demands on R.C. frame structures. *XIII Convegno ANIDIS 2009- L'Ingegneria Sismica in Itali*a. Bologna. 28 June-2 July. ISBN: 978-88-904292-0-0.]

Comitè Europèen de Normalisation (CEN), 2004. *Eurocode 8 – Design of Structures for earthquake resistance – Part 1: General rules, seismic actions and rules for buildings*. EN 1998-1, CEN, Brussels.

Ibarra L.F., Medina R.A., Krawinkler H., 2005. Hysteretic models that incorporate strength and stiffness deterioration, *Earthquake Engineering and Structural Dynamics*, **34**, 1489-1511.

Iervolino I., De Luca F., Cosenza E., 2010a. Spectral shape-based assessment of SDOF nonlinear response to real, adjusted and artificial accelelrograms, *Engineering Structures*, 32, 2776-2792.

Iervolino I., Giorgio M., Galasso C., Manfredi G., 2010b. Conditional hazard maps for secondary intensity measures, *Bulletin of Seismological Society of America*, **100**(6), 3312-3319.

Luco N., Bazzurro P., 2004. Effect of earthquake scaling on nonlinear structural response. Report for Pacific Earthquake Engineering Research (PEER) Center, Lifelines Program Project 1G00 Addenda, 2004. Available at http://peer.berkeley.edu/lifelines/lifelines_pre_2006/final_reports/1G00-FR.pdf.

Luzi L., Hailemikael S., Bindi D., Pacor F., Mele F., Sabetta F., 2008. ITACA (ITalian ACelerometric Archieve): A web portal for the dissemination of Italian strong-motion data, *Seismological Research Letters*, **79**, 716-722.

Manfredi G., 2001. Evaluation of seismic energy demand, *Earthquake Engineering and Structural Dynamics*, **35**, 21–38.

McGuire R.K., 2004. *Seismic hazard and risk analysis*. Report MNO-10. Earthquake Engineering Research Institute Publication, Oakland, CA, USA.

Miranda E. and Bertero V.V., 1994. Evaluation of strength reduction factors for earthquake-resistant design. *Earthquake Spectra*, **10**(2), 357-379.

Pacor F, Paolucci R, Ameri G, Massa M, Puglia R, 2011. Italian strong motion records in ITACA: overview and record processing. *Bulletin of Earthquake Engineering* DOI: 10.1007/s10518-011-9295-x.

Paolucci R, Pacor F, Puglia R, Ameri G, Cauzzi C, Massa M., 2011. Record processing in ITACA, the new Italian strong-motion database. In: Akkar S, Gulkan P, Van Eck T (eds) Earthquake data in engineering seismology, geotechnical, geological and earthquake engineering series, vol 14, Chapter 8, pp 99–113. Springer, Berlin.

Tothong P., Cornell C.A:, 2006. An empirical ground-motion attenuation relation for inelastic spectral displacement. *Bulletin of the Seismological Society of America*, **96**(6), 2146-2164.

Tothong P., Cornell C.A:, 2007. Probabilistic seismic demand analysis using advanced ground motion intensity measures, attenuation relationships, and near fault effects. *John A. Blume Earthquake Engineering Center, Department of Civil and Environmental*

Engineering, Stanford University, CA 2007. Available at http://blume.stanford.edu/Blume/TRList.htm.

Tothong P., Luco N., 2007. Probabilistic seismic demand analysis using advanced ground motion intensity measures. *Earthquake Engineering and Structural Dynamics*, **36**, 1837-1860.

Veletsos A.S., Newmark N.M., 1960. Effect of inelastic behavior on the response of simple systems to earthquake motions, *Proccedings of the 2nd World Conference on Earthquake Engineeirng*, Tokyo, Japan, 895-912.

Vidic T., Fajfar P., Fischinger M., 1994. Consistent inelastic design spectra: strength and displacement. *Earthquake Engineering and Structural Dynamics*, **23**, 507-521.

Chapter 3

REAL, ADJUSTED AND ARTIFICIAL RECORDS FOR CODE-BASED SEISMIC INPUT SELECTION

Iervolino I., De Luca F., Cosenza E. *Spectral shape-based assessment of SDOF nonlinear response to real, adjusted and artificial accelerograms*. Engineering Structures 32, 2010 pp. 2776-2792

Esposito M., 2009. *Accelerogrammi spettrocompatibili per la progettazione delle strutture: valutazione comparativa della risposta sismica*. Dipartimento di Ingegneria Strutturale, Università degli Studi di Napoli Federico II. Graduation Thesis. Advisors: E. Cosenza, I. Iervolino, F. De Luca.
[http://wpage.unina.it/flavia.deluca/tesi_en_file/TESI_Marilena.pdf] (in Italian)].

3.1 Authorship of Chapter

This chapter is based on two publications (cited above). It is the result of the work begun for the graduation thesis of Eng. Marilena Esposito with her thesis advisors. It covers some of the issues regarding code-based record selection and investigates, from a structural point of view, the possibility to employ artificial, adjusted and scaled record in nonlinear dynamic analyses, given the spectral compatibility asked by Codes.

3.2 Introduction

Seismic assessment of structures via nonlinear dynamic analysis requires seismic input selection. Seismic codes suggest different procedures to select ground motion signals, most of those assuming spectral compatibility to the elastic design spectrum as the main criterion (Iervolino et al., 2008a), for example Eurocode 8 (CEN, 2004), requires the average spectrum of the chosen

set to be above 90% of the design spectrum in the range of periods $0.2T_1$ – $2T_1$, where T_1 is the fundamental period of the structure. Practitioners have several options to get input signals for their analysis; e.g., real or real manipulated records and various types of synthetic and artificial accelerograms (Bommer and Acevedo, 2004). All these options are usually acknowledged by codes which may provide additional criteria or limitations for some of them. In the Italian seismic code (DM 14/01/2008), for example, artificial records, generated recurring to random vibration theory, should have duration of *at least 10s in their pseudo-stationary part*, and cannot be used in the assessment of geotechnical structures. Synthetic records, generated by simulation of earthquake rupture process, should refer to a characteristic scenario for the site in terms of magnitude, source-to-site distance and seismological source characteristics; finally real records should reflect the earthquake *dominating* the hazard at the site. However, practitioners not always can accurately characterize the seismological threat to generate synthetic signals or it is not possible to find a set of real records that fits properly code requirements in terms of a specific hazard scenario (Convertito et al., 2009).

In fact, despite in the last decades the increasing availability of databanks of real accelerograms has determined a spread use of this type of records; it may be very difficult to successfully apply code provisions to obtain code-compliant real record sets. In particular, provisions regarding spectral compatibility are hard to match if appropriate tools are not available (Iervolino et al., 2008a; Iervolino et al., 2009a). This is why the relatively easy and fast generation of artificial records, perfectly compatible with an assigned design spectrum, is still very popular for both practice and research purposes.

More recently, procedures to get the spectral compatibility of real records by wavelets adjustment were proposed (e.g., Hancock et al., 2006). This kind of manipulation is conceptually an extension of the more simple linear scaling of real records to modify (e.g., to amplify) the spectral shape to get a desired intensity level (Iervolino et al., 2005).

Although several studies tried to assess the *reliability* of each of these

procedures (e.g., Schwab and Lestuzzi, 2007), many of them are relatively narrow in scope without giving a general overview of the spectral compatibility issue. This work tries to address the spectral matching matter from the structural point of view in terms of ductility and cyclic response, having as reference a code-based design spectrum. To this aim six classes of 28 accelerograms, each of those comprised of four sets of 7, were considered: (1) unscaled real records; (2) moderately scaled real records; (3) significantly scaled real records; (4) wavelet-adjusted real records; (5) non stationary artificial records; (6) stationary artificial records. All sets are compatible with the elastic design spectrum for a case study in southern Italy.

The seismic responses of a large number of single degree of freedom (SDOF) systems, with different backbones, hysteretic relationships, and with various strength reduction factors (R), were considered. As structural response measures, or engineering demand parameters (EDPs), the ductility normalized with respect to the strength reduction factor and the equivalent number of cycles were considered to relate the ground motions to both peak and cyclic structural demand (Iervolino et al., 2006; Manfredi, 2001). Analyses aimed at comparing the differences, if any, in the EDPs associated to each class of records with respect to the unscaled real records, considered as a benchmark. Hypothesis tests on selected samples were also carried out to assess the statistical significance of the results found in terms of both peak and cyclic response.

3.3 Record classes

All the classes of records refer to the same 5% damped elastic design spectrum evaluated according the new Italian seismic code for a case-study site in Avellino (southern Italy, lat. 40.914, long. 14.780). The spectrum considered is that corresponding to the life-safety limit state of an ordinary construction with a nominal life of 50 years on A-type soil class, according to Eurocode 8 classification; see (DM 14/01/2008) for details.

For each class four spectrum compatible sets, made of seven records

each, were selected (if real) or generated (if artificial) because seven is the minimum sample to consider the average structural response as the design value according, among others, to the Italian and Eurocode 8 provisions. In the following the selection or generation processes are briefly reviewed, other information about the selection procedure can be found in (Esposito, 2009).

3.3.1. URR - Unscaled real records

The sets of unscaled real ground motions (URR) were selected using REXEL 2.5 (beta), the software freely available at http://www.reluis.it/, which allows to select combinations of 7 records contained in the European Strong Motion Data Base (http://www.isesd.hi.is/) and the Italian Accelerometric Archive (http://itaca.mi.ingv.it/ItacaNet/), which on average match a code-based or user-defined elastic spectrum in a desired period range and with specified upper and lower bound tolerances (Iervolino et al., 2009b). Because REXEL can also automatically build the code spectrum for an Italian site based on its geographical coordinates, 4 sets of records were selected, each of those matching on average the target in the 0.15s-2.0s period range. Magnitude (moment magnitude, M_w) and source-to-site distance (epicentral, R_e) range between 5.6-7.8 and 0km-35km, respectively, site conditions are of A-type.

Because the Italian code design spectra approximate closely uniform hazard spectra provided for the Italian territory, initially the selection aimed at finding records with M_w and R_e equal to 5.8 and 14km, respectively; i.e., equal to the mean from disaggregation of peak ground acceleration (PGA) at the site[2] available at http://esse1-gis.mi.ingv.it/ (official Italian hazard data). However, due to the lack of spectrum matching unscaled real record sets fitting these restraints, M_w range had to be relaxed obtaining average values of magnitude and distance for the class equal to 6.5 and 15 km, respectively.

In Figure 3.1a, the four sets are depicted along with the target spectrum.

[2] It is to recall here that, more accurately, disaggregation to be matched should be that for the hazard of the spectral ordinate at the fundamental period of the structure (Baker and Cornell, 2006).

All the set averages are selected to be within [-10%, +30%] tolerance range with respect to the code spectrum, and in most of the compatibility interval they approximate very well the design spectral shape. To measure such an approximation the average deviation (δ) from the target spectrum, see equation (3.1), may be introduced. In equation (3.1) $Sa_{o,med}(T_i)$ represents the pseudo-acceleration ordinate of the average real spectrum corresponding to the period T_i, while $Sa_s(T_i)$ is the value of the spectral ordinate of the code spectrum at the same period, and N is the number of values within the considered range of periods (0.15s – 2.0s). All the URR sets have similar δ values; in fact: it is equal to 0.163 for set 1, 0.134 for set 2, 0.152 for set 3 and 0.141 for set 4. The four URR sets have no records in common and come from seventeen different earthquakes, as it is shown in the Appendix B (Table B- to Table B-4).

$$\delta = \sqrt{\frac{1}{N}\sum_{i=1}^{N}\left(\frac{Sa_{o,med}(T_i) - Sa_s(T_i)}{Sa_s(T_i)}\right)^2} \tag{3.1}$$

In the following the SDOF response to various ground motion selection or generation methods will be compared referring to URR response. In fact, in this kind of studies it is necessary to define the "true" response (i.e., a point of comparison). Because the work herein presented is mostly aimed at comparing spectral matching in the light of code-compliant procedures, which often basically only prescribe the average spectrum of the set to match the design spectrum (Iervolino et al., 2008a; Convertito et al., 2009), the URR records are assumed as a benchmark. This means that if systematic difference in the response from another class of records with respect to URR will be found, this class will be considered "biased". However, this use of the *bias* term does not necessarily extends beyond this study as, in general, the URR may be not an unbiased baseline itself, even if allowed by the code, simply because, for example, selecting records that have a similar spectral shape, a selection bias can be created (Hancock et al., 2008; PEER report 2009/01, 2009).

3.3.2. SF – Scaled real records

REXEL also allows selecting sets of seven accelerograms compatible with the reference spectrum if linearly scaled in amplitude. In other words, before the search, the spectra are preliminarily normalized dividing the spectral ordinates by the corresponding PGA. These non-dimensional spectra are compared to the target spectrum also normalized. Records belonging to spectrum matching combinations found in this way require to be linearly scaled to comply with the original code spectrum. Because REXEL allows controlling the average scaling factor (SF) of the combination, two classes of four scaled records sets each, (i) SF equal to 5; (ii) and SF equal to 12, were selected from A-type site class accelerograms. The intent is to compare response to records moderately and significantly scaled.

- **SF5**

In the same range of periods in which there is spectral compatibility (0.15s – 2s), with the same tolerances, and in the same magnitude and distance intervals chosen for URR, four set of seven compatible accelerograms, each of those having a mean SF equal to 5, were selected, Figure 3.1b.

The 28 records (9 records in common with URR) come from 15 earthquake events (10 of them are in common with URR), as shown in Appendix B (Table B-5 to Table B-8).

In this case the deviations of the sets are smaller than URR records' deviations, as expected (Iervolino et al. 2008a; Iervolino et al., 2009a), being equal to: 0.082 for set 1, 0.087 for set 2, 0.069 for set 3 and 0.089 for set 4.

- **SF12**

Using REXEL also three sets of seven records whose mean SF was 12, were selected, each of those matching on average the target in the 0.15s-2.0s period range. Magnitude and source-to-site distance range between 5.5-7.8 and 0km- 50km. Because it was not possible to find another set with the desired characteristics via REXEL, the fourth set of seven accelerograms was "manually" selected in the same magnitude and distance ranges so that its deviation and its average scaling factor were similar to the other three

software-aided selected sets, Figure 3.1c.

These four sets have no events in common with the URR class and belong to 17 different earthquakes, as shown in Appendix B (Table B-9 to Table B-12). In this case, deviations of the sets are still smaller than deviations of URR and comparable to deviations of the SF5 sets, being equal to: to 0.072, 0.078, and 0.117 for the software selected sets and equal to 0.207 for the manually selected set, respectively.

3.3.3. RSPMatch - Wavelet adjusted records

RSPMatch2005 software[3] (Abrahamson, 1992; Hancock et al., 2006), was used to modify the URR accelerograms. Spectral matching software, as RSPMatch2005, make adjustments to recorded ground motions to provide a good match with a target response spectrum. Using spectrally-matched records as an input to time-history analysis helps to reduce the variability in the seismic demand, and therefore allows fewer records to be used to obtain stable estimates of the expected response (Hancock et al., 2008). Generally, RSPMatch2005 is able to provide an excellent match of the target spectrum across a wide range of periods (and, if required, at multiple damping levels), with relatively small adjustment to the seed accelerogram. Useful guidelines and reliable selecting criteria to choose set of records suitable to be adjusted by the software can be found elsewhere (e.g., Grant et al., 2008).

In this case the adjustment procedure was simply aimed at reducing dispersion of records, in a specific period range, with respect to the target. The procedure was pursued only for the 5% damping factor in the range of periods 0.15s-2.0s in which records were already compatible on average, Figure 3.1d.

It is to note that wavelet adjustment was applied in a relatively limited period range. Nevertheless, even if the matching in the 0.15s-2.0s interval produced individual spectrum modification also beyond that range (Figure 3.1d), the average of RSPMatch class is close to the target also in the 2s-4s

[3] Courtesy of Damian Grant, ARUP, USA.

range.

3.3.4. *Artificial records*

Generally speaking, generation procedures for artificial accelerograms are based on the random vibration theory and the spectral matching is carried out iteratively adjusting the Fourier amplitude spectrum of each accelerogram generated (Pinto et al., 2004). In this way, spectral matching procedures are carried out in the frequency domain by the use of a power spectral density function, the selection of which is the key issue and represents the main difference between various generation procedures.

The software considered in this study generate different kind of signals: the first one, Belfagor (Mucciarelli et al., 2004) produces non stationary signals based on the semi-empirical method of Sabetta and Pugliese (1996); the second one SIMQKE (Gasparini and Vanmarke, 1976) produces stationary signals that are subsequently enveloped in a trapezoidal shape to roughly simulate non-stationary characteristics of ground motion.

- **Belfagor sets**

Belfagor (http://www.unibas.it/utenti/mucciarelli/index.html) generates non stationary signals by using variable Fourier amplitudes empirically evaluated from the Sabetta and Pugliese ground motion prediction equation (Sabetta and Pugliese, 1996); in fact, the code asks for reference M_w, R_e, and soil type. Because of record's non-stationary character, these parameters influence strictly the shape of the signal even if the spectral matching procedure is based on a smooth code spectrum.

A class of 28 accelerograms was generated for the purposes of this study. The input M_w and R_e values for each signal were equal to those of the URR and *stiff soil type*, according to (Sabetta and Pugliese, 1996), was assumed. All the generated records have the same duration, 21.48s with a 0.005s time step (default values of Belfagor). The duration is slightly lower than the minimum prescribed by the Italian code for artificial records (25s); however this 15% difference is not believed to affect results (see also section 2.5).

Although not strictly necessary for the purposes of this study, the

accelerograms were randomly arranged in four sets of seven consistently with the other classes, Figure 3.1e.

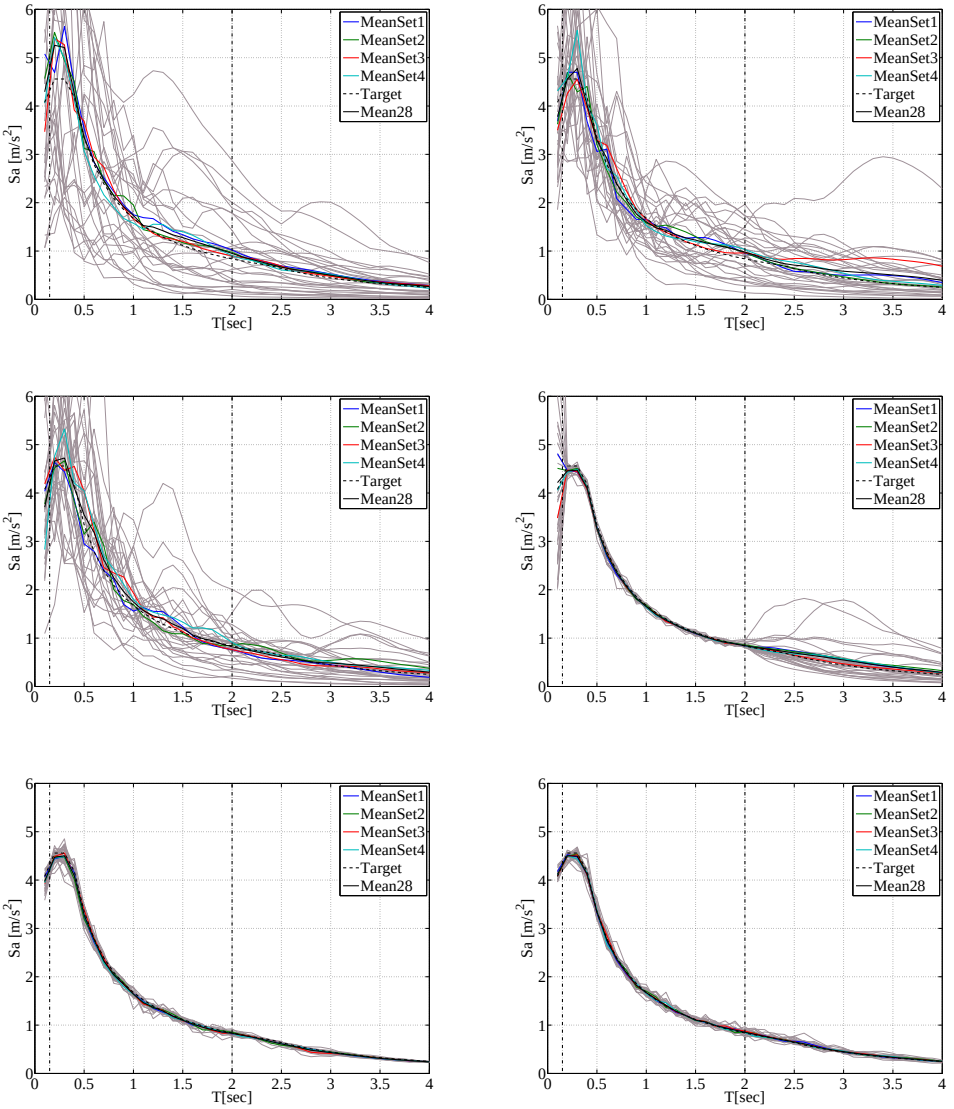

Figure 3.1. URR (a), SF5 (b), SF12 (c), RSPMatch (d), Belfagor (e), and Simqke (f) acceleration elastic spectra, compared to the target spectrum.

- **Simqke sets**

  A second class of artificial records was generated by Simqke

(http://bsing.ing.unibs.it/~gelfi/software/simqke/). This is the commonly used method for generating synthetic ground motions, which are compatible with a prescribed design spectrum. This method is based on simulation of stationary processes. The matching of the target spectrum may be improved by means of an iterative procedure. Other studies evaluated the influence of iterative option in the software that was not considered in this case (e.g., Schwab and Lestuzzi, 2007). In this case 28 records were generated in a single run of the software and subsequently they were separated in 4 groups of 7, Figure 3.1f.

They fully respect the Italian code's provisions in terms of duration of both stationary and non-stationary parts. In fact, as it was reported previously, this software simulates record non-stationary by enveloping the signal obtained in a trapezoidal shape, and the user can choose how long to make the beginning and ending of non stationary part.

3.4 Integral ground motion parameters

Each accelerogram of the six classes was processed to evaluate its characteristic other than the spectral shape, in particular in terms of integral intensity measures (IMs). Average values of Arias intensity (I_A), equation (3.2), and of Cosenza and Manfredi index (I_D), (Cosenza et al., 1993), equation (3.3), computed as the average on the sample of 28 records for each class, are reported in Figure 3.2. In Equation (3.2) and (3.3) a(t) is the signal's accelerometric time-history, whose duration is equal to t_E, and PGV represents the peak ground velocity.

$$I_A = \frac{\pi}{2 \cdot g} \int_0^{t_E} a^2(t)\, dt \tag{3.2}$$

$$I_D = \frac{2 \cdot g}{\pi} \frac{I_A}{PGA \cdot PGV} \tag{3.3}$$

It seems that the Simqke generation process is not able to reproduce characteristic Arias intensities of real events at least if compared to URR, SF5,

and SF12. Scaled real records have lower I_A values, on average, with respect to the URR as well as those adjusted via RSPMatch2005. However, when passing to I_D, which is supposed to be better related than I_A to structural cyclic response expressed in terms of equivalent number of cycles (Manfredi, 2001), both scaled and unscaled real records and RSPMatch have close average values of I_D. Both classes of artificial signals display higher values of I_D, especially the Simqke accelerograms because of the high I_A.

Also the significant duration (Sd), defined as the time interval between 5% and 95% of I_A accumulation, was computed. Table 3-1 reports average values of Sd for each class. Only Simqke records show duration clearly larger than others.

Table 3-1. Average values of Sd for the considered classes of records.

URR	SF5	SF12	RSPM	Belf	Simq
13.7s	12.5s	10.4s	13.8s	12.0s	18.0s

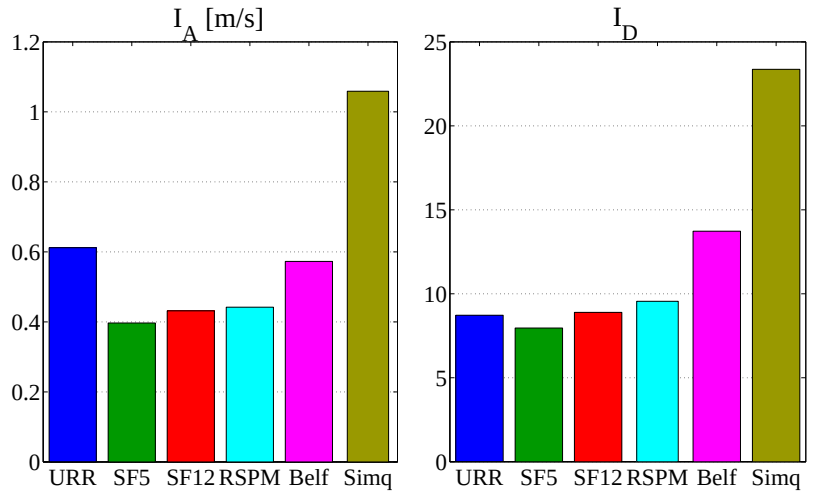

Figure 3.2. Average values of I_A and I_D for the considered classes of records.

Although it was discussed how integral parameters such as I_D are good IMs for cyclic response, one may argue that the correct value to match is not necessarily that of URR. To investigate this, in Figure 3.3 the probability of

exceedance of I_D conditional to the PGA of the target spectrum is reported for three M_w-R_e pairs. The first pair chosen (M_w=5.0 and R_e=5.0km) is the modal pair from disaggregation of the hazard for the design PGA at the site, the second pair (M_w=5.8 and R_e=14.0km) is the mean. For comparative purposes, a third couple of M_w and R_e (M_w=6.5 and R_e=15.0 km) was considered, it represents mean M_w and R_e of the URR class. The curves in Figure 3.3 were obtained via *conditional hazard analysis* according to the procedure[4] described in Iervolino et al., 2008b and Iervolino et al., 2009b.

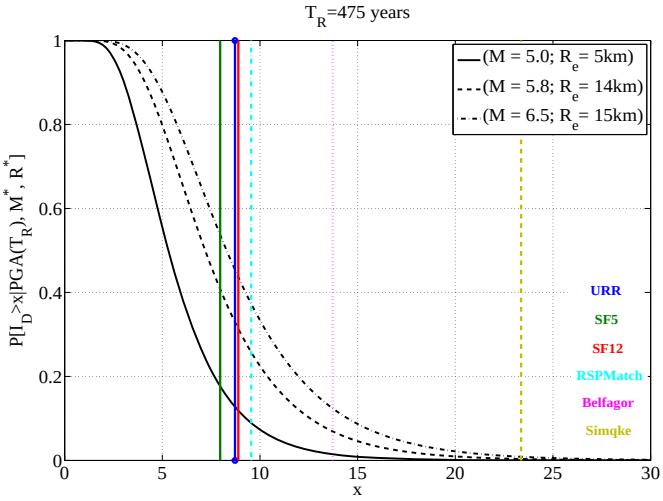

Figure 3.3. Comparison between probability of exceedance of I_D conditional to the PGA value of the target elastic spectrum and I_D medium values of each record category.

The mean I_D of all the classes of records can be compared with the I_D

[4] As discussed in (Iervolino et al., 2008b) and (Iervolino et al., 2009c) the conditional I_D distribution would require to account for all M_w and R_e pairs weighted by their contribution to hazard from disaggregation and this would be the "exact" result in terms of the distribution of integral ground motion features given the design peak acceleration. However, a simplified and approximated approach may be followed using only representative pairs form the joint M_w and R_e disaggregation distribution. This approach is also used herein; different representative pairs lead to slightly different (approximated) results.

distributions. It may be observed that the likely I_D values given the PGA at the site are 5.3 and 7.2 as median, 3.5 and 4.7 as 16% and 8.2 and 11.1 as 84% percentile, respectively for the mode and mean M_w and R_e from disaggregation. URR mean M_w and R_e give 5.3, 8.3 and 12.8 as 16%, 50% and 84% percentiles respectively.

All the three complementary cumulative distributions of I_D suggest that the artificial signals are characterized by unusual integral parameters although matching the same elastic spectrum of all the other record classes.

3.5 SDOF systems and demand measures

All records selected for each class were used as input for nonlinear dynamic analyses applied to 240 SDOFs. They belong to three classes of hysteretic behavior with elastic period varying from 0.1s to 2s, sampled with 0.1s step. Elastic-plastic with hardening (EPH) SDOF represents non-degrading and non-evolutionary structures. The post-yielding stiffness was assumed as 0.03 of the initial stiffness (k_{el}), Figure 3.4a. The second class of inelastic SDOFs has a non-degrading and evolutionary relationship; its backbone is elastic perfectly plastic (EPP) and it is characterized by a degrading stiffness; Clough and Johnston model (Clough and Johnston, 1966) was considered (Figure 3.4b). The third class of inelastic SDOFs has a softening backbone (ESD); a Takeda hysteretic rule was assumed (Takeda et al., 1970). The softening stiffness is equal to 10% of the elastic one and 10% of yielding strength was taken as the residual value. All ESD systems have ductility before reaching the residual strength, evaluated as the ratio between ultimate displacement (Δ_u) and yielding displacement (Δ_y) in the backbone curve, equal to 10. In the following, this ductility value will be called *ductility limit*, Figure 3.4c. In all panels of Figure 3.4, F_y is the yielding strength of the SDOF.

To have a response that ranges from mildly inelastic to severely inelastic, for all SDOF systems four strength reduction factors (R) were considered: 2, 4, 6 and 10. Note that the peak deformation experienced by an elastic structure is a ground motion specific quantity. Therefore, one can achieve the same value

of R either for each record in a dataset (*constant R approach*) or on an average sense (*constant strength approach*) keeping constant the yielding strength. The latter was adopted in this case, to simulate the effect of different sets of accelerograms on the same structure (same F_y value at a given oscillation period T), given the design spectrum. However, it should be emphasized that the two different approaches can lead to different conclusions as pointed out by some authors (e.g., Bazzurro and Luco, 2004).

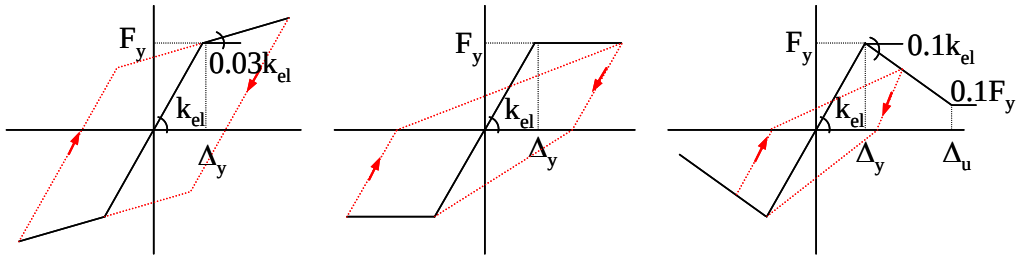

Figure 3.4. EPH (a), EPP (b), and ESD backbone curve (c).

3.6 Engineering demand parameters

EDPs chosen were selected to investigate both peak and cyclic seismic response. Displacement-based parameters is the ratio between displacement ductility and reduction factor (D_{kin}/R), the former evaluated as the ratio of the peak inelastic displacement ($Sd_{R=i}$) and yielding displacement, according to equation (3.4).

$$D_{kin} = \frac{Sd_{R=i}}{\Delta_y} \tag{3.4}$$

The cyclic response-related parameter is the equivalent number of cycles (N_e). This latter parameter is given by the cumulative hysteretic energy (E_H), evaluated as the sum of the areas of the hysteretic cycles (not considering contribution of viscous damping), normalized with respect to the largest cycle, evaluated as the area underneath the monotonic backbone curve from the yielding displacement to the peak inelastic displacement ($A_{plastic}$), equation (3.5). This allows separating ductility demand (already considered above in

D_{kin}) and cyclic demand (Manfredi, 2001).

$$N_e = \frac{E_H}{A_{plastic}} \tag{3.5}$$

3.7 Results and discussion

3.7.1. Elastic displacements and ratio to the target code spectrum

Elastic displacement spectra, evaluated as mean value on 28 records for each class, are compared to the target spectrum transformed from pseudo-acceleration, Figure 3.5a.

Figure 3.5b reports the ratio of the average spectrum of the class and the code spectrum, that is, the deviation of each class (Sd_{el}) with respect to the target spectrum ($Sd_{el\text{-}target}$), as it may help to understand the nonlinear results presented in the following. Although all classes are spectrum matching, real records spectra show the largest deviation with respect to the target, as it was anticipated. This is because real records match the target on average, while for the other three classes (adjusted and artificial records) each single records matches closely the target (see Figure 3.).

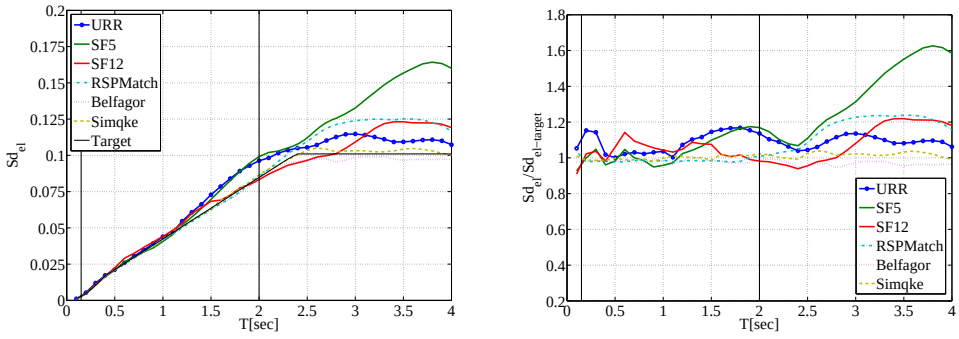

Figure 3.5. Average values of elastic displacement (a) and ratio to the target spectrum for the record classes (b).

From Figure 3.5b it is possible to recognize that all the average spectra of the six record classes selected are above 90%, and mostly below 20%, of the target in the 0s-4s range. This renders the classes suitable, according to

Eurocode 8 spectral matching provisions, for structures with a fundamental period up to 2s.

3.7.2. Ductility demand

Figure 3.6 shows ductility demand normalized with respect to the different R values investigated referring to the EPH system. For low R, normalized ductility seems to be similar for all six classes of records (Figure 3.6a and Figure 3.6b).

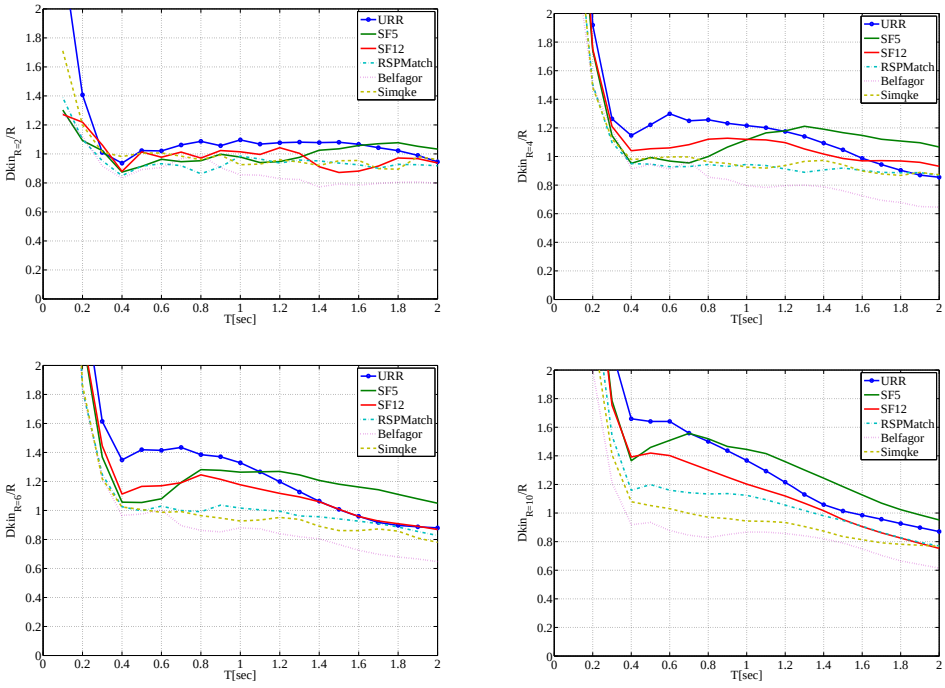

Figure 3.6. Average values of ductility demand for EPH system computed as mean value of 28 records.

The cases for high R values (Figure 3.6c and Figure 3.6d) emphasize an apparent underestimation of ductility for artificial records with respect to real records classes. In particular, results for R equal to 10 show different underestimation levels for adjusted and artificial classes of records: Belfagor class is followed by Simqke and RSPMatch. Ductility response indicates that

wavelet adjusting procedure gives a lower bias. On the other hand, it should be recalled that RSPMatch records are the same records as URR to which the adjustment procedure was applied. Linearly scaled records, indifferently if moderately or significantly, seem to show no trends with respect to URR. Although, the large scattering of real records with respect to the target, leads to large variability of the average estimated response from class-to-class of real records; e.g., Figure 3.6c and Figure 3.6d.

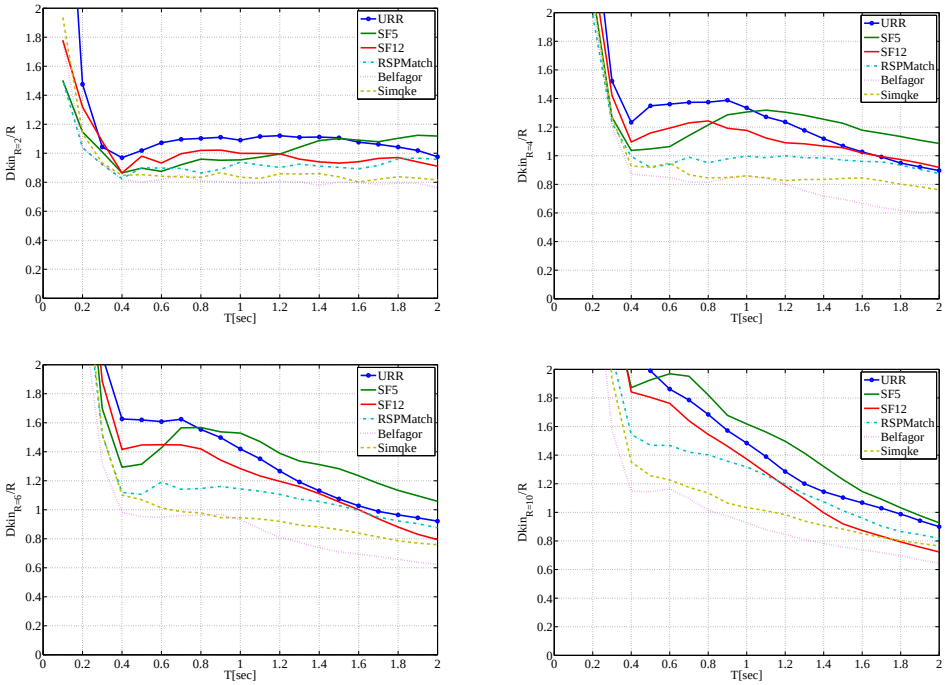

Figure 3.7. Average values of ductility demand for EPP system computed as mean value of 28 records.

Figure 3.7 shows normalized ductility results for EPP systems. The stiffness degrading behavior of these SDOFs tends to confirm conclusions found for EPH systems. However, when interpreting the results for these two backbones it should be recalled that URR class had a linear demand which was already generally above that of the artificial records. Moreover, hypothesis tests, (to follow), do not confirm these differences to be statistically significant.

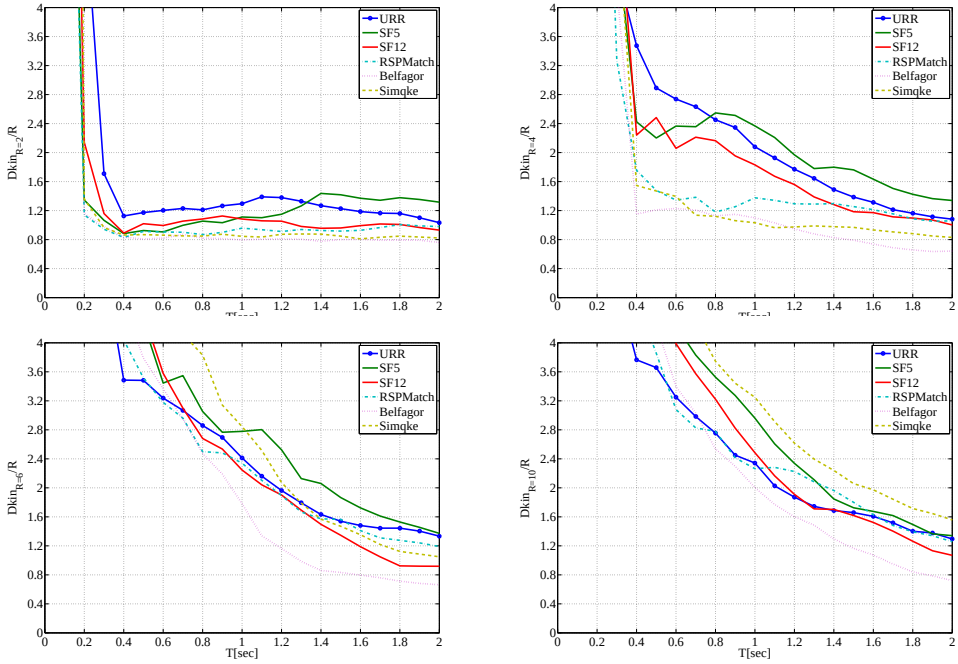

Figure 3.8. Average values of ductility demand for ESD system computed as mean value of 28 records.

Figure 3.8 shows normalized kinematic ductility demand for ESD systems; in this case the trends are less clear. For R factors up to 4 it is possible to recognize about the same trends found for EPH and EPP systems, see Figure 3.8a and Figure 3.8b, with some underestimation of nonlinear demand that is systematically about 100%, for artificial and adjusted records with respect to real records classes. For higher R values (6 and 10), see Figure 3.8c and Figure 3.8d, it is not possible to recognize the same trends; all classes except Simqke records, show similar ductility demands. This has an explanation related to modeling of the nonlinear systems; in fact, for R equal to 6 and 10 the ESD SDOFs exceed the *ductility limit* and start cycling on the residual strength branch of the backbone. This behavior which is systematic for all record classes has a smoothing effect on the differences among the classes of accelerograms. However, it seems to be confirmed also for ESD systems that SF5 and SF12

classes do not show any trend with respect to URR.

3.7.3. Equivalent number of cycles

N_e has the mentioned advantage of normalizing cyclic response with respect to peak demand, equation (3.5), allowing a comparison between the different classes of records in terms of cumulative demand only.

Figure 3.9 shows the values of this EDP for the EPH systems at different R values. For all the R investigated a strong overestimation in term of cyclic response may be observed for both classes of artificial records. Simqke records show the highest overestimation (e.g., twice than URR at low periods). Belfagor results shows that a generation procedure based on non-stationary characteristics of the earthquake gives more acceptable results in terms of cyclic response.

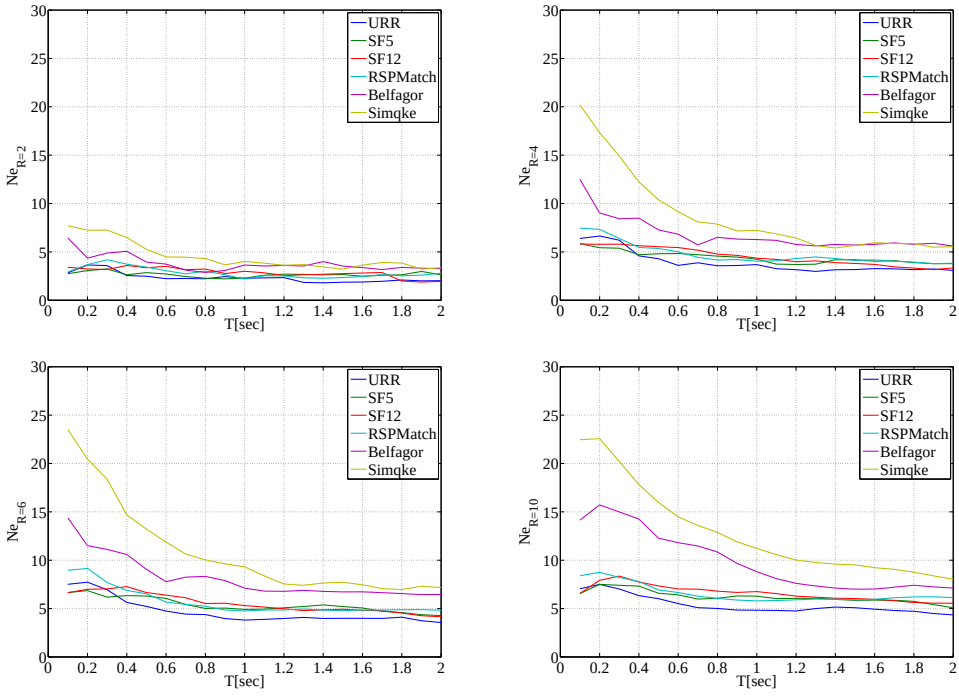

Figure 3.9. Average values of equivalent number of cycles for EPH system computed as mean value of 28 records.

Cyclic EDP results seem to be independent of strength reduction factor, at least for R values ranging from 4 to 10.The latter is an expected result, in fact, N_e represents the total hysteretic energy normalized with respect to energy of the maximum cycle.

SF5 and SF12 records have, again, a non systematic trend with respect to URR, confirming that scaling procedure does not introduce any bias even if the scaling factor is large. RSPMatch records give results very close to URR indicating that the wavelet adjustment does not influence the cyclic response.

Figure 3.10 shows the N_e results for the EPP systems. The same conclusions found for EPH systems hold. In this case the lower reduction factors (2,4) are characterized by the largest N_e, this effect is strictly related to a decrease in the total hysteretic energy with the strength reduction factor.

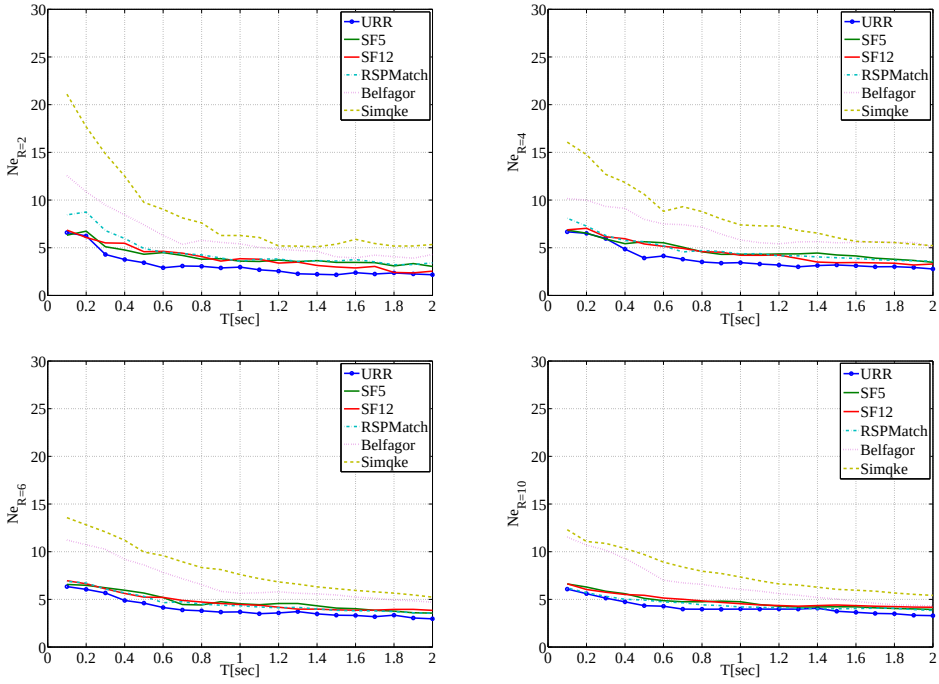

Figure 3.10. Average values of equivalent number of cycles for EPP system computed as mean value of 28 records.

Figure 3.11 shows N_e for ESD systems. Again, the same trends found for

EPH and EPP hold. Artificial records show cyclic response overestimation, while wavelet adjustment seems to introduce no bias with respect to URR. Moderately and significantly scaled real records also show no trends. Note that, for large strength reduction factors (6,10), N_e tends to be similar for all classes. This is because ESD systems, at high nonlinearity level, easily reach the residual strength branch of the backbone.

3.7.4. Prediction of cyclic response

Cyclic response overestimation of artificial records was a predictable result; in fact artificial records are characterized by higher values of integral parameters, especially I_D. Figure 3.12 shows, as an example, the I_D versus N_e plot of each record for EPH systems with R equal to 4, at two periods equal to 0.6s and 1.0s, Figure 3.12a and Figure 3.12b, respectively. Figure 3.13 shows I_D versus N_e plot for EPP system characterized by the same R at the same periods of Figure 3.12.

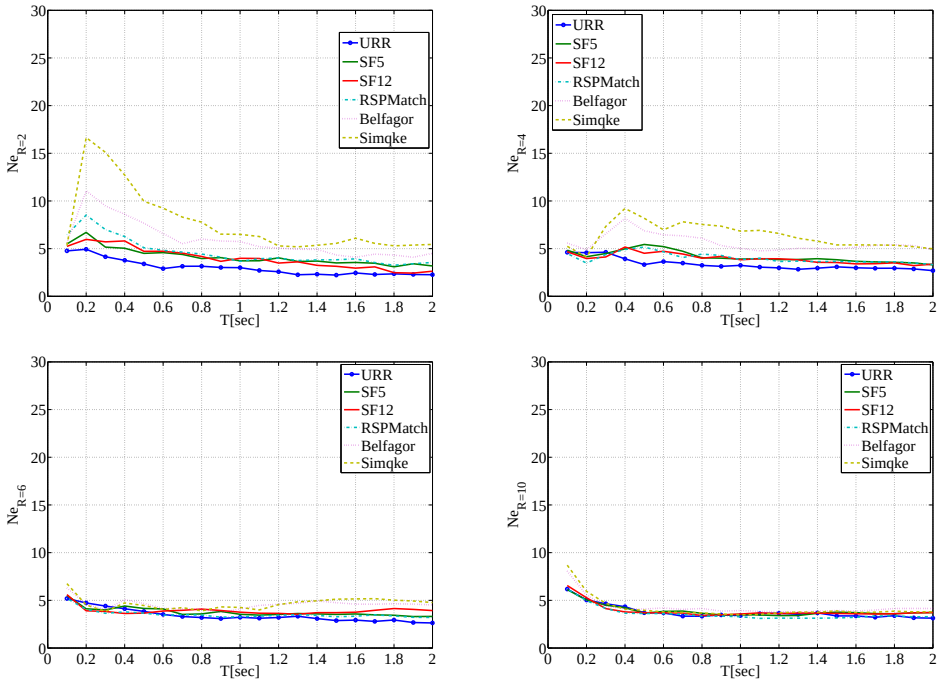

Figure 3.11. Average values of equivalent number of cycles for ESD system computed as mean value of 28 records.

Similarly to EPH systems, it is possible to note a fairly good correlation between the two parameters. Figure 3.14 refers to ESD systems; in this case the correlation is still good but become less recognizable for higher R values due to fact that at these nonlinearity levels the *ductility limit* of the degrading system does not emphasize differences between equivalent number of cycle's response of each class (i.e., Figure 3.11c and Figure 3.11d).

As a conclusion, considering I_D evaluated in section 3.4 for all records classes, and their compliance with the conditional hazard analysis, the latter can be suggested as an additional criterion in selection or generation procedures for accelerograms when the cyclic response represents a critical performance parameter for the structure to be analyzed.

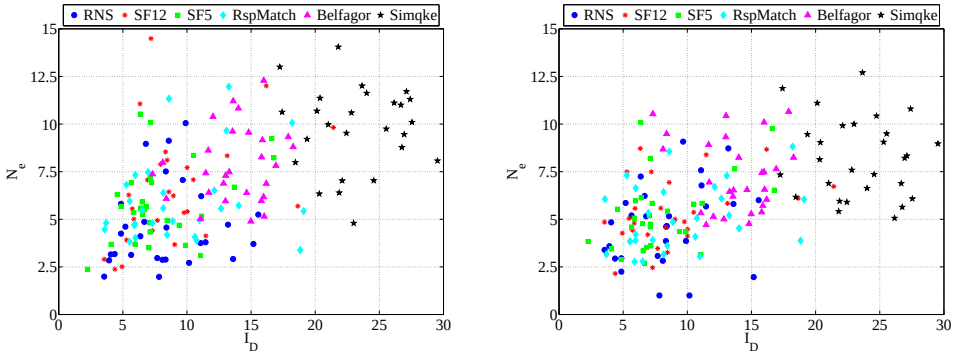

Figure 3.12. N_e versus I_D for R = 4 and T = 0.6s (a) and T = 1.0s (b) evaluated for system EPH for each record of each class.

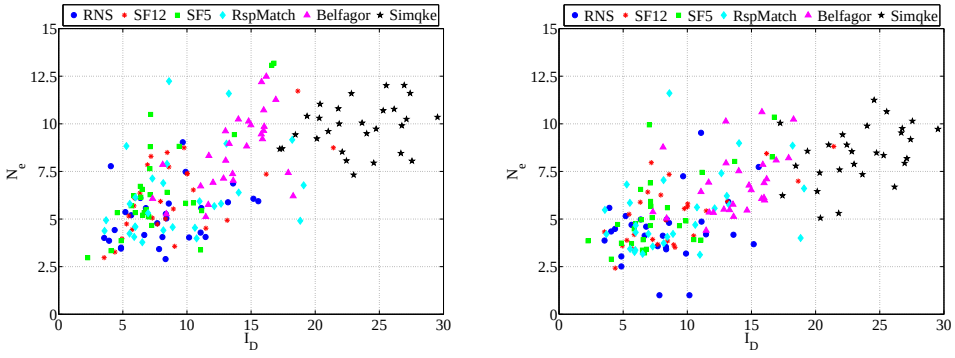

Figure 3.13. N_e versus I_D for R = 4 and T = 0.6s (a) and T = 1.0s (b) evaluated for system EPP for each record of each class.

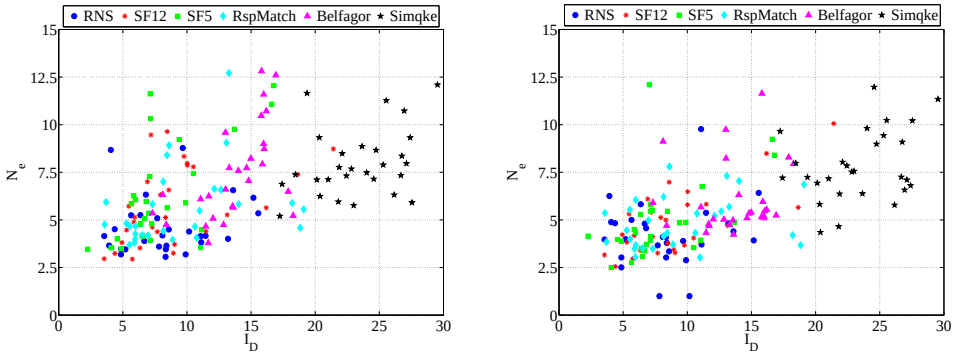

Figure 3.14. N_e versus I_D for R = 4 and T = 0.6s (a) and T = 1.0s (b) evaluated for system ESD for each record of each class.

3.8 Hypothesis tests

To finally draw conclusions from the results above, it may be helpful trying to quantitatively assess their significance. In particular, parametric hypothesis tests (Benjamin and Cornell, 1970) were performed to assess to what significance the median values of the response, from a given class of records, may be considered equal to that from URR for each oscillation period in the considered range. Hypothesis tests were performed for both peak and cyclic EDPs. Regarding peak response inelastic displacement $Sd_{R=i}$ (i=1,2,4,6,10) was chosen as the variable to test and it was considered to have lognormal distribution. What found for the inelastic displacement is valid also for D_{kin}, see equation (3.4), considering the *constant strength approach* adopted. Regarding cyclic response, N_e+1 was chosen as the variable to test, again, with lognormal distribution[5].

The null hypothesis to check was whether median EDPs for any class of records was equal (null hypothesis) or not (alternate hypothesis) to that from URR. To this aim a two-tails Aspin-Welch test (Welch, 1938) was preferred with respect to the standard *T-Student* test, as the former does not require the assumption of equal, yet still unknown, variances of populations originating

[5] Distribution assumptions were checked with the Lilliefors test (Lilliefors, 1967), and could not be rejected at 95% significance level.

the samples, which would be an unreasonable assumption given the natures of the compared record classes.

The test statistic employed is reported in equation (3.6) in which z_x and z_y are the sample means, s_x and s_y are the sample standard deviations and n and m are the samples sizes (in this case always equal to 28). The test statistic, under the null hypothesis, has an approximate Student-T distribution with a number of degrees of freedom given by Satterthwaite's approximation (Satterthwaite, 1941).

$$t = \frac{z_x - z_y}{\sqrt{\frac{s_x^2}{n} + \frac{s_y^2}{m}}} \tag{3.6}$$

Because URR were assumed as a benchmark, a preliminary test was performed to check if it was possible to reject the null hypothesis in terms of elastic displacement first. Table 3-2 presents *p-values* divided per period, bold are the rejection cases assuming a 95% significance level; i.e., choosing I-type risk (α) equal to 0.05. Periods values reported in the hypothesis tests tables are step by 0.2s for the sake of brevity.

Table 3-2. Aspin – Welch test results for elastic displacements, *p-values* lower than 0.05 are reported in bold.

Period (s)		*0.2*	*0.4*	*0.6*	*0.8*	*1*	*1.2*	*1.4*	*1.6*	*1.8*	*2*
Compared		*R = 1*									
URR	*SF12*	0.882	0.328	0.178	0.308	0.382	0.379	0.467	0.676	0.647	0.699
URR	*SF5*	0.997	0.390	0.243	0.682	0.666	0.462	0.361	0.323	0.282	0.281
URR	*RSPM*	0.895	0.172	0.271	0.312	0.278	0.249	0.229	0.273	0.295	0.194
URR	*Belf*	0.878	0.183	0.230	0.362	0.308	0.258	0.215	0.281	0.323	0.229
URR	*Simq*	0.826	0.162	0.237	0.284	0.246	0.189	0.192	0.195	0.220	0.172

In Table 3-3 to Table 3-14 the test results for different R values (2,4,6,10) and for EPH, EPP and ESD SDOF models are shown. Results for EPH system show that there are no rejections with respect to URR records at any reduction

factor. Results for EPP system are qualitatively similar to EPH with no rejections. In the case of ESD system it is recognizable a number of rejections in comparing real and artificial accelerograms. It is worth to note that, in this case, the results relative to high R values (6,10) are affected by the fact that ductility demand exceeds the *ductility limit* and rejections associated to Simqke records indicate displacements significantly higher than those of real record, see Figure 3.8c and Figure 3.8d.

Table 3-3. Aspin – Welch test results for inelastic displacements of EPH system, R=2, *p-values* lower than 0.05 are reported in bold.

Period (s)		*0.2*	*0.4*	*0.6*	*0.8*	*1*	*1.2*	*1.4*	*1.6*	*1.8*	*2*
Compared		*R = 2*									
URR	*SF12*	0.903	0.505	0.533	0.822	0.618	0.430	0.728	0.800	0.392	0.352
URR	*SF5*	0.777	0.528	0.564	0.932	0.690	0.652	0.360	0.276	0.248	0.220
URR	*RSPM*	0.914	0.521	0.534	0.737	0.381	0.362	0.250	0.270	0.183	0.119
URR	*Belf*	0.990	0.603	0.673	0.540	0.841	0.918	0.997	0.793	0.566	0.389
URR	*Simq*	0.623	0.089	0.227	0.638	0.643	0.309	0.320	0.211	0.230	0.057

Table 3-4. Aspin – Welch test results for inelastic displacements of EPH system, R=4, *p-values* lower than 0.05 are reported in bold.

Period (s)		*0.2*	*0.4*	*0.6*	*0.8*	*1*	*1.2*	*1.4*	*1.6*	*1.8*	*2*
Compared		*R = 4*									
URR	*SF12*	0.389	0.498	0.920	0.578	0.421	0.389	0.398	0.355	0.269	0.292
URR	*SF5*	0.279	0.830	0.512	0.966	0.530	0.362	0.255	0.162	0.134	0.166
URR	*RSPM*	0.813	0.723	0.495	0.946	0.590	0.599	0.387	0.218	0.140	0.124
URR	*Belf*	0.761	0.884	0.420	0.466	0.617	0.782	0.980	0.956	0.995	0.991
URR	*Simq*	0.803	0.530	0.826	0.932	0.715	0.496	0.170	0.165	0.113	0.069

Table 3-5. Aspin – Welch test results for inelastic displacements of EPH system, R=6, *p-values* lower than 0.05 are reported in bold.

Period (s)		*0.2*	*0.4*	*0.6*	*0.8*	*1*	*1.2*	*1.4*	*1.6*	*1.8*	*2*
Compared		*R = 6*									
URR	*SF12*	0.358	0.736	0.768	0.435	0.612	0.459	0.354	0.423	0.426	0.516
URR	*SF5*	0.366	0.956	0.853	0.469	0.661	0.446	0.288	0.177	0.158	0.228
URR	*RSPM*	0.891	0.927	0.960	0.969	0.730	0.426	0.244	0.179	0.190	0.319
URR	*Belf*	0.830	0.793	0.867	0.378	0.559	0.830	0.908	0.945	0.998	0.849
URR	*Simq*	0.745	0.846	0.797	0.909	0.787	0.487	0.323	0.206	0.137	0.318

Table 3-6. Aspin – Welch test results for inelastic displacements of EPH system, R=10, *p-values* lower than 0.05 are reported in bold.

Period (s)		*0.2*	*0.4*	*0.6*	*0.8*	*1*	*1.2*	*1.4*	*1.6*	*1.8*	*2*
Compared		*R = 10*									
URR	*SF12*	0.460	0.562	0.517	0.587	0.656	0.607	0.479	0.600	0.679	0.880
URR	*SF5*	0.545	0.825	0.578	0.477	0.534	0.436	0.260	0.295	0.365	0.325
URR	*RSPM*	0.764	0.923	0.977	0.787	0.520	0.478	0.266	0.316	0.461	0.554
URR	*Belf*	0.290	0.155	0.142	0.148	0.503	0.821	0.690	0.792	0.894	0.781
URR	*Simq*	0.788	0.657	0.601	0.581	0.872	0.754	0.410	0.417	0.399	0.327

Table 3-7. Aspin – Welch test results for inelastic displacements of EPP system, R=2, *p-values* lower than 0.05 are reported in bold.

Period (s)		*0.2*	*0.4*	*0.6*	*0.8*	*1*	*1.2*	*1.4*	*1.6*	*1.8*	*2*
Compared		*R = 2*									
URR	*SF12*	0.620	0.690	0.826	0.630	0.610	0.585	0.730	0.669	0.475	0.528
URR	*SF5*	0.878	0.710	0.824	0.928	0.749	0.712	0.350	0.289	0.270	0.230
URR	*RSPM*	0.541	0.770	0.835	0.822	0.483	0.590	0.429	0.365	0.164	0.131
URR	*Belf*	0.543	0.815	0.645	0.475	0.638	0.890	0.973	0.757	0.664	0.644
URR	*Simq*	0.976	0.633	0.789	0.625	0.896	0.787	0.608	0.738	0.457	0.388

Table 3-8. Aspin – Welch test results for inelastic displacements of EPP system, R=4, *p-values* lower than 0.05 are reported in bold.

Period (s)		*0.2*	*0.4*	*0.6*	*0.8*	*1*	*1.2*	*1.4*	*1.6*	*1.8*	*2*
Compared		*R = 4*									
URR	*SF12*	0.366	0.394	0.613	0.516	0.507	0.520	0.321	0.329	0.395	0.445
URR	*SF5*	0.490	0.680	0.805	0.741	0.494	0.407	0.260	0.204	0.193	0.212
URR	*RSPM*	0.591	0.626	0.699	0.816	0.677	0.433	0.238	0.185	0.152	0.193
URR	*Belf*	0.424	0.768	0.314	0.247	0.718	0.773	0.741	0.730	0.543	0.605
URR	*Simq*	0.350	0.911	0.783	0.365	0.735	0.895	0.612	0.324	0.360	0.404
URR	*Simq*	0.503	0.967	0.898	0.951	0.908	0.589	0.498	0.549	0.542	0.452

Table 3-9. Aspin – Welch test results for inelastic displacements of EPP system, R=6, *p-values* lower than 0.05 are reported in bold.

Period (s)		*0.2*	*0.4*	*0.6*	*0.8*	*1*	*1.2*	*1.4*	*1.6*	*1.8*	*2*
Compared		*R = 6*									
URR	*SF12*	0.273	0.328	0.422	0.428	0.523	0.444	0.385	0.499	0.713	0.849
URR	*SF5*	0.574	0.831	0.633	0.396	0.436	0.362	0.237	0.202	0.256	0.298
URR	*RSPM*	0.669	0.919	0.642	0.683	0.485	0.287	0.207	0.178	0.222	0.239
URR	*Belf*	0.878	0.559	0.432	0.592	0.804	0.649	0.774	0.791	0.713	0.671
URR	*Simq*	0.465	0.966	0.693	0.667	0.846	0.766	0.499	0.453	0.528	0.487

Table 3-10. Aspin – Welch test results for inelastic displacements of EPP system, R=10, *p-values* lower than 0.05 are reported in bold.

Period (s)		*0.2*	*0.4*	*0.6*	*0.8*	*1.0*	*1.2*	*1.4*	*1.6*	*1.8*	*2.0*
Compared		*R = 10*									
URR	*SF12*	0.195	0.313	0.346	0.488	0.504	0.487	0.616	0.868	0.977	0.975
URR	*SF5*	0.494	0.508	0.314	0.372	0.377	0.253	0.254	0.402	0.465	0.468
URR	*RSPM*	0.489	0.508	0.494	0.420	0.291	0.218	0.214	0.364	0.487	0.404
URR	*Belf*	0.487	0.415	0.720	0.533	0.637	0.795	0.957	0.944	0.948	0.941
URR	*Simq*	0.503	0.967	0.898	0.951	0.908	0.589	0.498	0.549	0.542	0.452

Table 3-11. Aspin – Welch test results for inelastic displacements of ESD system, R=2, *p-values* lower than 0.05 are reported in bold.

Period (s)		*0.2*	*0.4*	*0.6*	*0.8*	*1.0*	*1.2*	*1.4*	*1.6*	*1.8*	*2.0*
Compared		*R = 2*									
URR	*SF12*	0.491	0.981	0.914	0.654	0.761	0.747	0.864	0.709	0.545	0.552
URR	*SF5*	0.163	0.976	0.692	0.909	0.795	0.839	0.326	0.292	0.278	0.228
URR	*RSPM*	0.072	0.849	0.874	0.672	0.725	0.868	0.571	0.426	0.210	0.156
URR	*Belf*	0.080	0.882	0.434	0.416	0.438	0.648	0.772	0.879	0.845	0.738
URR	*Simq*	0.208	0.955	0.629	0.559	0.670	0.975	0.744	0.853	0.579	0.432

Table 3-12. Aspin – Welch test results for inelastic displacements of ESD system, R=4, *p-values* lower than 0.05 are reported in bold.

Period (s)		*0.2*	*0.4*	*0.6*	*0.8*	*1.0*	*1.2*	*1.4*	*1.6*	*1.8*	*2.0*
Compared		*R = 4*									
URR	*SF12*	**0.013**	0.796	0.883	0.460	0.457	0.475	0.454	0.420	0.496	0.600
URR	*SF5*	**0.046**	0.881	0.835	0.483	0.365	0.306	0.210	0.177	0.209	0.242
URR	*RSPM*	**0.010**	0.787	0.467	0.553	0.725	0.462	0.233	0.214	0.226	0.200
URR	*Belf*	**0.003**	0.212	0.364	0.443	0.845	0.743	0.786	0.714	0.481	0.513
URR	*Simq*	**0.000**	0.729	0.818	0.460	0.660	0.850	0.585	0.429	0.426	0.469

Table 3-13. Aspin – Welch test results for inelastic displacements of ESD system, R=6, *p-values* lower than 0.05 are reported in bold.

Period (s)		*0.2*	*0.4*	*0.6*	*0.8*	*1.0*	*1.2*	*1.4*	*1.6*	*1.8*	*2.0*
Compared		*R = 6*									
URR	*SF12*	**0.001**	**0.011**	0.112	0.474	0.520	0.444	0.590	0.909	0.529	0.661
URR	*SF5*	**0.004**	0.103	0.282	0.275	0.311	0.224	0.203	0.274	0.488	0.510
URR	*RSPM*	**0.027**	**0.036**	0.140	0.319	0.207	0.260	0.231	0.269	0.490	0.469
URR	*Belf*	**0.001**	**0.011**	**0.030**	0.210	0.556	0.750	0.502	0.535	0.271	0.270
URR	*Simq*	**0.000**	**0.000**	**0.000**	**0.002**	**0.017**	0.055	0.168	0.314	0.615	0.598

Table 3-14. Aspin – Welch test results for inelastic displacements of ESD system, R=10, *p-values* lower than 0.05 are reported in bold.

Period (s)		*0.2*	*0.4*	*0.6*	*0.8*	*1.0*	*1.2*	*1.4*	*1.6*	*1.8*	*2.0*
Compared		*R = 10*									
URR	*SF12*	**0.047**	**0.007**	0.114	0.114	0.253	0.275	0.366	0.564	0.650	0.930
URR	*SF5*	**0.012**	0.062	0.207	0.281	0.187	0.147	0.365	0.524	0.461	0.576
URR	*RSPM*	0.135	**0.015**	0.335	0.188	0.158	**0.046**	0.100	0.280	0.344	0.374
URR	*Belf*	**0.011**	**0.002**	0.079	0.278	0.337	0.258	0.621	0.948	0.612	0.439
URR	*Simq*	**0.005**	**0.000**	**0.002**	**0.004**	**0.002**	**0.003**	**0.008**	**0.027**	**0.038**	**0.042**

Table 3-15. Aspin – Welch test results for equivalent number of cycles of EPH system, R=2 *p-values* lower than 0.05 are reported in bold.

Period (s)		*0.2*	*0.4*	*0.6*	*0.8*	*1*	*1.2*	*1.4*	*1.6*	*1.8*	*2*
Compared		*R = 2*									
URR	*SF12*	0.812	**0.028**	**0.037**	**0.012**	0.101	0.224	**0.044**	**0.046**	0.587	0.658
URR	*SF5*	0.992	0.166	0.114	0.439	0.365	0.128	**0.043**	0.170	0.243	0.142
URR	*RSPM*	0.427	**0.003**	**0.033**	**0.018**	0.389	0.161	**0.036**	**0.026**	0.051	**0.015**
URR	*Belf*	**0.040**	**0.000**	**0.001**	**0.024**	**0.001**	**0.002**	**0.000**	**0.000**	**0.001**	**0.001**
URR	*Simq*	**0.000**	**0.000**	**0.000**	**0.000**	**0.000**	**0.002**	**0.000**	**0.000**	**0.000**	**0.001**

Table 3-16. Aspin – Welch test results for equivalent number of cycles of EPH system, R=4 *p-values* lower than 0.05 are reported in bold.

Period (s)		*0.2*	*0.4*	*0.6*	*0.8*	*1*	*1.2*	*1.4*	*1.6*	*1.8*	*2*
Compared		*R = 4*									
URR	*SF12*	0.597	0.071	**0.010**	**0.021**	0.116	0.074	0.177	0.307	0.593	0.402
URR	*SF5*	0.339	0.303	**0.024**	**0.036**	0.167	0.199	**0.045**	0.131	0.157	0.146
URR	*RSPM*	0.526	0.078	**0.010**	0.173	0.298	**0.043**	**0.020**	**0.028**	**0.044**	**0.047**
URR	*Belf*	**0.004**	**0.000**	**0.000**	**0.000**	**0.000**	**0.000**	**0.000**	**0.000**	**0.000**	**0.000**
URR	*Simq*	**0.000**	**0.000**	**0.000**	**0.000**	**0.000**	**0.000**	**0.000**	**0.000**	**0.000**	**0.000**

Table 3-17. Aspin – Welch test results for equivalent number of cycles of EPH system, R=6 *p-values* lower than 0.05 are reported in bold.

Period (s)		*0.2*	*0.4*	*0.6*	*0.8*	*1*	*1.2*	*1.4*	*1.6*	*1.8*	*2*
Compared		*R = 6*									
URR	*SF12*	0.781	**0.033**	*0.019*	**0.044**	**0.019**	0.139	0.158	0.193	0.459	0.195
URR	*SF5*	0.641	0.212	0.060	0.207	**0.023**	0.091	**0.045**	0.069	0.250	0.129
URR	*RSPM*	0.294	0.133	0.092	0.156	0.085	0.087	**0.046**	0.056	0.105	**0.020**
URR	*Belf*	**0.000**	**0.000**	**0.000**	**0.000**	**0.000**	**0.000**	**0.000**	**0.000**	**0.001**	**0.000**
URR	*Simq*	**0.000**	**0.000**	**0.000**	**0.000**	**0.000**	**0.000**	**0.000**	**0.000**	**0.000**	**0.000**

Table 3-18. Aspin – Welch test results for equivalent number of cycles of EPH system, R=10 *p-values* lower than 0.05 are reported in bold.

Period (s)		*0.2*	*0.4*	*0.6*	*0.8*	*1*	*1.2*	*1.4*	*1.6*	*1.8*	*2*
Compared		*R = 10*									
URR	*SF12*	0.408	**0.049**	0.059	**0.022**	**0.026**	0.070	0.180	0.148	0.202	0.081
URR	*SF5*	0.891	0.252	0.231	0.140	0.072	0.083	0.221	0.153	0.162	0.192
URR	*RSPM*	0.314	0.129	0.092	0.071	0.098	**0.033**	0.111	0.061	**0.029**	**0.013**
URR	*Belf*	**0.000**	**0.000**	**0.000**	**0.000**	**0.000**	**0.000**	**0.001**	**0.001**	**0.000**	**0.000**
URR	*Simq*	**0.000**	**0.000**	**0.000**	**0.000**	**0.000**	**0.000**	**0.000**	**0.000**	**0.000**	**0.000**

Table 3-19. Aspin – Welch test results for equivalent number of cycles of EPP system, R=2, *p-values* lower than 0.05 are reported in bold.

Period (s)		*0.2*	*0.4*	*0.6*	*0.8*	*1*	*1.2*	*1.4*	*1.6*	*1.8*	*2*
Compared		*R = 2*									
URR	*SF12*	0.571	**0.004**	**0.011**	**0.032**	0.092	0.051	0.054	0.180	0.394	0.322
URR	*SF5*	0.221	**0.025**	**0.009**	0.121	0.077	**0.013**	**0.010**	0.107	0.193	0.093
URR	*RSPM*	**0.047**	**0.002**	**0.003**	**0.020**	0.069	**0.007**	**0.001**	**0.002**	**0.008**	**0.001**
URR	*Belf*	**0.000**	**0.000**	**0.000**	**0.000**	**0.000**	**0.000**	**0.000**	**0.000**	**0.000**	**0.000**
URR	*Simq*	**0.000**	**0.000**	**0.000**	**0.000**	**0.000**	**0.000**	**0.000**	**0.000**	**0.000**	**0.000**

Table 3-20. Aspin – Welch test results for equivalent number of cycles of EPP system, R=4, *p-values* lower than 0.05 are reported in bold.

Period (s)		*0.2*	*0.4*	*0.6*	*0.8*	*1*	*1.2*	*1.4*	*1.6*	*1.8*	*2*
Compared		*R = 4*									
URR	*SF12*	0.396	0.060	**0.047**	**0.028**	0.065	0.051	0.250	0.292	0.500	0.196
URR	*SF5*	0.787	0.195	**0.020**	**0.030**	**0.061**	0.068	**0.018**	0.084	0.160	0.129
URR	*RSPM*	0.463	0.284	**0.038**	**0.021**	0.059	**0.034**	**0.023**	**0.027**	**0.048**	**0.020**
URR	*Belf*	**0.000**	**0.000**	**0.000**	**0.000**	**0.000**	**0.000**	**0.000**	**0.000**	**0.000**	**0.000**
URR	*Simq*	**0.000**	**0.000**	**0.000**	**0.000**	**0.000**	**0.000**	**0.000**	**0.000**	**0.000**	**0.000**

Table 3-21. Aspin – Welch test results for equivalent number of cycles of EPP system, R=6, *p-values* lower than 0.05 are reported in bold.

Period (s)		*0.2*	*0.4*	*0.6*	*0.8*	*1*	*1.2*	*1.4*	*1.6*	*1.8*	*2*
Compared		*R = 6*									
URR	*SF12*	0.345	0.149	0.061	0.126	0.200	0.236	0.254	0.169	0.116	**0.031**
URR	*SF5*	0.413	0.092	0.070	0.194	0.105	0.091	0.109	0.142	0.278	0.114
URR	*RSPM*	0.482	0.137	0.221	0.082	0.101	0.127	0.114	0.125	0.201	0.075
URR	*Belf*	**0.000**	**0.000**	**0.000**	**0.000**	**0.000**	**0.000**	**0.000**	**0.000**	**0.000**	**0.000**
URR	*Simq*	**0.000**	**0.000**	**0.000**	**0.000**	**0.000**	**0.000**	**0.000**	**0.000**	**0.000**	**0.000**

Table 3-22. Aspin – Welch test results for equivalent number of cycles of EPP system, R=10, *p-values* lower than 0.05 are reported in bold.

Period (s)		*0.2*	*0.4*	*0.6*	*0.8*	*1*	*1.2*	*1.4*	*1.6*	*1.8*	*2*
Compared		*R = 10*									
URR	*SF12*	0.463	0.131	0.230	0.144	0.282	0.359	0.347	0.059	0.047	0.027
URR	*SF5*	0.320	0.165	0.369	0.231	0.259	0.537	0.744	0.240	0.213	0.125
URR	*RSPM*	0.731	0.514	0.176	0.143	0.382	0.494	0.770	0.210	0.124	0.120
URR	*Belf*	**0.000**	**0.000**	**0.000**	**0.000**	**0.000**	**0.000**	**0.004**	**0.002**	**0.006**	**0.006**
URR	*Simq*	**0.000**	**0.000**	**0.000**	**0.000**	**0.000**	**0.000**	**0.000**	**0.000**	**0.000**	**0.000**

Table 3-23. Aspin – Welch test results for equivalent number of cycles of ESD system, R=2, *p-values* lower than 0.05 are reported in bold.

Period (s)		*0.2*	*0.4*	*0.6*	*0.8*	*1.0*	*1.2*	*1.4*	*1.6*	*1.8*	*2.0*
Compared		*R = 2*									
URR	*SF12*	0.116	**0.002**	**0.009**	**0.034**	0.076	**0.046**	0.051	0.189	0.347	0.337
URR	*SF5*	**0.022**	**0.013**	**0.007**	0.105	0.058	**0.007**	**0.015**	0.125	0.219	0.105
URR	*RSPM*	**0.002**	**0.001**	**0.001**	**0.015**	**0.047**	**0.004**	**0.001**	**0.002**	**0.006**	**0.002**
URR	*Belf*	**0.000**	**0.000**	**0.000**	**0.000**	**0.000**	**0.000**	**0.000**	**0.000**	**0.000**	**0.000**
URR	*Simq*	**0.000**	**0.000**	**0.000**	**0.000**	**0.000**	**0.000**	**0.000**	**0.000**	**0.000**	**0.000**

Table 3-24. Aspin – Welch test results for equivalent number of cycles of ESD system, R=4, *p-values* lower than 0.05 are reported in bold.

Period (s)		*0.2*	*0.4*	*0.6*	*0.8*	*1.0*	*1.2*	*1.4*	*1.6*	*1.8*	*2.0*
Compared		*R = 4*									
URR	*SF12*	0.094	**0.028**	**0.035**	0.084	0.131	0.063	0.135	0.227	0.350	0.108
URR	*SF5*	0.263	**0.036**	**0.007**	0.084	0.141	0.124	**0.033**	0.154	0.195	0.140
URR	*RSPM*	**0.002**	0.108	**0.018**	**0.007**	0.076	0.056	**0.037**	**0.043**	**0.048**	**0.041**
URR	*Belf*	0.464	**0.000**	**0.000**	**0.000**	**0.000**	**0.000**	**0.000**	**0.000**	**0.000**	**0.000**
URR	*Simq*	0.312	**0.000**	**0.000**	**0.000**	**0.000**	**0.000**	**0.000**	**0.000**	**0.000**	**0.000**

Table 3-25. Aspin – Welch test results for equivalent number of cycles of ESD system, R=6, *p-values* lower than 0.05 are reported in bold.

Period (s)		*0.2*	*0.4*	*0.6*	*0.8*	*1.0*	*1.2*	*1.4*	*1.6*	*1.8*	*2.0*
Compared		*R = 6*									
URR	*SF12*	**0.020**	0.167	0.408	0.065	0.168	0.218	0.095	**0.028**	**0.003**	**0.003**
URR	*SF5*	0.105	0.770	0.345	0.422	0.418	0.389	0.209	0.127	0.151	0.053
URR	*RSPM*	0.067	0.267	0.592	0.417	0.905	0.382	0.235	0.183	0.182	0.065
URR	*Belf*	0.989	0.181	0.063	**0.009**	**0.007**	**0.000**	**0.000**	**0.000**	**0.000**	**0.000**
URR	*Simq*	0.829	0.368	0.103	**0.036**	**0.015**	**0.004**	**0.001**	**0.000**	**0.000**	**0.000**

Table 3-26. Aspin – Welch test results for equivalent number of cycles of ESD system, R=10, *p-values* lower than 0.05 are reported in bold.

Period (s)		*0.2*	*0.4*	*0.6*	*0.8*	*1.0*	*1.2*	*1.4*	*1.6*	*1.8*	*2.0*
Compared		*R = 10*									
URR	*SF12*	0.417	0.079	0.707	0.530	0.390	0.675	0.630	0.272	0.325	0.070
URR	*SF5*	0.947	0.652	0.735	0.439	0.769	0.782	0.896	0.306	0.394	0.133
URR	*RSPM*	0.964	**0.023**	0.829	0.736	0.963	0.394	0.345	0.910	0.736	0.362
URR	*Belf*	0.085	0.662	**0.033**	**0.007**	0.073	0.330	0.329	0.062	**0.024**	**0.005**
URR	*Simq*	**0.003**	0.508	0.337	0.088	0.382	0.497	0.457	0.153	0.118	**0.042**

In Table 3-15 to Table 3-26 the test results for different R values on equivalent number of cycles respectively for EPH, EPP and ESD systems are shown. As it was expected, considering the results in section 3.7.3, there are a large number of rejections for this EDP for all kinds of SDOF models, especially for Belfagor and Simqke accelerograms. RSPMatch records do not lead to a significant number of rejections.

For ESD models (Table 3-23 to Table 3-26) rejections at all periods indicate always an overestimation of artificial records. The number of rejections tends to reduce at high nonlinearity levels. In fact, in the previous section it was observed that, when ductility demand exceeds the *ductility limit*, the equivalent number of cycles tends to be similar for all six classes. Scaled real records present only a few rejections with respect to URR records.

3.9 Conclusions

Different ways to achieve spectrum matching record sets were compared in terms of post-elastic seismic peak and cyclic responses. This was pursued considering SDOFs with three different force-displacement backbones and hysteretic rules at different nonlinearity levels. The ductility and equivalent number of cycles response of 240 systems were analyzed with respect to six classes of records: real unscaled, real with moderate linear scaling factor, real with significant linear scaling factor, real adjusted with wavelets, and two different types of artificial records.

The *life-safety* design elastic spectrum, for a case study site in southern

Italy, was considered; all the classes of records match it on average or by means of individual records.

Results indicate that the linearly scaled records do not show any-systematic trend with respect to the unscaled records' results independently of the backbone and response parameters, suggesting that scaling is a legitimate technique, as many studies point out, if the spectral shape is controlled.

RSPMatch2005 wavelet-adjustment procedure shows small, if any, bias in terms of peak and cyclic responses. Conversely, both classes of artificial records, but especially non-stationary accelerograms, in some cases seem to underestimate peak demand (ductility). Artificial records, especially those stationary, gave strong cyclic response overestimation (at least until ductility demand let the hysteresis to reach the residual strength of the backbone, although this is more a modeling issue).

Hypothesis tests were carried out with the aim of assessing quantitatively how much these results are significant. Tests have shown a statistical significance of the bias of artificial records only in terms of cyclic response. Regarding peak response, test results suggest that underestimation of artificial records with respect to unscaled real records does not have statistical significance. In fact, it is significant only in the case of the degrading systems (ESD) at high nonlinearity levels, when modeling hypotheses have a strong influence.

It is to note that, as it is well known, the cyclic response overestimation could have been predicted by some integral parameters of ground motion, which, if appropriate hazard analysis tool is available, could be used as an additional criterion for record selection especially in those cases when cyclic behavior has an important role in determining the seismic performances.

REFERENCES

Abrahamson N.A., 1992. Non-stationary spectral matching. *Seismological research letters*. 63(1), 30.

Baker J.W., Cornell C.A., 2006. Spectral shape, epsilon and record selection. *Earthquake Engineering and Structural Dynamics*, 35(9), 1077–1095.

Bazzurro P., Luco N., 2004. *Post-elastic response of structures to synthetic ground motions*. Report for Pacific Earthquake Engineering Research (PEER) Center Lifelines Program Project 1G00 Addenda. CA, US.

Benjamin J., Cornell A., 1970. *Probability, statistics and decision for civil engineers*, Mc Graw-Hill, NY, USA.

Bommer J.J, Acevedo A.B., 2004. *The use of real earthquake accelerograms as input to dynamic analysis*. Journal of Earthquake Engineering. 8(Special Issue I), 43-91.

Clough R.W., Johnston S.B., 1966 Effect of stiffness degradation on earthquake ductility requirements. Proceedings of *Japan Earthquake Engineering Symposium*, Tokyo, Japan.

Comité Européen de Normalisation, 2004. *Eurocode8, Design of Structures for earthquake resistance – Part1: General rules, seismic actions and rules for buildings*. EN 1998-1, CEN, Brussels.

Convertito V., Iervolino I., Herrero A., 2009. The importance of mapping the design earthquake: insights for southern Italy. *Bulletin of the Seismological Society of America*, 99(5), 2979–2991.

Cosenza E., Manfredi G., Ramasco R., 1993. The Use of Damage Functionals in Earthquake-Resistant Design: a Comparison Among Different Procedures. Earthquake Engineering and Structural Dynamics, 22(10), 855-868.

Decreto Ministeriale del 14/1/2008, 2008. Approvazione delle nuove norme tecniche per le costruzioni. G.U. n. 29 del 4/2/2008 (in Italian).

Esposito M., 2009. Accelerogrammi spettrocompatibili per la progettazione delle strutture: valutazione comparativa della risposta sismica. Dipartimento di Ingegneria Strutturale, Università degli Studi di Napoli Federico II. Graduation Thesis. Advisors: E. Cosenza, I. Iervolino, F. De Luca. Available at http://wpage.unina.it/iuniervo/ (in Italian)

Gasparini D.A., Vanmarke E.H., 1976. *Simulated earthquake motions compatible with prescribed response* spectra. MIT civil engineering research report R76-4. Massachusetts Institute of Technology, Cambridge, MA.

Grant D.N., Greening P.D., Taylor M.L. and Ghosh B, 2008. Seed record selection for spectral matching with RSPMatch2005. Proceedings of *14thWorld Conference on Earthquake Engineering*, October 12-17, Beijing, China.

Hancock J., Watson-Lamprey, J., Abrahamson N.A., Bommer J.J., Markatis A., McCoy E., Mendis E., 2006. An improved method of matching response spectra of recorded earthquake ground motion using wavelets. *Journal of Earthquake Engineering*, 10(Special Issue I), 67-89.

Hancock J., Bommer J.J., Stafford P.J., 2008. Number of scaled and matched accelerograms required for inelastic dynamic analyses. *Earthquake Engineering and Structural Dynamics*, 37(14), 1585-1607.

Iervolino I., Cornell C.A., 2005 Record selection for nonlinear seismic analysis of structures. *Earthquake Spectra*, 21(3), 685-713.

Iervolino I., Manfredi G., Cosenza E., 2006. Ground motion duration effects on nonlinear seismic response. *Earthquake Engineering and Structural Dynamics*, 30, 485–499.

Iervolino I., Maddaloni G., Cosenza E. 2008a. Eurocode 8 compliant real record sets for seismic analysis of structures. *Journal of Earthquake Engineering*, 12(1), 54-90.

Iervolino I. , Giorgio M., Galasso C., Manfredi G.; 2008b. Prediction relationships for a vector valued ground motion intensity measure accounting for cumulative damage potential, 14th World Conference on Earthquake Engineering, Beijing, China, October 12-17.

Iervolino I., Maddaloni G., Cosenza E., 2009a. A note on selection of time-histories for seismic analysis of bridges in Eurocode 8. *Journal of Earthquake Engineering*, 13(8), 1125–1152.

Iervolino I., Galasso C., Cosenza E., 2009b. REXEL: computer aided record selection for code-based seismic structural analysis. *Bulletin of Earthquake Engineering*. 8:339-362.

Iervolino I., Galasso C., Manfredi G., 2009c. Conditional hazard analysis for secondary intensity measures. *Bulletin of the Seismological Society of America*. (submitted).

Lilliefors H.W., 1967. On the Komogorov-Smirnov test for normality with mean and variance unknown. *Journal of the American Statistical Association*, 62, 399-402.

Manfredi G., 2001. Evaluation of seismic energy demand. *Earthquake Engineering and Structural Dynamics*, 35, 21–38.

Mucciarelli M., Spinelli A., Pacor F., 2004. Un programma per la generazione di accelerogrammi sintetici "fisici" adeguati alla nuova normativa. XI *Convegno ANIDIS, "L'Ingegneria Sismica in Italia"*. January 25-29, Genoa, Italy.

PEER ground motion selection and modification working group – Haselton C.B., editor, 2009. Evaluation of Ground Motion selection methods: prediction median interstory drift response of buildings. PEER report 2009/01 available at http://peer.berkeley.edu/publications/peer_reports/reports_2009.

Pinto P.E., Giannini R., Franchin P., 2004. *Seismic reliability analysis of structures*. IUSS Press, Pavia, Italy.

Sabetta, F., Pugliese, A., 1996. Estimation of response spectra and simulation of non stationary earthquake ground motions. *Bulletin of the Seismological Society of America*, 86(2), 337-52.

Satterthwaite F.E., 1941. Synthesis of variance. *Psychometrika*, 6(5), 309-316.

Schwab P., Lestuzzi P., 2007. Assessment of the seismic nonlinear behaviour of ductile wall structures due to synthetic earthquakes. *Bulletin of Earthquake Engineering*, 5, 67-84.

Takeda T., Sozen M.A., Nielsen N.N., 1970. Reinforced concrete response to simulated earthquakes, *Journal of Structural Engineering Division*, ASCE, 96(12), 2557–2573.

Welch B. L., 1938. The significance of the difference between two means when the population variances are unequal. *Biometrika*, 29, 350-62.

PART II

DEMAND PREDICTION

Chapter 4

ANALYSIS METHODS: CRITICAL REVIEW OF THE RECENT ITALIAN SEISMIC CODE

De Luca F., Verderame G.M., Manfredi G. *La verifica sismica di edifici esistenti in cemento armato: criticità dell'attuale approccio normativo italiano*. 26° convegno nazionale AICAP, Padova 19-21 Maggio 2011; (in Italian).

4.1 Authorship of Chapter

This chapter is based on the publication (cited above). It deals with some critical aspects regarding analysis methods in the Italian seismic code, developed within the activities of the Rete dei Laboratori Universitari di Ingegneria Sismica – ReLUIS for the research program funded by the Dipartimento di Protezione Civile 2010-2013.

4.2 Introduction

Demand prediction represents the second phase of Performance Based Earthquake Engineering. It deals with the evaluation of the engineering demand parameters (EDP) given the intensity measure selected in the *hazard* phase of PBEE. Even if the actual PBEE approach deals with this phase suggesting to employ the most accurate structural analysis tools available in literature, it is worth to note that actually the aspect of demand prediction, in general, is something that is implicitly considered in structural engineering itself and in any case it has to be carried out with a structural analysis method selected between the different possibilities available that, in turn, correspond to different levels of accuracy and computational effort.

Analysis methodologies represent the primary tool for an earthquake engineer. Earthquake engineering was born together with structural analysis

methods. In fact, (see chapter 1), it can be stated that earthquake engineering began when the first engineer decided to design a structure with a few percent of its weight as horizontal load; that day earthquake engineering and lateral force method were born.

Actually analysis methodologies are strictly coupled with structural modeling: there is no need to employ a detailed analysis approach unless the structural model employed is able to provide a detailed structural response.

In the following the methodological aspects of structural analysis methods will be examined taking for granted that each methodology asks for a proper modeling approach. Especially in the case of nonlinear modeling, the approach is not necessarily univocal (e.g. lumped plasticity, fiber modeling, assumption of the hysteretic loop …); each different modeling approach is characterized by pros and cons.

On the other hand not only the aspect of nonlinear modeling can play a key role in demand prediction. An example can be the linear modeling approach for reinforced concrete structures in which it is necessary to choose a single stiffness for the elements that should be representative of an evolutionary stiffness that passes through a cracking phase up to a yielding phase. Important scientists and philosophers of the past, such as Carl Nilsson Linnaeus and Gottfried Wilhelm von Leibniz, would suggest that *Natura non facit saltus*. Hence, if nature does not make jumps, often mathematical modeling has to, and the choice of a single representative characteristic, such as stiffness in structural modeling of reinforced concrete elements (e.g. Elwood et al., 2007), has to be an aware solution dealing with the specific target of the analysis.

4.3 Structural analysis methods

Analysis methodologies can be classified in two big families according to the approach chosen for the classification. Each family differs because of the basis of the classification: if it is made on the basis of actions or on the basis of response. Thus an analysis method is static or dynamic or it is linear or

nonlinear. The above classifications end up in four different analysis methodologies which represent, in turn, the four analysis options provided by most of the recent seismic codes. It is worth to note different approaches are possible once a given methodology between the four is considered.

Analysis methods are going to be reviewed from the less accurate to the most accurate evaluating pros and cons of each single solution. It is implicit that with the increasing accuracy there is an increasing computational effort.

4.3.1. Linear static analysis or lateral force method

This method is the classical and basic approach to earthquake engineering, as it was already emphasized above. It is based on the fundamental hypothesis that the first mode of the structure is representative of the whole structural behavior. It consists in applying an inverted triangle distribution of forces, whose shape recalls the shape of the first mode of regular buildings. The static forces are applied in each of the principal direction of the structure and then effects of the forces in the two directions are combined. The basic hypothesis of the method leads to limitations in the employment of such an analysis approach for non regular structures. On the other hand this simple straightforward method can help in dimensioning structures and roughly quantifying the effect of seismic forces.

In this method of analysis, the hazard at the site is represented by the seismic base shear force evaluated as the product of the whole mass of the building and the elastic spectral acceleration at the first fundamental period of the structure in the direction considered. In some cases additional coefficients accounting for different approximations are provided (e.g. a coefficient that accounts approximately for the participant mass ratio of the fundamental mode).

This method is *force-based*, since the response of the analysis is evaluated in term of forces. On the other hand modern design emphasizes the role of ductility that cannot be computed when a force-based linear analysis method is employed. To this aim codes and literature introduce a reduction factor R or a behavior factor q accounting for ductility. Such factors allow accounting for

ductility even in a force based approach. Regarding this latter aspect, basically coming from the *equal displacement rule* between maximum displacement of an elastic and an elastic plastic single degree of freedom (Veletsos and Newmark, 1960), it should be emphasized that the general meaning of such a reduction factor is to bring back resulting demands from the analysis to the elastic limit before nonlinear behavior is experienced by the structure; so, allowing a force-based approach that accounts for ductility. In the case of lateral force analysis the reduction factor or the behavior factor are applied to the base shear force, and they reduce it.

4.3.2. Linear dynamic analysis

Linear dynamic analysis has the advantage of considering all the fundamental modes characteristic of the structure. It would be natural to think that when a dynamic analysis is performed, whether linear, as in this case, or nonlinear, the seismic input would be characterized by accelerometric waveforms. Actually the latter observation is not exactly right, since; in general, when referring to linear dynamic analysis, a modal response spectrum analysis is the objective. Thus, let us consider the differences between such approaches in the framework of linear dynamic analysis.

A linear dynamic analysis, strictly speaking, is an analysis applied to a linear model of the structure in which the input is characterized by accelerometric waveforms resulted by seismic input selection, based on the hazard analysis at the site. The approach in such analysis, given its linear characteristics, would be *force-based* as well as in the case of lateral force method, with the advantage of considering the interaction of the modes of the structure with the typical frequencies of an earthquake defined by accelerometric waveforms. Such an analysis approach provides structural response as a function of time.

The previous described approach also known as linear time-history analysis or response history analysis is not what codes provide when referring to linear dynamic analysis. In fact, as it will be better detailed in section 4.4, codes in general refer to a modal response spectrum analysis. The genesis of

this latter method is the general idea of determining the peak response of a structure, to be employed in design, directly from the response spectrum of the ground motions, avoiding a time-history. So, the modal response analysis is based on the combination of different linear static analyses in which the shapes of the force distributions are proportional to the modal shape of the i^{th} mode. Such an approach allows considering for each static analysis, in which the procedure is split, the i^{th} peak response referred to the i^{th} mode in which base shear force is evaluated as the product of the elastic spectral acceleration at the period of the i^{th} mode and the mass excited by the i^{th} mode. Hence, the peak modal responses r_{io} (i=1,2,..,n) evaluated for each mode has to be combined to obtain the peak value r_o of the total response. The combination is the most critical aspect of such modal analysis approaches; in this phase approximation needs to be introduced. In fact, the peak responses of each mode are attained at different times given the waveform, so the combination should consider also this aspect. In literature combination rules are provided accounting for the typical trend of the peak responses as an effect of earthquake waveforms. In the following the description of modal combination rules by Chopra (2007) is provided.

The assumption that all modal peaks occur at the same time and their algebraic sign is ignored provides an upper bound limit to the peak value of the total response. This approach, also known as ABSSUM, see equation (4.1), is too conservative, so, it is not employed in structural design applications. Other possible approach is the square-root-of-sum-of -squares, SRSS, rule for modal combination, developed in Rosenblueth (1951), see equation (4.2).

$$r_o \simeq \sum_{i=1}^{n} \left| r_{io} \right| \tag{4.1}$$

$$r_o \simeq \left(\sum_{i=1}^{n} r_{io}^2 \right)^{1/2} \tag{4.2}$$

The peak response in each mode is squared, the squared modal peaks are summed, and the square root of the sum provides an estimate of the peak total

response. This modal combination rule provides excellent response estimates for structures with well-separated natural frequencies. This limitation has not always been recognized in applying this rule to practical problems, and at times it has been misapplied to systems with closely spaced natural frequencies, such as piping systems in nuclear power plants and multistory buildings with unsymmetrical plan.

The complete quadratic combination (CQC) rule for modal combination, see equation (4.3), is applicable to a wider class of structures as it overcomes the limitations of the SRSS rule. Each of the n^2 terms on the right side of equation (4.3) is the product of the peak responses in the i^{th} and j^{th} modes and the correlation coefficient ρ_{ij} for these two modes; ρ_{ij} varies between 0 and 1 and ρ_{ij} is equal to 1 for $i=k$. Thus equation (4.3) can be rewritten as equation (4.4) to show that the first summation on the right side is identical to the SRSS combination rule of equation (4.2); each term in this summation is obviously positive. The double summation includes all the cross $(i \neq k)$ terms; each of these terms may be positive or negative. A cross term is negative when the modal static responses assume opposite signs. Thus the estimate for r_o obtained by the CQC rule may be larger or smaller than the estimate provided by the SRSS rule.

$$r_o \simeq \left(\sum_{i=1}^{n} \sum_{j=1}^{n} \rho_{ij} r_{io} r_{jo} \right)^{1/2} \tag{4.3}$$

$$r_o \simeq \left(\sum_{i=1}^{n} r_{io}^2 + \underbrace{\sum_{i=1}^{n} \sum_{j=1}^{n} \rho_{ij} r_{io} r_{jo}}_{i \neq j} \right)^{1/2} \tag{4.4}$$

Starting in the late 1960s and continuing through the 1970s and early 1980s, several formulations for the peak response to earthquake excitation were provided in literature. Some of these are identical or similar to equation (4.3) but differ in the mathematical expressions given for the correlation

coefficient (Rosenblueth and Elorduy, 1969; Der Kiureghian, 1981). Der Kiureghian (1981) formulation is now widely used in code, see section 4.4.

It is worth to note that numerical applications (Chopra, 2007) show that ABSSUM can be very conservative and that SRSS and CQC provides essentially the same estimates when cross-correlation coefficients are small. Other than the previous observations, largely expected, it should be emphasized that peak response estimates by SRSS and CQC rules can be, in some cases, smaller than the results of a time-history analysis, even if the latter cannot be considered a general trend. Another interesting observation is that the error between the peak estimates by SRSS and CQC respect to a time history varies with the response quantity considered (e.g. story shears at different levels, in reason of the different effect of higher modes on such response quantities, can be characterized by different errors respect to the corresponding peak demands evaluated via time-history analysis). Finally it is important to observe that such differences observed when employing spectra of single accelerograms are smoothed by the typical smoothed functional form of code spectra.

Other relevant problem for complex structures is the number of modes to consider in the analysis. Generally codes consider all the modes with mass participant ratios that exceed a specific value and a number of total modes so that the sum of participant mass ratios reaches an acceptable percentage of the total mass of the structure. Given the linear characteristic of this analysis, also in this case it is provided a reduction factor, generally applied to the response spectrum considered) that accounts indirectly for ductility and allows a force-based approach for the results.

4.3.3. Nonlinear static analysis or pushover method

Nonlinear static analysis represents a straightforward way for the estimation of nonlinear response of structures. The idea is to apply an incremental force distributions, keeping its shape fixed, and to register the response in a synthetic form, considering the base shear, on the vertical axis, and the displacement of a control point (generally located at the roof) at each

of the increasing step of the analysis, on the horizontal axis.

The main general hypothesis at the basis of this analysis procedure is that the response of a multi degree of freedom (MODF) system can be approximated with the response of an equivalent single degree of freedom (SDOF) system.

Once the pushover curve is obtained the possible procedures consist in different subsequent steps: (i) define a capacity curve of an equivalent single degree of freedom; (ii) fit a piecewise linear function (typically bilinear) to define the period and backbone of an equivalent SDOF; (iii) use a pre-calibrated R-μ-T (reduction factor – ductility – period) relationship for the extracted piecewise linear backbone to obtain SDOF seismic demand for a given spectrum; (iv) translate the SDOF response to the MDOF "target displacement" (usually at the roof level) and use the static pushover curve to extract MDOF response demands for the entire structure; (v) compare demands to capacities; see (Fajfar and Fischinger, 1988) for example. Further details regarding the nonlinear static analysis can be found in chapter 5.

An example of static pushover curve of a simple RC frame is provided in Figure 4.1. Figure 4.1a shows the geometry of the frame considered and Figure 4.1b shows the pushover curve in the case of second order effects (P-Δ) are accounted or not. In the example provided a lumped plasticity model was considered for frames and a plastic behavior after yielding was considered for hinges in the elements, the latter modeling solution was aimed at emphasizing P-Δ. The non-smooth shape of the pushover curve suggests the soft storey mechanism found at the third level of the structure, as an example of how the synthetic representation of the pushover curve, and substantially its shape, can suggest the collapse mechanism characterizing the structure.

Another example of static pushover curves is provided in Figure 4.2 in which two RC frames, sharing the same global geometry (Figure 4.2a), are designed accounting for gravity loads only and in high ductility class (DCH) according to the recent Italian seismic code. Differences in the shapes of the two pushover curves (Figure 4.2b) emphasize the different seismic response

and the different collapse mechanisms registered; a soft storey at the first level for the gravity load design and a global mechanism for the DCH design. For further details on this example please see De Luca et al. (2009). Also in this example a lumped plasticity model was employed, in this case P-Δ was not accounted for in the nonlinear modeling of the elements but mechanical softening was considered, in fact, the backbones of plastic hinges were characterized by strength degradation after the attainment of the maximum bending moment.

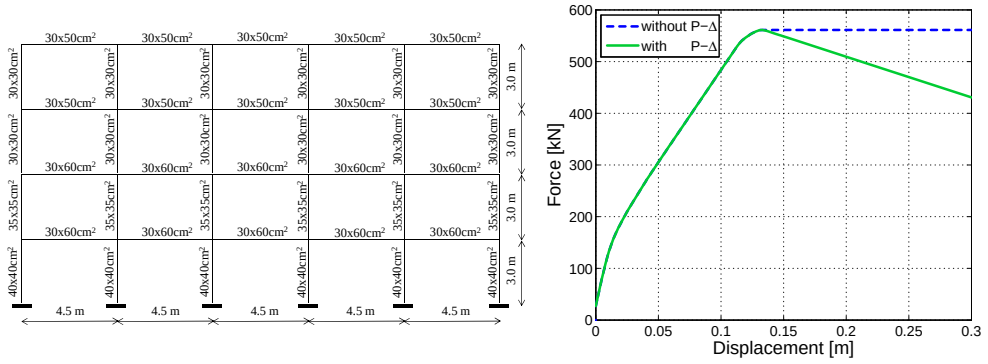

Figure 4.1.Example of a simple RC frame, (a) geometry and section dimensions, (b) static pushover curve with and without P-Δ effect.

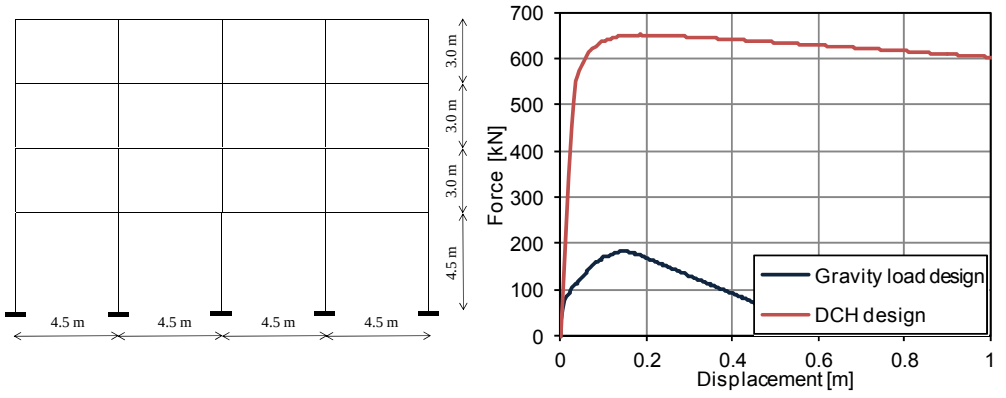

Figure 4.2. Global geometry of an RC frame designed for gravity load and in high ductility class according to Italian Code (a), corresponding pushover curves of the two structures (b), see De Luca et al. 2009 for details.

The key issues in static pushover analysis are the approximations implicit in the method: (i) the assumption of the load path, (ii) the MDOF to SDOF equivalence, (iii) the piecewise linear approximation. Each of the above approximations have been studied and enhanced methodologies have been carried out to adapt the load path (Antoniou and Pinho, 2004), to account for higher mode response (Chopra and Goel, 2002) and to control the error introduced by the piecewise linear fit of the curve (see chapter 5). Every enhancement in the static pushover conventional procedure asks for further computational efforts that results in losing its practical and straightforward approach to nonlinear response of structure. Thus, the best solution is to be aware of pros and cons of such procedure (e.g. Krawinkler and Seneviratna, 1998) and switch to another analysis method or integrate it with another analysis method if approximations results in an inadequate response.

4.3.4. Nonlinear dynamic analysis

Nonlinear dynamic analysis is the most accurate analysis method available. It asks for a nonlinear model that accounts for both monotonic and hysteretic response of structures. Taking for granted the reliability of the mathematical model employed (it is a significant hypothesis since a lot of issues are related with nonlinear modeling of structures, see Filippou and Fenves, 2004); the analysis method consists in the evaluation of the response of a structure once an acceleration waveform is applied to it. The time-dependent response of the structure is obtained through direct numerical integration of its differential equations of motion. This kind of analysis, even if generally computational demanding, allows considering faithfully the nonlinear response of a structure (not considering approximations implicit in the mathematical modeling of the structure). The main issue in this analysis methodology is the selection of records representative of the hazard at the site. A lot of recent studies focus on the best approach to be followed (e.g. PEER report 2009/01, 2009).

It should be observed that a nonlinear time-history analysis, in which

record selection is made on the basis of the hazard at the site, not necessarily produces the nonlinear response of a structure; an example can be strategic structures in which an intentional overestimation of the forces is applied during design and if is not considered an high return period for hazard estimation, the structure can lead to elastic response. Aimed at relating directly response and hazard, so, aimed at a direct estimation of the $dG(EDP|IM)$, incremental nonlinear dynamic analysis method was carried out (Vamvatsikos and Cornell, 2002). Such an accurate method to estimate nonlinear structural response has become more common thanks to the improved computational capabilities of personal computers.

Incremental dynamic analysis (IDA) represents the conceptual extension of incremental static analysis (pushover) at nonlinear time-history analysis. It has been adopted by the U.S. Federal Emergency Management Agency (FEMA) guidelines (FEMA-350, 2000; FEMA-440, 2005) as the state-of-the art method to determine the global collapse capacity. The general idea is to perform a nonlinear time-history analysis for each intensity measure level and to employ peak response in term of engineering demand parameters in a plot versus increasing intensity measure. The optimization of such a computational demanding process can enjoy of different tools such as accelerograms scaling and optimization algorithms (Luco and Bazzurro, 2007; Vamvatsikos and Cornell, 2004). The normal plot approach followed in IDA consists in putting the EDP on the horizontal axis and the IM on the vertical one. An example of IDA evaluated on thirty records is shown in Figure 4.3, in which a simple plane structure was considered (the same considered in Figure 4.1a). The IM in this example is the elastic 5% damped spectral acceleration at the first period of the structure $Sa(T_1,5\%)$ and the EDP is the maximum interstorey drift (MIDR) in Figure 4.3a, while in Figure 4.3b on the horizontal axis is plotted the demand capacity ratio evaluated considering as capacity limit the ultimate chord rotation according to the approach suggested in Jalayer et al. (2007). Figure 4.3b shows also the results in term of 16°, 50° and 84° fractiles accounting for variability of seismic demand.

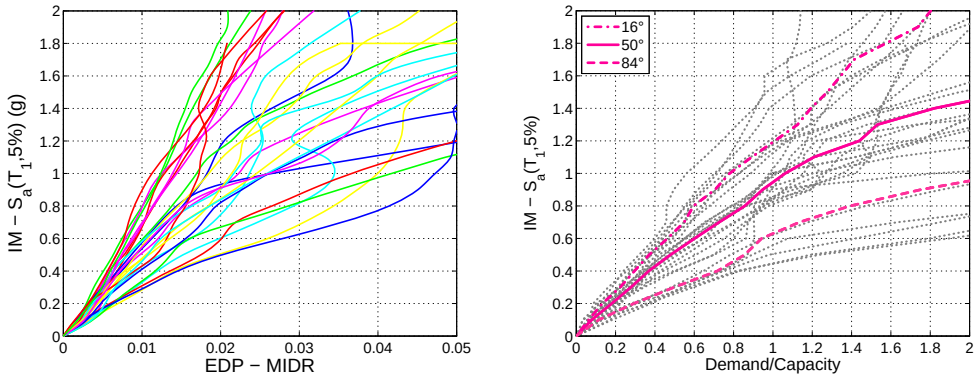

Figure 4.3. IDA example on a simple plane RC structures in which Sa(T1,5%) is the considered IM. On the horizontal axis (a) MIDR , (b) demand over capacity ratio evaluated considering ultimate chord rotations of the structures according to the approach in Jalayer et al. (2007).

It is worth noting that correspondences can be found between the shape of a IDA curve and the shape of a pushover curve (Vamvatsikos and Cornell, 2005), it is simple to understand that if the pushover is not characterized by softening, so mechanical and geometrical softening is not considered in modeling and analysis, the corresponding IDA curve never reaches the plateau, that in an IDA curve means collapse.

4.4 Code approaches

Seismic codes suggest different ways to carry out the analysis methods described above, in general, other than providing alternative proposal they adopt literature suggestions and apply restriction to the employment of a given analysis methods accounting for its implicit approximations.

In Eurocode 8 part 1 (CEN, 2004a) the four analysis methods described in the previous section are considered.

Lateral force method can be employed when the structure can be considered regular in elevation, according to criteria provided in the code, and if the fundamental period of the structure does not exceeds the value of 2.0 seconds and four times T_D, one of the characteristic periods defined by code

spectrum at the site. When employing this analysis method an approximate formulation for the evaluation of the period can be considered (if the height of the structure do not exceeds 40 meters); such an approximate formulation results in a very conservative evaluation of force demands.

As it was already anticipated in section 4.3, ductility is accounted for by means of the behavior factor q in Eurocode. It is an approximation of the ratio of the seismic forces that the structure would experience if its response was completely elastic with 5% viscous damping to the seismic forces that may be used in the design, with a conventional elastic analysis model, still ensuring a satisfactory response of the structure.

For modal response spectrum analysis, the routine method for the design of structures according to Eurocode 8 (CEN, 2004a), since compliance to regularity criteria in plan and elevation is not requested, the code prescribes to consider an number of modes so that the sum of the effective modal masses amounts at least 90% of the total mass of the structure and all modes with effective modal masses greater than 5% are taken into account. Modal combination of the responses can be made according to SRSS rule if the relevant modal responses may be regarded as independent of each other. If the latter condition is not verified CQC rule shall be adopted.

Regarding nonlinear static analysis, Eurocode 8 suggests the capacity spectrum method approach provided in Fajfar (1999). At least two vertical distributions of the lateral loads have to be considered (a *modal* pattern and a *uniform* pattern). It is worth to note that no restrictions are considered for this kind of analysis, unless some specific procedures for the estimation of torsional effects for structures with a predominantly torsional first mode of vibration.

In the case of nonlinear time-history analysis sets of three or at least seven accelerograms can be considered if the demand is evaluated as the maximum of the set or as the mean of the sets respectively (further details regarding this aspect can be found in chapter 3).

In Eurocode 8 part 3 (CEN, 2005), for existing buildings, linear analysis (both static and dynamic) are allowed considering the elastic spectral

acceleration or the elastic spectrum without the application of any reduction factor and applying these methods according to a *displacement-based* approach (it means that verification of ductile mechanisms should be based on deformations). This kind of analyses are subjected to an applicability condition that checks that the demand is uniformly distributed over the structure, so, allowing the application of equal displacement rule at single element level. The condition is based on the control that the ratio between the maximum demand capacity ratio and minimum one, selected between the element demand capacity ratios that exceeds 1, results within 2.5. The latter condition emphasizes that in the case of existing building a linear analysis method should be considered as an exception. Eurocode 8 part 3 allows also the so called q factor approach so resulting in the same analysis method considered for new design building but limiting the value of the q factor to 1.5, unless compliance criteria for local and global ductility according Eurocode 8 part 1 (CEN, 2004a) are met.

American regulation for existing buildings (ASCE/SEI 41-06, 2007) provides a clear overview of the limitations and approaches followed in different analysis methodologies. According to ASCE/SEI41-06 linear procedures are appropriate where the expected level of nonlinearity is low. The latter is measured by component demand capacity ratios of less than 2. In addition it is provided that linear procedures (both static and dynamic) shall be permitted for building which do not have irregularities. Limitations are provided also for nonlinear static procedures and substantially refer to the case in which higher mode effects are significant. The effect of higher modes can be considered significant if story shears evaluated with a modal response spectrum analysis, accounting for 90% of total mass, exceeds 130% of the corresponding story shear considering only first mode response. In such cases a nonlinear static analysis is allowed if a linear dynamic analysis is also performed to supplement the nonlinear static.

In American regulations, the seismic base shear for lateral load method is evaluated according to a coefficient approach, so, in addition to the product

between spectral acceleration at the fundamental period and mass also three coefficients are considered: a coefficient that relates elastic and inelastic response (related to the strength reduction factor), a coefficient that accounts for cyclic stiffness degradation and a coefficient that accounts for the effective mass participation to the first mode (a similar coefficient, named λ, is also employed in CEN, 2004a). Regarding linear dynamic methods both SRSS and CQC are allowed and a number of modes accounting for 90% of the total mass have to be considered. It is interesting that in ASCE/SEI 41-06 linear time history analysis is considered as alternative linear dynamic analysis method.

Nonlinear static analysis, other than being characterized by the limitations above, is performed in ASCE/SEI 41-06 according to the coefficient method provided by FEMA-440 (2005). It is worth noting that, given the findings in FEMA-440 (2005), showing that multiple load patterns do little to improve the accuracy of nonlinear static procedures, ASCE/SEI 41-06 recommends a single pattern based on the first mode shape. The coefficient method employed consists in the evaluation of the target displacement accounting for three modification factors, a coefficient to adapt equivalent SODF to MODF response, a coefficient aimed at relating maximum inelastic displacements to displacements calculated for linear response, and the latter coefficient accounting for cyclic stiffness degradation.

As it is expected, no limitations are provided by Eurocodes (CEN, 2004a; CEN, 2005) and American regulations (ASCE/SEI 41-06, 2007) when nonlinear dynamic analysis is employed.

4.5 Critical aspects of the recent Italian seismic code

The Italian Code, once the Decreto Ministeriale 14/1/2008 (DM 14/1/2008) and the Circolare 617/2009 (CS. LL. PP., 2009) have been released, changed completely and a radical upgrade in the design and assessment principles was carried out. Performance Based Design became the compulsory approach. On the other hand, some critical issues arose when this code has been applied in these three years and the experience after the 2009 L'Aquila

earthquake helped in this sense. Further upgrades and improvements can come from the comparison with the European Codes and American guidelines and thanks to the recent enhancements of the research community. All these factors are going to help the enhancement project of the Code promoted by the Consiglio Superiore dei Lavori Pubblici. Different critical aspects in the Italian code can be found in the approach to analysis methodologies, especially in the case of specific prescriptions for existing buildings.

For lateral load method Italian code prescribes the same limitations of Eurocode 8 (CEN, 2004a). Regarding response spectrum analysis, the Italian code prescribes always the employment of the CQC rule for modal combination, accounting for 85% of the total mass and for all the modes characterized by a modal mass ratio higher than 5%. On the other hand, the expression for the evaluation of the correlation coefficients, explicitly provided in the code, considers the special case of the Der Kiureghian (1981) coefficient formulation in which damping of the modes ($\xi_i=\xi_j$) are equal. The specialized coefficient, for $\xi_i=\xi_j=\xi$, is shown in equation (4.4), while the extended expression according to Der Kiureghian (1981) is shown in equation (4.5), in both the expressions $\beta_{ij}=T_j/T_i$. Now, the latter is a side problem for ordinary structures, in which normally damping is assumed equal to 5% for all modes. On the contrary, if for example based isolated structures are of concern, the correlation coefficients evaluated according to equation (4.4) cannot be considered reliable and equation (4.5) should be employed.

$$\rho_{ij} = \frac{8\xi\beta_{ij}^{3/2}}{\left(1-\beta_{ij}\right)\left[\left(1-\beta_{ij}\right)^2 + 4\xi^2\beta_{ij}\right]} \tag{4.4}$$

$$\rho_{ij} = \frac{8\sqrt{\xi_i\xi_j}\left(\beta_{ij}\xi_i + \xi_j\right)\beta_{ij}^{3/2}}{\left(1-\beta_{ij}^2\right)^2 + 4\xi_i\xi_j\beta_{ij}\left(1+\beta_{ij}^2\right) + 4\left(\xi_i^2+\xi_j^2\right)\beta_{ij}^2} \tag{4.5}$$

Regarding nonlinear static analysis, Italian code restricts its employment to the applicability of at least one modal pattern out of three principal patterns.

The first two load paths can be applied if the fundamental mode excites at least 75% of the total mass and the third one can be applied only if the fundamental period is higher than the characteristic period of the spectrum (T_C). The first pattern is a linear distribution proportional to story height and masses at each level (the same employed in lateral force method), the second pattern is a modal pattern accounting for first mode shape, the third pattern is a distribution proportional to the story shear distribution calculated by combining modal responses from a response spectrum analysis of the building. Such principal load patterns can be accompanied by one of the two secondary patterns, a uniform distribution and an adaptive distribution.

Now this applicability limits recall the similar principal force distributions provided in FEMA-356 (2000). It is worth noting that, other than being out-of-date according to subsequent FEMA-440 and ASCE/SEI 41-06 (see the previous section), the limit of the third load pattern is different; in fact, FEMA-356 distribution recalls that such a distribution shall be used when the period of the fundamental mode exceeds 1.0 second. In addition to the previous observation, it should be noted that Italian code does not provide the possibility to apply a modal response analysis coupled with a nonlinear static analysis, so, in the case of impossibility to apply nonlinear static analysis, especially in the case of existing building, the result is that practitioners go for linear analyses with q factor approach. The latter is not well-suited for existing buildings, given uncertainties on the evaluation of q.

As it was anticipated at the beginning of this section most of the problematic aspect in the new Italian seismic code arises regarding existing buildings. The explicative document to the Italian code (CS.LL.PP., 2009) recalls substantially Eurocode part 3 approach but considering some slight differences to such an approach that can create some problems, especially if the limitations to nonlinear static analysis above are considered.

The critical aspects concern linear analysis applicability condition and the q factor approach. First of all, according to CS. LL. PP. (2009) for linear analysis with elastic spectrum, two applicability conditions are provided. The

first one is relaxed respect to the one provided in Eurocode 8 part 3, since the ratio between maximum and minimum demand capacity ratios limited to 2.5 have to be checked between the elements that exceeds a demand capacity ratio equal to two. On the other hand, an applicability condition on brittle mechanisms have to be checked, the latter requests that all the elements show a ductile behavior , so that the shear capacity is not exceeded by the maximum shear produced by flexure (V_{flex}), see chapter 6. The latter conditions results in a very strict limit since beams, columns and beam-column joints have to be checked and it is very likely that columns or beam-column joints are not verified according to this applicability condition. The two applicability conditions together prevents, in any reasonable situation for existing building, the linear model to be accepted. The second applicability condition is also provided by Eurocode 8 (CEN, 2005), in a note, but in this case it is explicitly considered that brittle failures can be avoided with a local intervention on the brittle element; thus, this condition can be controlled afterwards, without preventing the employment of linear analysis method.

The resulting landscape of analysis methods for existing buildings according to Italian code is quite problematic: in fact, unless the static pushover analysis is applicable, practitioners have to choose between q factor approach, for which no restrictions are provided, and nonlinear dynamic analysis. It is not even necessary to stress which one is the most followed choice.

The linear analysis with q factor approach according to Italian code has itself some problems. First of all it should be emphasized that such a *force-based* method is considered in codes (CEN, 2005; CS. LL. PP., 2009) only to allow two specific situations: (i) to allow a positive seismic assessment for buildings that may have been (recently) designed in accordance to Eurocode 2 (CEN, 2004b) and Eurocode 8 (CEN, 2004a) ; (ii) to facilitate retrofitting of buildings by adding a new lateral-load-resisting system capable of sustaining the full seismic action, (Fardis, 2009).

The problems in q factor approach for existing buildings in the Italian

code are two. The first problem is that two behavior factors can be considered for the same structure, one for ductile mechanisms to be chosen in the interval [1.5;3] and the other one for brittle mechanisms always equal to 1.5. The latter approach produces a misuse and a misinterpretation of the behavior factor. Behavior factor should be interpreted with the same meaning assumed for new design structures, and should not be forced to a lower value when local and global ductility conditions in the structure allow the assumption of a higher factor (e.g. equal to 3). The second problem is practically huge; in fact, Italian code (CS.LL.PP, 2009) explicitly asks that in the case of q factor approach the demand for brittle mechanisms should be taken from the analysis (in which it was compulsory to assume q equal to 1.5). The approach is different if compared to Eurocode (CEN, 2005) in which demand of brittle mechanisms is always computed according to the flexural limit that can be reached in the element. The Italian prescriptions results in very prohibitive demands on which retrofitting intervention should be dimensioned and, in some cases, such interventions have to be applied to elements that are characterized by a ductile behavior ($V_{shear}>V_{flex}$). In most of cases local intervention, such as the application of fiber reinforced material wrapping or steel jacketing, in the case of RC elements, become not sustainable as retrofitting solutions. Finally in any case such an approach leads to disproportionate retrofitting costs.

4.6 Conclusion and perspectives

The general review provided in this chapter regarding analysis methodologies, other than recalling some interesting, well known, aspects of the methodological approaches for seismic structural analyses, emphasized some weaknesses of the recently released Italian code. Such aspects should be object of a revision since an upgrade process of the code has already begun. The general aim of the above observations is to clarify some aspects other than being an exercise of pointless criticism, hoping in a more and more aware employment of advanced tools for design and retrofitting by practitioners.

Finally it has to be highlighted that the recent upgrade of the code, even

with the critical aspects emphasized, represented a revolutionary innovation in the Italian regulation context.

REFERENCES

American Society of Civil Engineers (ASCE), 2007. Seismic Rehabilitation of Existing Buildings, ASCE/SEI 41-06, Reston, Virginia.

Antoniou S., Pinho R., 2004. Advantage and limitations of adaptive and non-adaptive force-based pushover procedures, *Journal of Earthquake Engineering* **8**, 497-522.

Chopra A.K., 2007. Dynamics of the Structures, Prentice Hall, Upper Saddle River, New Jersey, 3rd edition.

Chopra A.K. and Goel R.K., 2002. A modal pushover analysis procedure for estimating seismic demands for buildings, *Earthquake Engineering and Structural Dynamics*, **31**, 561-582, 2002.

Comité Européen de Normalisation (CEN), 2004a. Eurocode 8 – Design of Structures for earthquake resistance – Part 1: General rules, seismic actions and rules for buildings. EN 1998-1, CEN, Brussels.

Comité Européen de Normalisation (CEN), 2004b. Eurocode 2 – Design of concrete structures – Part 1-1: General rules and rules for buildings. EN 1998-1-1, CEN, Brussels.

Comité Européen de Normalisation (CEN), 2005. Eurocode 8 – Design of Structures for earthquake resistance – Part 3: assessment and retrofitting of buildings. EN 1998-3, CEN, Brussels.

CS.LL.PP. Circolare 617, 2009. Istruzioni per l'applicazione delle Norme Tecniche per le Costruzioni, Gazzetta Ufficiale della Repubblica Italiana 47, 2/2/2009 (in Italian).

De Luca F., Elefante L., Iervolino I., Verderame G.M., 2009. Strutture esistenti e di nuova progettazione: comportamento sismico a confronto. XIII Convegno ANIDIS, Bologna 28 Giugno – 2 Luglio. (in Italian).

Der Kiureghian A., 1981. A response spectrum method for random vibration analysis of MDF systems, *Earthquake Engineering and Structural Dynamics*, **9**, 419-435.

Decreto Ministeriale del 14 gennaio, 2008. Approvazione delle nuove norme tecniche per le costruzioni. G.U. n. 29 del 4/2/2008 (in Italian).

Elwood K.J., Matamoros A., Wallace J.W., Lehman D., Heintz J., Mitchell A., Moore M. Valley M., Lowes L.N., Comartin C., Moehle J.P., 2007. Update to ASCE/SEI 41 concrete provisions, *Earthquake Spectra*, **23**(3), 493-523.

Fajfar P., Fischinger M., 1988. N2 – A method for non-linear seismic analysis of regular structures, *Proceedings of the 9th World Conference on Earthquake Engineering*, Tokyo, 111-116.

Fajfar P., 1999. Capacity spectrum method based on inelastic demand spectra. *Earthquake Engineering and Structural Dynamics*, **28**, 979-993.

Fardis M.N., 2009. Seismic design, assessment and retrofitting of concrete buildings based on EN-Eurocode 8, Springer, August.

Federal Emergency Management Agency (FEMA), 2000. Recommended seismic design criteria for new steel moment-frame buildings. Report No. FEMA-350, SAC Joint Venture, Federal Emergency Management Agency, Washington, DC.

Federal Emergency Management Agency (FEMA), 2000. Prestandard and commentary for the seismic rehabilitation of buildings. Report No. FEMA-356, Washington, D.C.

Federal Emergency Management Agency (FEMA), 2005. Improvement of nonlinear static seismic analysis procedures. Report No. FEMA-440, Washington, D.C.

Filippou F.C. and Fenves G.L. , 2004. Methods of analysis for earthquake-resistant structures. In: Bozorgnia Y. and Bertero V.V. Editors *Earthquake Engineering: From engineering seismology to performance-based engineering*, CRC Press, chapter 6.

Jalayer F., Franchin P., Pinto P.E., 2007. A scalar damage measure for seismic reliability of RC frames. *Earthquake Engineering and Structural Dynamics*, **36**, 2059-2079.

Krawinkler H., Seneviratna G.P.D.K., 1998. Pros and cons of a pushover analysis of seismic performance evaluation, *Engineering Structures*, **20**, 452-464.

Luco N., Bazzurro P., 2007. Does amplitude scaling of ground motion records result in biased nonlinear structural drift responses? Earthquake Engineering and Structural Dynamics, **36**, 1813-1835.

PEER ground motion selection and modification working group – Haselton C.B., editor, 2009. Evaluation of Ground Motion selection methods: prediction median interstory drift response of buildings. PEER report 2009/01 available at http://peer.berkeley.edu/publications/peer_reports/reports_2009.

Rosenblueth E., 1951. A basis for aseismic design. Ph.D thesis, University of Illinois, Urbana, Ill.

Rosenblueth E., Elorduy J., 1969. Response of linear systems to certain transient disturbances. *Proceedings of the 4th World Conference on Earthquake Engineering*, Santiago, Chile, vol. I, 185-196.

Vamvatsikos D. and Cornell C.A., 2002 Incremental Dynamic Analysis, *Earthquake Engineering and Structural Dynamics*, **31**, 491-514.

Vamvatsikos D. and Cornell C.A., 2004. Applied Incremental Dynamic Analysis. *Earthquake Spectra*, **20**, 523-553.

Vamvatsikos D., Cornell C.A.m 2005. Direct Estimation of Seismic Demand and Capacit of Multidegree-of-Freedom Systems through Incremental Dynamic Analysis of Single Degree of Freedom Approximation. ASCE Journal of Structural Engineering, **131**(4), 589-599.

Veletsos A.S., Newmark N.M., 1960. Effect of inelastic behavior on the response of simple systems to earthquake motions, *Proccedings of the 2nd World Conference on Earthquake Engineeirng*, Tokyo, Japan, 895-912.

.

Chapter 5

OPTIMIZED PIECEWISE LINEAR FITS OF CAPACITY CURVES FOR EQUIVALENT SDOF ANALYSIS

De Luca F., Vamvatsikos D., Iervolino I. Near-optimal bilinear fit of capacity curves for equivalent SDOF analysis. COMPDYN 2011 3rd International Conference on Computational Methods in Structural Dynamics and Earthquake Engineering, 25-28 May, Corfu, Greece, 2011.
De Luca F., Iervolino I., Vamvatsikos D. Improving the static pushover analysis in the Italian Seismic Code by proper piecewise-linear fitting of capacity curves. XIV Convegno ANIDIS 2011, Bari 18-22 September, 2011.
De Luca F., Iervolino I., Vamvatsikos D. Optimized piecewise linear fits of static pushover curves for equivalent SDOF analysis. Earthquake Engineering and Structural Dynamics, (under review).

5.1 Authorship of Chapter

This chapter is based on the three publications (cited above) that resulted from the collaboration with Dr. Dimitrios Vamvatsikos at the University of Cyprus in spring 2010. The core of this work is the development of an incremental dynamic analysis based methodology for the assessment of the error introduced by piecewise linear fits of capacity curves in nonlinear static analysis procedures and the consequent optimizing fitting rules to decrease this error. The final result of the collaboration with Dr. Vamvatsikos is an optimized three points piecewise linear fit for all the kind of capacity curves.

5.2 Introduction

In the last decades, improvements in the computational capabilities of personal computers have allowed the employment of nonlinear analysis

methods in many earthquake engineering problems. In this framework, nonlinear static analysis is becoming the routine approach for the assessment of the seismic capacity of existing buildings. Consequently, nonlinear static procedures (NSPs) for the evaluation of seismic performance, based on static pushover analysis (SPO), have been codified for use in practice. All such approaches consist of the same five basic steps: (a) perform static pushover analysis of the multi-degree-of-freedom (MDOF) system to determine the base shear versus (e.g., roof) displacement response curve; (b) fit a piecewise linear function (typically bilinear) to define the period and backbone of an equivalent single degree of freedom system (SDOF); (c) use a pre-calibrated R-μ-T (reduction factor – ductility – period) relationship for the extracted piecewise linear backbone to obtain SDOF seismic demand for a given spectrum; (d) translate the SDOF response to the MDOF "target displacement" (usually at the roof level) and use the static pushover curve to extract MDOF response demands for the entire structure; (e) compare demands to capacities; see (Fajfar and Fischinger, 1988) for example.

NSP is a conventional method without a rigorous theoretical foundation for application on MDOF structures (Krawinkler and Seneviratna, 1998), as several approximations are involved in each of the above steps. On the other hand, its main strength is that it provides an estimate of structural demand and capacity in a simple and straightforward way. Although several improvements and enhancements have been proposed since its introduction, any increase in the accuracy of the method is worth only if the corresponding computational effort does not increase disproportionately. Extensively investigated issues are the choice of the pattern considered to progressively load the structure and the implication of switching from the nonlinear analysis of MDOF system to the analysis of the equivalent SDOF sharing the same (or similar) capacity curve. Regarding the shape of the force distributions, it was observed that an adaptive load pattern could account for the differences between the initial elastic modal shape and the displacement shape in the nonlinear range (Bracci et al., 1997; Elnashai, 2001;Antoniou and Pinho, 2004).

Contemporarily, other enhanced analysis methodologies were proposed to account for higher mode effects and to improve the original MDOF-to-SDOF approximation (e.g., Chopra and Goel, 2002). Regarding the demand side, efforts have been made to improve the estimation of the target displacement, especially by providing advanced R-μ-T to better evaluate the inelastic seismic performance at the SDOF level; (e.g., Vidic et al., 1994; Miranda and Bertero, 1994).

One of the issues not yet systemically investigated is the approximation introduced by the imperfect piecewise linear fit of the capacity curve for the equivalent SDOF. The necessity to employ a *multilinear* fit (an inexact, yet common, expression to describe a single-variable piecewise linear function) arises due to the use of pre-determined *R-μ-T* relationships that have been obtained for idealized systems with piecewise linear backbones. This has become even more important recently since nonlinear modeling practice has progressed towards realistic member models, which may accurately capture the initial stiffness using uncracked section properties and/or include in-cycle strength degradation. The gradual plasticization of such realistic elements and models introduces a high curvature into the SPO curve that cannot be easily represented by one or two linear segments. It is an important issue whose true effect is often blurred, being lumped within the wider implications of using an equivalent SDOF approximation for an essentially MDOF system. On the other hand, recent studies have shown the influence of accounting for uncracked stiffness in the structural response of reinforced concrete structures (Aschheim, 2008).

The effect of the piecewise linear approximation will be investigated in stages, practically following the progression of modern *R-μ-T* relationships from the simple bilinear to the more complex quadrilinear backbone shapes by adding one linear segment at a time. Thus, starting with an elastic segment, it will be successively added a perfectly-plastic or positive-stiffness "hardening" segment, a negative stiffness "softening" segment and a low-strength zero-stiffness "residual" plateau. In essence, the optimal fitting of four different

shapes will be examined comprising (a) bilinear elastoplastic, (b) bilinear elastic-hardening (c) trilinear elastic-hardening-negative and (d) quadrilinear elastic-hardening-negative-residual. While the first two cases are typical in most NSP guidelines, (e.g. CEN, 2004; FEMA-356, 2000), the latter two have also become an option in recent codes (ASCE/SEI 41-06, 2007; FEMA-440, 2005), or literature (Vamvatsikos and Cornell, 2006; Dolsek and Fajfar, 2004).

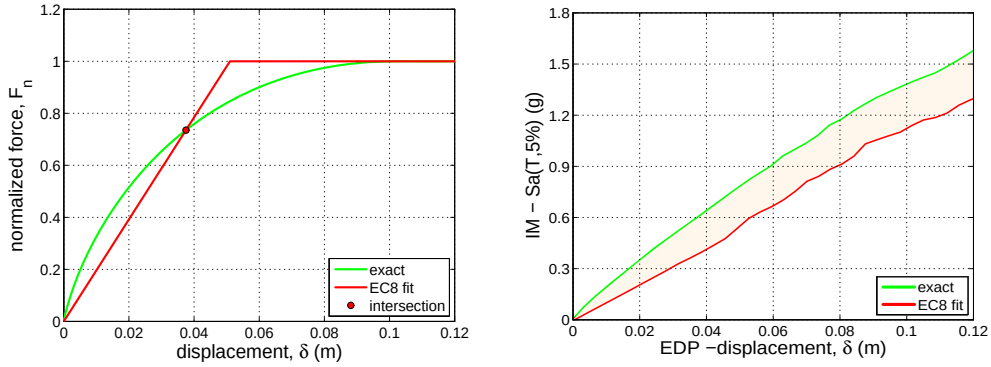

Figure 5.1. (a) Example of exact capacity curve versus its elastoplastic bilinear fit according to EC8 and (b) the corresponding median IDA curves showing the negative (conservative) bias due to fitting for T=0.5 s.

The approach employed will be based on the accurate assessment of the effect of the capacity curve fit on the NSP results. This is achieved by proper quantification of the bias introduced into the estimate of the seismic response at the level of the SDOF itself. Incremental dynamic analysis, IDA, (Vamvatsikos and Cornell, 2002), will be used as benchmark method to quantify the error introduced by each candidate fit with respect to the exact capacity curve of the SDOF. Figure 5.1a shows a typical example, where an elastoplastic backbone is fitted to a highly-curved SPO shape according to the equal area criterion, i.e., by equalizing the area discrepancy above and below the fitted curve. Such an approximation actually follows the Eurocode 8 (EC8) provisions (CEN, 2004) and it is not far from the ASCE/SEI 41-06 (2007) guidelines for a target displacement deep within the plastic plateau. The corresponding median IDA curves displayed in Figure 5.1b in terms of spectral

acceleration (the intensity measure, or IM) versus displacement (the engineering demand parameter, or EDP) show that the fitted backbone produces nearly 25% higher demand at all intensity levels. Thus, even code-mandated fitting rules may lead to an unintended hidden bias that will be shown to be generally conservative but may often become unreasonably high.

In the sections to follow the methodology considered will be fleshed out and applied to quantify the approximation errors. By extensive investigation of numerous candidate piecewise linear fits, a set of fitting rules will be established that can offer an optimal standardized approximation, suitable for immediate application in NSPs with superior performance to anything else currently in existence.

5.3 Methodology

The main target is the quantification of the error introduced in the NSP-based seismic performance assessment by the replacement of the original capacity curve of the system, termed the "exact" or "curved" backbone, with a piecewise linear approximation, i.e., the "fitted" or "approximate" curve (e.g., Figure 5.1a). This will enable a reliable comparison between different fitting schemes in an attempt to minimize the observed discrepancy between actual and estimated performance. In all cases, to achieve an accurate and focused comparison of the effect of fitting only, it is necessary to disaggregate the error generated by the fit from the effect of approximating an MDOF structure via an SDOF system. Thus, all the investigations are carried out entirely at the SDOF level, using a variety of capacity curve shapes, different periods and hysteresis rules and using IDA as the method of choice for assessing the actual performance of the different alternatives.

5.3.1. Exact versus approximate SDOF systems

An ensemble of SDOF oscillators is considered with varying curved shapes of force-deformation backbones. The first part of the investigation addresses non-softening behaviors; the backbones, in fact, display a

monotonically decreasing stiffness that starts from elasticity and ends at a final zero or positive stiffness that remains constant for all higher deformations (e.g., Figure 5.1a). According to their final constant stiffness, these will be termed "generalized elastoplastic" and "generalized elastic-hardening" systems, respectively. They are all fitted accordingly with bilinear elastoplastic or elastic-hardening shapes. The second part of the investigation focuses on backbones displaying negative stiffness, i.e., softening, termed "generalized elastic-hardening-softening" systems. First the use of an elastoplastic fit that is extended beyond the peak of the backbone to take into account the early negative slope will be investigated (e.g., the approach recommended by the current Italian building code, CS. LL. PP., 2009). Then, the higher fidelity three- or four-segment piecewise linear fit for backbones with non-trivial softening behavior, will be addressed.

For each considered curved backbone shape, 5% of critical viscous damping was used and appropriate masses were employed to obtain a range of matching "reference" periods of 0.2, 0.5, 1 and 2 seconds. The concept of the "reference" period, instead of the actual initial (tangent at zero displacement) period, is introduced because of the highly curved shape of some backbones. In some cases they show a strictly localized significant change in the initial stiffness, resulting in periods lower than 0.01 sec. Since this initial stiffness disappears almost immediately for any kind of loading history, a more representative reference period is required for each exact capacity curve. The reference period (T herein) was defined as the secant period at 2% of the displacement corresponding to the peak force capacity.

Actually, in the vast majority of the cases there was insignificant difference between the initial tangent period and the reference secant period. In all cases, both the exact and the approximate system share the same mass, but, due to the typically lower initial stiffness of the latter, the "equivalent" period of the fitted curve tends to be higher than the "reference" one, thus replicating the approach followed in the conventional NSP methodology (Fajfar and Fischinger, 1988). In addition, it is assumed that the backbone curve

itself suffices to capture via its shape all the in-cycle degradation effects (e.g., due to plasticization, P-Delta effects, etc.) without needing to use approximate coefficients (FEMA-356, 2000) or two separate analyses with and without P-Delta (FEMA-440, 2005).

In order to draw general conclusions, independent of the hysteretic behavior assumed, two distinct hysteretic rules were initially considered for the each curved backbone and its bilinear fit in the case of generalized elastoplastic behavior. The first is a standard kinematic strain hardening model without any cyclic degradation characteristics. The second is a pinching hysteresis featuring cyclic stiffness degradation (see Ibarra et al. 2005). In all cases, when comparing an original system with its approximate having a piecewise linear backbone, the same hysteretic rules are always employed, so that both systems display the same characteristics when unloading and reloading in time-history analyses. In other words, all differences observed in the comparisons to follow can be attributed to the fitted shape of the approximate backbone, obviously also capturing any differences due to mismatches between the exact ("reference") and the "equivalent" oscillator period.

When working with the backbone shapes and their fits it is useful to avoid the appearance of arbitrary scales and units of force F or displacement δ. Thus, using the normalized counterparts, F_n and δ_n, becomes attractive. Unfortunately, the concise definition of a yield point on curved backbones is impractical, unless tied to some preselected fitting rules; therefore it is not possible to use a strength reduction factor, or equivalent ductility, without bias. Instead, it was chosen to uniformly normalize force and displacement by the reference values of 1kN and 0.10m, respectively. These values correspond to the point where the generalized elastic-plastic backbones reach their plastic plateau (e.g. Figure 5.1a) by becoming fully plasticized. More complex backbone curves have been generated by building upon the elastoplastic ones in a consistent manner, so that the reference values generally represent a point in the "hardening" region, between near-elastic behavior and peak strength,

where a nominal yield point would normally reside.

For each exact shape of the SDOF's capacity curve and for each period value, several piecewise linear fit approximations have been considered according to different fitting rules. These include typical code-suggested fits, e.g., as laid out in Eurocode 8 (CEN, 2004), FEMA-356 (2000), ASCE/SEI 41-06 (2007), and the Italian Code (Circolare 617/2009, CS.LL.PP., 2009). In addition several bilinear, trilinear and quadrilinear fits, including solutions available in literature (Vamvatsikos and Cornell, 2006; Dolsek and Fajfar, 2004; Han et al., 2010), have been investigated. Different fitting criteria, e.g., varying initial stiffness, yield point definition, and softening slope, have been employed in an attempt to pinpoint the consistent characteristics that can define an optimal or near-optimal fit. In all cases, the aim is to provide a standardized approximation that delivers accuracy yet remaining independent of the NSP target displacement, to offer a single representation of the static pushover curve for a wide range of limit-states considered. To enable a precise comparison that will allow distinguishing among relatively similar backbones in consistent performance terms, as it was previously stated, incremental dynamic analysis, IDA, (Vamvatsikos and Cornell, 2002) will be employed.

5.3.2. Performance –based comparison via IDA

IDA is arguably the most comprehensive analysis method available for determining the seismic performance of structures. It involves performing a series of nonlinear dynamic analyses by scaling a suite of ground motion records to several levels of intensity, characterized by a scalar IM, and recording the structural response via one or more EDPs. The results typically appear in terms of multiple IDA curves, one for each record, plotted in the IM versus EDP space. These can be in turn summarized into the 16, 50, 84% fractile curves of EDP given IM (EDP|IM) or, equivalently (Vamvatsikos and Cornell, 2004), as the practically identical 84, 50, 16% fractile curves of IM given EDP (IM|EDP). The summarized curves thus provide the (central value and the dispersion) of the distribution of EDP seismic demand given the IM intensity of the earthquake or, vice-versa, the distribution of a structure's IM-

capacity that a ground motion's intensity should reach to achieve the given value of EDP response.

To perform IDA for each exact and approximate oscillator considered, a suite of sixty ground motion records was used, comprising both horizontal components from thirty recordings (Vamvatsikos and Fragiadakis., 2006) from the PEER NGA database (http://peer.berkeley.edu/peer_ground_motion_database). They are all characterized by relatively large moment magnitude (between 6.5÷6.9) and moderate distances of the recording site from the source (15km÷35km), all recorded on firm soil and bearing no marks of directivity. Using the *hunt & fill* algorithm (Vamvatsikos and Cornell, 2004), 34 runs were performed, per record, to capture each IDA curve with excellent accuracy. The IM of choice was $S_a(\tau)$, the 5%-damped spectral acceleration at the period τ of the oscillator, this being the reference period for the exact systems or the equivalent for the fitted ones. The oscillator displacement δ (or its normalized counterpart δ_n) was used as the corresponding EDP, being the only SDOF response of interest for NSP.

Once the IM and EDP are decided, interpolation techniques allow the generation of a continuous IDA curve from the discrete points obtained by the 34 dynamic analyses for each ground motion record. The resulting sixty IDA curves can then be employed to estimate the summarized IDA curves for each exact and approximate pair of systems considered. Still, in order to be able to compare an exact system with reference period T with its approximation having an equivalent period T_{eq}, it was necessary to have their summarized IDA curves expressed in the same IM. In this case it is chosen to be $S_a(T)$, i.e. the spectral ordinate at the reference period of the curved backbone oscillator. Thus, while the approximate system IDA curves are first estimated as curves in the $S_a(T_{eq})$ – δ (or δ_n) plane, they are now transformed to appear on $S_a(T)$ – δ axes. This is achieved on a record-by-record basis by multiplying all 34 $S_a(T_{eq})$ values comprising the i-th IDA curve (i=1,2,…,60) by the constant spectral ratio $[S_a(T)/S_a(T_{eq})]_i$ that characterizes the i-th record (Fragiadakis et al., 2006).

The error is evaluated for every value of displacement in terms of the

relative difference between the two system median S_a-capacities, both evaluated at the reference period T of the exact system, see equation (5.1). Alternatively, one could use the relative error in the median displacement response given the level of spectral acceleration, see equation (5.2)

$$e_{50}(\delta_n) = \frac{S_{a,50}^{fit}(\delta_n) - S_{a,50}^{exact}(\delta_n)}{S_{a,50}^{exact}(\delta_n)} \tag{5.1}$$

$$e_{50}(S_a) = \frac{\delta_{n,50}^{fit}(S_a) - \delta_{n,50}^{exact}(S_a)}{\delta_{n,50}^{exact}(S_a)} \tag{5.2}$$

Similarly, the same definitions can be used to estimate the errors for different demand or capacity fractile values, e.g., 16% or 84%, or even for the dispersion in response or capacity, which, assuming lognormality, can be defined as one half the difference between the corresponding 84% and 16% values. Thus, two different ways of measuring the discrepancy between IDA curves are available, e.g., for the two median IDA curves shown in Figure 5.1b. In one case "horizontal statistics" are employed, working with the median EDP given IM, and in the other case "vertical statistics" of IM given EDP. As Vamvatsikos and Cornell (2004) have shown, the median IDA curve is virtually the same, regardless of how it is calculated, while, as discussed earlier, the 16, 84% fractiles are simply flipped. In addition, while there might be differences in the error estimates using these two different methods, these are only an issue of scale. Figure 5.2a, Figure 5.2b compare the two error quantification methods for the median IDAs shown in Figure 5.1b (an example of generalized elastic-plastic behavior). The observed trends are actually the same, but simply inverted: obviously, an overestimation in response becomes an underestimation in capacity and vice-versa.

Why then should one method be preferred over the other? There are three important reasons that make the IM-based method (IM|EDP) a more attractive solution. First, parameterizing the error in terms of the displacement

response simplifies its visualization as displacement is directly mapped to specific regions of the oscillator force-deformation backbone. Thus, it is possible to see directly in Figure 5.2b, when it is compared vis-à-vis Figure 5.2a, whether it is the "elastic" or the "post-elastic" part that is causing the accumulation of error. Figure 5.2a is much more difficult to understand, especially if more complex backbones, than the ones used here, are considered. Second, comparing the exact versus the fitted equivalent system on the basis of S_a-capacity, links directly to comparison in terms of seismic performance, as expressed by the mean annual frequency (MAF) of violating limit-states defined by the oscillator displacement (Vamvatsikos, 2011).

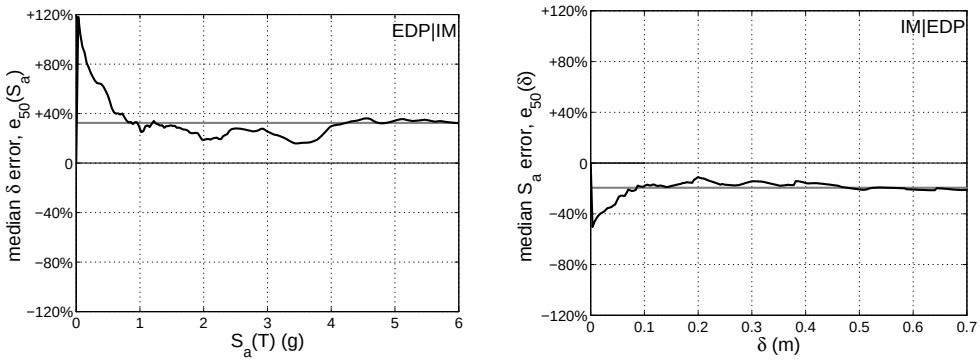

Figure 5.2. The mean relative error in the median capacity (black line) shown with the overall average (grey line) as introduced by the bilinear fit in Figure 1. It is expressed on the basis of (a) response given intensity (EDP|IM) and (b) intensity given response (IM|EDP).

An over/under-estimation of S_a-capacity maps to a consistent (although not commensurable) under/over-estimation of the MAF of limit-state exceedance, provided that the difference between the reference and the equivalent period is not overly large. Finally, when collapse enters the problem it is obvious that the error in displacement may easily diverge when at a given intensity level one system has collapsed, while the other has not. In fact, on the contrary, this is never a problem for the S_a-based error. These are all compelling reasons to recommend only the S_a-based comparison for general use.

5.4 Bilinear fits for non-softening behavior

Bilinear elastic-plastic or elastic-hardening fits are the fundamental force-deformation approximations employed in NSP guidelines. The simplicity of the bilinear shape means that the only need is to estimate the position of the nominal "yield point" and select a value for the constant post-elastic stiffness. Eurocode 8 (CEN, 2004), following the original N2 method (Fajfar and Fischinger, 1988), suggests an elastic-plastic idealized backbone based on the balancing of the area discrepancy above and below the fit. FEMA documents (FEMA-356, 2000; FEMA-440, 2005) generally employ a bilinear elastic-hardening curve. While a third softening segment was also considered indirectly by FEMA-356 (2000), for demand estimation, FEMA-440 (2005) and consequently ASCE/SEI 41-06 (2007) only use it to limit the allowable value of the *R*-factor to protect against global collapse. In all cases, the idealized elastic-hardening shape is fitted through an iterative procedure: the nominal yield point and the post-yield slope are selected to achieve a balance of the misfit areas above and below the capacity curve up to the target displacement, while also requiring that the elastic segment remains secant at 60% of the nominal yield strength.

In order to develop an improved bilinear fit, the fitting of the initial "elastic" segment is investigated separately and then the post-elastic non-negative stiffness part is added. Generalized elastic-plastic systems will be first studied, where the stiffness becomes zero beyond a displacement of 0.10 m, followed by generalized elastic-hardening backbones were the post-yield stiffness is positive. In all cases the target is developing a standardized fitting rule that performs well for a continuum of limit-states in the non-negative stiffness region.

5.4.1. Bilinear fits of generalized elastic-plastic systems

First a family of generalized elastic-plastic capacity curves is considered that exhibit a stiffness gradually decreasing with deformation, starting from the initial elastic and reaching zero slope. The shapes are mainly characterized

by the rate and magnitude of the changes in stiffness with increasing displacement. Figure 5.3a and Figure 5.3b give an example of the shapes employed and emphasize two opposing cases. The first (Figure 5.3a) is not characterized by significant curvature, while the second (Figure 5.3a) shows a significant change in slope that can be representative of the behavior of a model that accounts for uncracked stiffness or displays progressive plasticization of elements.

Three basic fitting rules are compared: (a) the "FEMA-style" fit (*60% fit*), (b) the "EC8-style" fit using a simple equal area criterion (*equal area*), and (c) the *10% fit*, defined so that the intersection between the capacity curve and the fitted elastic segment is at 10% (instead of 60% for the "FEMA-style" fit) of the maximum base shear. The latter is a simple standardized rule that has been derived from extensive testing to better (near-optimally) capture the early seismic behavior. In all three cases the post-yield linear segment is chosen to match the exact plastic-plateau. Strictly speaking this marks a slight deviation from the actual FEMA fit which stipulates a variable post-elastic segment depending upon the target displacement and the area-balancing rule; on the other hand our approach may be thought of being representative of the code-mandated fit for a target displacement deep into the plastic plateau.

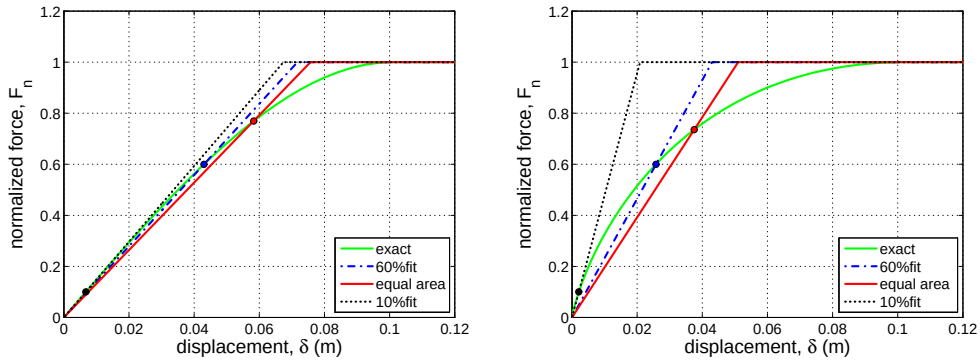

Figure 5.3. Comparison of generalized elastic-plastic capacity curves and their corresponding fits having (a) insignificant versus (b) significant changes in initial stiffness Note: 0.1 displacement becomes 1.0 normalized.

Figure 5.3a shows that when the capacity curves are not characterized by

significant stiffness changes, the three fits are very similar to each other. They differ significantly though when the initial stiffness diminishes rapidly, as in Figure 5.3b. To investigate the differences between the different fitting rules when applied to the two different backbones, IDA is performed for each of the actual and approximate SDOF systems for a range of periods. Figure 5.4 to Figure 5.7 show the comparison in terms of the normalized difference in the median S_a-capacity, see equation (5.1) for T equal to 0.2, 0.5, 1.0 and 2.0 s, respectively.

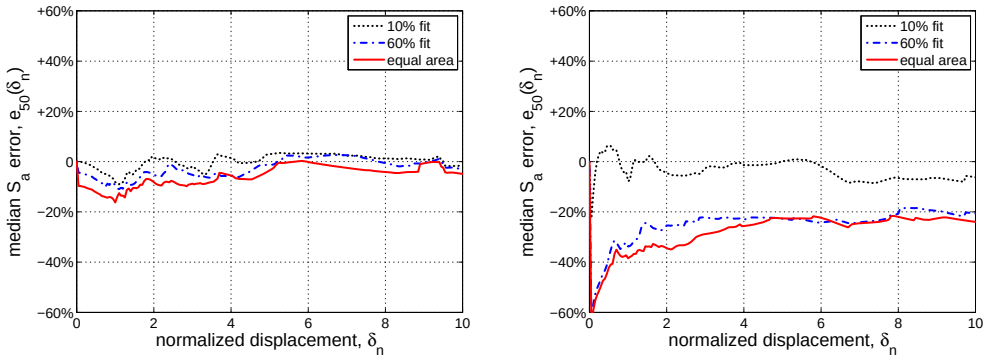

Figure 5.4. The relative error in the median S_a-capacity of the 10%, 60% and equal area fits for T = 0.2 s, when applied to the capacity curves of Figure 5.3: (a) insignificant versus (b) significant changes in initial stiffness.

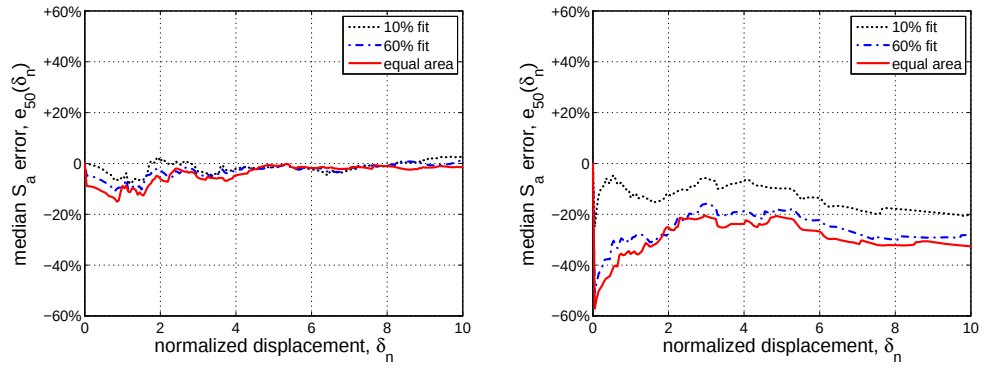

Figure 5.5. The relative error in the median S_a-capacity of the 10%, 60% and equal area fits for T = 0.5 s, when applied to the capacity curves of Figure 5.3: (a) insignificant versus (b) significant changes in initial stiffness.

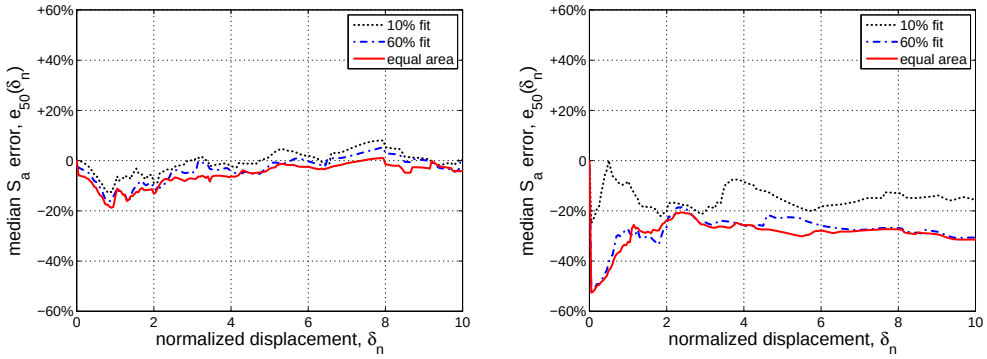

Figure 5.6. The relative error in the median S_a-capacity of the 10%, 60% and equal area fits for T = 1.0 s, when applied to the capacity curves of Figure 5.3: (a) insignificant versus (b) significant changes in initial stiffness.

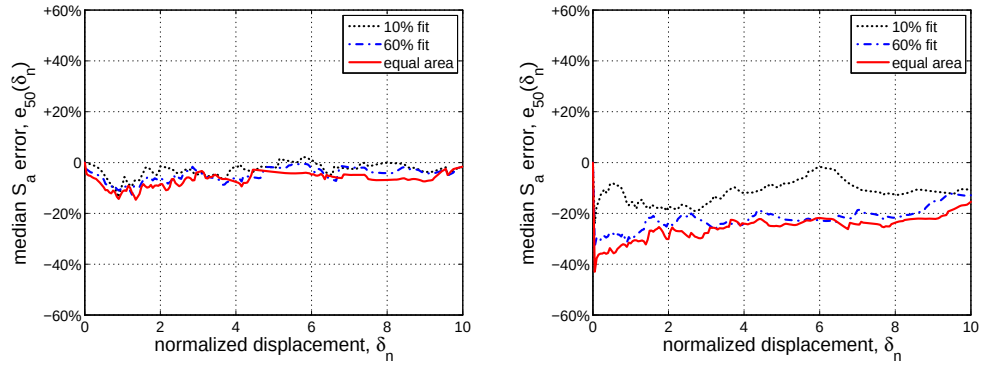

Figure 5.7. The relative error in the median S_a-capacity of the 10%, 60% and equal area fits for T = 2.0 s, when applied to the capacity curves of Figure 5.3: (a) insignificant versus (b) significant changes in initial stiffness.

Obviously, the shape of the original backbone has a significant impact. In all cases, the error increases with curvature while its maximum always appears at the earlier backbone segments. Curiously, the 10% fit leads to a remarkable decrease in the error for any deformation level, even for the highly curved shape of Figure 5.3b where it clearly violates any notion of equal area (or *equal energy*) that seems to be prevalent in current guidelines. It leads to a slightly non-conservative estimation of the capacity for displacements before the full plasticization (for δ_n up to 1) and only for short-period systems, T = 0.2 s (Figure 5.4). In addition, even in case of highly-curved backbones (Figure 5.4b)

only a 10% underestimation appears at most. Conversely, code approaches are always conservative for all the displacement levels and all the shapes considered, but at a cost of almost 20%÷40% underestimation of capacity. The trends identified are generally confirmed for all other periods considered. As noted previously, such conclusions are mirrored when operating on demands, e.g., via equation (5.2) rather than capacities. Thus, for example, code fits are found to cause a significant (conservative) overestimation of displacement demand at all levels of intensity in comparison to the near-optimal 10% fit.

To verify the above observations, a sample of five different generalized elastic-plastic shapes (see Figure 5.8a) was also considered for each of the two hysteretic rules described in section 2 and shown in Figure 5.8b.

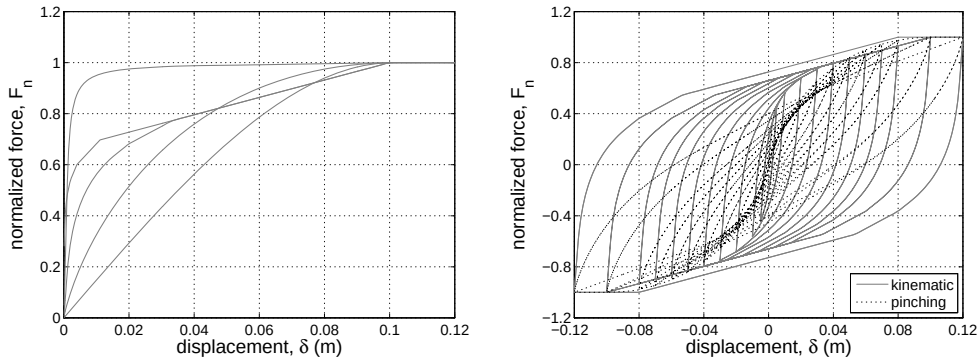

Figure 5.8. (a) The backbones and (b) the two hysteretic rules considered for the generalized elastic-plastic system sample.

Figure 5.9 to Figure 5.12 display the statistics of the relative error on the median S_a-capacity evaluated at each period for the proposed 10% fit versus the conventional FEMA-style 60% fit. The bias is evaluated up to δ_n = 2, where most of the significant differences appear. The hysteretic rules were found to be relatively insignificant, as the magnitude of the error depends primarily on the shape of the fitted backbone (see also Vamvatsikos and Cornell, 2006); this result has also been confirmed for other types of backbones and essentially frees us from the problem of having a hysteresis-dependent optimal fit. Hysteresis aside, all the previously drawn conclusions are confirmed.

The 10% fit enjoys an insignificant bias, on average, for all the periods considered and its error never exceeds 20%. FEMA-style fits (60% fit), and similarly EC8-style approximations, again show a strictly negative; i.e., conservative, bias of 20% or even 60%, depending on the shape of the original backbone, most of which is concentrated at the low displacement range. However, if the target displacement falls in this region, a strict application of the code guidelines would reduce the latter effect as they call for a more localized fit.

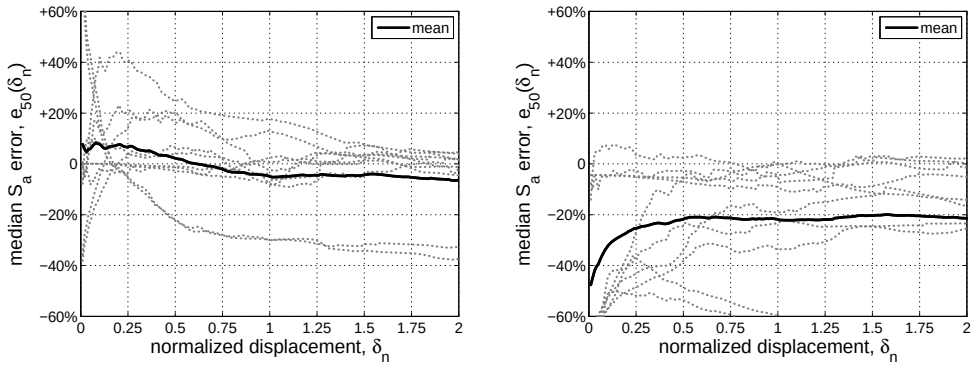

Figure 5.9. The mean of the relative error in the median S_a-capacity for (a) the 10% fit and (b) the 60% fit, for a reference period of T = 0.2 s and for ten generalized elastic-plastic systems, represented by. the grey dotted lines.

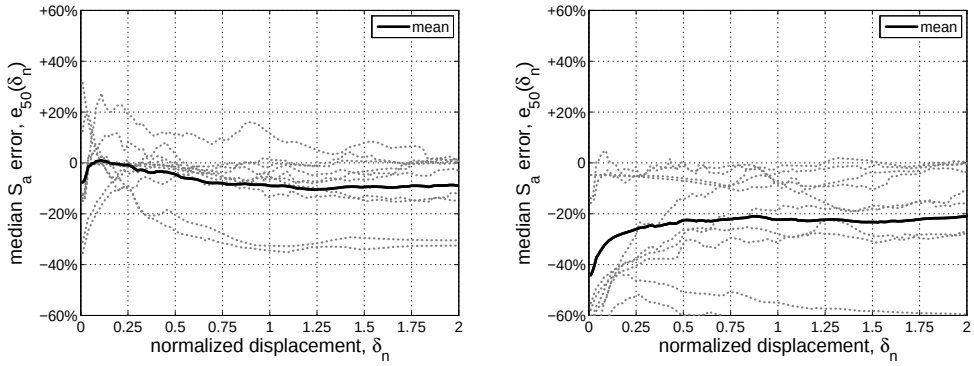

Figure 5.10. The mean of the relative error in the median S_a-capacity for (a) the 10% fit and (b) the 60% fit, for a reference period of T = 0.5 s and for ten generalized elastic-plastic systems, represented by. the grey dotted lines.

The above stated results must still be viewed with caution whenever the equivalent "fitted" and the reference "exact" period differ significantly (Vamvatsikos, 2011). Since the 10% rule, by nature, maintains a close match to the actual period, our conclusions regarding its excellent performance remain robust. On the other hand, the code-based fits may result to disproportionately large equivalent periods for highly-curved backbones. Then, the results of a more accurate MAF-based performance comparison might differ from the S_a-based results discussed above depending on the nature of the seismic hazard.

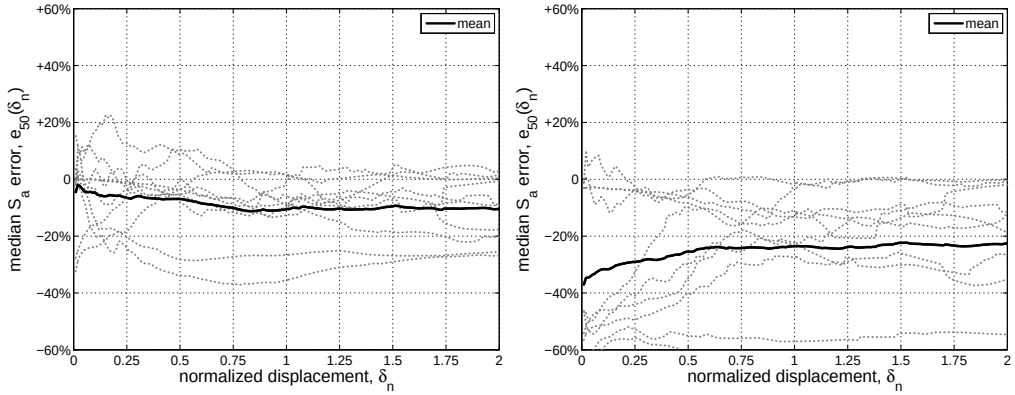

Figure 5.11. The mean of the relative error in the median S_a-capacity for (a) the 10% fit and (b) the 60% fit, for a reference period of T = 1.0 s and for ten generalized elastic-plastic systems, represented by. the grey dotted lines.

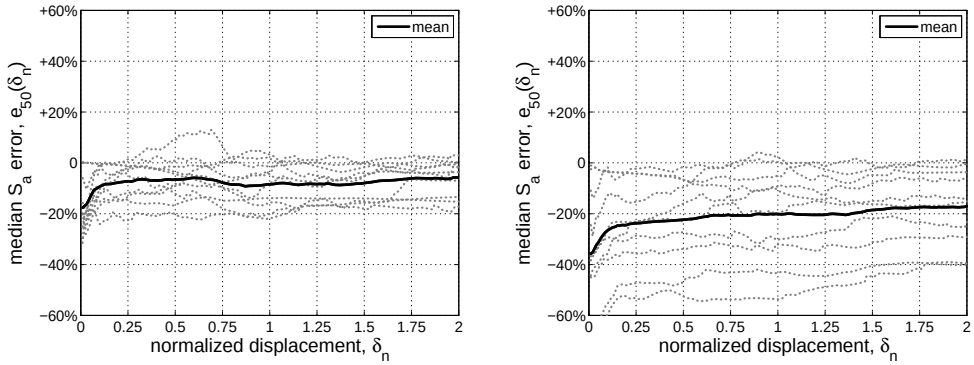

Figure 5.12. The mean of the relative error in the median S_a-capacity for (a) the 10% fit and (b) the 60% fit, for a reference period of T = 2.0 s and for ten generalized elastic-plastic systems, represented by. the grey dotted lines.

Actually, it is possible that employing a code-based fit for NSP assessment may prove to be unconservative due to this effect. For example, if using a uniform-hazard spectrum with significant differences between short and long-period hazard, the 20%÷40% conservative bias predicted earlier can be nullified or reversed. This restriction should be kept in mind for all comparisons in the following sections.

Error comparisons for the S_a-capacity dispersion (record to record) are not shown as all fits generally achieve equally good estimates. Of course, differences appear in the region preceding the nominal yield point of each approximation. Therein the fitted system will predict no dispersion, being essentially elastic and perfectly predicted by S_a, whereas the actual one shows some small variability due to early inelasticity. This is to be expected and it cannot weigh in favor of one fit over another.

Summing up, it can be stated that capturing the initial stiffness of the actual backbone is of primary importance. Existing guidelines fail to achieve this for highly curved backbones, leading to biased results that may become overly conservative. Thus, the optimal fit should capture, as close as possible, the initial stiffness of the backbone, being careful to avoid unreasonable estimates for initially ultra-stiff systems that very quickly lose their initial properties. Thus, fitting the "elastic" secant at 5% or 10% of the maximum base shear, as opposed to 0.5% or 1%, is considered a robust strategy that delivers excellent results.

5.4.2. Bilinear fits of generalized elastic-hardening systems

The second family of shapes investigated is characterized by a generalized elastic-hardening behavior. Only the pinching hysteretic rule was considered, given the insignificant differences observed earlier when compared to the kinematic hardening. Each backbone investigated is characterized by different curvatures and final hardening stiffness, allowing a wide coverage of the typical shapes that can be obtained considering different structural behaviors and modeling options.

In analogy with the previous subsection, two different backbones will be

presented in detail. The first (Figure 5.13a) is characterized by mild changes in the oscillator stiffness, in contrast to the second (Figure 5.13b). The target displacement is assumed to be equal to 0.2m. The EC8 fit is not applied as it is restricted to elastic-plastic approximations which are clearly inferior for the shapes shown in Figure 5.13.

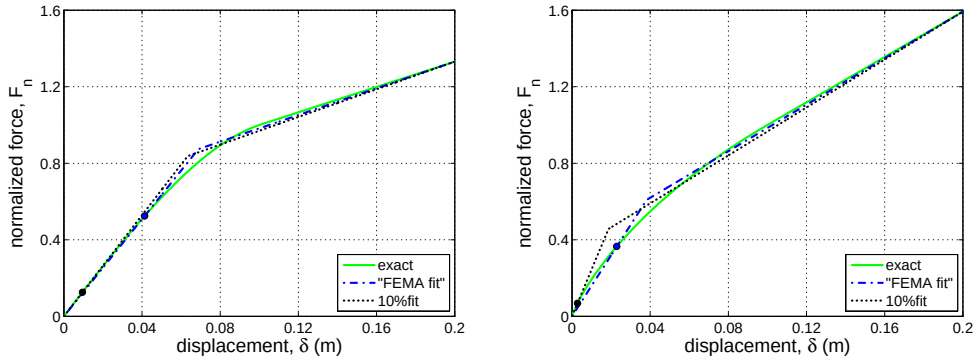

Figure 5.13. Comparison of generalized elastic-hardening capacity curves and their corresponding fits having (a) insignificant versus (b) significant changes in initial stiffness. Note 0.2 displacement becomes 2.0 normalized.

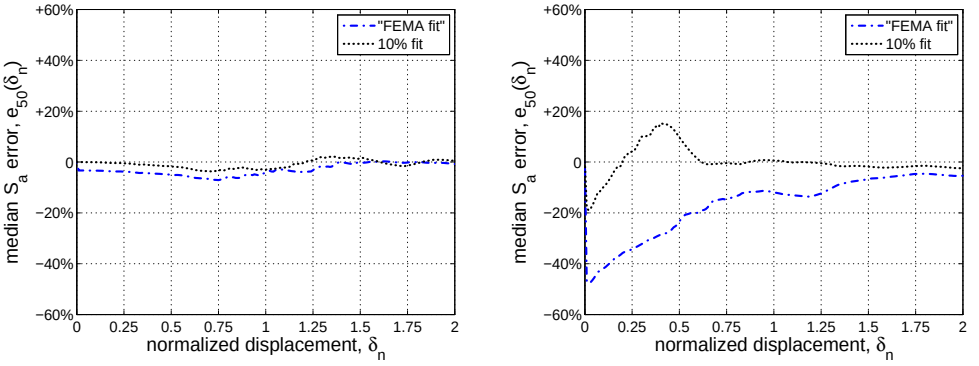

Figure 5.14. The relative error in the median S_a-capacity of the "FEMA fit" and 10% fit for T = 0.2 s, when applied to the capacity curves of Figure 5.13: (a) insignificant versus (b) significant changes in initial stiffness.

On the other hand, the "FEMA fit" rule can be applied without problems, although, strictly speaking it might call for slightly different approximations depending on the value of the target displacement. Still, the results and the

corresponding conclusions remain the same in all cases. The alternative fit proposed, based on the 10% rule, determines the initial stiffness at 10% (instead of 60%) of the nominal yield shear defined in accordance with FEMA, while the post-elastic stiffness is determined by minimizing the absolute area discrepancy between the capacity curve and the fitted line.

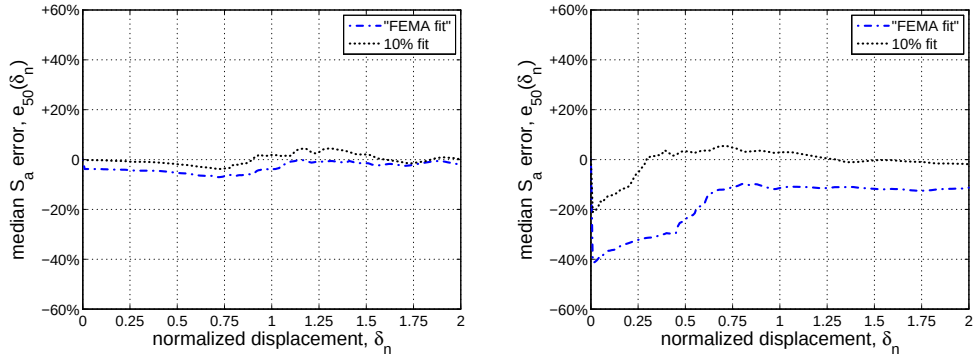

Figure 5.15. The relative error in the median S_a-capacity of the "FEMA fit" and 10% fit for T = 0.5 s, when applied to the capacity curves of Figure 5.13: (a) insignificant versus (b) significant changes in initial stiffness.

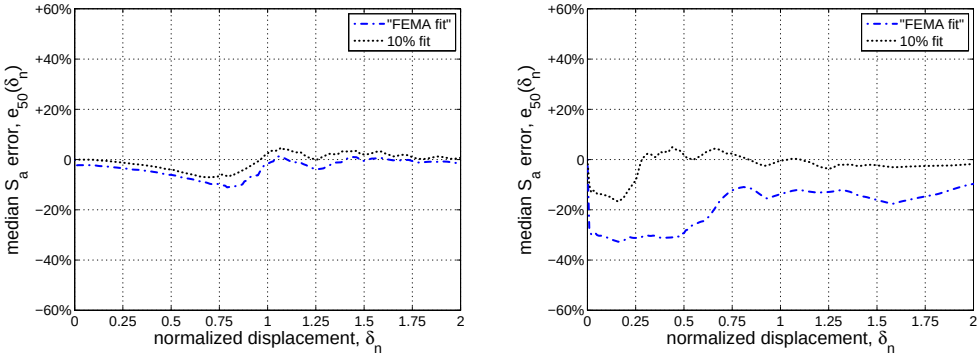

Figure 5.16. The relative error in the median S_a-capacity of the "FEMA fit" and 10% fit for T = 1.0 s, when applied to the capacity curves of Figure 5.13: (a) insignificant

The area minimization leads to similar results as the balancing of areas above and below the fitted line. While easy to apply graphically, the latter is an ill-defined problem that can yield mixed results: imagine two coincident equal-size linear segments where one, the "approximation", is rotated by an arbitrary

angle around the common center. Obviously, the rotated segment always satisfies the area balancing rule as a valid approximation to the original. Only when it becomes coincident it does satisfy the minimum area criterion. Thus, area minimization is algorithmically and mathematically superior. In total, the proposed rule came out as the simplest standardizable rule with a near-minimum error for this family of backbones. In fact, many other alternatives were considered, they are not shown for the sake of brevity. It suffices to say that capturing the initial stiffness by a secant in the range of 5%÷10% of the peak strength (or the nominal yield point) remains the most important aspect of any successful fit. The definition of the nominal yield point is made according to FEMA (FEMA-356, 2000; FEMA-440, 2005) provisions, thus the imposed intersection at 10% in alternative to the suggested 60% represents the only difference with the codified approach.

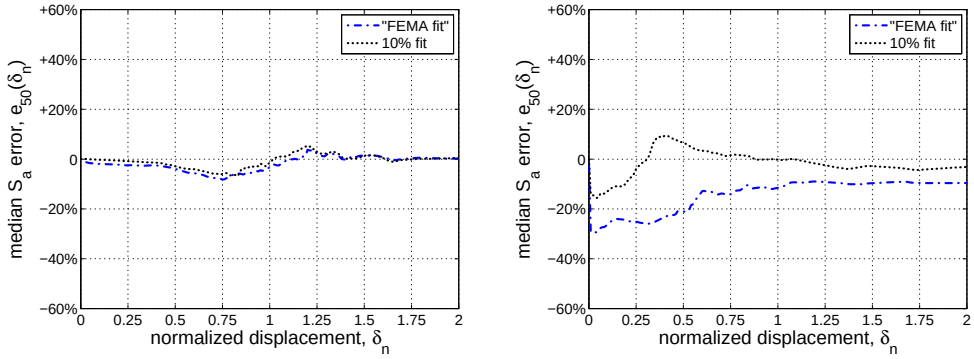

Figure 5.17. The relative error in the median S_a-capacity of the "FEMA fit" and 10% fit for T = 2.0 sec, when applied to the capacity curves of Figure 5.13: (a) insignificant versus (b) significant changes in initial stiffness.

The results of the proposed and the FEMA fitting procedures applied to the example shapes appear in Figure 5.13. Obviously, when the stiffness of the backbone is not characterized by abrupt changes in the curvature (Figure 5.13) both fits tend to be practically the same. Figure 5.14 to Figure 5.17 show the error introduced by each fit, for both backbone shapes considered in Figure 5.13, in the cases of T = 0.2, 0.5, 1.0 and 2.0 s, respectively.

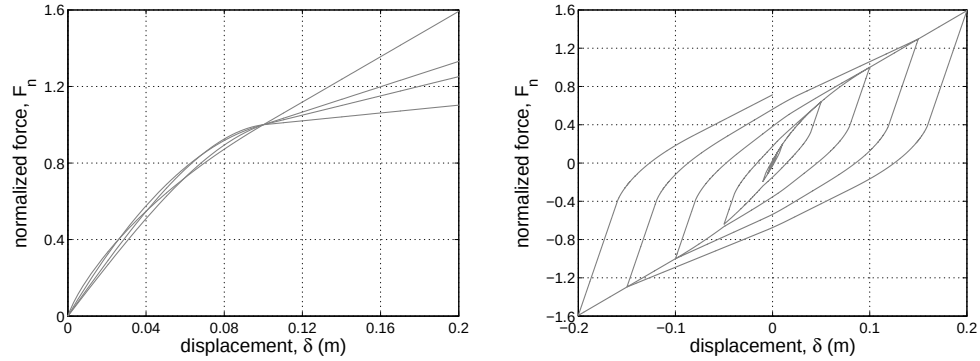

Figure 5.18. (a) The backbones and (b) the hysteretic rule considered for the generalized elastic-hardening system sample.

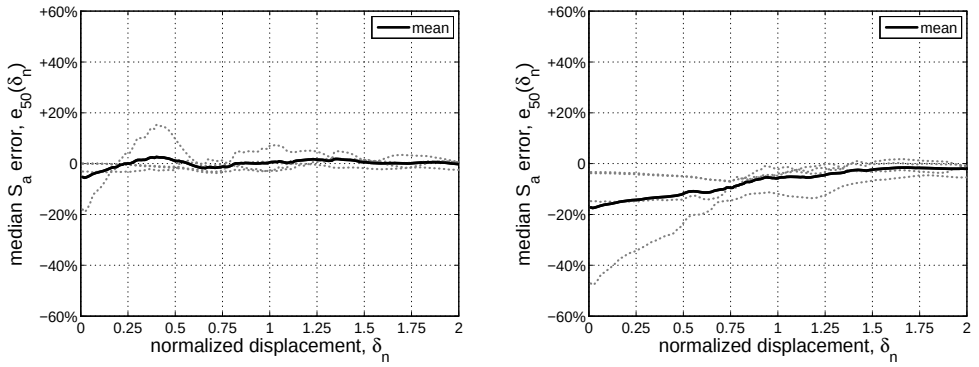

Figure 5.19. The mean of the relative error in the median S_a-capacity for (a) the 10% fit and (b) the "FEMA fit", for a reference period of T = 0.2 sec and for four generalized elastic-plastic systems, represented by the grey dotted lines.

In analogy with the results presented for the elastic-plastic case, most of the error is concentrated at the beginning of the backbone. In the case of the backbone with low changes in the stiffness (low curvature), it can be observed that the error is very small and very similar for both fits. A higher curvature of the backbone increases the error introduced by the fit and emphasizes that, although at the target displacement the backbones and their fits in both cases are coincident, this is not enough to warrant the same error. The earlier fitted segments, and especially the equivalent period extracted, can make a significant difference. As the *10% fit* manages to capture the initial stiffness better, it provides better predictive capability for higher displacements as well.

Capturing the initial stiffness is the key issue in the fitting procedure, while the fitted hardening segment is an additional improvement. In fact, replacing the hardening segment with a plastic plateau intersecting the actual backbone at the target displacement (in this case 0.2 m) gave quite satisfactory results, at least for the cases at hand.

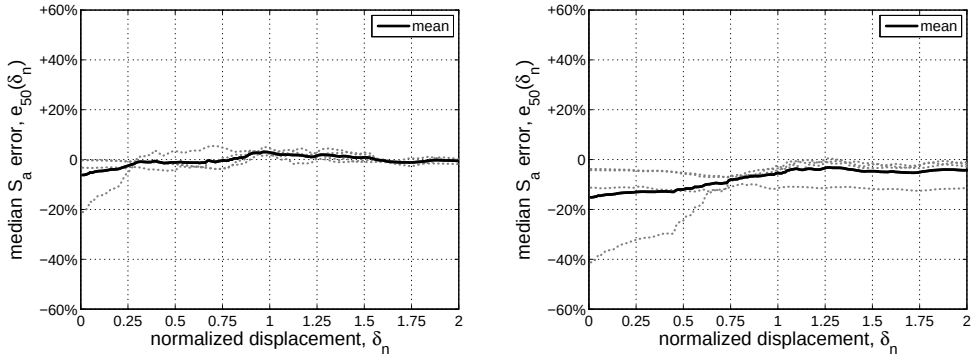

Figure 5.20. The mean of the relative error in the median S_a-capacity for (a) the 10% fit and (b) the "FEMA fit", for a reference period of T = 0.5 sec and for four generalized elastic-plastic systems, represented by the grey dotted lines.

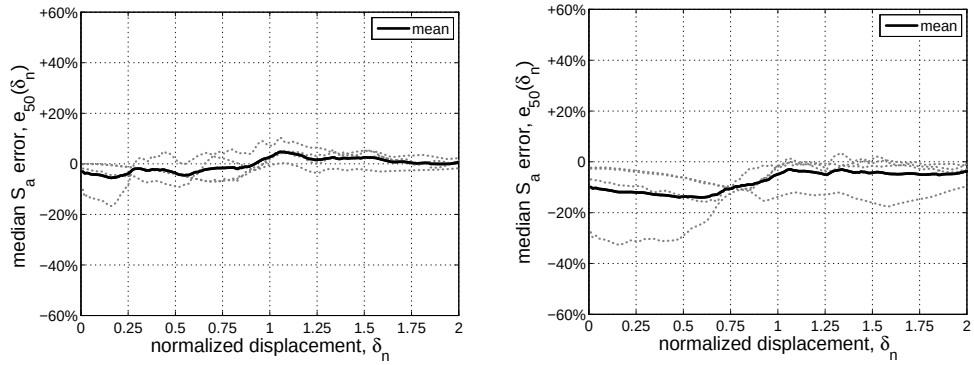

Figure 5.21. The mean of the relative error in the median S_a-capacity for (a) the 10% fit and (b) the "FEMA fit", for a reference period of T = 1.0 sec and for four generalized elastic-plastic systems, represented by the grey dotted lines.

For further verification a family of four different shapes is considered, shown in Figure 5.18a where only the pinching hysteretic rule is used (Figure 5.18b). In Figure 5.19 to Figure 5.22 the relative errors in the median S_a-

capacity, are compared for T = 0.2s, 0.5s, 1.0s and 2.0s. Again, the proposed fit leads to a small and relatively unbiased error, which seldom exceeds 10%. In this case the sample of backbones considered for the elastic-hardening case was smaller than the elastic-plastic case, but the robustness of the general results, showing the same trends in both cases, supports the remarks. It should be noted that the results of the FEMA approximation will improve somewhat at low displacements if we refit for a lower target displacement, but not enough to alter the above conclusions.

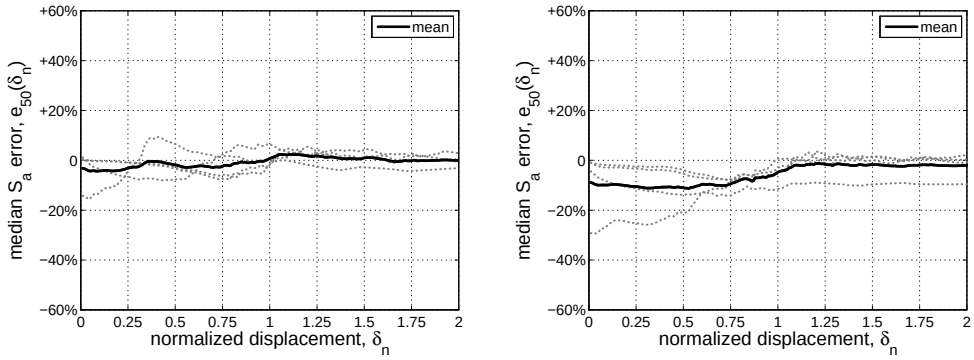

Figure 5.22. The mean of the relative error in the median S_a-capacity for (a) the 10% fit and (b) the "FEMA fit", for a reference period of T = 2.0 sec and for four generalized elastic-plastic systems, represented by the grey dotted lines.

5.5 Multilinear fits for softening behavior

Fitting the negative stiffness part of the static pushover curve has lately become an option in NSP. In some cases (e.g., Italian provisions, CS. LL. PP., 2009) an elastoplastic fit is simply extended to cover some portion of the early negative stiffness range while in others (e.g. FEMA-440, 2005) an additional negative stiffness linear segment is utilized. Until fairly recently, the negative-stiffness segment was typically employed only indirectly either to achieve demand modification (FEMA-356, 2000) or to set a limit on the allowable R-factor (ASCE/SEI 41-06, 2007; FEMA-440 2005) due to the lack of appropriate R-μ-T relationships. With the emergence of SPO2IDA (Vamvatsikos and Cornell, 2006), it is now possible to achieve full-range direct seismic demand

and capacity estimation for trilinear or quadrilinear backbone approximations that include negative stiffness.

5.5.1. *Elastoplastic fits for generalized elastic-hardening-negative systems*

The recent seismic Italian seismic code (CS. LL. PP., 2009) suggests that elastoplastic systems with extended plateaus may be used to capture negative-stiffness behaviors up to a 15% loss of the peak base shear capacity. Specifically, the Italian code is essentially a derivative of the FEMA-356 rule where a 60%-secant defines the initial stiffness and an area-balancing criterion is used to get the plastic plateau which may now be extended into the negative stiffness range. Obviously, the yield strength of such a fit is always lower than the peak strength of the exact backbone.

To verify the feasibility of such an approach a direct search was undertaken for different plateau levels and "elastic" secant values that could provide the optimal solution. Out of the large number of candidate fits tried, only four will be showcased (Figure 5.23a) on a highly-curved backbone out of a family of twelve (Figure 5.23b).

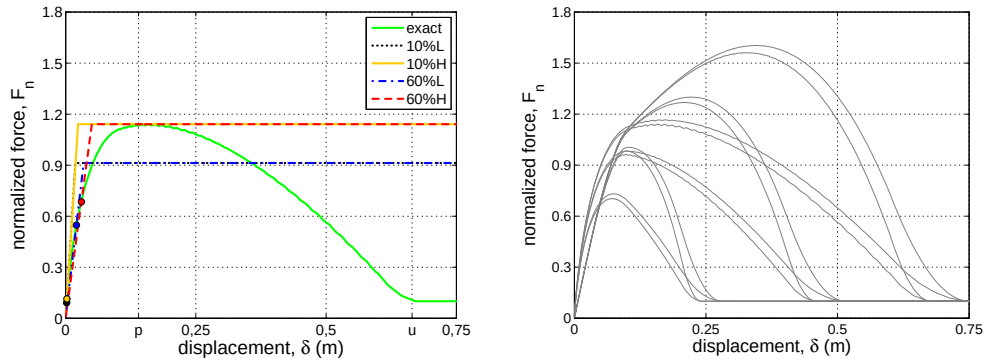

Figure 5.23 (a) An example of generalized elastic-hardening-negative capacity curve having significant changes in initial stiffness and its corresponding fits, (b) the backbones considered for the generalized elastic-hardening-negative system sample.

The initial stiffness is set at 10% and 60% of nominal yield strength

combined with two plateau levels at 80% (L) and 100% (H) of peak shear strength respectively. The corresponding candidate rules are named 10%L, 10%H, 60%L and 60%H, and their performance is shown in Figure 5.24a and Figure 5.24b for 0.2 s and 1.0 s, respectively. Results show that capturing the initial part of the backbone is still important, as the 10% fit substantially improves results whenever there are significant curvature changes in the exact backbone. Furthermore, foregoing any notions of area-minimization or balancing to match the peak point (H versus L fits) instead, is always beneficial. The Italian fit rule will always have a plateau height between 80% and 100% therefore it displays a performance right between the 60%H and 60%L cases, in general showing a 20%÷40% conservative bias.

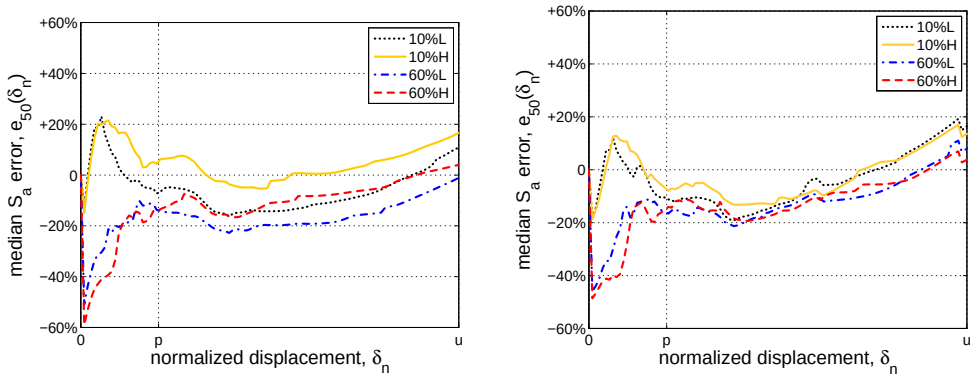

Figure 5.24. The relative error in the median S_a-capacity of the 10%L, 10%H, 60%L and 60%H fits for (a) T = 0.2 s and (b) T = 1.0 s, when applied to the capacity curve of Figure 5.23a.

The sample family of twelve backbones considered (Figure 5.24b) was also tested for the two opposing rules of 60%L and 10%H. Figure 5.25 to Figure 5.28 display the relative median *Sa*-capacity errors plotted against a displacement axis that has been normalized for each backbone separately to ensure that the peak (p) and the ultimate (u) displacement points are aligned. The results verify that the 10%H fit is an unbiased fit approach with robust performance, at least up to the point where the structure loses about 20% of its maximum strength. Consequently, it makes sense to suggest that an optimized

rule should forego any strict area-minimization (or balancing) considerations in favor of accurately capturing the maximum base shear strength. Failing to follow this approach, the Italian code rule was, again, found to be generally conservative, in analogy with other code fits. On the other hand, the limit that it enforces when extending the plastic plateau finds a solid confirmation in the results; in fact, none of the bilinear fits considered can adequately simulate the softening behavior beyond 20% shear loss, resulting in a systematical unconservative underestimation of the actual response.

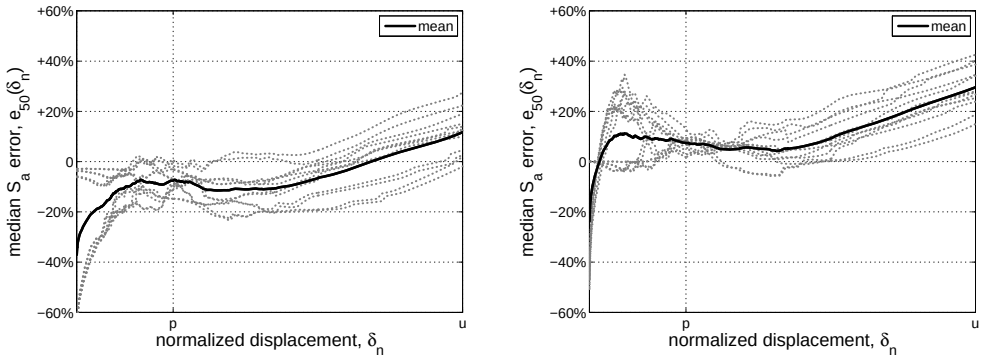

Figure 5.25. The mean of the relative error in the median S_a-capacity for (a) the 60%L and (b) 10%H fits, applied to the capacity curves of Figure 19b, for T = 0.2 s.

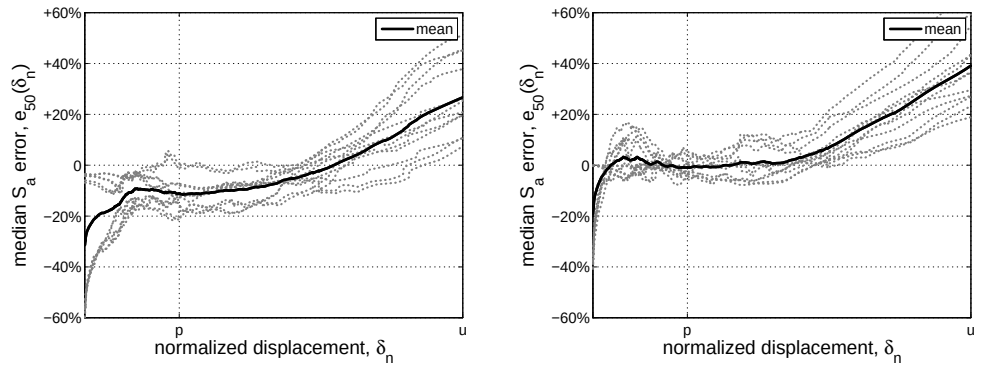

Figure 5.26. The mean of the relative error in the median S_a-capacity for (a) the 60%L and (b) 10%H fits, applied to the capacity curves of Figure 19b, for T = 0.5 s.

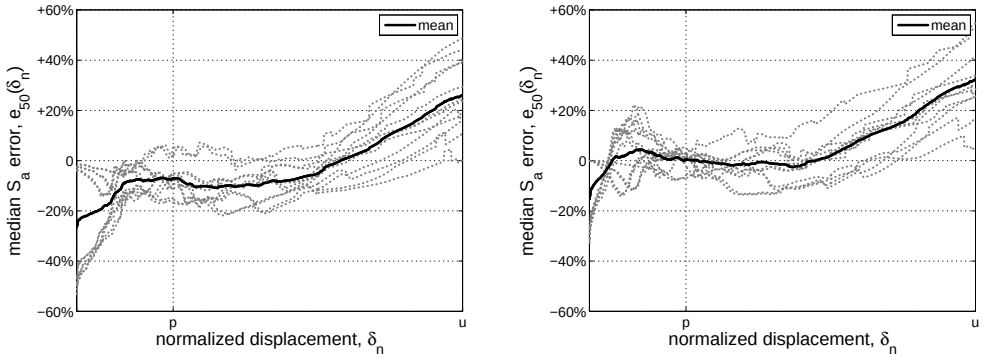

Figure 5.27. The mean of the relative error in the median S_a-capacity for (a) the 60%L and (b) 10%H fits, applied to the capacity curves of Figure 19b, for T = 1.0 s.

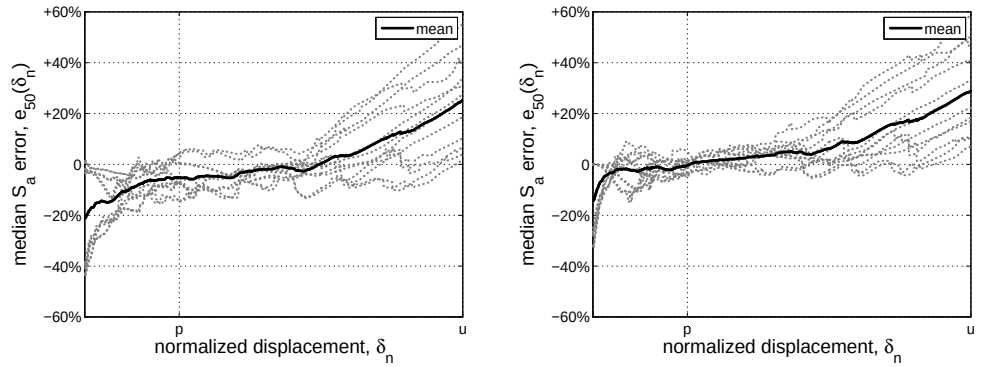

Figure 5.28. The mean of the relative error in the median S_a-capacity for (a) the 60%L and (b) 10%H fits, applied to the capacity curves of Figure 19b, for T = 2.0 s.

5.5.2. *Multilinear fits of generalized elastic-hardening-negative systems*

It is easy to recognize that if the softening behavior is characterized by mild changes in the negative slope, any negative stiffness segment that links the peak point with any other specific point in the softening branch (such as 60% of the nominal yield strength suggested in ASCE/SEI 41-06) will allow a reliable fit that captures softening behavior. The difficulties in determining a single reliable slope for the softening branch arise when the capacity curve is characterized by significant changes such as a steep segment followed by a milder one or a milder slope followed by a steeper one and any combinations

of the two. Such phenomena, while rare in the hardening range, can appear quite frequently in the softening range, thus, typically complicating the fit.

A wide family of capacity curves with non-trivial softening shapes is employed to establish a reliable fitting criterion independent from the specific shape considered, to be employed in any situation. In addition, a large number of competing fitting-rules was considered of which only the most promising will be shown. Figure 5.29 show two examples of generalized elastic-hardening-negative backbones that differ in two main aspects: the first (Figure 5.29a) is characterized by a nearly linear initial elastic part with a somewhat steep-mild (i.e. first steep then mild) trend in the softening segment; the second one (Figure 5.29b), conversely, is characterized by significant curvature in the elastic-hardening part of the backbone and a mild-steep trend in softening.

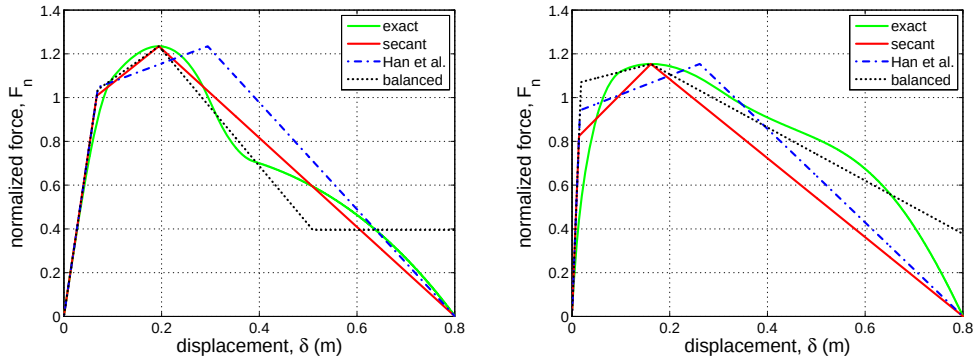

Figure 5.29. Comparison of generalized elastic-hardening-negative capacity curves and their corresponding fits having (a) steep-mild (b) mild-steep trend in the softening slope.

Three different fitting approaches are shown for each backbone. To provide a reference basis, for all three fits, the pre-peak part of the backbone is approximated according to the optimal rule of section 5.4.2, i.e. using a 10% rule with area-minimization for the hardening segment that terminates at the peak strength. To determine the softening segment, which extends from the peak point to the ultimate, three different approaches are considered: (a) the first, termed *secant*, employs the slope linking the peak point with the ultimate; (b) the second, termed *Han et al.*, which follows the graphical approach

suggested in (Han et al., 2010), provides as softening slope the bisector between the *secant* slope and the softening segment that captures the slope at the end of the backbone ending up at the peak strength; (c) the third, termed *balanced*, uses area-minimization to fit the slope utilizing both a negative slope and a horizontal residual strength segment wherever needed. In all cases, the fit is terminated at the ultimate displacement, if necessary by assuming a vertical drop to zero strength.

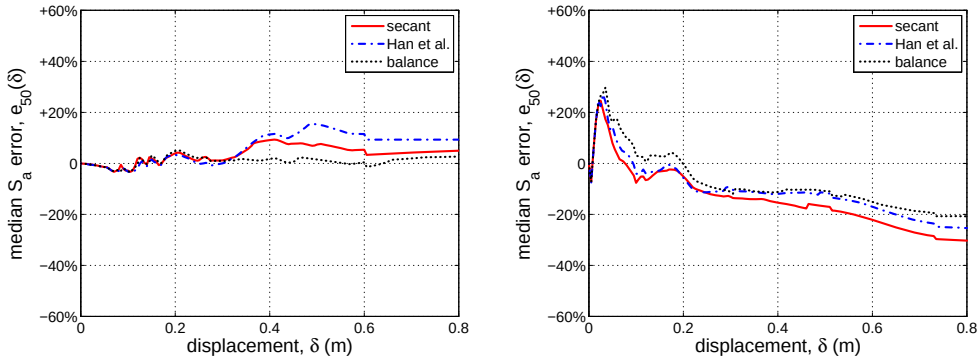

Figure 5.30. The relative error in the median S_a-capacity of the secant, Han et al and balanced fits for T = 0.2 s, when applied to the capacity curves of Figure 5.29: (a) steep-mild versus (b) mild-steep trend in the softening slope.

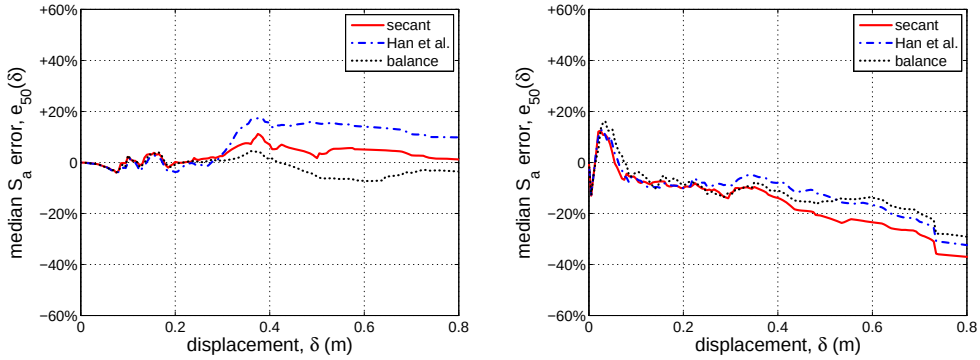

Figure 5.31. The relative error in the median S_a-capacity of the secant, Han et al and balanced fits for T = 0.5 s, when applied to the capacity curves of Figure 5.29: (a) steep-mild versus (b) mild-steep trend in the softening slope.

The errors introduced by each fit are shown in Figure 5.30 and Figure 5.33 respectively for T = 0.2 s, 0.5s, 1.0s and 2.0s. For the steep-mild case (Figure 5.29b) the balanced and the secant fit are clearly the best, with the former being slightly on the conservative side. In the mild-steep case, the balanced and the Han et al. approach are practically indistinguishable, clearly outperforming the secant fit. Taking into account numerous tests, not shown, it is the area-minimization fit that generally offers the best performance across different shapes and periods. Still, it is not strictly optimal.

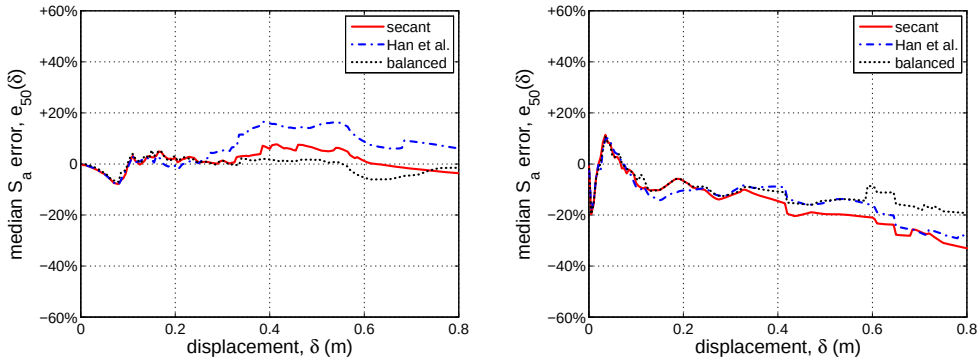

Figure 5.32. The relative error in the median S_a-capacity of the secant, Han et al and balanced fits for T = 1.0 s, when applied to the capacity curves of Figure 5.29: (a) steep-mild versus (b) mild-steep trend in the softening slope.

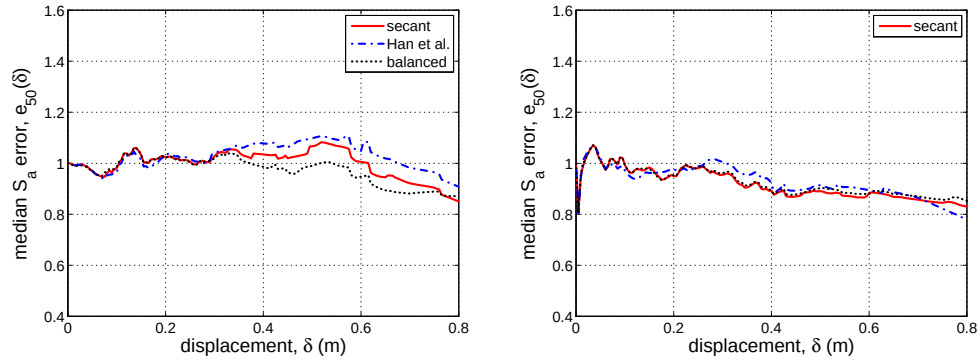

Figure 5.33. The relative error in the median S_a-capacity of the secant, Han et al and balanced fits for T = 2.0 s, when applied to the capacity curves of Figure 5.29: (a) steep-mild versus (b) mild-steep trend in the softening slope.

Curiously, all three fits are conservatively biased in the case of Figure 5.29b. They were found to be even more so for extreme steep-mild behavior in Figure 5.34a. In both these highly curved backbones, a linear softening segment, or a softening-residual segment combination that would produce near-zero error would need to be high above and to the right of the actual backbones, clearly enveloping them in the negative stiffness range.

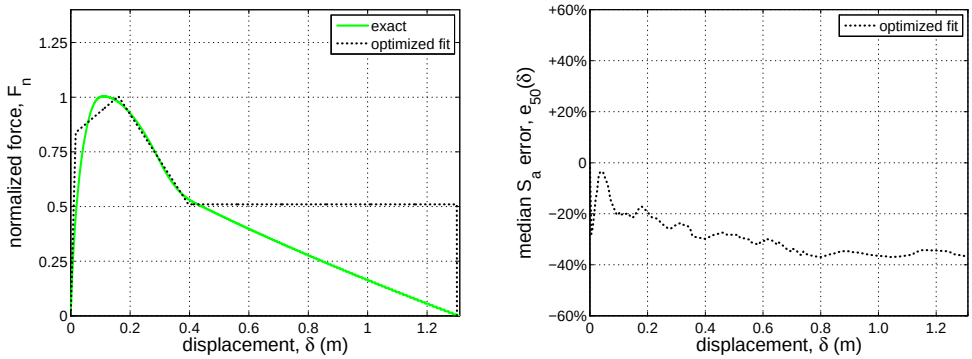

Figure 5.34. A generalized elastic-hardening-negative capacity curve having *extreme* mild-steep negative slope and its corresponding optimized fit, (a) the curve (b) relative median Sa-capacity errors for T=1.0 s.

Apparently, the inherent curvature of the actual backbone has a protective effect on the system that cannot be replicated by a linear segment and cannot be easily captured in a practical format. A possible explanation is that typical ground motion records (even of non-pulse-like ordinary type) produce most of the damage in just one or two large pushes in the nonlinear range. Perhaps the change in stiffness, and correspondingly in the tangent period, take the edge off any large nonlinear excursion that can proceed unchecked in a constant-stiffness linear segment. Especially for the extreme steep-mild case of Figure 5.34a this effect is so strong that even using a residual plateau that starts at the intersection of the two different slopes and maintains the same strength until the ultimate displacement is not enough to reach a fully unbiased solution (Figure 5.34b). Nevertheless, the latter amendment to the area-minimization rule was found to be the only simple practical rule that can reliably reduce the bias in all such cases to an acceptable level of 20%÷30%.

Therefore, this will form the final part of our "optimal" practical fitting rule.

5.6 Definition and testing of the optimized fit

Combining all previous results, it is now possible to propose an "optimal" fitting rule that, while not strictly optimized, manages to maintain low error and low bias and can be standardized to be applicable to a wider range of capacity curve shapes than the ones investigated. Essentially, it is based on fitting the distinct regions of structural behavior observed in all realistic pushover curves, namely "elastic", "hardening" and "softening"; see (Vamvatsikos, 2011). These will be approximated by linear segments defined by three specific points, namely the nominal yield (y), the nominal peak strength (p) and the ultimate displacement (u) point:

a) The "elastic" pre-nominal-yield part is captured by a secant linear segment with initial stiffness matching the secant stiffness of the capacity curve at 5%÷10% of the peak or the nominal yield base shear. Using the peak is preferable as, without any loss of accuracy, it allows a fast estimation without needing multiple iterations.
b) The "hardening" pre-peak non-negative stiffness segment is chosen to terminate at the maximum base shear while minimizing the absolute area difference (formally the integral of the difference) of the fitted and the exact curve between the displacements corresponding to the nominal peak and the nominal yield points, as defined by the intersection of this segment with the preceding and succeeding one.
c) The "softening" post-peak negative stiffness segment is also defined by minimizing the absolute area difference between the fitted and the exact curve in the negative stiffness region. It may be further augmented by a fourth, residual plateau segment. If the negative stiffness region is characterized by steep slopes that partway down grow significantly milder, the plateau should be drawn at the intersection of these two distinct zones. If instead the negative stiffness progressively grows steeper, then any residual should be fitted according to the area-minimization rule.

To properly assess the error induced by the proposed rules, a new separate sample of curves is needed for blind testing. Forty capacity curves were randomly generated considering relatively highly curved shapes with non-trivial softening behavior, thus including either steep-mild or mild-steep negative slopes combined with various rates of change in the initial stiffness, as shown in Figure 5.35a.

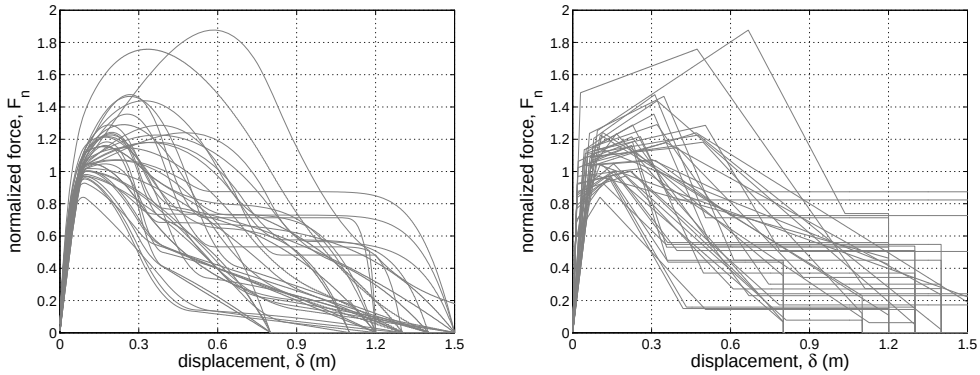

Figure 5.35. Blind testing sample of (a) capacity curves and (b) their optimized fits.

Essentially they are complex shapes meant to provide a severe test for the proposed rule. Each curve was fitted according to the "optimal" fitting rule, resulting in the forty fits showed in Figure 5.35b. The relative median capacity errors appear in Figure 5.36 and Figure 5.37 for 0.2 and 0.5 seconds and 1.0 and 2.0 seconds, respectively. To facilitate comparison, the displacement axis has been non-homogeneously normalized to match the three characteristic points (y, p, u) of the exact pushover curves. The mean value of the error never exceeds 20% and the trend is always conservative except for the first part of the hardening behavior (between y and p points) when low period values are considered (see Figure 5.36a). Still, due to the deliberate complexity of the tested curves, even the low errors shown may be higher than average.

In Figure 5.38 normal probability plots of the errors are shown at the three characteristic points for T = 0.2 and 2.0 seconds and for all the forty curves considered, showing a strong resemblance to a normal distribution. Table 5-1 shows mean and standard deviation of the relative errors at the three

characteristic points *y*, *p* and *u*, respectively for T = 0.2 s, 0.5 s, 1.0 s, and 2.0 s; the data shows that the distributions are generally conservative (negative errors). Some slightly unconservative bias can be found only at the yielding point (*y*) for T = 0.2 s.

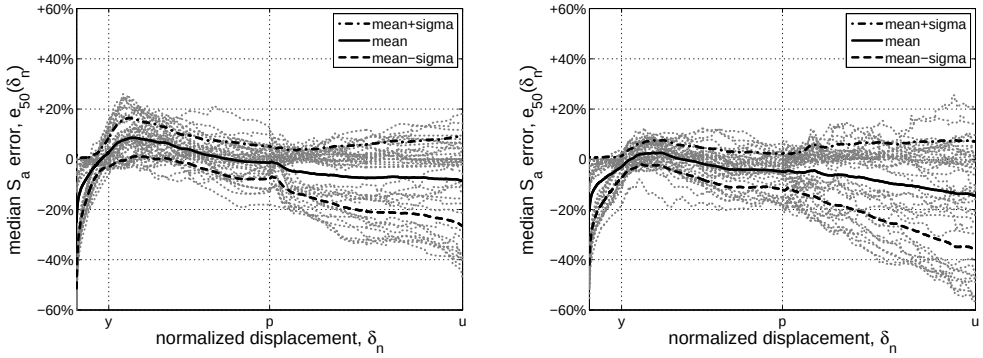

Figure 5.36. The statistics of the relative error in the median S_a-capacity for T = 0.2 sec (a) and for T = 0.5 sec (b), in the case of elastic-hardening-negative SDOF systems considered for blind testing of the optimized fit (grey dotted lines).

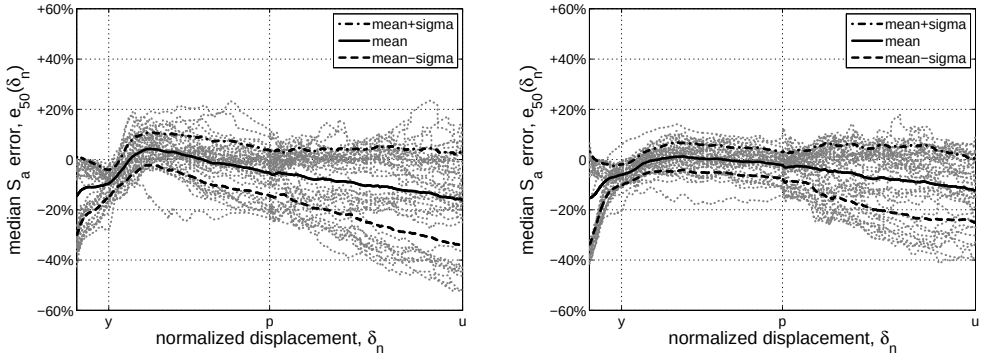

Figure 5.37. The statistics of the relative error in the median S_a-capacity for T = 1.0 sec (a) and for T = 2.0 sec (b), in the case of elastic-hardening-negative SDOF systems considered for blind testing of the optimized fit (grey dotted lines).

A Kolmogorov-Smirnov hypothesis test (Massey, 1951) was performed on the sample of forty relative errors at each of the three characteristic points (*y*, *p* and *u*) for each of the four periods. At the 95% significance level this cannot reject the null hypothesis that they follow normal distributions with the

means and standard deviations shown in Table 5-1; the only exception is the ultimate (u) point for T = 0.2 s (see Figure 5.38a) due to some large tail values. Using such results, it is possible to have at least some general sense of the epistemic uncertainty introduced by the optimized piecewise linear approximation at the three different ranges of behavior. It goes without saying that the results for current code-based fits are far more dispersed and heavily biased towards the conservative range.

Table 5-1. Mean and standard deviation of the relative median error in Sa-capacity at the characteristic points y, p, u.

	T = 0.2 s			T = 0.5 s			T = 1.0 s			T = 2.0 s		
	y	*p*	*u*	*y*	*p*	*u*	*y*	*p*	*u*	*y*	*p*	*u*
μ	0.028	-0.013	-0.086	-0.030	-0.049	-0.143	-0.096	-0.053	-0.163	-0.060	-0.023	-0.122
σ	0.060	0.066	0.182	0.044	0.071	0.218	0.056	0.091	0.186	0.042	0.053	0.129

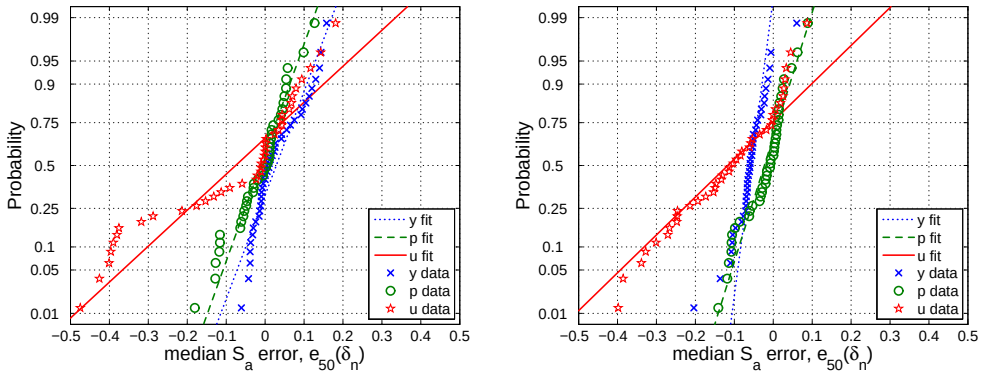

Figure 5.38. Probability plot for normal distribution of the relative errors in the median S_a-capacity evaluated at the three significant points y, p and u for T = 0.2 (a) and T=2.0 (b) seconds.

5.7 Conclusions

An optimal piecewise linear fit is presented for static pushover capacity curves that can offer nearly-unbiased low-error approximation of the dynamic response of realistic systems within the framework of Nonlinear Static Procedures. Incremental Dynamic Analysis is used to rigorously assess

different fits on an intensity-measure capacity basis, allowing a straightforward performance-based comparison that is largely independent of site hazard. An easy to apply optimal rule was derived that is based on using appropriate linear segments to capture the three typical ranges of structural behavior appearing in realistic pushover curves: (a) "elastic" where the initial stiffness should always be captured by a secant at 5%÷10% of the peak strength regardless of any area-balancing or minimization rules, (b) "hardening", where it is important to maintain the actual peak shear strength but not necessarily the corresponding displacement (c) "softening", where the ultimate displacement should always be matched while the linear segment itself should closely fit the negative stiffness pushover curve. In the latter case, if a significant lessening of the slope is observed with increasing displacements then an additional enveloping residual-plateau segment should be employed.

In addition, it was found that simple elastoplastic fits capturing the initial stiffness and the maximum strength may serve as very simple approximations in most practical situations even venturing into the early negative stiffness region. On the other hand, all codified approaches tested generally err on the conservative side, although high changes in initial stiffness may reverse this finding for certain sites. In general though, the error in code fits always increases disproportionately when encountering significant changes in stiffness, representative of models that account for uncracked stiffness or the gradual plasticization and failure of elements. In particular, the area-balancing fitting process prescribed by most codes is often the culprit. Its indiscriminate use ignores the strong beneficial effect of backbone shape and curvature, invariably introducing bias. The proposed optimized fit is found to significantly reduce the error introduced by the piecewise linear approximation, offering a practical solution to upgrade existing guidelines.

REFERENCES

American Society of Civil Engineers (ASCE), 2007. Seismic Rehabilitation of Existing Buildings, ASCE/SEI 41-06, Reston, Virginia.

Antoniou S., Pinho R., 2004. Advantage and limitations of adaptive and non-adaptive force-based pushover procedures, *Journal of Earthquake Engineering* **8**, 497-522.

Aschheim M., Browning J., 2008. Influence of cracking on equivalent SDOF estimates of RC frame drift, *ASCE Journal of Structural Engineering*, **134**(3), 511-517.

Bracci J.M., Kunnath S.K., A.M. Reinhorn, 1997. Seismic performance and retrofit evaluation of reinforced concrete structures, *Journal of Structural Engineering*, **123**, 3-10.

Chopra A.K. and Goel R.K., 2002. A modal pushover analysis procedure for estimating seismic demands for buildings, *Earthquake Engineering and Structural Dynamics*, **31**, 561-582, 2002.

Comité Européen de Normalisation, 2004. Eurocode 8 – Design of Structures for earthquake resistance – Part 1: General rules, seismic actions and rules for buildings. EN 1998-1, CEN, Brussels.

CS LL PP Circolare 617, 2009. Istruzioni per l'applicazione delle Norme Tecniche per le Costruzioni, Gazzetta Ufficiale della Repubblica Italiana 47, 2/2/2009 (in Italian).

Dolsek M., Fajfar P., 2004. Inelastic spectra for infilled reinforced concrete frames, *Earthquake Engineering and Structural Dynamics*, **33**, 1395–1416.

Elnashai A.S., 2001. Advanced inelastic static (pushover) analysis for earthquake applications, *Structural Engineering and Mechanics*, **12**, 51-69.

Fajfar P., Fischinger M., 1988. N2 – A method for non-linear seismic analysis of regular structures, *Proceedings of the 9th World Conference on Earthquake Engineering*, Tokyo, 111-116.

Federal Emergency Management Agency (FEMA), 2000. Prestandard and commentary for the seismic rehabilitation of buildings. Report No. FEMA-356, Washington, D.C.

Federal Emergency Management Agency (FEMA), 2005. Improvement of nonlinear static seismic analysis procedures. Report No. FEMA-440, Washington, D.C.

Fragiadakis M., Vamvatsikos D., Papadrakakis M., 2006. Evaluation of the influence of vertical irregularities on the seismic performance of a nine-storey steel frame, *Earthquake Engineering and Structural Dynamics*, **35**, 1489-1509.

Han S.W., Moon K., Chopra A.K., 2010. Application of MPA to estimate probability of collapse of structures, *Earthquake Engineering and Structural Dynamics*, **39**, 1259-1278.

Ibarra L.F., Medina R.A., Krawinkler H., 2004. Hysteretic models that incorporate strength and stiffness deterioration, *Earthquake Engineering and Structural Dynamics*, **34**, 1489-1511.

Krawinkler H., Seneviratna G.P.D.K., 1998. Pros and cons of a pushover analysis of seismic performance evaluation, *Engineering Structures*, **20**, 452-464.

Massey F.J., 1951. The Kolmogorov-Smirnov Test for Goodness of Fit, *Journal of the American Statistical Association*, **46**, 68-78.

Miranda E. and Bertero V.V., 1994. Evaluation of strength reduction factors for earthquake-resistant design, *Earthquake Spectra*, **10**(2), 357-379.

Vamvatsikos D. and Cornell C.A., 2002 Incremental Dynamic Analysis, *Earthquake Engineering and Structural Dynamics*, **31**, 491-514.

Vamvatsikos D. and Cornell C.A., 2004. Applied Incremental Dynamic Analysis. *Earthquake Spectra*, **20**, 523-553.

Vamvatsikos D., Cornell C.A., 2006. Direct estimation of the seismic demand and capacity of oscillators with multi-linear static pushovers through Incremental Dynamic Analysis, *Earthquake Engineering and Structural Dynamics*, **35**(9), 1097–1117.

Vamvatsikos D., Fragiadakis M., 2010. Incremental dynamic analysis for estimating seismic performance sensitivity and uncertainty, *Earthquake Engineering and Structural Dynamics*, **39**, 141-163.

Vamvatsikos D., 2011. Some thoughts on methods to compare the seismic performance of alternate structural designs. In: Dolsek M. (ed), Protection of Built Environment Against Earthquakes. Springer: Dordrecht.

Vamvatsikos D., De Luca F., 2011. Optimal-fitting algorithm for piecewise linear approximation of static pushover curves, (in preparation).

Vidic T., Fajfar P., Fischinger M., 1994. Consistent inelastic design spectra: strength and displacement, *Earthquake Engineering and Structural Dynamics*, **23**, 507-521.

PART III

MODELING OF DAMAGE STATES

Chapter 6

BRITTLE FAILURES IN EXISTING REINFORCED CONCRETE BUILDINGS

De Luca F., Verderame G.M., Manfredi G. A simplified tool for the assessment of shear failures in existing RC buildings. XIV Convegno ANIDIS 2011, Bari 18-22 Settembre, 2011.

6.1 Authorship of Chapter

This chapter is based on the publication (cited above). It deals with some issues regarding brittle failures in existing reinforced concrete buildings, developed within the activities of the Rete dei Laboratori Universitari di Ingegneria Sismica – ReLUIS for the research program funded by the Dipartimento di Protezione Civile 2010-2013.

6.2 Introduction

Concrete and reinforced concrete structures are used as building materials in every country. The universal nature of reinforced concrete construction stems from the wide availability of reinforcing bars and the constituents of concrete , gravel, sand, and cement, the relatively simple skills required in concrete construction, and the economy of reinforced concrete compared to other forms of constructions (Macgregor J.G., 1997).

Reinforced concrete structures consist of a series of "individual members" that interact to support the loads placed on the structures. When a structure or a structural member becomes unfit for its intended use, it is said to have reached a limit state. The attainment of such limit states is checked by means of a comparison between demands and capacities. The latter is also the basic step for the definition of damage measures DM and consequently for the

evaluation of $dG(DM|EDP)$ in the PBEE framework.

In a more general framework of design in both seismic and non-seismic prone areas, limit states for reinforced concrete structures can be divided into three basic groups, according to the classification made by Macgregor (1997).

- Ultimate limit states. These involve a structural collapse of part or all of the structure. Such a limit state should have a very low probability of occurrence since it may lead to loss of life and major financial losses. The major ultimate states are:
  a. *Loss of equilibrium* of a part or all of the structure as a rigid body. Such a failure would generally involve tipping or sliding of the entire structure and would occur if the reactions necessary for the equilibrium could not be developed.
  b. *Rupture* of critical parts of the structure, leading to partial or complete collapse.
  c. *Progressive collapse*. In some cases a minor localized failure may cause adjacent members to be overloaded and fail, until the entire structure has collapsed. Progressive collapse is prevented or slowed by correct structural detailing to tie the structure together and to provide alternative load paths in case of localized failure. Since such failures may occur during construction, the designer should be aware of construction loads and procedures. A structure is said to have general structural integrity if it is resistant to progressive collapse.
  d. *Formation of a plastic mechanism*. A mechanism is formed when the reinforcement yields to form plastic hinges at enough sections to make the structure unstable.
  e. *Instability* due to deformations of the structure. This type of failure involves buckling.
  f. *Fatigue*. Fracture of members due to repeated stress cycles of service loads may cause collapse.
- Serviceability limit states. These involve disruption of the functional use of the structure but not collapse per se. Since there is less danger of loss of life,

a higher probability of occurrence can generally be tolerated than in the case of an ultimate limit state. The major serviceability limit states include:

a. *Excessive deflection* for normal service. Excessive deflection may cause machinery to malfunction, may be visually unacceptable, and may lead to damage to nonstructural elements or to changes in the distribution of forces.
b. *Excessive crack width.* Although reinforced concrete must crack before the reinforcement can act, it is possible to detail the reinforcement to minimize the crack widths. Excessive crack widths lead to leakage through the cracks, corrosion of the reinforcement, and gradual deterioration of the concrete.
c. *Undesirable vibrations.* Vertical vibrations of floors or bridges and lateral and torsional vibrations of tall buildings may disturb the users. Vibrations has rarely been a problem in reinforced concrete buildings.

- Special limit states. This class of limit states involves damage or failure due to abnormal conditions or abnormal loadings and includes:
  a. *Damage or collapse in extreme earthquakes.*
  b. *Structural effects of fire, explosions, or vehicular collisions.*
  c. *Structural effects of corrosion or deterioration.*
  d. *Long-term physical or chemical instability* (normally not a problem with concrete structures).

In seismically prone areas such limit states are specialized in term of specific performance levels; "operational" and "immediate occupancy" are serviceability limit states, while life safety" and "near collapse" are ultimate limit states. Each one of the above performance levels are paired off with discrete hazard levels. Operational level corresponds to a *frequent* earthquake, expected to take place during the conventional working life of the building (a mean return period of approximately 25 years. Immediate occupancy level corresponds to an *occasional* earthquake with a mean return period between 75 and 200 years. Life safety level corresponds to a *rare* earthquake with a mean return period of 500 years. Finally, near collapse level corresponds to a *very*

rare earthquake or *maximum considered* with an approximate return period in the order of 1000 to 2500 years.

Given the limit states approach, shared in building codes all over the world, PBEE, in particular, focuses on the ability of the engineered facility to fulfill its intended purpose, taking into account the consequences of its failure to meet it. Conventional structural design codes, by contrast, are process-oriented, emphasizing the means, namely the prescriptive, easy to apply, but often opaque rules that disguise the pursuit of satisfactory performance. These rules have been developed over time as a convenient means to provide safe-sided, yet economical solutions for common combinations of building layout, dimensions and materials. They leave limited room for the designer to exercise judgment and creativity and do not provide a rational basis for innovative designs that benefit from recent advances in technology and structural materials, (Fardis, 2009). Different performance criteria are defined for the verification of structural or non-structural elements under the various performance levels.

In Code provisions a specific limit state is defined by the attainment of a deformation or strength capacity at global or local level. For example, according to European and Italian provisions for existing reinforced concrete structures, the near-collapse and life safety limit states are represented by the attainment of a specific value of the chord rotation (deformation) or of the shear capacity (strength) in the first element of the structure. Thus, according to this vision, a local collapse is a collapse of the whole structure. It is to be noted that while for brittle failures this vision has always a real counterpart in term of damage, on the contrary the ductile failure of a single element does not implies necessary a significant damage in the rest of the structure. Thus, for reinforced concrete structures, more than other materials, the behavior and the capacity of individual members play a key role in the assessment.

6.3 Failure modes in existing reinforced concrete buildings

Existing substandard buildings have been designed for very low lateral force resistance, if any. So, they are expected to develop significant inelastic action, even under a moderate earthquake. To sustain it, they should have considerable ductility, at both the local and the global level. In existing substandard buildings potential plastic hinge regions are not detailed for ductility. Besides, members are not capacity-designed against pre-emptive brittle failure in shear. More important, though, existing substandard buildings seldom have the strong and stiff vertical spine necessary for spreading inelastic deformation demands throughout their height and avoid storey mechanism. If they have one in the form of strong walls, it is more by coincidence than by design. Even more important, as a rule, their overall structural layout is seismically deficient, (Fardis, 2009).

Owing their poor structural layout, the lack of a strength hierarchy engineered to control the inelastic response mechanism, deficient or discontinuous load path, etc., existing substandard buildings may experience certain concentration of seismic deformation demands to few of their elements in the event of a strong earthquake. Unfortunately these elements may be ill-prepared to withstand the increased demands, as they lack detailing for ductility and are not protected from pre-emptive brittle failures. Non-ductile failures of members or connections, due to poor detailing, are plenty in reconnaissance reports (see chapter 7). Regarding flexural plastic hinges, failed column end regions are characterized by little confining reinforcement and ties not anchored by a 135° hook. Furthermore, columns without engineered earthquake resistance have normally been designed only for gravity compression with a nominal eccentricity. So, they are not only undersized and poorly detailed, but also have low flexural and shear resistance against lateral load. By contrast, the beams of seismically deficient buildings normally have substantial flexural and shear resistance thanks to their design for gravity loads. So, unlike column failure, which abound, beam failures are rare, (Fardis,

2009).

6.4 Capacity models for ductile mechanisms

Current code prescriptions allow to evaluate the rotational capacities from hybrid (mechanical-empirical) or empirical formulations, for reinforced concrete members (Panagiotakos and Fardis, 2001). The reliability of such formulations is strictly linked to the characteristics of the database employed in term of number of samples and homogeneity, (e.g. ribbed or smooth bars, conforming or non-conforming elements).

The ultimate rotational capacity is generally evaluated referring to a fixed strength decay (20%) respect to the peak resistance, evaluated on the force-displacement envelope curve. It is clear that this definition is strongly influenced by the maximum resistance condition, as well as the post-peak degradation, monotonic or cyclic. It is difficult to define a relationship between the element parameters and the rotational capacity, due to the complex phenomena influencing the post-elastic deformation behavior and to the natural variability affecting these phenomena. Codes (CEN, 2005; CS. LL. PP., 2009), consistently with the methodologies developed in literature, propose two main approaches: a mechanical-empirical approach, based on plastic hinge length concept, and a purely empirical approach, (Verderame et al., 2010).

Different proposals can be found in literature for the evaluation of ultimate capacity of reinforced concrete elements (e.g. Panagiotakos and Fardis, 2001; Rossetto, 2002; Lam et al., 2003; Fardis, 2006; Perus et al., 2006; Perus and Fajfar, 2007; Haselton and Deierlein, 2007; Zhu et al., 2007; Haselton et al., 2008; Fardis, 2009); development of empirically calibrated expressions is allowed by experimental databases, made available by authors (Panagiotakos and Fardis, 2001; Berry et al., 2004) that collected results of experimental tests carried out by many others.

Given the complexity of the phenomena involved, the purely empirical approach should be preferred, since the hybrid approach simply moves all the empirical aspects in the evaluation of the plastic hinge length. On the other

hand, still regarding the evaluation of the rotational capacities by means of the purely empirical approach and in general regarding the evaluation of moment - chord rotation backbones (M-θ), it is possible to recognize two different solutions developed on the basis of the two main databases available in literature (Panagiotakos and Fardis, 2001; Berry et al., 2004), the European one, founded on Fardis' approach and the American one, provided by PEER.

The European approach provides the yielding and the ultimate chord rotation, θ_u, (referring to the fixed 20% strength decay respect to the peak resistance), without any provision regarding chord rotation at peak strength; the latter is a consequence of the uncertainties in dealing with the definition of the peak strength point in the experimental tests. On the other hand, the ultimate chord rotation defined by means of such an approach accounts in itself for all the source of degradations (cyclic and in-cycle). Such yielding and ultimate chord rotations are based on Panagiotakos and Fardis' database that comprises more than one thousand tests.

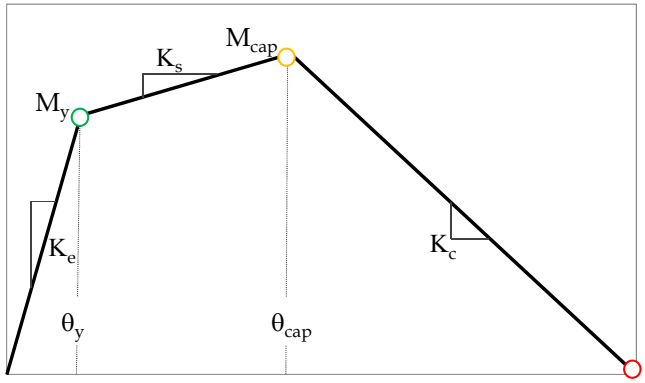

Figure 6.1. Moment–chord rotation (M-θ) backbone according to the experimental calibration by Haselton et al. (2008) on the Ibarra et al. (2005) model. [Adapted from Haselton et al., 2008].

The American approach, calibrated on Berry et al. (2004) database that comprises approximately five hundred columns, on the contrary, provide a full M-θ backbone definition (see Figure 6.1), calibrating the yielding (θ_y), the capping (θ_{cap}) and the post-capping chord rotations (θ_{pc}) on the element model

developed by Ibarra et al. (2005). It could be inferred that the capping chord rotation empirical formulation provided in Haselton et al. (2008) can be employed as characteristic abscissa for the peak strength and could, in some way, integrate the results of European approach. Unfortunately, the θ_{cap} is evaluated on the non-deteriorated backbone and an additional parameter accounts for the cyclic and in-cycle deterioration (λ); thus, preventing any integration with the European approach. The two formulations are shown in equations (6.1) and (6.2), for the definition of the specific term in the equations please see Fardis (2009) and Haselton et al. (2008).

$$\theta_u^{pl} = a_{st}^{pl}\left(1-0.52a_{cy}\right)\left(1+\frac{a_{sl}}{1.6}\right)\left(1-0.44a_{w,r}\right)\left(1-\frac{a_{w,nr}}{4}\right)\left(0.25\right)^{\nu} \left(\frac{\max\left(0.01;\omega_2\right)}{\max\left(0.01;\omega_1\right)}\right)^{0.3} f_c^{0.2}\left[\min\left(9;\frac{Lv}{h}\right)\right]^{0.35} 25^{\left(\frac{\alpha\rho_s f_{yw}}{f_c}\right)} 1.275^{100\rho_d} \tag{6.1}$$

$$\theta_{cap}^{pl} = 0.12\left(\frac{\max\left(0.01,\frac{\rho' f_y}{f'_c}\right)}{\max\left(0.01,\frac{\rho f_y}{f'_c}\right)}\right)^{0.225} \left(1+0.55a_{sl}\right)\left(0.16\right)^{\nu} \left(0.02+40\rho_{sh}\right)^{0.43}\left(0.54\right)^{0.01c_{units}f'_c}\left(0.66\right)^{0.1s_n}\left(2.27\right)^{10.0\rho} \tag{6.2}$$

On the other hand, the European approach has different advantages regarding the prediction of ultimate chord rotation capacity. In fact, first of all Fardis' database is larger, secondly the ultimate chord rotation capacity according to the European approach (CEN, 2005) allows accounting for absence of detailing for earthquake resistance in the elements, or for smooth bars, so, finally, it becomes the most attractive solution for existing elements. The difficulties in the comparison of the two approaches are, in some way, already emphasized in Haselton et al. (2008) when comparing the ultimate chord rotation by Fardis with the capping and the post capping rotational capacity according to these authors.

An example of the preferable accuracy of the European approach can be

found in the recent updates of the whole Fardis' database made for smooth bars. In fact, recently, the database of element reinforced with smooth bars has been enlarged with further experimental tests (Verderame et al., 2008a and 2008b), allowing the calibration of a new coefficient, less penalizing, to account for the presence of smooth reinforcement in the elements (CEN, 2009). Subsequent studies on the same issue (Verderame et al., 2010) have shown that the coefficient for smooth bars could be further improved (see Figure 6.2) respect to the solution proposed in literature and codes (CEN, 2005; Fardis, 2006 and CEN, 2009). Figure 6.2 shows the trend of the correction coefficients for smooth bars according to different authors and codes as function of the lap length (l_o) normalized by the diameter of the longitudinal bars (d_{bL}). The correction coefficient, as it is expected, increases with the lap length, and becomes constant as soon as l_o/d_{bL} is equal to 50.

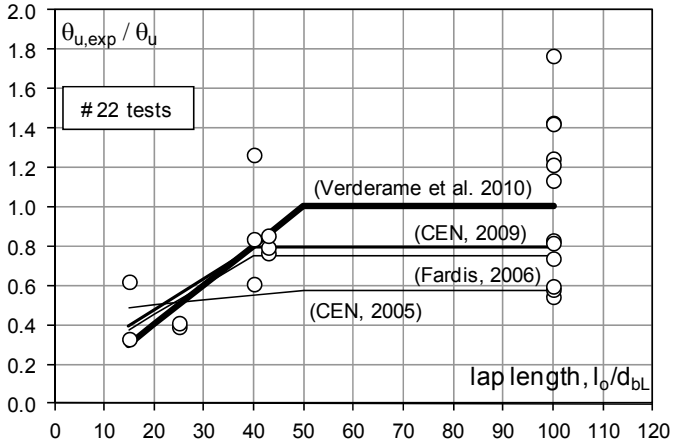

Figure 6.2. Comparison between the correction proposed coefficient in Verderame et al. (2010) and the ones reported in CEN (2005), Fardis (2006) and CEN (2009). [Courtesy of the authors of the paper Verderame et al., 2010].

6.5 Capacity models for brittle failure mechanisms

Brittle failure mechanisms are something that should never be registered in a capacity designed building. On other hand, brittle failure represents a significant issue in the framework of the assessment of existing buildings, as it

was emphasized in section 6.3. Capacity design rule, in fact, is the fundamental of all new generation seismic codes; any building designed according to Eurocode8 (CEN, 2004a) or recent Italian seismic code (DM 14/1/2008) cannot be characterized by brittle failures. Such an approach prevents brittle failures or other undesirable failure mechanisms by deriving the design action effects of selected regions from equilibrium conditions. For elements it is assumed that plastic hinges, with their possible overstrengths, develop at the end sections of the element and shear demand is evaluated as the maximum shear that can be registered because of flexural behavior. In existing reinforced concrete buildings brittle failures often represent a significant quota of the retrofitting costs. Brittle failures can develop in beams, columns and beam-column joints.

6.5.1. Shear capacity models in codes and literature

In the main framework of brittle failures of beams and columns the choice of a reliable shear capacity model becomes an imperative since different approaches are available in codes and literature.

Shear capacity models available in literature and codes can be quite different to each other and can be based whether on analytical theories or experimental databases. While flexural strength is based on general principles recognized as reliable in the scientific community and its evaluation is almost the same in all the codes all over the world, because of a very good accordance with experimental results; shear failure mechanisms are physically more complex and different interpretations of the mechanical phenomenon lead to different theories and models. The latter is the reason why codes and literature can suggest different shear capacity models and some of the most recent follow the regression approach on experimental data that results as the most reliable when analytical models fail in the prediction of a phenomenon. An example can be the evaluation of chord rotation capacities that in the last ten years has followed the experimental basis, (e.g. Panagiotakos and Fardis, 2001; Haselton et al. 2008), see section 6.4.

The shear capacity model employed in design, according to Eurocode 2

(CEN, 2004b) and Eurocode 8 part 1 (CEN, 2004a), is the variable strut inclination model; such a model is not well suited for design against seismic loads. The value to be assumed for the inclination of the strut (θ) is comprised in the mandatory ranges of 21.8° and 45° according to Eurocode 8 and it can be evaluated as the inclination that equalizes the resistance of the tension (V_{Rsd}) and the compression (V_{Rcd}) struts, according to equation (6.3), in which the value of the transversal mechanical reinforcement ratio (ω_{sw}) is expressed in equation (6.4). The expression for V_{Rsd} and V_{Rcd} are shown in equations (6.5) and (6.6).

$$\cot\theta^* = \sqrt{\frac{0.5\cdot\alpha_c}{\omega_{sw}} - 1} \tag{6.3}$$

$$\omega_{sw} = \frac{A_{sw}}{b\cdot s}\cdot\frac{f_{yw}}{f_c} \tag{6.4}$$

$$V_{Rsd} = 0.9\cdot d\cdot\frac{A_{sw}}{s}\cdot f_{yw}\cdot\left(\cot\alpha + \cot\theta\right)\cdot\sin\alpha \tag{6.5}$$

$$V_{Rcd} = 0.9\cdot d\cdot b\cdot\alpha_c\cdot 0.5\cdot f_c\cdot\frac{\left(\cot\alpha + \cot\theta\right)}{\left(1+\cot^2\theta\right)} \tag{6.6}$$

$$V_{Rd} = \min\left(V_{Rsd}, V_{Rcd}\right) \tag{6.7}$$

If the resulting θ* is not comprised in the mandatory ranges, the shear capacity is evaluated with θ equal to 45° or 21.8°, if the value obtained is respectively higher than 45° or lower than 21.8°, resulting in the minimum between the tensile and compression shear resistance, see equation (6.7). In equation (6.3) to (6.6), α is the transversal reinforcement inclination, α_c is a coefficient dependent to the axial load and d is the distance from the compression fiber to centroid of longitudinal tension reinforcement; for further details regarding this model see Cosenza et al. (2008).

It is to be noted that in Eurocode 8 and Italian Code the shear design is made according to capacity design rule (employing the shear demand corresponding to the flexural capacity of the elements); thus assuring a shear-

flexure hierarchy that prevents any brittle failure. The strut inclination is fixed to 45° in the case of beams designed in high ductility class (DCH), leading to a very conservative capacity equal to the classical Ritter-Mörsch model for elements that are meant to experience high ductility demand, such as beams. In fact, in such cases the minimum value in equation (6.7) is V_{Rsd} that is brought back to the Ritter-Mörsch model when θ is equal to 45°. Moreover, in critical regions of elements, are always the code mandated transversal reinforcement details that rule the design procedure. The latter is the reason why, even if the variable strut inclination model is not suitable for seismic loads, the shear design procedure according to Eurocode 8 results in elements and, consequentially, in buildings that comply the safety requirements according Eurocode 0 (BS EN 1990, 2002).

The shear capacity model employed for assessment in Eurocode 8 part 3 (CEN, 2005), for existing buildings, is the regression model based on the large database of 239 columns collected by Biskins et al. (2004), with the additional coefficient γ_{el} equal to 1.15 accounting for the dispersion of the regression model. First of all the regression model is different if the shear span ratio (Lv/h) is lower or equal than 2, see equation (6.8) or higher to 2, see equation (6.9); in the first case the failure is controlled by diagonal compression, in the second it is controlled by diagonal tension. Both the empirical formulas account for shear strength degradation according to the plastic ductility factor $\mu_{\Delta pl}$, equal to the chord rotation demand over the yielding chord rotation minus 1, (θ/θ_y-1). The shear strength degradation because of cyclic loads varies linearly between $\mu_{\Delta pl}$ equal to 0 and 5, the latter is the value at which the maximum degradation is attained.

$$V_{EC8,squat} = \frac{1}{\gamma_{el}}\frac{4}{7}\left(1-0.02\min\left(5;\mu_{\Delta pl}\right)\right)\left(1+1.35\frac{N}{A_c f_c}\right) \left(1+0.45\cdot 100\rho_{tot}\right)\sqrt{\min\left(f_c;40\right)}b\cdot z\cdot\sin 2\delta \tag{6.8}$$

$$V_{EC8,slender} = \frac{1}{\gamma_{el}}\left[V_N + V_c + V_w\right] \tag{6.9}$$

Eurocode 8 part 3 prescribes that the shear capacity is the minimum value obtained by this regression model and the variable strut inclination one. On the other hand, it has to be noted that in most practical cases the regression model represents the minimum, as it will be shown in the following subsection 6.5.3. Discarding the case of squat columns (Lv/h<2), because of no practical interest for typical situations; the regression model, for elements that fail in diagonal tension, accounts for three contributions: the classical 45-degrees truss model (V_w), supplemented with concrete contribution (V_c), where both depend on cyclic displacement ductility demand and finally the axial load contribution (V_N). The latter is an effect that was already considered in previous shear strength degradation models (e.g. Priestley et al., 1994). Equations (6.10) to (6.12) reports explicitly the three contributions in equation (6.9), where all the symbols are the same employed in Eurocode 8 (CEN, 2005).

$$V_N = \frac{h-x}{2L_V}\cdot\min\left(N;0.55A_c f_c\right) \tag{6.10}$$

$$V_c = \left(1-0.05\min\left(5;\mu_{\Delta pl}\right)\right)\cdot\left[0.16\max\left(0.5;100\rho_{tot}\right)\cdot\left(1-0.16\min\left(5;\frac{L_V}{h}\right)\right)\sqrt{f_c}A_c\right] \tag{6.11}$$

$$V_w = \left(1-0.05\min\left(5;\mu_{\Delta pl}\right)\right)\cdot\left(\rho_w b\cdot z\cdot f_{yw}\right) \tag{6.12}$$

According to American provisions for existing buildings (ASCE/SEI 41-06, 2007), shear strength shall be calculated with the additive formula provided by ACI 318 (ACI 318-05, 2005), see equations (6.13) to (6.15) in which A_g is the gross cross-sectional area. Specific provisions are considered in yielding regions and in the case of not properly detailed elements, for details see section 6.3.4 in ASCE/SEI 41-06 (2007). For concrete moment frames, shear strength in columns can be evaluated according to Sezen and Mohele' s regression model (2004), see equations (6.16) to (6.17). Such model accounts for shear strength degradation caused by ductility demand by means of the coefficient k and it is calibrated on an experimental database of 51 columns (see section 6.5.2). k coefficient is equal to 1 (no degradation) if the displacement ductility is less than or equal to 2, it is equal to 0.7 in regions where displacement ductility is

greater than or equal to 6, and varies linearly for displacement ductility between 2 and 6. It is possible to note the strict analogy with Eurocode 8 part 3 model and with the regression model by Biskinis et al. (2004).

$$V_{ACI318} = V_c + V_w \tag{6.13}$$

$$V_c = 0.166\left(1 + \frac{N}{13.8A_g}\right)\sqrt{f_c} \cdot b \cdot d \tag{6.14}$$

$$V_w = \frac{A_{sw} \cdot f_{yw} \cdot d}{s} \tag{6.15}$$

$$V_{Sezen} = k \cdot V_w + k \cdot V_c \tag{6.16}$$

$$V_w = \frac{A_{sw} \cdot f_{yw} \cdot d}{s} \tag{6.17}$$

$$V_c = \left(\frac{0.5\sqrt{f_c}}{Lv/d} \cdot \sqrt{1 + \frac{N}{0.5 \cdot \sqrt{f_c} \cdot A_g}}\right) \cdot 0.8A_g \tag{6.18}$$

- **The Italian issue**

While other codes prescribe, for existing buildings, a clear path to be followed for the evaluation of shear capacity in reinforced concrete members, the recent Italian code provisions for seismic zones do not provide any model for the assessment. Regarding the design of new elements the model adopted is the variable strut model and prescriptions are the same of Eurocode 8 part 1 (CEN, 2004a). For the assessment, the code itself (DM 14/1/2008) does not provide any specific rule, giving only general criteria, while the explicative documents to the code (CS. LL. PP., 2009) follows, in general, the same prescription of Eurocode 8 part 3.

Regarding shear capacity models to be employed for the assessment, the explicative document to the Code (CS. LL. PP., 2009) gives some suggestions without providing any explicit capacity model. It is written that the same approach of design case in non seismic regions should be followed (so, the variable strut inclination model) accounting for a concrete contribution V_c at most equal to the one for elements without transversal reinforcement. Now,

this suggestions make no sense unless an additive formula is employed as it used to be according to the old Italian code prescriptions (DM 9/1/1996) and the only possible solution that complies these suggestions is the classical Ritter-Mörsch model, discarding any concrete contribution and employing a particular case of the variable strut inclination model ($\cot\theta = 1$). Such an approach can be, evidently, very conservative in most cases and it does not fit with the general rule that assessment procedure should lead to a realistic evaluation of the capacity of a structure. The reason of such an ambiguous prescription is caused by a misprint. In fact, most of the explicative document to the actual code (CS. LL. PP., 2009) was taken by another document that was released after the 2003 Umbria-Marche earthquake (OPCM 3274, 2003), the latter was, in turn, taken mostly form Eurocode 8 part 3. The OPCM 3274 (2003) took into account the fact that the main code at the time used to have an additive formula (DM 9/1/1996). Thus, such prescription in the explicative document of the new code (CS. LL. PP., 2009) was not changed respect to OPCM 3274, while the new version of the code (DM 14/1/2008) switched to variable strut inclination model.

The problem created by this misprint is now going to be solved by a new upgraded release of both the code (DM 14/1/2008) and its explicative document (CS. LL. PP., 2009).

6.5.2. *Experimental results versus analytical formulations: models' comparisons*

The models described in the previous subsection are now investigated with respect to experimental tests. The database considered is composed of 51 rectangular columns characterized by light transversal reinforcement, data are available in Sezen and Mohele (2004). The reason why this database, employed for the evaluation of analytical model by Sezen and Mohele, was selected for the numerical versus experimental comparison herein, is that it is fully available in literature and all the necessary details on the experimental tests can be found in Sezen (2002).

The main properties of the columns in the database are shown in Figure

6.3 to Figure 6.6. Materials' mechanical properties distribution are shown in Figure 6.3; the frequency distribution of reinforced concrete compressive strength (f_c) varies from 15 MPa to 45 MPa, so covering a wide range that can be representative of both existing and new reinforced concrete properties. Steel yielding strength frequency distribution of the longitudinal reinforcement (f_y) varies in the range 300 t0 600 MPa, a large amount of specimens is characterized by 350 and 450 MPa, so regarding longitudinal reinforcement these two values can be good representatives of the typical yielding strengths of existing steel (350 MPa) and more recent steel (450 MPa). Steel yielding strength frequency distribution of the transversal reinforcement (f_{yw}) is in average higher than the strength of the longitudinal steel and also characterized by a wider variability.

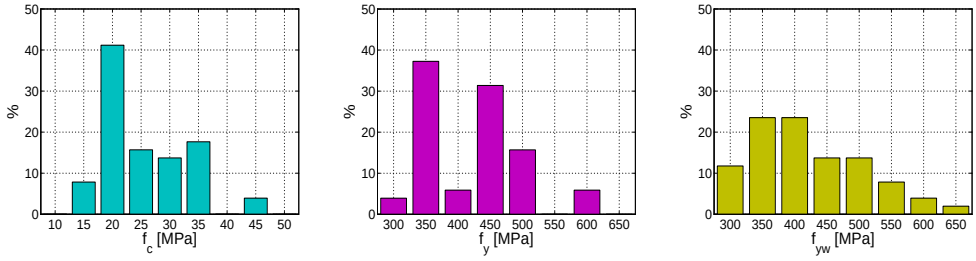

Figure 6.3. Sezen and Mohele's database, data frequency distributions: material properties, reinforced concrete compressive strength (f_c), steel yielding strength of longitudinal reinforcement (f_y) and transversal reinforcement (f_{yw}).

Figure 6.4 shows frequency distribution of shear span ratio (Lv/h) and ductility (μ_Δ) in the database. It is worth noting that shear span ratios are not equally distributed in the range [2;3.5] and most of the specimens are characterized my small shear span ratios. Ductility frequency distribution varies in the range [1;8] and its ranges can be considered representative of different situations, useful for a quite generalized characterization of the behaviour of elements as function of the ductility demand.

Figure 6.5 shows the frequency distribution of transversal (ρ_w) and longitudinal (ρ_{tot}) reinforcement ratios. The database is characterized by high percentage of longitudinal reinforcement ratio that ranges from 0.01 to 0.04

with a large amount of specimens characterized by 0.02; such values are considered high if the targets are existing buildings in the Mediterranean area. Transversal reinforcement ratio is quite low, the latter represents the main characteristic of the database by Sezen and Mohele, in fact the authors emphasize that the analytical model obtained on such database is for "lightly reinforced columns".

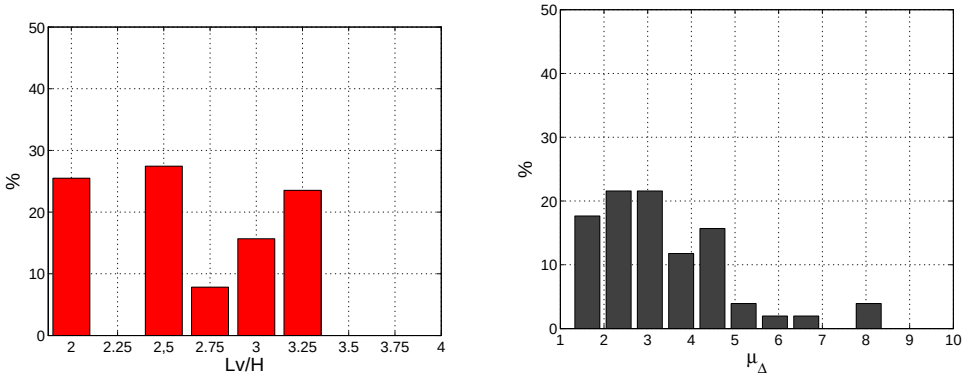

Figure 6.4. Sezen and Mohele's database, data frequency distributions: shear span ratio (Lv/h) and ductility (μ_Δ).

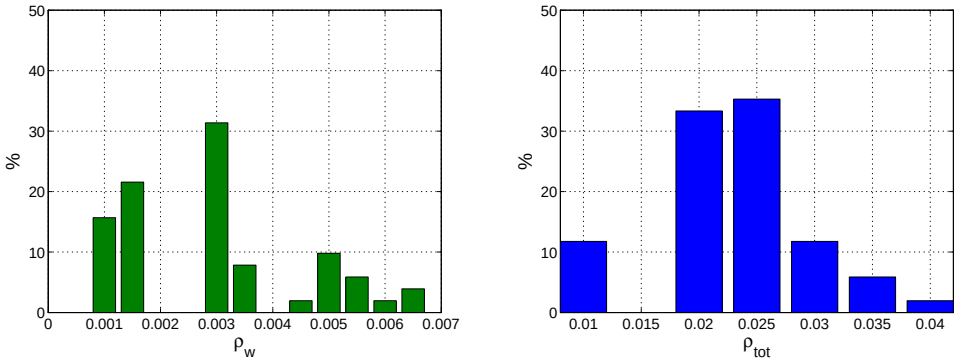

Figure 6.5. Sezen and Mohele's database, data frequency distributions: transversal (ρ_w) and longitudinal (ρ_{tot})geometrical reinforcement ratios.

Figure 6.6 shows the frequency distribution of transversal and longitudinal mechanical reinforcement ratios; the plot was intentionally represented in a wider range ($\omega_{sw} \in [0;0.25]$ and $\omega_{tot} \in [0;2.5]$) representative of

both existing and new design elements; on the other hand it should be noted that the whole database in term of both longitudinal and transversal mechanical reinforcement ratios can be representative of the typical values characteristic of existing reinforced concrete buildings.

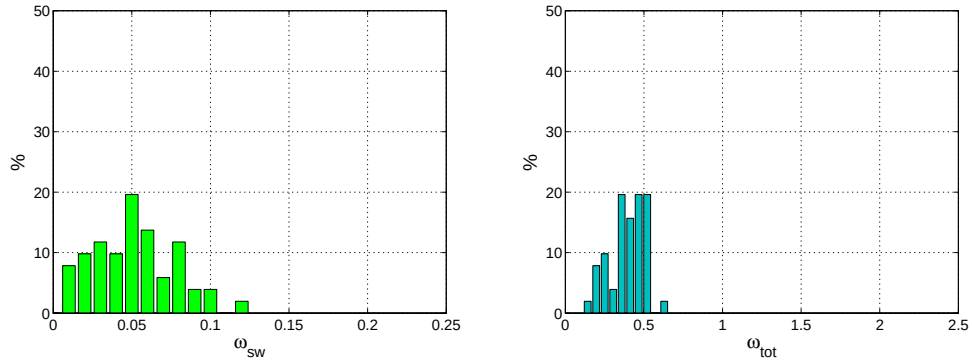

Figure 6.6. Sezen and Mohele's database, data frequency distributions: transversal (ω_{sw})and longitudinal (ω_{tot})mechanical reinforcement ratios.

The analytical models considered in section 6.5.1 are compared with the experimental results of the database. Table 6-1 shows the mean (μ), the standard deviation (σ) and the coefficient of variation (COV) of the ratio between the experimental shear capacities and the shear capacities obtained by the analytical models considered (V_{exp}/V_{model}). Results are shown for the models by Sezen and Moehele (*Sezen*), by Biskinis (*Bisk*), for the variable strut inclination (*NTC*), the classical Ritter-Mörsch (*45°*) and the Eurocode 8 part 3 formulations (*EC8*). It is worth to note that the only difference between *Bisk* and *EC8* formulations is the presence of the coefficient γ_{el} equal to 1.15.

Table 6-1. Mean and standard deviation of the experimental over analytical ratio for the capacity models considered.

V_{exp}/V_{model}	Sezen	Bisk	NTC	45°	EC8
μ	1.06	0.96	1.04	2.59	1.10
σ	0.17	0.19	0.47	1.20	0.21
COV	0.16	0.19	0.45	0.46	0.19

Statistics showed in Table 6-1 emphasize how the models that accounts

for shear strength degradation give a response closer to the experimental observations with mean values close to 1 and low dispersion. Evidently, Sezen and Mohele' s model, calibrated on the database, is the one with the best performances and Biskinis' s formulation, without the application of the correction coefficient, suggested in Eurocode 8, can be the only slightly unconservative analytical model. Surprisingly, the variable strut inclination model shows a mean value even closer to 1 if compared to all the degrading models considered, on the other hand, its dispersion is very high. Classical Ritter-Mörsch truss is a very conservative approach and highlights the fundamental role played by concrete contribution on the shear strength capacity. Shear strengths of all the specimens of the database versus the analytical prediction, according to all the models considered, are mapped in Figure 6.7.

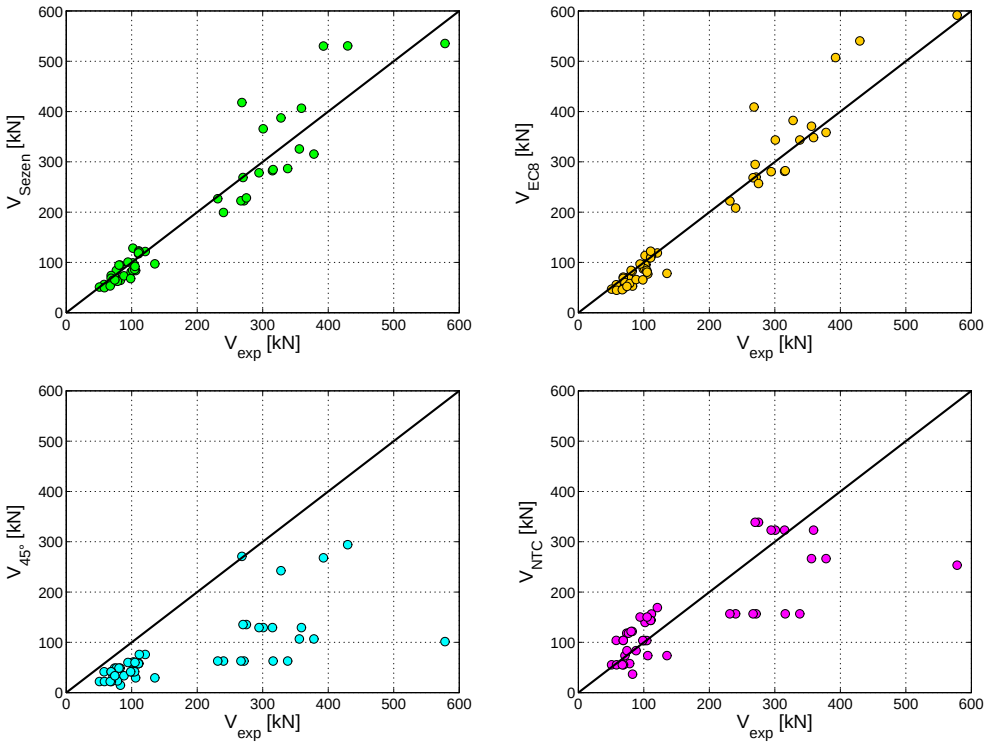

Figure 6.7. Performance of the analytical models considered respect to Sezen and Mohele (2004) database. (a) Sezen and Mohele' s model (*Sezen*), (b) Eurocode 8 part 3

model (*EC8*), (c) Ritter Morsch' s model (*45°*), (d) Variable strut inclination model (*NTC*).

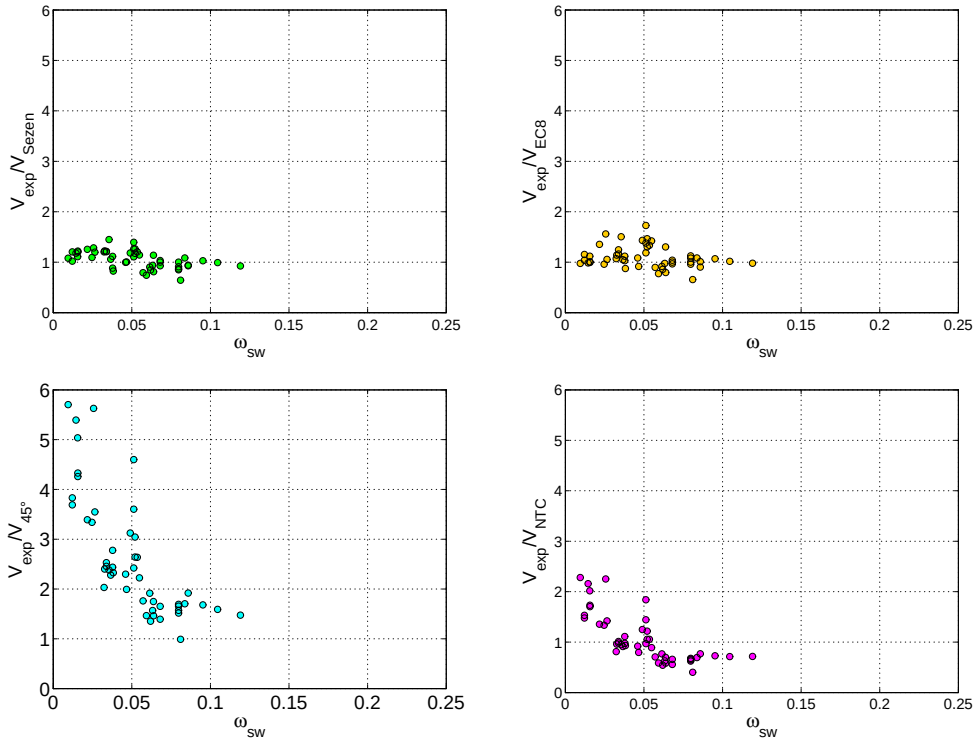

Figure 6.8. Trend with transversal mechanical reinforcement ratio of the experimental over analytical ratio for the capacity models considered. (a) Sezen and Mohele' s model (*Sezen*), (b) Eurocode 8 part 3 model (*EC8*), (c) Ritter Morsch' s model (*45°*), (d) Variable strut inclination model (*NTC*).

For a better characterization of the estimation trend of each single analytical model, the ratio between experimental and analytical strengths is plotted versus the transversal mechanical reinforcement ratio (ω_{sw}), see Figure 6.8. Non degrading models are characterized by most of the error in range of very low transversal reinforcement ratios and it worth to note that the variable strut inclination model is the only one that can become unconservative for ω_{sw} higher than 0.03. The variable strut inclination ratio (V_{exp}/V_{NTC}) can get to 0.4. Observing that the 1/0.4 is equal to 2.5 it is easy to understand that the limit of cotθ equal to 2.5 is not properly calibrated for cyclic shear demand and ω_{sw}

ranging in the interval [0.03;0.1]; the typical range characteristic of existing reinforced concrete elements.

6.5.3. Non dimensional shear strength: models' comparison

The shear strength capacity models, compared by means of the experimental data available in Sezen and Mohele database are now compared in non-dimensional form in a wider range of ω_{sw} and ω_{tot}. It is worth to note that once a model is adopted by a code no restrictions are generally applied to the model, thus it can be employed in general situations, discarding the limits of the experimental database on which it was calibrated or the analytical hypotheses made to obtain it. According to the results of the previous sections, Eurocode 8 part 3 capacity model seems to be the most reliable solution for existing buildings, not only because of the good performances showed respect to the experimental database considered above but because the experimental database on which it is calibrated is wider and allows covering a wider range for parameters governing the shear capacity in RC elements.

The comparison, in this subsection, is made considering shear capacities of the classical Ritter-Mörsch, the variable strut inclination and the Eurocode 8 (for slender columns) models normalized by the ultimate axial force of the section (bhf_c). Such a simplified approach requires some approximations. Ritter-Mörsch and variable strut inclination have been simplified assuming the value of k_2 coefficient equal to 0.8, see equation (6.19) and (6.20). Eurocode 8 model, see equation (6.21), requires a larger number of hypotheses that still do not affect the general results of the comparison. The value of the neutral axis (x) in the formula was assumed equal to $\nu h/0.8$, in which ν is the normalized axial force; this x is obtained according to three main hypotheses, assuming the stress block stress-strain relationship for concrete: (i) the reinforcement is made of only two registers, (ii) the area of steel in compression and tension is equal and (iii) both steel in compression and tension have attained yielding, so that the stress in the steel is equal to f_y, see Cosenza et al. (2008) for further details. k_1 coefficient, equal to 0.9(h-c)/h, was fixed to 0.8. Moreover ν cannot exceed 0.55, the geometrical reinforcement ratio (ρ_{tot}) is higher than 0.5% and Lv/h is

lower than 5. As it was described previously, the maximum value of the shear strength degradation coefficient in Eurocode 8 model is equal to 0.75, so in equation (6.21), β coefficient is equal to 0 in the case of absence of any degradation and equal to 0.25 in the case of maximum shear strength degradation. By means of the non-dimensional expressions of the shear capacity in equations (6.19) to (6.21), it is possible to show the ratio between the capacities of the models considered. Fixing the value of ρ_{tot} to 0.01 and f_c to 20 MPa to simulate an example of likely characteristics for an existing building, the ratio between Eurocode 8 formulation (V_{EC8}) and Ritter-Morsch ($V_{45°}$), in both the cases of absence of degradation and maximum degradation of the shear capacity can be plotted as function of ν and ω_{sw}, respectively in the case of Lv/H equal to 3 and 5, see Figure 6.9 and Figure 6.10. The same plot, with same hypotheses, can be made considering the ratio between V_{EC8} and the variable strut inclination model (V_{NTC}), see Figure 6.11 and Figure 6.12.

$$\frac{V_{45°}}{bHf_c} = \omega_{sw} \cdot \frac{0.9\left(h-c\right)}{h} = \omega_{sw} \cdot k_2 \tag{6.19}$$

$$\frac{V_{NTC}}{bHf_c} = \omega_{sw} \cdot k_2 \cdot \cot\theta^* \tag{6.20}$$

$$\frac{V_{EC8}}{bHf_c} = \frac{1}{\gamma_{el}}\left\{\frac{\nu h}{2L_V}\left(1-1.25\nu\right)+\left(1-\beta\right)\cdot\left[\frac{16}{0.9}\omega_{tot}\left(1-0.16\frac{L_v}{h}\right)\frac{\sqrt{f_c}}{f_y}+\omega_{sw}\cdot k_1\right]\right\} \tag{6.21}$$

The ratio $V_{EC8}/V_{45°}$ shows how the maximum shear strength degradation in V_{EC8} can lead to a capacity that is even lower than the value obtained with Ritter-Mörsch model, this effect is emphasized with the increasing of the shear span ratio (Lv/H) and the decreasing of ν, since the normalized axial force rules the weight of V_N in the Eurocode formulation, that represents the only contribution without degradation, see equation (6.10). On the other hand, the ratio of V_{EC8} with V_{NTC} emphasizes how, in the practical range of interest of ω_{sw} for existing buildings, from 0.02 to 0.1, approximately, V_{NTC} can lead to an overestimation of the shear capacity that cannot be acceptable in the

assessment framework, in which no structural details and reinforcement limits are applied as it is conversely made when design is of concern. This results is the confirmation of the results already shown in Figure 6.8. The value of cotθ equal to 2.5 seems to be not well calibrated in the case of lightly transversal reinforced elements subjected to cyclic load, in which V_{Rsd} rules the minimum capacity, see equation (6.7).

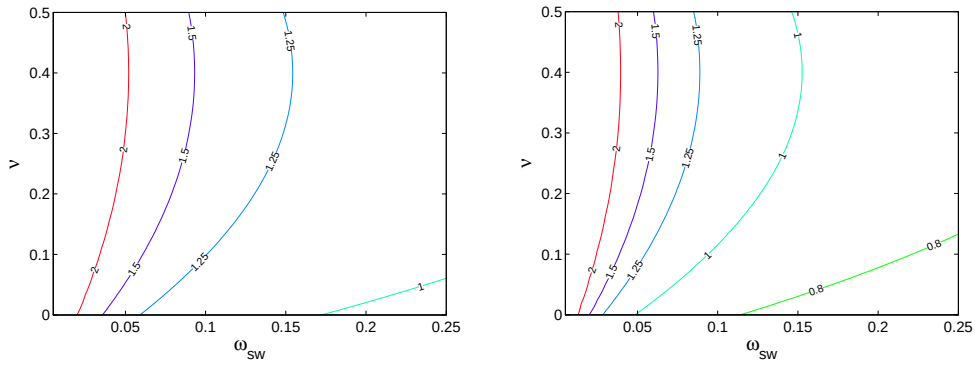

Figure 6.9. Ratio between EC8 shear capacity without (a) and with strength degradation and Ritter-Mörsch model in the case of Lv/h equal to 3.

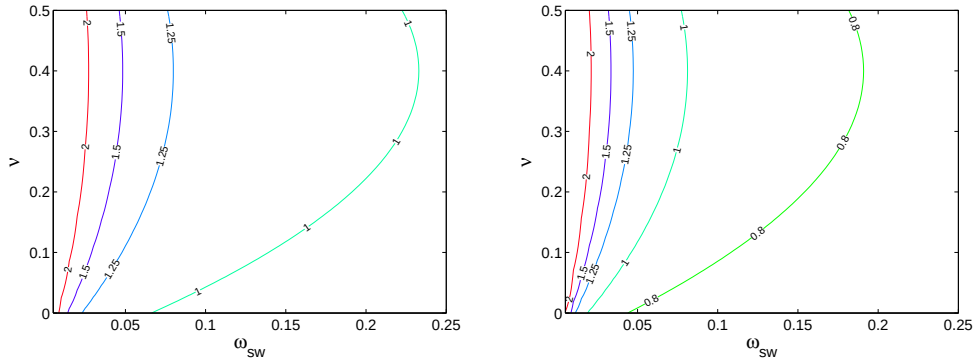

Figure 6.10. Ratio between EC8 shear capacity without (a) and with strength degradation and Ritter-Mörsch model in the case of Lv/h equal to 5.

On this latter aspect the recent released draft of Model Code 2010 (CEB FIP Model Code, 2010) provides a limitation to the value of the maximum cotθ to be employed for cyclic shear resistance at the ultimate limit states in members with shear reinforcements in the seismic design framework (par.

7.4.3.5 in second volume of Model Code 2010).

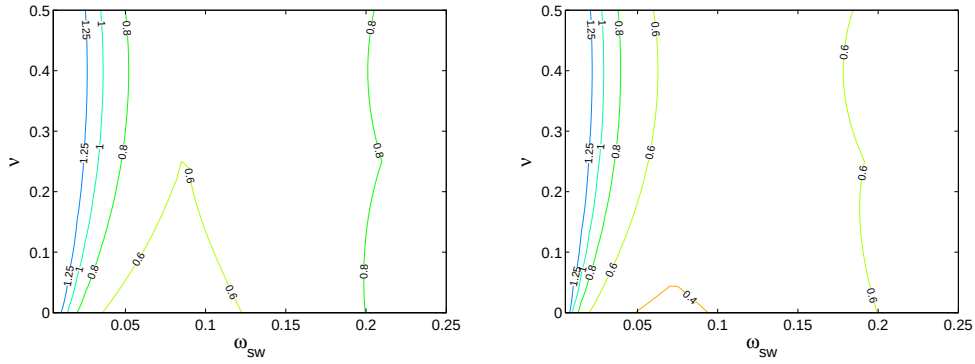

Figure 6.11. Ratio between EC8 shear capacity without (a) and with strength degradation and variable strut inclination model in the case of Lv/H equal to 3.

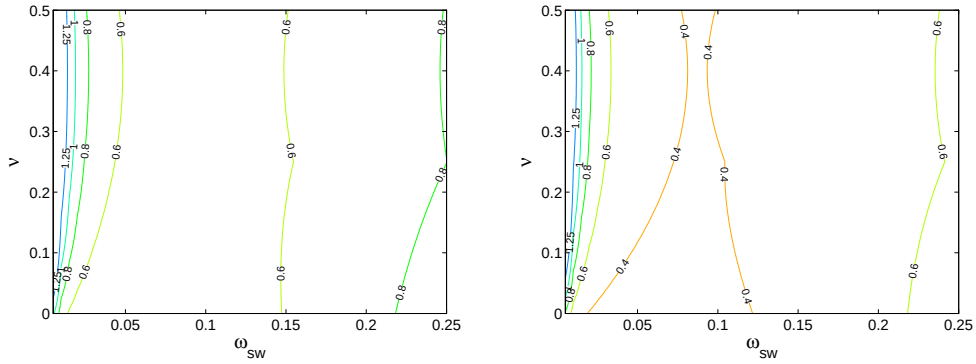

Figure 6.12. Ratio between EC8 shear capacity without (a) and with strength degradation and variable strut inclination model in the case of Lv/H equal to 5.

In Model Code 2010 cotθ is assumed equal to 1 if ductility demand in the element exceeds the value of 2, while it is assumed equal to 2.5 in the case of zero plastic rotation (θ<θy), linear interpolation is considered in-between of these values. It is worth to note that Model Code 2010 does not provide the variable strut inclination approach followed by Eurocode and Italian code (CEN, 2004a; CEN, 2004b; DM 14/1/2008); it provides an additive formulation. With a concrete contribution to shear capacity to be added to the formula in equation (6.5), see equation (6.22). The concrete contribution depends on a coefficient k_v coefficient whose formulation changes according to the level of

approximation. The levels of approximation differ in the complexity of the applied methods and in the accuracy of results. Level I is meant for conception and design of new structures, level II is meant for design and brief assessment, while level III may be used for the design of members in a complex loading state or more elaborate assessments of structures. k_v coefficient is evaluated as a function of the geometrical percentage of transversal reinforcement (ρ_w) for level I, it is equal to zero for level II, and it is a function of ρ_w and of the longitudinal strain at the mid-depth of the member (ε_x); for further details see Model Code 2010 (CEB FIP Model Code, 2010).

$$V_{c,ModelCode\ 2010} = k_v \frac{\sqrt{f_{ck}}}{\gamma_c} \cdot b \cdot z \tag{6.22}$$

6.5.4. *A practice-oriented approach for the assessment of shear failures*

Shear failures can limit strictly the global displacement capacity of existing RC building. A brittle failure, in fact, even if it represents a local event in a building, leads the structure to collapse. The latter is the reason why capacity design rule is applied to new design buildings and brittle failures are prevented by imposing shear-flexure hierarchy, so that the behavior of all the elements can be always assumed as ductile, see Figure 6.13.

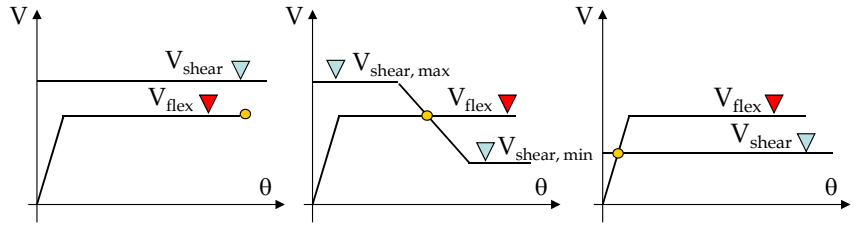

Figure 6.13. Ductile, brittle and limited ductility behavior in RC elements.

While in new buildings ductile behavior is assured because of design, RC elements in existing buildings can show brittle failures or limited ductility behavior (if a degrading shear capacity model is employed). Thus it is fundamental to classify element behavior in the assessment framework. Herein

a simplified tool for the assessment of brittle failure in RC buildings is carried out employing an approximated classification procedure. The general idea is to create a failure domain once the shear capacity model is chosen. Such a failure domain is obtained by means of an equation that equalize the maximum shear flexural demand (V_{flex}), that corresponds to the shear value attained when both the maximum bending moments are attained in the two end sections of the element, with the shear capacity (V_{shear}), see equation (6.23). The equation can be represented in the 2D plane of transversal and longitudinal mechanical reinforcement ratios (ω_{sw}-ω_{tot}), normalizing both V_{flex} and V_{shear} by means of the maximum axial load of the section (bhf_c).

$$\frac{V_{flex}}{bhf_c} = \frac{V_{shear}}{bhf_c} \tag{6.23}$$

By means of the simplified expressions of the shear capacities showed in the previous subsection it is possible to obtain the failure domains for each shear capacity model considered and employed in codes European and Italian codes: Ritter-Mörsch (*45°*), variable strut inclination (*NTC*) and Eurocode 8 part 3 (*EC8*), in both the hypotheses of absence (β=0) or maximum shear strength degradation (β =0.25). The maximum shear flexural demand needs to be expressed in a simplified way assuming some conservative basic hypothesis: (i) the longitudinal reinforcement is made of two registers, ($A_{tot}=A_s+A_s'$); (ii) there is the same steel area in tension and compression, ($A_s=A_s'$) (iii) both the compression and tension reinforcement have attained yielding ($\sigma_s=f_y$). Such hypotheses allow expressing non-dimensional V_{flex} in the form showed in equation (6.24); and the boundary of brittle and ductile failure domains can be obtained in the form shown in equations (6.25) to (6.27) respectively for Ritter-Mörsch, variable strut inclination and Eurocode 8 part 3 model for slender columns (Lv/h<2).

$$\frac{V_{flex}}{bhf_c} = \frac{h}{L_v}\left[\frac{\nu}{2}(1-\nu) + \frac{\omega_{tot}}{2}k_1\right] \tag{6.24}$$

$$\omega_{tot,45°} = \frac{2L_v}{k_1 h}\omega_{sw}\cdot k_2 - \frac{\nu(1-\nu)}{k_1} \tag{6.25}$$

$$\omega_{tot,NTC} = \frac{2L_v}{k_1 h}\omega_{sw}\cdot k_2 \cdot \cot\theta^* - \frac{\nu(1-\nu)}{k_1} \tag{6.26}$$

$$\omega_{tot,EC8} = \frac{\left(\frac{1-\gamma_{el}}{2}\right)\cdot\nu + \left(\frac{\gamma_{el}-1.25}{2}\right)\cdot\nu^2 + (1-\beta)\frac{L_V}{h}\cdot\omega_{sw}\cdot k_1}{\frac{\gamma_{el}\cdot k_1}{2} - \frac{(1-\beta)}{0.9}\frac{L_V}{h}\cdot\left(16-2.56\cdot\frac{L_V}{h}\right)\cdot\frac{\sqrt{f_c}}{f_y}} \tag{6.27}$$

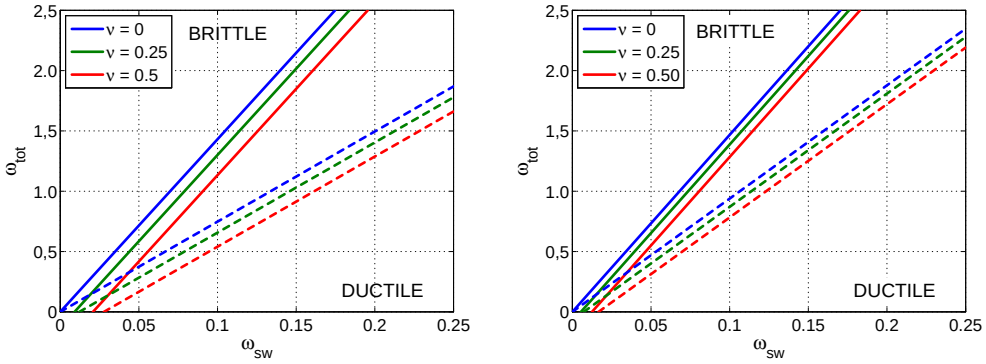

Figure 6.14. Fast assessment domains for Eurocode 8 shear capacity model without (solid lines) and with (dashed lines) shear degradation in the case of Lv/h equal to 3 (a) and 5 (b).

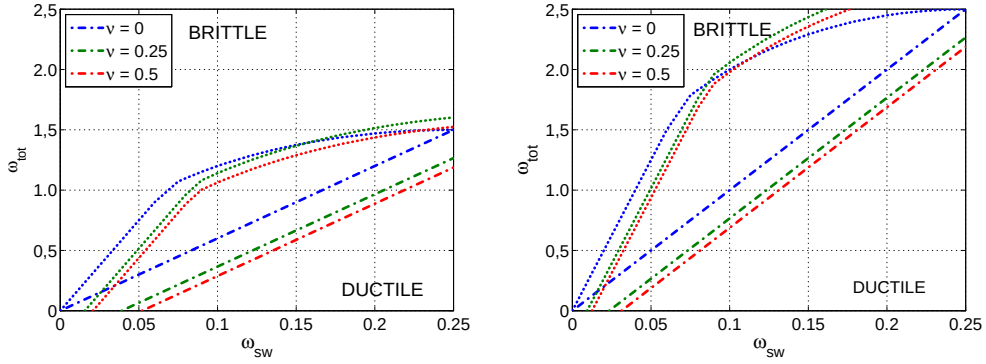

Figure 6.15. Fast assessment domains for variable strut inclination (dotted lines) and Ritter-Mörsch (dotted-dashed lines) shear capacity models in the case of Lv/h equal to 3 (a) and 5 (b).

The failure domains point out the ω_{sw} and ω_{tot} values leading to brittle or ductile behaviors. Figure 6.14 and Figure 6.15 show the failure domains for the shear capacity models considered and Lv/h respectively equal to 3 and 5. It can be observed that Lv/h rules strictly the classification of the element and increasing ν values, as expected, decrease the ductile area.

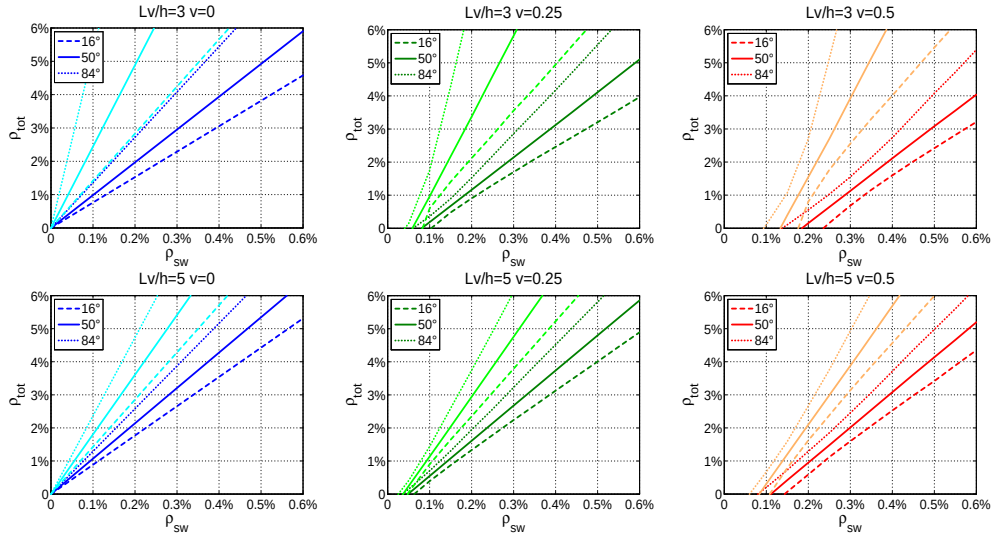

Figure 6.16. Material uncertainties in the fast assessment domains for Eurocode 8 shear capacity model without and with shear degradation, 16°. 50° and 84° percentiles for AQ50 steel pdf (Ricci et al. 2011) and concrete pdf evaluated according to Iervolino et al. (2007).

The failure domains obtained can help in the framework of fast assessment, when the amount of brittle failures is of concern because of its impact on retrofitting costs. Moreover an interesting employment of such a tool can be in the framework of large scale assessment; given the age of construction and data frequencies of geometry data (storey heights and section dimensions) of a building stock. In such cases, it is possible to obtain ω_{sw} and ω_{tot} from code prescriptions for reinforcements and material properties at the time of construction, so that elements can be classified and brittle failure occurrence in the building stock can be assessed. On the other hand material properties are always characterized by uncertainties and a probabilistic characterization of their properties can help in such a fast assessment

framework.

An example of the influence of material properties is shown in Figure 6.16 in which the domains are obtained in the 2D plane ρ_{sw}-ρ_{tot} and two normal probability density function (pdf) are assumed for concrete compressive strength, f_c, and for the steel of transversal and longitudinal reinforcement, respectively f_{yw} and f_y. The mean value of f_c was assumed equal to 25 MPa with a COV equal to 0.25 according to Iervolino et al. (2007), while f_y and f_{yw} distributions are assumed considering an AQ50 steel whose mean is equal to 371 MPa and the COV is equal to 0.09 according to Ricci et al. (2011) database. A Monte Carlo simulation was performed and f_y and f_{yw} values were assumed with the same pdf, sampling independently their realizations. Results for Lv/h equal to 3 and 5 and ν equal to 0, 0.25 and 0.5 are shown for the EC8 model in both the case of absence and maximum shear strength degradation, see Figure 6.16. EC8 model with maximum shear strength degradation shows a smaller variability than the case of absence of degradation. Furthermore the case of maximum degradation represents the proper choice for the fast assessment, since it is more conservative. So a proper fractile (e.g. 16°) can be assumed when this simplified assessment tool is employed.

The results of this practical-oriented approach suggest how the occurrence of brittle failures can be more frequent in building designed according to old seismic criteria rather than buildings designed for gravitational loads only. In buildings designed according to old seismic criteria, horizontal forces led to higher longitudinal reinforcement ratios in columns and at the same time transversal reinforcement used to be the same. In fact, transversal reinforcement used to be not designed in both cases because shear design procedure was based on a threshold criterion and seldom shear stresses, in both gravity load design and old seismic design, exceeded the threshold prescribed (in the Italian old code it used to be equal to 5 MPa). Given this situation the common ω_{sw} can lead to ductile or brittle failures according to the amount of longitudinal reinforcement ratio, ω_{tot}, see Figure 6.14 and Figure 6.15.

6.5.5. "Non conventional" brittle failures?

In the conventional framework of the assessment of existing buildings, shear capacity is evaluated only according to a strut model, but it is possible that shear stresses may cause a sliding type of failure along a well-defined plane (e.g. at the interface between concrete cast at different times). Because of external tension, shrinkage, neither treated nor checked casting surface or accidental causes, a crack may form along such a plane even before shear failure occurs (Park and Paulay, 1972). The term *interface shear transfer* is used to designate this mechanism, and possible formulations according to shear friction theory are discussed subsequently.

This kind of shear failure is generally not considered in columns because of the presence of axial force, N, and because of the presence of vertical reinforcement well distributed around the periphery of element section, giving more reliance to dowel resistance against sliding of vertical bars (Paulay and Priestley, 1992).

The mechanism of interface shear is different in initially uncracked and initially cracked concrete. In initially uncracked surfaces, the resistant mechanism is characterized by adhesion V_a and friction V_f. When the crack is formed, adhesion contribution is not present anymore but a friction contribution due to clamping action ($V_{f,c}$) is added to the friction contribution due to axial force ($V_{f,N}$) and a new additional contribution due to dowel action (V_d) can develop, see equation (6.28).

$$V_R = V_{f,N} + V_{f,c} + V_d \tag{6.28}$$

Shear friction theory in its original version (Birkeland and Birkeland, 1966) is based on the determination of clamping action due to yielding stress in reinforcement that produces a compression stress on two sides of the crack. As a result of the interlocking at the interface, the sliding movement leads to a vertical movement perpendicular to the crack; as a consequence, longitudinal reinforcement across the crack surface yields in tension. This theory is based on the following hypotheses: reinforcement should be properly anchored on

both sides of the crack, sufficiently to develop yield in steel; whereas concrete must be well confined by stirrups. Therefore, consistent with the original formulation proposed by Birkeland and Birkeland (1966) and adopted by international codes (CEN, 2005; ACI 318-05, 2005), the contribution due to clamping action is given in equation (6.29), in which A_{sl} is the area of shear-friction reinforcement, f_y is the yield strength of reinforcement and μ is the coefficient of friction. This coefficient depends on the treatment of the sliding surface.

$$V_{f,c} = \mu \cdot A_{sl} \cdot f_y \tag{6.29}$$

Obviously, due to the frictional nature of the resistance mechanism, an increase in the external axial load (that is, in the compression state on the interface area) leads to an increase in the shear strength $V_{f,N}$.

Experimental studies (Hofbeck et al., 1969) demonstrate that shear friction theory gives a conservative estimate of the shear transfer strength of initially cracked concrete and that dowel action assumes an important role in this particular situation.

The contribution of dowel action is due to the shear displacement subjected by reinforcement across the section. In European (CEN, 2005) and Italian (DM 14/1/2008) codes this contribution is expressed according to equation (6.30). Hence, interface shear strength is given by equation (6.31).

$$V_d = 0.25 \cdot A_{sl} \cdot f_y \tag{6.30}$$

$$V_R = \mu \cdot (A_{sl} \cdot f_y + N) + 0.25 \cdot A_{sl} \cdot f_y \tag{6.31}$$

Friction coefficient μ depends on the treatment of the sliding surface. International code prescriptions in relation to this coefficient are quite different; ACI proposes to assume μ equal to 1.40, 1.00 and 0.60 for monolithic concrete, intentionally roughed surfaces and untreated surfaces respectively, while European codes (CEN, 2005; DM 14/1/2008) adopt values equal to 0.60 for smooth interfaces and to 0.70 for rough interfaces.

Finally it is worth to note that according to ASCE/SEI 41-06 (2007) *shear*

friction strength shall be calculated according to ACI 318, taking into consideration the expected axial load to gravity and earthquake effects. Furthermore according to the same provisions (ASCE/SEI 41-06, 2007), *where rehabilitation involves the addition of concrete requiring overhead work with dry-pack, the shear friction coefficient μ, shall be taken as equal to 70% of the value specified by ACI 318*. This latter observation emphasizes how in the case of strong vertical components of the earthquake and or in the case of poor executive detailing, this kind of brittle failure, normally discarded for in cast structures, becomes critical and worth to be considered as it will be shown in chapter 7. Another relevant contribution to the shear friction model is provided in Model Code 2010 (CEB FIP Model Code, 2010), in which specific design is considered for the interface between concrete cast at different times and a detailed tables of adhesion and friction coefficient is given.

6.5.6. Beam-column joints

Beam and columns flexure and shear mechanisms have been discussed above as isolated members on the assumption that they can somehow be joined together to develop continuity. The design of joints requires a knowledge of the forces to be transferred through the joint and the likely ways in which transfer occurs, (Macgregor, 1997). Force transfer mechanism in concrete joints is ruled by bond and shear, as it will be clearly shown in the following, literally citing Fardis' approach regarding this aspect (Fardis, 2009).

Bending moments in beams due to gravity loading normally have the same sign at opposite faces of their joint with vertical member. By contrast, beam bending moments due to seismic shear forces are very high in the joint itself. Figure 6.17(a) illustrates the reason for the magnitude of this shear:

- With the joint considered as part of the beam, the change in the beam moment from a (high) negative value to a positive one across the joint produces a vertical shear force, $V_{jv} = \Sigma M_b/h_c = \Sigma V_b L_{cl}/2h_c$, where M_b and V_b denote the beam seismic moments and shears at the face of the joint, L_{cl} the beam clear span and h_c the depth of the column.
- With the joint considered as part of the column, the change of the column

bending moment from a high value just above the joint to an equally high value with opposite sign just below, produces a horizontal shear force, $V_{jh} = \Sigma M_c/h_b = \Sigma V_c H_{cl}/2h_b$, where M_c and V_c denote column seismic moments and shears above or below the joint, H_{cl} the clear storey height and h_b the beam depth.

The joint shear forces produce a nominal shear stress in the concrete of the joint: $v_j = \Sigma M_c/(h_c h_b b_j) = \Sigma M_b/(h_c h_b b_j)$, where $(h_c h_b b_j)$ is the volume of the joint, with b_j its effective width normal to the plane of bending, conventionally taken by seismic design codes as a function of the dimension of beams and columns framing into the joint, see CEN (2004a) for details.

Shear stresses are introduced in a joint mainly by bond along the bars of the beam and the column (or wall) around the core of the joint. Because the nominal shear stress in the concrete of the joint is the same, no matter whether it is computed from the horizontal or the vertical shear force, V_{jh} or V_{jv}, it is more convenient to compute it from the horizontal shear, V_{jh}, which is based on the forces transferred via bond stresses along the top bars of the beam. Note that, even when beam column hierarchy ($\sum M_{Rc} \geq \gamma_{Rd} \sum M_{Rb}$, see CEN, 2004a for details) is not fulfilled, the beams framing into a joint normally yield before the column or the wall. If they don't, the horizontal joint shear is overestimated if computed from the top bars of the beam, and hence is on the safe side for the joint.

So, the joint may be considered as a series system of two (independent) mechanisms of force transfer:

- from the beam and column (or wall) longitudinal bars to the core of the joint, by bond;
- from each side of the joint core to the opposite, through shear (see Figure 6.17b).

This implies that:

- if one of the two force transfer mechanisms fails, the joint fails as well; and
- the overall (shear) deformation of the joint is the sum of the individual deformations of the two mechanisms (see Figure 6.18).

Force transfer to the joint core by bond along the longitudinal bars passing through the joint or anchored in it causes slippage along these bars. Slippage shows up as fixed-end rotation, θ_{sl}, of the end of the member where the longitudinal bars belong (see Figure 6.18). Force transfer through the joint by shear causes an angular distortion (shear strain) of the joint core, γ_j (Figure 6.18). The total deformation of the joint is an apparent shear deformation, equal to the sum of γ_j and of the fixed-end rotations, θ_{sl}, at the ends of all (four, in an interior joint) members framing into the joint (unless such a fixed-end rotation is incorporated in the chord rotation of the member. The total shear deformation of a frame panel made up of two beams and two columns is

equal to the sum of:

- the average apparent shear deformation of the four joints at the corners of the panel; plus
- the average chord rotation at the (four) column ends on either side of the panel, θ_c; plus
- the average chord rotations at the (four) beam ends above and below the panel, θ_b.

It is interesting that, although it adds to $\theta_c + \theta_b$, the angular distortion (shear deformation) of the joint core, γ_j, takes place in the opposite sense with respect to the sum of $\theta_c + \theta_b$ (see Figure 6.18): the joint diagonal that shortens is the one parallel to the panel diagonal that gets longer during the deformation of the panel. This is consistent with the opposite sign of the joint shears, V_{jv}, and V_{jh}, with respect to those in the members themselves (see Figure 6.17a).

If there is no pull-out (or -through) of the beam or column bars around the joint core, shear stresses develop within the joint core with a nominal value equal to the ratio of $\Sigma M_c = \Sigma M_b$ to the volume of the joint, $h_c h_b b_j$. Shear failure of the joint, (as it will be shown in chapter 7), is far more brittle than any failure of plastic hinges around the joint, even in the columns. So, it should be prevented through design and detailing of the joint. To this end, the maximum possible shear force that can develop in the joint is established from capacity design calculations, on the basis of the capacity of the beams or the columns framing

into the joint (whichever is weaker) to deliver shear through bond along the outermost beam or column bars passing through the joint. If the sum of moment resistances of the beams framing into a joint, M_{Rb}, is less than that of the columns, M_{Rc}, ($M_{Rb} < M_{Rc}$), the shear input in the joint is governed by the beams. If pull-out (or -through) of the beam top bars does not take place, the maximum possible value of the horizontal shear force in an interior joint, V_{jh}, can be computed as:

- the maximum possible tensile force in the top bars at one face of the joint, $A_{s1}fy$,
- plus the maximum possible compressive force in the top flange at the opposite face,
- minus the shear force V_c in the column above the joint.

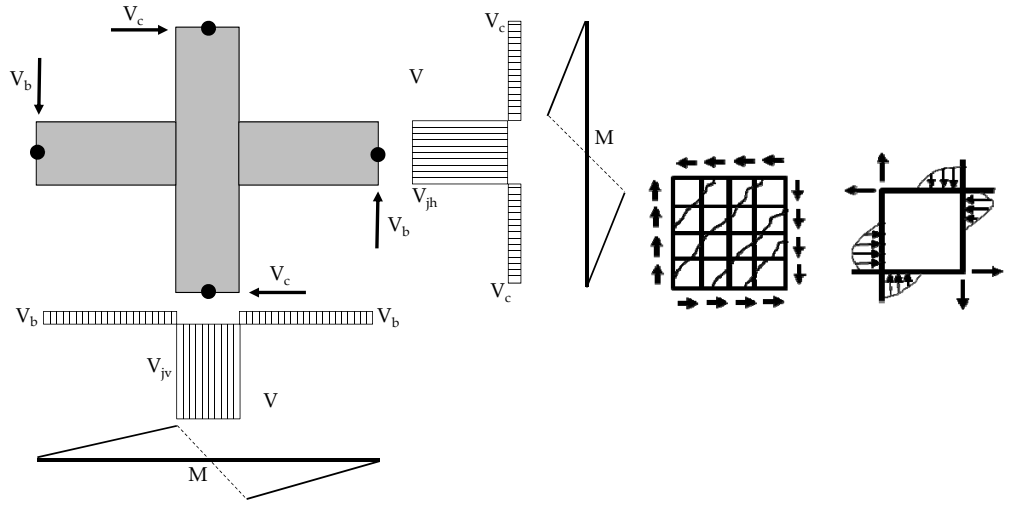

Figure 6.17. Interior beam-column joints: (a) shear forces within the joint; (b) shear resistance mechanisms. [Adapted from Fardis, 2009].

According to Eurocode 8 part 1 (CEN, 2004a), the expression for the evaluation for the horizontal shear force acting on the concrete core of the joints may be assumed equal to equation (6.32) for interior beam column joints; in which As_1 and As_2 are the cross-sectional area of the beam top reinforcement at one face of the joint and of its bottom reinforcement at the opposite face and

V_C is the column shear at beam plastic hinging. At interior beam-column joints equation (6.33) should be satisfied in which η is equal to 0.6(1-fc/250), b_j is the joint effective width, h_c is the distance between extreme layers of column reinforcement, ν is the normalized axial force in the column above the joint and f_c is given in MPa.

$$V_{jh} = \gamma_{Rd}\left(A_{s1} + A_{s2}\right)f_y - V_C \tag{6.32}$$

$$V_{jh} \le \eta f_c \sqrt{1 - \frac{\nu}{\eta}} \cdot b_j \cdot h_c \tag{6.33}$$

For existing reinforced concrete buildings Eurocode 8 part 3 (CEN, 2005) refers to the approach provided in Eurocode8 part 1 (CEN, 2004a) considering mean material properties from in-situ tests divided by the appropriate confidence factor (based on the Knowledge Level reached) and divided by the partial factor of the material, as made for all brittle failure mechanisms.

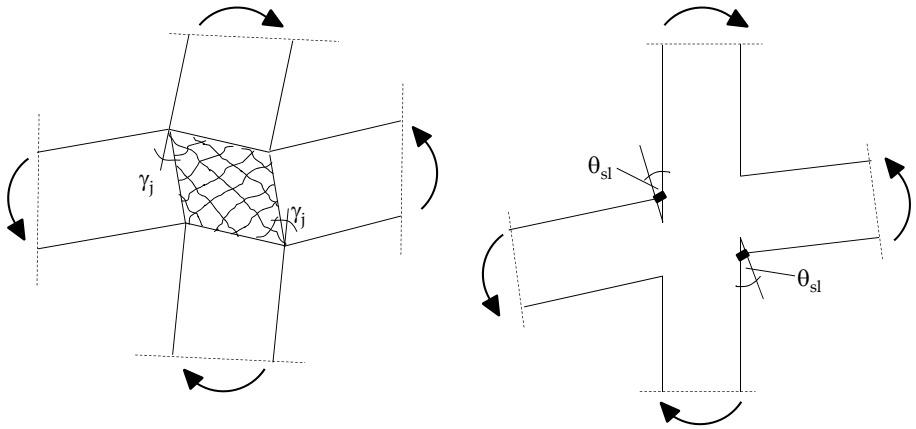

Figure 6.18. Interior beam-column joints: joint deformation. [Adapted from Fardis, 2009].

It is worth noting that the absence of capacity design in beam-column joints can lead to brittle failure and it is a frequent situation in existing RC buildings given also the strict capacity provided by codes and limited at the attainment diagonal cracking ($\sigma_I = f_{ct}$) by the principal stress in tension and compression. In fact, experimental tests on beam-column joints shows that

damage is attained after diagonal cracking, so such elements have a reserve, even if small, respect to design and assessment criteria provided by Codes, (e.g. Mitra and Lowes, 2007).

6.6 Infilled RC structures: interaction with non-structural elements

Masonry infills in reinforced concrete buildings are generally considered non-structural elements. On the other hand it is not always safe discarding their structural contribution, especially in the case of substandard existing buildings. According to Part 3 of Eurocode 8 (CEN, 2005), wherever there are no specific provisions for masonry infills, the pertinent ones of Part 1 (CEN, 2004a) apply; if walls take at least 50% of the base shear from a linear analysis, the interaction of the structure with the masonry infills may be neglected. This may be taken to imply that it is allowed then to disregard the infills in the structural model. However, this is not always a safe assumption. An asymmetric layout of the infills in plan may cause torsional response to the translational horizontal components of the seismic action; so, according to Eurocode 8 part 1 (CEN, 2004a) infills with strongly asymmetric or irregular layout in plan should be included in a 3D structural model and a sensitivity analysis of the effect of the stiffness and position of the infills should carried out (e.g., disregarding one out of three or four infill panels per planar frame). If the layout of infills in plan is not so asymmetric or irregular to warrant including them in the analysis model, the requirement in CEN (2004a) to double the accidental eccentricity in an analysis that neglects them applies for existing buildings as well. The provisions in CEN (2004a) about infills with irregular distribution in elevation address the problem in a fully force-based context. So, they can only guide the decision about including or not in the structural model heightwise irregularly distributed infills. An amplification factor (η) is included to amplify the seismic internal forces in the columns (bending moments, axial forces, shears) from the analysis for the design seismic action. Such amplification factor depends on the ratio between the total

reduction of resistance of masonry infills in the storey and the design seismic shear of the storey (see section 4.3.6 in CEN, 2004). If the value of η is less than 1.1, heightwise distribution of infills is not a sufficient reason for including them. Thus, according to Eurocode 8 part 1, infills in principle are still considered as nonstructural elements but, in any case, special provisions should be applied if masonry infills are vulnerable to out-of-plane failures (e.g. when the slenderness ratio, evaluated as the ratio of the smaller of length or height to thickness, is greater than 15). Out-of-plane failures of infills represent another critical issue that damage observed after earthquake reconnaissance emphasizes (Dolce and Manfredi, 2010).#

Therefore, the analysis of seismic response of existing RC buildings should take into account the presence of infill elements and interaction between these elements and the primary RC structural system. Effect of infills on the whole structural behavior depends on different factors that are briefly recalled in the following and have been studied in dedicated papers.

Firstly, the evaluated fundamental period of the infilled structure (Ricci et al., 2010) changes significantly if compared to the period of the bare frame model, since the structure is significantly stiffer. Furthermore, infill presence can change regularity characteristics of the structure in plan and in elevation and consequently can affect the mode of vibration of the building, as previously emphasized. In other studies made after other earthquakes that struck the Mediterranean area it is already emphasized the importance of infill contribution in the evaluation of seismic performances of RC buildings (Dolsek and Fajfar, 2001).

Secondly, infills are characterized by a brittle behavior and the high contribution in strength they supply to a RC building suddenly decrease for low values of drift (Dolsek and Fajfar, 2004). On the other hand, it is worth to note that infill impact on the structural performances of buildings becomes a critical issue when RC primary elements are designed according to obsolete criteria and the structure is characterized by an insufficient global and local ductility. The latter can be observed when seismic performances of

contemporary and existing infilled frame structures are compared (Dolsek and Fajfar, 2005). Infilled RC building behavior can be significantly different if low or high level of seismic intensity is attained (Dolsek and Fajfar, 2001).

If infill distribution is irregular in plan or elevation, their contribution introduces a source of irregularity (e.g. *Pilotis effect*) and the possibility to register soft-storey mechanisms is dramatically increased, especially when no capacity design criterion has been employed in the design of the bare frame (Dolsek and Fajfar, 2001).

Mechanical properties of the infills represent another critical factor that can vary the effect of infills on the performances of the whole structure, since they are considered nonstructural elements and their properties, not systematically checked, can vary significantly (Colangelo, 2005) because of the local building practice. Regarding this latter issue, it is important to stress the relative weight that infills have respect to the mechanical properties of the bare frame. Because of all the variables considered (seismic intensity level, old or contemporary design approach, distribution and mechanical properties of the infills) it is tough to say if structural contribution of these "nonstructural" elements increases or decreases the overall seismic capacity of the building.

6.7 Conclusions and perspectives

Reinforced concrete structures capacity limits represents a relevant issue in PBEE for RC structures. According to the different mode of failure of elements considered, different capacity models are provided in codes and literature. In the framework of assessment of existing buildings some specific issues arises and becomes critical, such as brittle failures, caused by the absence of capacity design or pernicious interaction with masonry infills. Regarding brittle failure mechanisms there is still much to do in term of experimental results and analytical models, even if a positive trend can be found regarding this aspect thanks to the recent regression approaches based on experimental results, that have been recently adopted by different codes.

The key issue is that the mechanical phenomenon is physically complex

and different interpretations lead to different theories and models. The latter is the reason why codes and literature can suggest different brittle capacity models that can lead to different capacities.

In the whole context of assessment of existing buildings, practice-oriented approaches can be useful as fast assessment tools for the evaluation of the impact of brittle failures on the total retrofitting costs. Such tools can lead, additionally, to important general considerations on the occurrence of brittle failures in building stocks.

Other critical issue are beam-column joint failures, mainly governed by shear and bond mechanisms. Force distribution in these elements allows shear and moment transfer, producing diagonal cracking. Hence, when no transversal reinforcement is present in the joint (typical situation of existing buildings) failure due to diagonal compression in the concrete is quite likely to occur.

In the context of assessment of existing buildings, also "non-conventional" modes of failures can play a key role. In fact, mode of failures such as sliding shear mechanism, normally discarded in conventional design thanks to a proper detailing of the elements, can occur easily and become the principal cause of structural collapses. Finally local interaction between reinforced concrete elements and masonry infills can increase the shear demand in elements.

REFERENCES

ACI 318-05, 2005. Building code requirements for structural concrete (ACI 318-05) and commentary (ACI 318R-05). ACI committee 318 structural building code. American Concrete Institute.

American Society of Civil Engineers (ASCE), 2007. Seismic Rehabilitation of Existing Buildings, ASCE/SEI 41-06, Reston, Virginia.

Berry M., Parrish M., Eberhard M., 2004. PEER structural performance database: user's manual (version 1.0). Pacific Earthquake Engineering Research Center, University of California, Berkeley.

Biskinis D.E., Roupakias G. K., Fardis M.N., 2004. Degradation of shear strength of reinforced concrete members with inelastic cyclic displacement, *ACI Structural Journal*, **101**(6), 773-783.

Birkeland, P. W., and Birkeland, H. W., 1966. Connections in Precast Concrete Construction. *ACI Journal, Proceed*ings **63**(3), March, 345-368.

BS EN 1990, 2002. Eurocode – Basis of Structural Design.

CEB FIP Model Code, 2010. First complete draft, April 2010. Fib Bulletin 56, Model Code 2010 - First complete draft, Volume 2, chapters 7-10.

Colangelo F., 2005. Pseudo-dynamic seismic response of reinforced concrete frames infilled with non-structural brick masonry, *Earthquake Engineering and structural Dynamics*, **34**, 1219-1241.

Comité Européen de Normalisation (CEN), 2004a. Eurocode 8 – Design of Structures for earthquake resistance – Part 1: General rules, seismic actions and rules for buildings. EN 1998-1, CEN, Brussels.

Comité Européen de Normalisation (CEN), 2004b. Eurocode 2 – Design of concrete structures – Part 1-1: General rules and rules for buildings. EN 1998-1-1, CEN, Brussels.

Comité Européen de Normalisation (CEN), 2005. Eurocode 8 – Design of Structures for earthquake resistance – Part 3: assessment and retrofitting of buildings. EN 1998-3, CEN, Brussels.

Comité Européen de Normalisation, 2009. Corrigenda to EN 1998-3, document CEN/TC250/SC8/N437A. CEN, Brussels.

Cosenza E., Manfredi G., Pecce M., 2008. Strutture in cemento armato. Basi della progettazione, Hoepli, Milano.

CS.LL.PP. Circolare 617, 2009. Istruzioni per l'applicazione delle Norme Tecniche per le Costruzioni, Gazzetta Ufficiale della Repubblica Italiana 47, 2/2/2009 (in Italian).

Decreto Ministeriale del 14 gennaio, 1992. Norme tecniche per il calcolo, l'esecuzione delle opere in cemento armato, normale e precompresso e per le strutture metalliche, Gazzetta Ufficiale della Repubblica Italiana 65, 18/3/1992.

Decreto Ministeriale del 9 gennaio, 1996. Norme tecniche per il calcolo, l'esecuzione e il collaudo delle strutture in cemento armato, normale e precompresso e per le strutture metalliche, Gazzetta Ufficiale della Repubblica Italiana 29, 5/2/1996.

Decreto Ministeriale del 14 gennaio, 2008. Approvazione delle nuove norme tecniche per le costruzioni. G.U. n. 29 del 4/2/2008 (in Italian).

Dolce M., Manfredi G., 2009. Research Needs in Earthquake Engineering Highlighted by the 2009 L'Aquila Earthquake, The State of Earthquake Engineering Research in Italy: the ReLUIS-DPC 2005-2008 Project. Editors: Gaetano Manfredi and Mauro Dolce.

Dolšek M, Fajfar P, 2001. Soft storey effects in uniformly infilled reinforced concrete frames, *Journal of Earthquake Engineering* , **5**(1), 1-12.

Dolšek M, Fajfar P., 2004. Inelastic spectra for infilled reinforced concrete frames, *Earthquake Engineering and Structural Dynamics*, **33**, 1395-1416.

Dolšek M, Fajfar P., 2005. Simplfied non-linear seismic analysis of infilled reinforced concrete frames, *Earthquake Engineering and Structural Dynamics*, **34**., 49-66.

Fardis M.N., 2006. Design rules for FRP retrofitting according to Eurocode 8 and their background. Lecture to Fib Course 2006 .Retrofitting of concrete structures through externally bonded FRPs with emphasis on seismic applications, Mexico.

Fardis M.N., 2009. Seismic design, assessment and retrofitting of concrete buildings based on EN-Eurocode 8, Springer, August.

Haselton C.B., Deierlein G.G., 2007. Assessing seismic collapse safety of modern reinforced concrete moment frame buildings. PEER Report No. 2007/08. Pacific Earthquake Engineering Research Center, University of California, Berkeley.

Haselton C.B., Liel A.B., Taylor Lange S., Deierlein G.G., 2008. Beam-column element model calibrated for predicting flexural response leading to global collapse of RC

frame buildings. PEER Report No. 2007/03. Pacific Earthquake Engineering Research Center, University of California, Berkeley.

Hofbeck J.A., Ibrahim I.O. and Mattock A.H., 1969. Shear transfer in reinforced concrete. *ACI Journal*, **66**(13), February, 119-128.

Ibarra L.F., Medina R.A., Krawinkler H., 2004. Hysteretic models that incorporate strength and stiffness deterioration, *Earthquake Engineering and Structural Dynamics*, **34**, 1489-1511.

Iervolino I., Manfredi G., Polese M., Verderame G.M., Fabbrocino G., 2007. Seismic risk of RC building classes, *Engineering Structures*, **29**, 813-820.

Lam S.S.E.,Wu B.,Wong Y.,Wang Z.Y., Liu Z.Q., Li C.S., 2003. Drift capacity of rectangular reinforced concrete columns with low lateral confinement and high-axial load. *ASCE Journal of Structural Engineering*, **129**(6), 733–742.

Macgregor J.G., 1997. Reinforced Concrete Mechanics and Design. Prentice Hall Edition, New Jersey.

Mitra N., Lowes N.L., 2007. Evaluation, Calibration, and Verification of a Reinforced Concrete Beam–Column Joint Model. *ASCE Journal of Structural Engineering*, **133**(1), 105-120.

Ordinanza del Presidente del Consiglio dei Ministri n. 3274 del 20/3/2003, 2003. Primi elementi in materia di criteri generali per la classificazione sismica del territorio nazionale e di normative tecniche per le costruzioni in zona sismica. G.U. n. 105 dell'8/5/2003 (in Italian).

Panagiotakos T.B., Fardis M.N., 2001. Deformation of reinforced concrete members at yielding and ultimate. *ACI Structural Journal*, **98**(2), 135–148.

Park R., Paulay T., 1975. Reinforced Concrete Structures. Wiley, New York.

Paulay T., Priestley M.J.N., 1992. Seismic Design of Reinforced Concrete Structures and Masonry Buildings. Wiley, New York.

Perus I., Poljansek K., Fajfar P., 2006. Flexural deformation capacity of rectangular RC columns determined by the CAE method. *Earthquake Engineering and Structural Dynamics*, **35**(12), 1453–1470.

Perus I., Fajfar P., 2007. Prediction of the force-drift envelope for RC columns in flexure by the CAE method. *Earthquake Engineering and Structural Dynamics*, **36**(15), 2345–2363.

Priestley M. J. N.; Verma R., Xiao Y., 1994. Seismic Shear Strength of Reinforced Concrete Columns, *Journal of the Structural Division ASCE*, **120**(8), 2310-2329.

Ricci P., Verderame G.M., Manfredi G., 2010. Analytical investigation of elastic period of infilled RC MRF buildings, *Engineering Structures*, **33**(2), 308-319.

Ricci P., Verderame G.M., Manfredi G., 2011. Analisi statistica delle proprietà meccaniche degli acciai da cemento armato utilizzati tra il 1950 e il 1980. *XIV Convegno ANIDIS L'Ingegneria Sismica in Italia*, 18-22 September, Bari, Italy (in Italian).

Rossetto T., 2002. Prediction of deformation capacity of non-seismically designed reinforced concrete members. In: Proceedings of the 7th U.S. national conference on earthquake engineering, Boston, July 21–25.

Sezen, H., 2002. Seismic Behavior and Modeling of Reinforced Concrete Building Columns," PhD dissertation, Department of Civil and Environmental Engineering, University of California, Berkeley, (http://library.eerc.berkeley.edu/archives/sezen/).

Sezen H., Moehle J.P., 2004. Shear strength model for lightly reinforced concrete columns, *ASCE Journal of Structural Engineering*, **130**(11), 1692-1703.

Verderame G.M., Fabbrocino G., Manfredi G., 2008a. Seismic response of RC columns with smooth reinforcement. Part I: monotonic tests. *Engineering Structures*, **30**(9), 2277–2288

Verderame G.M., Fabbrocino G., Manfredi G., 2008b. Seismic response of RC columns with smooth reinforcement. Part II: cyclic tests. *Engineering Structures*, **30**(9), 2289–2300

Verderame G.M., Ricci P., Manfredi G., Cosenza E., 2010. Ultimate chord rotation of RC columns with smooth bars: some considerations about EC8 prescriptions, *Bulletin of Earthquake Engineering*, **8**(6), 1351-1373.

Zhu L., Elwood K.J., Haukaas T., 2007. Classification and seismic safety evaluation of existing reinforced concrete columns. *ASCE Journal of Structural Engineering,* **133**(9), 1316–1330.

Chapter 7

EXISTING REINFORCED CONCRETE BUILDING PERFORMANCES: EARTHQUAKE DAMAGE OBSERVATION

Ricci P., De Luca F., Verderame G.M. 6th April 2009 L'Aquila earthquake, Italy: reinforced concrete building performance. Bulletin of Earthquake Engineering, 9(1), 2011 pp. 285-305.

Verderame G.M., De Luca F., Ricci P., Manfredi G.. Preliminary analysis of a soft-storey mechanism after the 2009 L'Aquila earthquake. Earthquake Engineering and Structural Dynamics, 40(8), pp. 925-944, 2011.

7.1 Authorship of Chapter

This chapter is based on the two publications (cited above). It is the result of a field campaign made by a DIST team in the days right after the 6th April 2009 L'Aquila earthquake to which Dr Paolo Ricci and Dr Gerardo Verderame took part. The field photos have been studied and analyzed in the light of Italian building code provisions of the last century and account for the specific characteristics of L'Aquila building stock. Such an approach can be placed in the Performance Based Earthquake Engineering framework between the aspects of *modeling of damage states* and *failure and loss estimation*; actually this kind of field campaigns represent a test bed for the whole complex of PBEE approach and for its further improvements. The filed photos of a soft storey mechanism suggested a further, more detailed, visual survey carried out on this structure. This latter investigation gave the chance to pursue a back analysis of the causes of the collapse of this case study building form an analytical point of view.

7.2 Introduction

Field campaigns represent an important tool for design and retrofitting practice and can be considered the main basis for improvements in codes and local building practice. Many examples of in-field campaigns after strong earthquakes (Decanini et al. 2004; Hosseini 2005; Loh et al. 2003; Rossetto and Peiris 2009) can be found in literature, they are all aimed at identifying the main structural causes of damage as well as the main characteristics of strong motion. A photographic documentation that was collected in the first days after the L'Aquila earthquake mainshock is provided in the following, focusing the target on reinforced concrete buildings. Damage and structural performances of RC buildings are described and analyzed, and attempts are made to identify the main weaknesses of the building stock. The principal causes of structural and non-structural damage are determined, herein, by a three-step process. The first step involves a data overview aimed at evaluating the impact of RC structures on the whole building stock and a detailed review of design codes in force at the time of construction of the buildings in the area. The second step involves analysis of the earthquake's main characteristics (see also Appendix C); the main aim of this step is the comparison with seismic demand provided for by codes. The third step involves analysis of the photographic documentation in the light of the previous steps, with a view to determining structural weaknesses that can be targeted as the main causes of global and local collapses and non-structural damage. Within the analysis of photographic documentation of collapse, a case study structure is selected and a back analysis to assess analytically the causes of the failure is carried out.

7.3 Reinforced concrete building stock in L'Aquila and seismic design criteria

An historical overview of the urban expansion of L'Aquila city and its actual characteristics in term of building stock (age of construction, building type, number of stories) are evaluated to point out the general characteristics of

the area struck by the earthquake and, above all, to highlight the impact of reinforced concrete buildings and their characteristics on the whole stock. Aimed at completing this preliminary step for the analysis of the damage observed in reinforced concrete buildings, an overview of seismic code provisions in Italy, with a special attention to L'Aquila area, is provided, ending up with a detailed review of seismic codes provisions regarding reinforced concrete structures from the beginning of XX century.

7.3.1. L'Aquila building stock

The layout of the ancient city of L'Aquila is characterized by two major streets crossing at right-angles at a place called "Quattro Cantoni". The historical centre (Figure 7.1) is situated on a raised hill overlooking the surrounding area. It is encircled by medieval walls, which still stand almost completely undamaged.

The first structures beyond the ancient perimeter were the sports facilities in Viale Gran Sasso, built in the 1930s. However, urbanization accelerated after World War II, especially during the 1960s and 1970s, following the opening of the highway to Rome. In 1965 and 1975 two urban plans were enacted. Expansion mainly occurred in on the north-western side of the city, leading in a few years to the complete saturation of the urban area bounded by the same highway (Figure 7.1). Later expansion radiated out from the historical centre on all sides, except to the south-west, the course of the Aterno river (Figure 7.1).

The current urban structure of L'Aquila is that of an historical centre surrounded by densely-packed suburbs, comprising the quarters of Pettino, Santa Barbara and Torrione, and less densely populated areas in the North-Western, including Coppito, Sant'Antonio and Torretta quarters. The remaining area within the city's administrative boundaries includes several villages in the surrounding area.

According to data from the Italian National Institute of Statistics (*Istituto Nazionale di Statistica*, ISTAT), see Figure 7.2 and Figure 7.3, collected in 2001, which represent the most recent official source for information about the

building stock in Italy, and hence in the L'Aquila area.

Data that identify age of construction of the buildings (Figure 7.2) indicate that 55% of the entire stock was built after 1945. 24% of buildings are reinforced concrete structures, 68% masonry structures and 8% structures of unspecified type (Figure 7.3a). A low overall incidence of RC structures shows that after 1945 new masonry structures were still being built and that the number of RC structures increased gradually over time. Based on the distribution of number of storeys (Figure 7.3b), only 5% of the buildings have more than three storeys. Assuming that all buildings with more than three storeys are RC structures, it may still be inferred that the vast majority of L'Aquila RC buildings are no more than three storeys tall.

Figure 7.1. L'Aquila: historical centre (black line), the Aterno river (blue line) and the highway (yellow line) (Google Earth©)

If the interstorey height is considered to vary between 3.0 and 3.5 meters, approximate formulation provided by the Eurocode (CEN, 2004) for RC frame structures gives for three-storey buildings a fundamental period of 0.4 seconds.

Working hypotheses assumed in this section, which were useful in defining points of comparison between codes, are mostly confirmed by representative samples of buildings employed in other field campaigns carried out for the same earthquake (e.g. Liel and Lynch, 2009).

According to previous observations, in the following section 7.4.1, when comparing different Italian Code spectral shapes, the comparison is focused on

period values that range from 0 to 0.4 seconds. The latter assumption allows a comparison between constant acceleration branches of the spectra. A general review of design prescriptions in recent decades is employed to identify the main weaknesses of the building stock and to finally compare seismic demand given by codes with the demand of the earthquake event considered in this study.

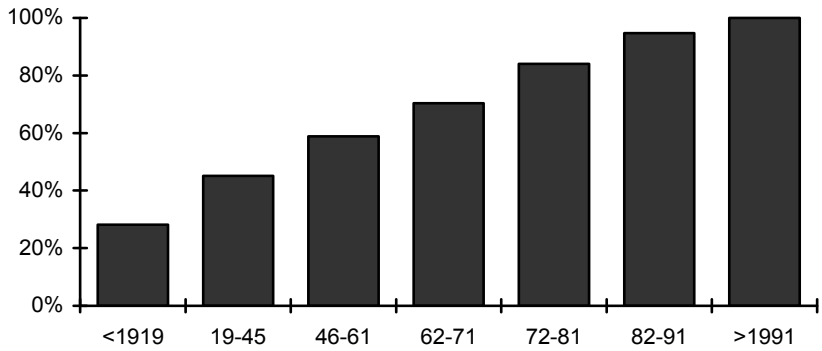

Figure 7.2. 2001 census ISTAT data for L'Aquila: age of construction.

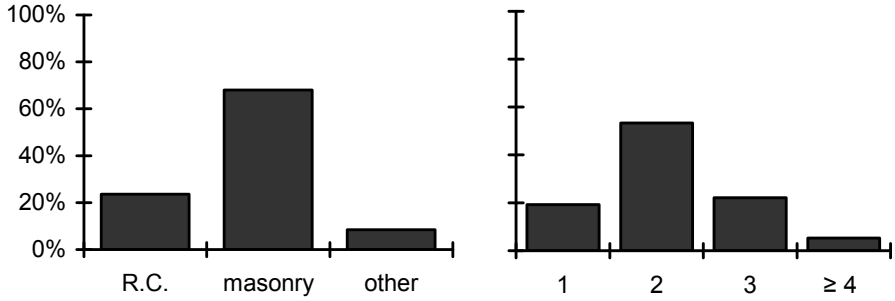

Figure 7.3. 2001 census ISTAT data for L'Aquila: (a) building type, (b) number of stories.

7.3.2. Seismic design criteria

L'Aquila and its neighborhood were first legally recognized as a seismic zone in 1915. A specific law (RDL 573, 1915) was passed after the catastrophic seismic event occurring in January 1915 that struck Abruzzo (the Marsica earthquake) killing more than 29,000 people.

In 1927 (RDL 431, 1927) a more detailed seismic classification was

introduced; this classification divided the Italian seismic area into two different categories; L'Aquila belonged to the less restricted one (second category). Seismic provisions were simply achieved by limiting the number of storeys: for the second category zone the 1927 law allowed construction of three-storey buildings, and for specific situations even four-storey buildings were accepted. Horizontal forces were equal to 1/10 of the storey weight for structures up to 15 meters tall or 1/8 for structures higher than this limit. This code gave specific prescriptions for RC structures including prescriptions for dimensions of beam and column sections and the least amount of steel reinforcement required.

In the following years, between 1930 and 1937, three seismic codes were enacted (RDL 682, 1930; RDL 640, 1935; RDL 2105, 1937) and their main concern was evaluation of seismic forces. For seismic vertical action the additional load was determined as equal to 1/3 of the structural weight, thus reducing the amount applied in the 1915 regulations. In second category zones the ratio between seismic horizontal forces and vertical forces due to gravity loads (base shear coefficient) was initially 0.05 (RDL 640, 1935) and then 0.07 (RDL 2105, 1937). These prescriptions were confirmed in 1962 (Legge 1684, 1962) with less restrictive limits about building height and setting the maximum number of storeys at seven. Under this law further areas of the country were classified as seismic.

In 1975 (DM 3/3/1975) a fundamental innovation was introduced into the analytical procedure: for the first time within Italian regulations the dynamic properties of the structures were considered. Starting from this year, seismic action could be determined by means of static and dynamic analyses. In the static analysis, the resultant of lateral force distribution applied to the building was given by equation (7.1), where W is the total weight of the structural masses; R the response coefficient, assumed as a function of the fundamental period of the structure; coefficient C represents the seismic action, see equation (7.2), and is defined by means of S, the seismic intensity parameter. Coefficients ε and β respectively express soil compressibility

(ε=1.00-1.30) and the possible presence of structural walls (β=1.00-1.20).

$$F_h = C \cdot R \cdot \varepsilon \cdot \beta \cdot W \tag{7.1}$$

$$C = \frac{S - 2}{100} \tag{7.2}$$

$$F_h = 0.07 \cdot W \tag{7.3}$$

For second category zones, S was assumed equal to 9. If coefficients ε and β were considered equal to 1, respectively corresponding to stiff soil and absence of structural walls, a structure, whose fundamental period was lower than 0.8 seconds, was characterized by a base shear coefficient (F_h /W) of 0.07 and it was the same as that adopted up to 1975, see equation (6.3).

The coefficient given by the product of C and R should be interpreted as a design inelastic acceleration demand: it took into account dynamic properties of the structure and a strength reduction factor evaluated upon dissipative capacity of the structure. Nevertheless, lateral forces applied to the building were proportional to the height of the slab at each storey determined from the foundation level, assuming a linear distribution with an "inverted triangular" shape that is more suitable to represent the actual dynamic behavior of the structure, compared with previous code prescriptions.

New generation codes explicitly express this kind of dissipative capacity of the structures; Eurocode 8 (CEN, 2004) does it by means of the "behavior factor". According to the Eurocode 8 definition, the behavior factor *q* is an approximation of the ratio of the seismic forces that the structure would experience if its response was completely elastic with 5% viscous damping to the seismic forces that may be used in the design, with a conventional elastic analysis model, still ensuring a satisfactory response of the structure. The values of *q*, which also account for the influence of the viscous damping being different from 5%, are given for various materials and structural systems according to the relevant ductility classes.

Regarding seismic input, even if different new seismic design codes were approved (DM 24/1/1986; DM 16/1/1996), no changes have been introduced

regarding this aspect since 1975. On the other hand, in this period, the Limit State method was introduced and, for Ultimate Limit State assessment, design acceleration was supposed to be increased by a factor of 1.50, thus obtaining an acceleration of (1.50 ·0.07g), equal to 0.105g.

Furthermore, it is worth noting that the first prescriptions close to the *performance-based seismic design* approach, such as the attainment of both proper local and global ductility capacity, were provided in 1997 with an explanatory document attached to the 1996 code (CS. LL. PP., 1997). In this document there were limits for longitudinal and transversal reinforcement of beams and columns with specific prescription in the end zone of each structural element (critical region). In the 1997 document, additional prescriptions were provided regarding proper anchorage of bars, and it was prescribed to lengthen longitudinal and transversal reinforcement of the column in beam-column joints. The latter prescription regarding beam-column joints was aimed at giving a proper local ductility to the element. Although this document (CS. LL. PP., 1997) represented an important step towards *performance-based design* criteria in Italy, lack in prescriptions about regularity criteria in plan and elevation is still recognizable and these criteria remained qualitative, without any specific quantitative definition to help in regularity classification.

In the 2003 seismic code (OPCM 3274, 2003) and its following modifications (OPCM 3431, 2005) an innovative seismic input definition was introduced, representing the first real upgrade towards the Eurocode 8 approach. In this document an elastic spectrum was provided with a defined shape in which the only value to be changed, considered a function of the seismic zone, was the anchorage Peak Ground Acceleration (PGA) on stiff soil type (ground type A). L'Aquila belonged to the second category and the PGA value on ground type A was 0.25g. This spectrum was to be amplified considering site specific characteristics, taking into account other ground types and topographic conditions. The elastic acceleration spectrum was to be reduced by the q factor value depending on the specific structural type, thus obtaining a design acceleration spectrum. This document explicitly introduced

in Italy the *strength hierarchy* concept, ensuring the development of inelastic deformations in the highest possible number of ductile elements and not in elements with lower rotational capacity (that is, in beams and not in columns, due to the different axial load), but also providing over-strength to brittle failure mechanisms with respect to ductile ones. Furthermore, proper quantitative definition of regularity criteria in plan and in elevation was introduced, fixing maximum variation of mass, stiffness and strength over building height.

The most recent Italian code (DM 14/1/2008) defines maximum acceleration expected at the site no longer with division in terms of seismic zones but as a function of geographic coordinates of the site. For L'Aquila (latitude 42.38; longitude 13.35), the PGA is 0.261 g on ground type A for a 10% probability of exceedance in 50 years. In the case of L'Aquila, 2003 and 2008 PGA values are very close to each other.

7.3.3. Non structural elements and damage limitation criteria

The 1975 and 1986 codes (DM 3/3/1975; DM 24/1/1986) laid down the first stipulations concerning structural maximum allowable deformation under seismic loads, but verification was not mandatory unless specific requirements in terms of interstorey displacement limitation were necessary to preserve functionality of connection or restraint elements.

In the 1996 code non-structural damage limitation was first introduced. Assuming η_p and η_d are the elastic interstorey displacement demand respectively produced by earthquake loads and other loads, total interstorey displacement demand η_t was evaluated according to equation (7.4), where λ was considered a function of the importance factor and of the specific use of the building; it was given equal to 2, 3 and 4 for importance coefficient (I) respectively equal to 1.0, 1.2 and 1.4. When the Limit State method was employed in verification, a χ value of 1.5 was assumed.

$$\eta_t = \left(\eta_p \pm \lambda \cdot \eta_d\right) / \chi \tag{7.4}$$

The interstorey displacement demand evaluated according to equation (6.4) had to be lower than prescribed interstorey capacity in order to ensure that no expulsion of internal or external infill panels took place. Interstorey displacement capacity was limited to 0.002 h, where h was the interstorey height, if infill panels were brittle and firmly connected to the structure, or to 0.004 h if infill panels did not interact with structure deformation.

The 1997 explanatory document to the 1996 code (CS.LL. PP., 1997) further specified the evaluation of frame-infills interaction; in specific conditions, such as an effective connection between panel and frame, the contribution of nonstructural elements could be taken into account in structural analysis. Deformability of the composite frame-infills system could be determined assuming an equivalent strut model to account for infill presence, calibrated according to infill mechanical characteristics.

Infill verification took into account different collapse mechanisms (horizontal sliding failure, diagonal cracking failure and corner crushing failure) and axial load variation in columns due to interaction with infills had to be considered.

According to the 2003 seismic code (OPCM 3274, 2003) a damage limitation spectrum was defined dividing the elastic spectrum by a 2.5 reduction factor. Interstorey drift ratio (IDR), the ratio between interstorey displacement (evaluated by assuming the damage limitation spectrum as seismic input) and interstorey height, was compared with 0.005 when infills were firmly connected to the concrete frame or with 0.01 when infills did not suffer damage due to their deformability or to the nature of the connection with the surrounding RC frame. A comparison between 1996 and 2003 damage limitation requirements makes it evident that a higher IDR capacity was assumed but a more severe seismic input was considered.

Non-structural elements required additional and specific verification, which in the case of infill panels concerned possible out-of-plane failure mechanisms. This kind of verification could be ignored if specific design procedures aimed at avoiding brittle collapse or out-of-plane failure were

adopted. Furthermore, a very irregular distribution of the infill panels in plan or in elevation (not quantitatively defined) was penalized by the code, assuming a higher value of seismic action, in order to account for possible damage concentration due to irregularity. Possible local interaction mechanisms in partially infilled frame bays were considered by specific and additional prescriptions on the amount of reinforcement and shear demand in columns adjacent to the infill panels.

The current seismic code in Italy (DM 14/1/2008) prescribes a specific Damage Limitation spectrum evaluated according to a hazard analysis corresponding to 63% exceedance probability in the considered life cycle of the building (50 years for ordinary buildings). Damage Limitation capacity limits are the same as those provided by the 2003 code and prescriptions about irregular distribution of infills are unchanged.

7.4 Earthquake characteristics

On 6th April 2009 an earthquake of magnitude M_w = 6.3 struck the Abruzzo region; the epicenter was only about 6 km from the city of L'Aquila. The event resulted in casualties and damage to buildings, lifelines and other infrastructures.

This was the third largest earthquake recorded by strong-motion instruments since 1972, after the 1976 Friuli (M_w = 6.4) and the 1980 Irpinia (M_w = 6.9) events. The event was generated by a normal fault, the epicenter coordinates being latitude 42.334 and longitude 13.334. The area has been hit by destructive earthquakes in the past, with events being documented since 1300 BC (Stucchi et al. 2007). The three strongest earthquakes occurred respectively in 1349 (epicentral intensity I_0=IX-X MCS), 1461 (I_0=X) and 1703 (I_0=X) (Ameri et al. 2009).

The L'Aquila earthquake mainshock was registered by 55 stations of the National Accelerometric Network (*Rete Accelerometrica Nazionale*, RAN), the stations being located from 4.8 to 278 km from the epicenter. The closest

stations both to the epicentre and to the centre of L'Aquila are located on the fault trace (AQA, AQV, AQG and AQK), see Appendix C for further details. The maximum PGA registered was 613.8 cm/s² on the East-West component of station AQV, whose soil type was classified according to cross-hole test results as type B (Chioccarelli et al. 2009; Ameri et al. 2009).

Elastic response spectra of the four closest stations (Figure 7.4) are evaluated after baseline correction and filtering on the registered signals (Chioccarelli et al. 2009); both horizontal components (Figure 7.4a) and vertical components (Figure 7.4b) are reported. Vertical components of the registered signals showed quite strong spectral acceleration values especially in the high frequency range, see Appendix C.

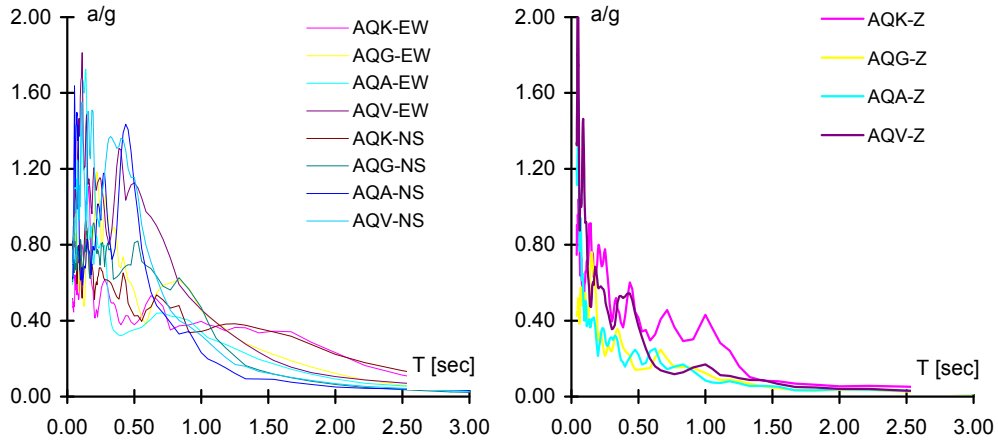

Figure 7.4. Elastic response spectra of horizontal (a) and vertical (b) components of L'Aquila mainshock registered signals (stations AQA, AQV, AQG and AQK).

A reliable comparison with spectral results reported in Figure 7.4 is provided by Figure 7.5, where hazard maps for the L'Aquila area are reported in terms of PGA (see Figure 7.5a) and in terms of spectral acceleration for a 0.4-second period, $S_a(T=0.4)$, with 10% of exceedance probability in 50 years on stiff soil (official Italian hazard data available at http://esse1-gis.mi.ingv.it), (see Figure 7.5b).

From these maps it may be recognized that PGA for L'Aquila is in the range (0.25-0.275)g while $S_a(T=0.4)$ is in the range (0.50-0.60)g. PGA and

S_a(T=0.4) ranges suggested by official Italian hazard data can be compared with the corresponding data recorded at the four stations closest to the epicenter.

Maximum PGA was 0.63g in the EW component of station AQV and minimum PGA was 0.34g in the NS component of station AQK, while S_a(T=0.4) ranged from the minimum 0.32g of the EW component of station AQA to the maximum 1.36g of the EW component of station AQV. Considering possible soil amplification, not included in Figure 7.5 maps, it may still be noted that registered values exceed the expected value for a return period (Tr) of 475 years. Registered signals and earthquake characteristics can provide further information for the critical analysis of damage observed on RC buildings.

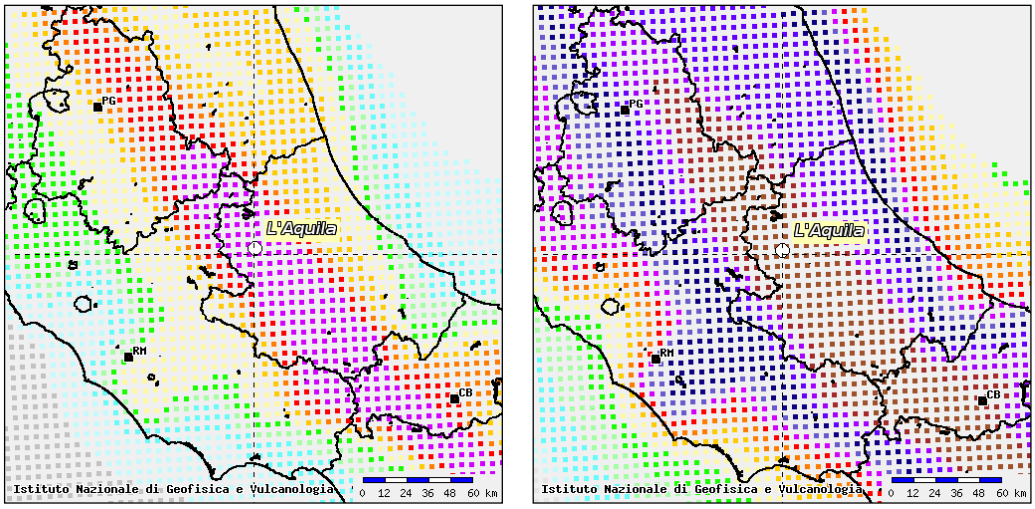

Figure 7.5. Hazard map of 10% probability of exceedance in 50 years for L'Aquila zone: PGA (a) and spectral acceleration at 0.4 seconds (b).

7.4.1. Spectral consideration

Seismic demand defined by previous codes can be considered equal to the lowest seismic capacity of structures designed according to them. The seismic demand of old codes can be easily compared with the current code seismic demand and actual seismic demand registered during the 2009

L'Aquila event.

Eurocode 8 (CEN 2004) and the Italian Code (DM 14/1/2008) provide a Newmark-Hall functional expression for the elastic spectrum. By means of official Italian hazard data, given the specific geographic coordinates and ground type, the elastic spectrum may be defined for the considered site. Material, reinforced concrete in this study, and ductility class are necessary to define the behavior factor q (see section 7.3); the latter is employed to pass from the elastic spectrum to the design spectrum.

Both Eurocode 8 and the Italian code provide two ductility classes depending on the hysteretic dissipation capacity. Both classes correspond to buildings designed, dimensioned and detailed in accordance with specific earthquake-resistant provisions, enabling the structure to develop stable mechanisms associated with large dissipation of hysteretic energy under repeated reversed loading, without suffering brittle failures.

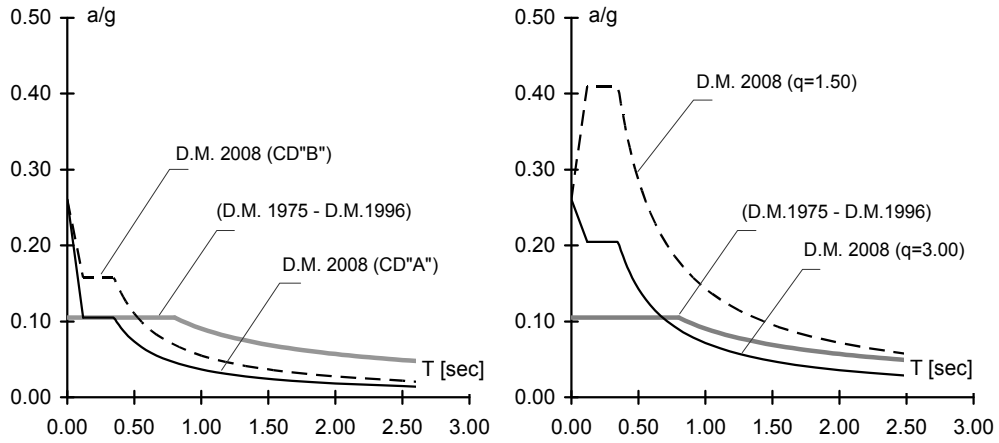

Figure 7.6. Inelastic old code spectra compared with current code spectra for new design structures (a) and existing structures (b).

Design spectrum defined by the Italian Code (DM 14/1/2008) for the Life Safety Limit State can be compared with the 1996 Ultimate Limit State spectral shape; the former was evaluated for both ductility classes, namely high ductility class (CD "A") and low ductility class (CD "B"), assuming a behavior factor q determined for new design RC frame structures (Figure 7.6a).

Another interesting comparison can be made between the 1996 inelastic spectral shape and design response spectra evaluated for existing RC structures considering extreme values of q factor (1.5-3.0) according to the current Italian seismic code (CS. LL. PP., 2009), see Figure 7.6b. Indeed, both Eurocode 8 and the Italian Code provide different values of behavior factor q for new design and existing buildings, presuming that the latter cannot be characterized by properly high hysteretic dissipation capacity.

According to the Ultimate Limit State spectrum adopted in Italy between 1975 and 1996, a constant value of 0.105g was assumed for spectral ordinates between 0 and 0.8 seconds. This value for design inelastic acceleration can be reasonably considered representative of the minimum base shear coefficient of the great majority of L'Aquila RC buildings, if properly designed according to codes until 2003 and given ISTAT data (Figure 7.1).

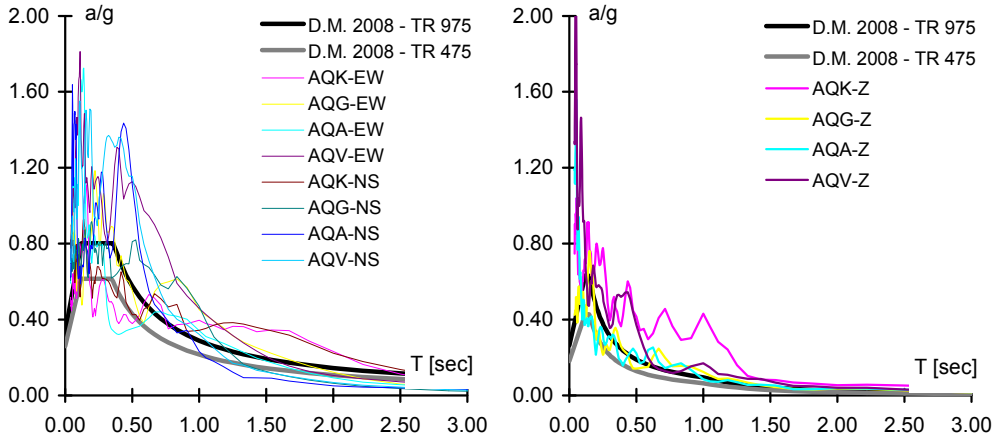

Figure 7.7. Current elastic code spectra compared with recorded signal spectra for horizontal (a) and vertical component (b).

Comparing constant acceleration branches of the various spectra shown in Figure 7.6a it may be noted that a building designed in CD "A", and regular in plan and elevation, so characterized by a q factor of 5.85, according to the current Italian Code, is designed for the same seismic demand as in the old codes. However, it has to be considered that previous codes provided neither

design rules nor detailed structural prescriptions able to ensure global and local ductility required by the current code, which allows adoption of a q factor of 5.85.

Generally, existing structures are unable to show a highly ductile behavior and it is not possible to ensure that the structure develops global mechanisms associated with large dissipation of hysteretic energy. This is why actual codes considerably limit q in such cases, allowing it in the range (1.5-3.0). The choice of a value in this range should be made according to regularity criteria and the employment of material properties.

Hence, a proper comparison has to be carried out between the current seismic demand spectra provided for existing structures and the former code spectrum (Figure 7.6b). The latter comparison leads to a ratio of at least 2 between the current seismic demand and the old seismic demand.

Design procedures and details according to new generation codes, such as Eurocode, (BS EN 1990, 2002), for the Ultimate Limit State, considering the second reliability class (RC2), according to the same Eurocode definition (BS EN 1990, 2002), lead to an annual failure probability of at least $1 \cdot 10^{-6}$.

A ratio of current to old code demands, as calculated above, of at least 2, does not mean Life Safety limits are exceeded for all buildings; on the other hand, the percentage of building failure over the whole population, in this case, would definitely be higher than $1 \cdot 10^{-6}$.

If the elastic demand spectra of the registered signals are compared with the current code's elastic demand spectra, determined for different return periods (T_R 475 and 975 years) on soil class A, it may be noted that the spectra of the registered signals exceed code demand in most of the frequency range considered. Figure 7.7a compares elastic spectra determined from horizontal components of the registered signals in stations AQK, AQG, AQA and AQV, while Figure 7.7b compares vertical components of the same signals with the vertical code spectra.

In Section 6.3.3 it was emphasized that damage limitation limit state prescriptions and verifications essentially aim to avoid or reduce infill damage,

and most notably that this kind of prescription was first introduced into the Italian code only in 1996 and better detailed and completed in 2003.

Hence, according to ISTAT data, it is reasonable to assume that most of the RC buildings in L'Aquila were constructed without any deformability control or verification (see Figure 7.2). On the other hand it should be emphasized that, even if a design procedure according to 1996 or, better, according to the 2008 code had been employed, involving Damage Limitation verification, the strong PGA characterizing the L'Aquila event would nonetheless have produced widespread damage to non-structural elements such as infills in many buildings in the area.

In the following a comparison between Damage Limitation spectra is proposed. The DM 1996 Damage Limitation spectrum can be extrapolated from the definition of elastic displacement demand, see equation (7.4) in the previous section. If a negligible influence of non-seismic loading is assumed ($\eta_p \approx 0$) and coefficient λ is assumed equal to 1, the displacement demand in verification of the limit state method is given by equation (7.5). The acceleration spectrum employed to calculate η_d was that proposed in Figure 7.6a with a constant acceleration branch equal to 0.105g. Hence, if the Ultimate Limit State spectrum according to the 1996 code is multiplied by (2/1.5) and ε, β and I are assumed equal to 1, the expression equation (7.6) can be extrapolated and the damage limitation spectrum according to the 1996 code is obtained. This spectrum can be easily compared with Damage Limitation spectra of 2003 and the one according to current Italian seismic codes (DM 14/1/2008).

$$\eta_t = \left(2 \cdot \eta_d\right)/1.5 \tag{7.5}$$

$$\begin{aligned} a/g &= 0.14 && \text{for } T \le 0.8\,\text{sec} \\ a/g &= 0.14 \cdot 0.862/T^{2/3} && \text{for } T > 0.8\,\text{sec} \end{aligned} \tag{7.6}$$

Figure 7.8 shows Damage Limitation spectra according to different Italian codes, released in 1996, 2003 and 2008. Values corresponding to the constant acceleration part of the spectra are 0.14 g, 0.25 g and 0.242 g

respectively.

As explained in Section 6.3.3, deformation capacity assumed by the 1996 code and later codes (2003 and 2008) strictly differ. As an example, given the same constraint condition between infill panels and the RC frame, the ratio between assumed capacities in the 1996 code and in later codes is 1/2.5; conversely, the ratio between respective demands is 1.7÷1.8. Based on this simple comparison, it may be concluded that the 1996 Damage Limitation restrictions were stricter.

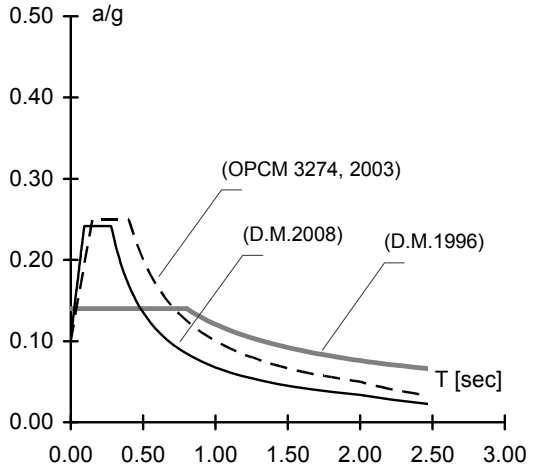

Figure 7.8. Comparison of damage limitation spectra: 1996, 2003 and 2008 codes.

7.5 Structural damage

In this section the main structural damage to RC structures after the L'Aquila earthquake is presented. Photographic documentation (Verderame et al., 2009) was produced on the days immediately following the 6th April 2009 mainshock. Generally speaking, damage to structural elements is not so frequent and it seldom involves the whole structural system.

The main structural damage that involved RC columns can be easily recognized as failure caused by mechanisms that capacity design rules tend to avoid or at least to limit. During an earthquake, columns are characterized by high flexural and shear demand; maximum flexural demand combined with

axial force produced by gravity loads and seismic loads are located at the end of the element; in these zones (critical regions) rotational ductility demand concentrates. Therefore, it is necessary to give an adequate rotational capacity and to avoid buckling of compressed longitudinal reinforcements.

Modern seismic codes, such as Eurocode 8 (CEN 2004), provide prescriptions to increase rotational capacity of the section: the upper limit on the longitudinal reinforcement percentage leads to a higher ultimate curvature of the section; proper hoop spacing and cross-tie presence give, due to a more efficient confinement action on concrete, an additional increase in section curvature capacity; finally, proper spacing between hoops avoids buckling in longitudinal reinforcement, or at least fixes an acceptable upper bound limit for which this phenomenon occurs.

However, the prescriptions and structural details presented above are typical of modern design concepts that first appeared in Italy in 1997. It is therefore possible to find RC columns with longitudinal reinforcement percentage exceeding 4% limit or hoops closed with 90° hooks, or with insufficiently thick spacing (15-20 cm).

Figure 7.9a presents a corner column of an RC building in the historical centre of L'Aquila, probably erected between 1950 and 1960. Damage occurred at the bottom end section of the element. The presence of smooth bars and a small hoop diameter (6 mm), closed with 90° hooks, can be observed, but the most significant detail is the absence of any transversal reinforcement in the first 30–40cm of the element immediately adjacent to the beam-column joint region. Figure 7.9b shows a circular column belonging to a building in the residential zone of Pettino, built in the 1980s: typical damage due to axial force and bending moment is recognizable; the concrete cover was crushed due to high compression strains and longitudinal bar buckling. In this case hoop spacing is, once again, not thick enough, as in the case of Figure 7.9a, but probably in this case the column was designed in accordance with code prescriptions at the time of construction.

High shear demand can produce brittle failures with an outstanding

reduction in column dissipative capacity. In order to prevent brittle failures, shear demand has to be determined according to flexural capacity of the element; applying to shear demand an amplifying coefficient to allow for variability in steel properties (CEN 2004) can prevent brittle failure occurrence. These prescriptions have been laid down since 2003 in the Italian code; no control of the failure mechanism used to be applied before this code was released. All the above considerations can be confirmed by brittle failure of the columns reported in Figure 7.10 and Figure 7.11.

Figure 7.9. Column with smooth bars and poor transversal reinforcement (a); damage to a column due to axial force and bending moment (b)

With regard to the rectangular column in Figure 7.10a, whose section is 30·100 cm², belonging to a 1980s' building, shear failure is evident, involving the top end section. Transversal reinforcement has hoop spacing of approximately 15-20cm, and is definitely under-designed with respect to column section size, that is, with respect to the inertia of the section, thus leading to premature shear failure of the element. The brittle failure mechanism is highlighted by the crushing of the concrete within the reinforcement and the complete opening of the third and fourth hoops from

the top end of the element.

Figure 7.10. Shear failure of: (a) rectangular and (b) circular columns.

Figure 7.11. Shear failure of: (a) column adjacent to partial infilling panels, (b) squat column adjacent to basement level concrete walls

Figure 7.10b shows shear failure of a 30cm-diameter circular column; in this case it is possible to recognize insufficient hoop spacing, which leads to the typical diagonal cracking characteristic of shear failure mechanisms and longitudinal bar buckling in the column.

In order to stress the non-secondary role played by column – infill interaction in determining brittle failures in the structural elements, Figure 7.11a shows the damage that columns present in these kinds of situation. It is possible to recognize the brittle failure in the column due to the local interaction with the concrete infill partially covering the bay frame, reaching 1/3 of the total column height. Partial infilling that effectively interacts with the column reduces the slenderness of the element and consequently produces a higher shear demand that exceeds column shear capacity. This kind of phenomenon involves all the columns interacting with the concrete partial infilling.

Figure 7.11b gives an example of a basement that is partially below the ground level. According to common building practice, basement levels are characterized by walls, often realized in concrete, aimed at a retaining function of the adjacent embankment; concrete wall height is limited with respect to column height to allow the fitting of windows. This structural solution leads to a strict reduction in column slenderness with a consequent increase in shear demand; moreover, decreasing shear span can modify the shear span ratio of the element up to a squat column behavior. This situation is of no secondary importance since the shear resistance mechanism of a squat column differs with respect to the typical behavior of a slender element. Differences between shear capacity formulations proposed in Eurocode 8 (CEN 2005) for existing buildings for slender and squat columns testify to the difference between shear failure mechanisms. Hence, if local interaction between the column and concrete wall is not allowed for, premature brittle failure due to excessive concrete compression can often occur.

Columns belonging to staircases can easily show brittle failures as well. Most common staircase types generally possess discontinuity elements in the

regular RC frame scheme composed by beams and columns. Indeed, on one side a staircase consists of inclined axis elements (beam or slab); on the other, squat columns are created by the intersection of inclined axis elements with the column.

Figure 7.12. Shear failure in squat columns of the staircase.

Staircase elements lend a considerable lateral stiffness to the whole structural system, first due to axial stiffness of the inclined elements and secondly to higher lateral stiffness of squat columns. These contributions are easily appreciable via linear analyses. On the other hand, staircase elements can represent a weak point because they possess higher shear demand that can lead to brittle failure mechanisms. Figure 7.12 shows a staircase composed by inclined beams; the squat column in the corner has typical shear failure. Poor transversal reinforcement, both in terms of hoop spacing and diameter, can be recognized.

Shear failures were found in reinforced concrete walls as well. As an example, in Figure 7.13 two reinforced concrete walls, respectively with two different shape factors, are shown; damage consists of a spread diagonal cracking. Low longitudinal and transversal reinforcement percentages can be recognized, especially compared with minimum values prescribed by design codes based on capacity design approach.

Beam-column joints can completely change the structural behavior of the whole building and their failure should necessarily be avoided in a proper seismic design approach: such elements possess brittle failure mechanisms. In beam-column joints, demand coming from beams and columns is concentrated and both the concrete panel and longitudinal bars are subjected to high gradients of shear and flexural demand.

Figure 7.13. Failure in reinforced concrete walls.

Joint failure mechanisms are mainly governed by shear and bond mechanisms; force distribution, which allows shear and moment transfer, produces diagonal cracking and hence joint failure due to diagonal compression in the concrete is quite likely to occur, thus producing a reduction in strength and stiffness in the connection.

Generally speaking, joint design is limited by concrete compressive stress; the diagonal stress induced by the elements meeting in the joint cannot exceed concrete compressive stress. In order to keep structural continuity when concrete cracking occurs, a proper transversal reinforcement along the whole element should be provided. The presence of transversal reinforcement

allows stresses to be transferred by means of a strut and tie mechanism, even if the cracking phase has passed in the concrete. The latter mechanism can be developed if longitudinal reinforcement, transversal reinforcement and concrete struts contribute to truss formation. If capacity design prescriptions are followed, preventing brittle failure in joints gives the chance to develop ductile mechanisms in the other structural elements.

Specific design rules for beam-column joints appeared in the Italian design prescriptions only in 2003 (OPCM 3274, 2003). Indeed, in the explanatory document to the 1996 code (CS. LL. PP. 65, 1997) the transversal reinforcement in the joints was simply required to be at least equal to the hoop spacing in the columns.

Damage from the 6th April 2009 earthquake clearly shows how hazardous failure of joints can be. Figure 7.14a shows an external beam-column joint, characterized by an extensive cracking in the joint panel. The absence of transversal reinforcement leads to local buckling of the longitudinal bars that consequently results in concrete cover spalling. Interestingly, the absence of proper transversal reinforcement in the joint also leads to a loss of anchorage in beam longitudinal reinforcement.

Figure 7.14b shows typical diagonal cracking failure in a concrete panel belonging to an external joint. Cracking begins at the intersection between the joint and upper column and ends at the intersection between the joint and lower column, producing the loss of monolithic connection. Absence of hoops, in this situation too, leads to buckling in the external longitudinal bars and involves lower column bars without transversal reinforcement in the first 30–40cm.

Another noteworthy aspect in RC damage after the L'Aquila earthquake is a peculiar loss of connection at the lower joint-column interface; this aspect is emphasized and becomes a critical issue when there is insufficient longitudinal and transverse reinforcement both within the joint and at the column end.

Generally speaking, the presence of a separation (previously present or

otherwise) at the interface between the column and beam-column joint, if both elements – column and joint – are well designed, complying with modern seismic prescriptions, should not prevent the development of a ductile failure mechanism in the column. According to current code prescriptions, (i) a minimum amount of longitudinal reinforcement, evenly distributed around the periphery of the section, and (ii) an adequate, effectively anchored transversal reinforcement, both in the beam-column joint and at the column end, have to be adopted, thus avoiding brittle failure along the interface section between column and joint (Paulay and Priestley, 1992).

Figure 7.14. Joint failure with evident (a) longitudinal bar buckling and (b) diagonal cracking failure in concrete joint panel.

Figure 7.15a reports a brittle failure mechanism due to the lack of transverse and longitudinal reinforcement that led to loss of continuity at the intersection between the joint and lower column, being the probable final cause of the failure. Figure 7.15b shows a clear separation in concrete at the joint-column interface; in this case, due to a complete spalling of the concrete cover, the reinforcement in the element may be recognized and it may be noted that the first hoop in the column is partially open. The lack of transverse reinforcement in the element made the separation at the joint-column interface

critical.

Figure 7.15. Failure mechanisms at joint – column interface surfaces

7.6 Nonstructural damage

As a general rule, infill failure mechanisms can be classified as: (i) horizontal sliding in the central zone of the infill panel, (ii) diagonal cracking due to tensile stress in the central zone of the infill panel, (iii) corner crushing in the direct contact application zone.

Figure 7.16 shows infill panels in building façades characterized by a diagonal cracking mechanism. In Figure 7.16a damage is concentrated at the first storeys of the building and diagonal cracking is more emphasized by the plaster layer because the external layer of the infill is made up of solid clay bricks that experienced limited damage.

Figure 7.16b shows a typical corner crushing mechanism. Out-of-plane failure of the infilling external layer allows the corner crushing mechanism of the internal layer to be observed; other evidence is the crack, which visibly involves the plaster but is also probably deeper, localized at the top of the column adjacent to the infill panel, as a consequence of column-infill local interaction.

The great majority of external infill panels consist of double layer infill

panels; internal layers are generally made with clay bricks, connections between the two layers by the interposition of brick elements discretely, or lined up. The low efficacy of this system is emphasized in Figure 7.17a.

Figure 7.16. Infill panel failures: diagonal cracking (a), and corner crushing (b) mechanisms.

Figure 7.17. External infill panel failures without connection between layers (a) and with ineffective connection (b).

Furthermore, in most of the observed cases, internal infilling layers are restrained at the four corners of the RC frame while external layers are constrained only by the upper and the lower beam by means of a small pawl. This constructive solution leads to a decrease in the interaction mechanism between RC frame and external infill panel, for both in-plane and out-of-plane seismic forces. The low efficacy of the restraint applied to the external panel,

coupled with the ineffective or completely absent connections between the two layers, leads to damage limited in most cases to the external infill panel which can easily show an out-of-plane failure due to seismic action in both directions, as can be observed in Figure 7.17b. Both neither local nor global interaction effects between infills and the RC structure are negligible. As was previously emphasized, local interaction between infill panel and adjacent columns can lead to (i) a reduction in the effective height of the column, an increase in shear demand and a consequent brittle failure of the column when the infill panel partially occupies the frame bay; (ii) shear concentration demand at the end of the column and consequent brittle failure when diagonal compression is applied by the panel on the RC element.

Figure 7.18. Soft storey mechanism examples in L'Aquila: Via Porta Napoli.

As a global phenomenon infill-structure interaction increases global stiffness of the complex system and consequently spectral acceleration demand. Besides, it can represent a source of irregularity in plan or elevation (e.g. *pilotis*) when the infill distribution is irregular.

Some particular cases of structural failure after the L'Aquila event and

mainly caused by irregularities in plan or elevation are reported in Figure 7.18 and Figure 7.19. The first structure considered (see Figure 7.18) was situated in the centre of L'Aquila (Via Porta Napoli); it was irregular in elevation and the second storey had an evident discontinuity in terms of infill distribution; in the left wing of the building there was a sort of porch. Thus, damage was concentrated on the second storey, leading to complete failure of the upper levels.

The structure proposed in Figure 7.19 was placed in the residential zone of Pettino (Via Dante Alighieri), close to L'Aquila, it is the object of the detailed analytical study in the next section.

Figure 7.19. Soft storey mechanism examples in L'Aquila: Via Dante Alighieri (Pettino).

7.7 A case study: preliminary analysis of a soft storey mechanisms

In this section one of the few collapsed buildings after L'Aquila earthquake is assumed as case study. The building has an irregular shape in

plan, similar to a T; infill distribution makes the structure irregular in elevation due to the presence of garage entrances. The building showed a soft-storey mechanism at the first storey and observed damage points to collapse as a result of a brittle failure mechanism. The failure can be explained by infill irregularities in elevation and by a local interaction between infills and adjacent columns, which probably led to a brittle failure of some columns at the first level, and consequently leading to the collapse of the whole building.

Given the likely scenario collapse inferred by observed damage, an analytical model of the building was built up taking into account nonlinear behavior of the infills; local interaction with columns was also considered by means of a three strut macro-model (Chrysostomou et al., 2002; El-Dakhakhni et al., 2003; Crisafulli, 1997). Two parametric hypotheses based on Italian code (CS. LL. PP., 2009) prescriptions were assumed for infill mechanical properties. Time history analyses were carried out assuming as seismic input the three components of the real registered signals during the mainshock in the vicinity of the case study structures. The study represents a preliminary approach because of the uncertainties regarding knowledge of the building.

Given the brittle failure highlighted by damage, beside capacity models suggested by codes (CEN, 2005), other shear failure mechanisms not typical for columns (Paulay and Priestley, 1992) were considered.

Numerical results seem to confirm the collapse scenario inferred by damage observation; the lack of proper structural and executive details was addressed as the main cause that made a critical issue the local interaction between columns and infills, other than the strong vertical component registered.

7.7.1. Damage observation

In the following, geometrical and structural characteristics of the case study building and the damage experienced due to the April 6th event are discussed. Pre- and post-event photographic images (Verderame et al., 2009) and a further in-situ survey allowed the determination of the geometry of the structure. Survey was rapidly carried out due to the severe damage of the

building. Moreover, some insights into the possible reasons for the collapse are reported.

- **Structure description**

The case study structure is part of a group of residential buildings realized during 1980s in Pettino (L'Aquila).

The morphology in plan is irregular, approximately T-shaped. Three storeys and an attic are present; the first storey is used as a store and a garage, the other storeys are used as habitation. The structure is a three-dimensional RC frame, likely designed for both gravity and seismic loads according to the seismic code prescriptions in force at the time of construction. L'Aquila was classified as a category II seismic zone and the design acceleration on stiff soil was equal to 0.07g (). Infill distribution is irregular in elevation due to the presence of openings at the first storey.

Figure 7.20. Pre-event view of case study building, placed in Pettino (L'Aquila) (Virtual Earth).

Figure 7.20 reports some aerial photographs of the building before the seismic event; some elements are clearly shown: the irregular plan, the number of stories, the attic storey and the garage openings at the first level.

No architectonic or structural drawing is available. Nevertheless, in-situ survey, together with a metric evaluation of photographic images, allowed defining the building global dimensions, number and length of bays in external frames. In particular, global dimensions in plan are approximately

(25×30) meters while interstorey height is about equal to 3 meters. Similarly, dimensions of structural elements and reinforcement details can be drawn from the empirical observation of failed elements. Columns at the first storey have a (300×500)mm² section. Deformed bars are employed as reinforcement; longitudinal reinforcement consists of eight 12 mm diameter bars, symmetrically distributed along the major section dimension, while transverse reinforcement is made by stirrups (diameter equal to 6 mm), 150 mm spaced. Infill panels consist of a double layer of hollow clay brick infills typical of Italian building practice. Thicknesses of external and internal layers are equal, respectively, to 120 and 80 mm.

- **Structural damage**

Building collapse involved only first storey elements. In Figure 7.21, moderate cracking in the upper storey infills is shown.

Figure 7.21. Building collapse mechanism. Damage along South-East (a) and South-West (b) wings of the building (Verderame et al., 2009).

Collapse mechanism is not translational. The position of first storey failed columns suggests that the building collapsed under a torsional mechanism, as simply schematized in Figure 7.22.

First storey columns in the most distant frame from the centre of the masses frame (1-2-3) show displacements approximately equal to tens of centimeters in X direction and very small in Y direction; in similar way columns in the perpendicular frame (15-23-31) show displacements of few centimeters in Y direction and very small in X direction. Corner columns are

totally separated from the rest of the building. Columns #1 and #22 reported in Figure 7.22 kept their original position, without showing any plastic rotation; therefore, the actual position of the collapsed building with respect to these elements is evidence of the movement associated to the collapse mechanism that resulted after the failure of the first columns. Due to this collapse movement, the structure, from the second storey on, completely lost its connection with columns #1 and #22. Collapsed columns #3 and #38 show evident damage; these elements were involved in the rotational collapse movement of the remaining part of the structure and their conditions seem to suggest that the building crashed into them. Moreover, it should be noted that in both kinds of damaged columns (#1, #22 and #3, #38) the longitudinal reinforcement was torn up from the concrete core of the column, due to the absence of a proper restrain; the absence of transversal reinforcement in beam-column joints, the low diameter of the stirrups in columns and the deficiency in closure detail of these stirrups can be highlighted as contributory causes that favored this specific observed damage.

Observation of failed columns shows that no ductile mechanism was developed; loss of contact between column and upper joint is not involved in such a mechanism. Similarly, it can be excluded that geometric non-linear effects such as P-Δ are involved in the collapse. As a matter of fact, this effect is related to high rotational (ductility) demands typical of a *flexure-controlled failure*, which are not shown by failed elements.

Failure is certainly due to a brittle mechanism. Nevertheless, columns' collapse appears to be different from a conventional brittle shear failure, due to a truss mechanism in compressed concrete or in transverse reinforcement. In this case, failure of the elements follows the development of diagonal cracks; moreover, crushed concrete struts and/or yielded transverse reinforcement can be clearly observed after failure.

On the contrary, surfaces at the top of failed columns and at the bottom of corresponding joints in the present building are rather smooth (see Figure 7.23), leading to the hypothesis of a likely frictional failure, located along weak

surfaces probably corresponding to a casting separation. Longitudinal bars crossing these surfaces were not restrained by transverse reinforcement, due to the stirrups spacing and to the complete absence of stirrups in beam-column joints.

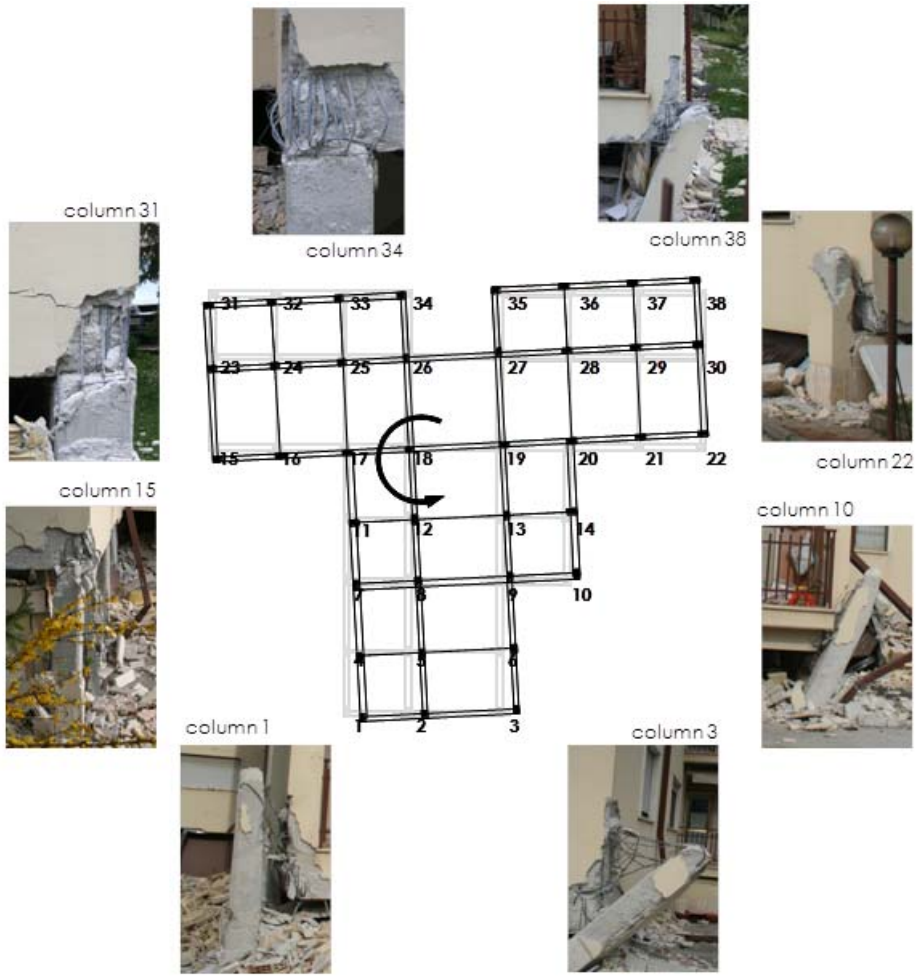

Figure 7.22. Building collapse: column damage points out a rotational movement.

Moreover, transverse reinforcement is closed with 90 degree hooks, therefore not providing an effective anchorage. This kind of failure seems to be confirmed by damage shown in Figure 7.23b, in a structural element adjacent to a failed infill panel: concrete cover is crushed and longitudinal

reinforcement is not restrained. There is no transverse reinforcement in the joint, and the first stirrup at the top of the column is opened. A clean, deep crack has clearly developed along the interface between the top of the column and the joint.

Figure 7.23. Damage highlights not properly treated casting surface (a, b) and absence of stirrups in the joint area (b), (Verderame et al., 2009).

Upper storeys show no significant damage in structural elements, or in infill walls. The light damage in the upper stories is clearly due to the rigid post-collapse movement mentioned above.

A likely collapse scenario can be described thanks to the above observation: shear friction failures occurred in the columns characterized by larger seismic loads due to their position in plan (probably #3 and #38). The brittle failure of the first columns and the loss of contact with the above structure at the connection between the top of the first storey columns and beam-column joints produced a rigid collapse movement that made the building crashing into columns #3, #10 and #38 and contemporarily losing any connection with columns on the other side (#1, #15, #31 and #34), which did not show any plastic rotation and stand exactly in the same position they had before the earthquake. It is to note that the only column in which it is still possible to recognize a shear friction failure is column #31, in the other cases the collapse rigid movement hid the original brittle failure mechanism

occurred in the columns, which can be considered the main cause of the whole building collapse according to the likely scenario made up from damage observation.

7.7.2. Modeling issues

Available information gathered by damage observation, pre-event configuration of the structure and time of construction (between 1980's and 1990's) were used to build up the structural model of the building, aimed at highlight the probable causes of the collapse by means of a numerical approach. Furthermore, it was possible to infer some information from code and building practices of the time (DM 3/3/1975) and to provide a simulated design procedure (Verderame et al. 2010) of some parts of the structure.

First, configuration and global dimension in plan were determined (Figure 7.24) using photographic material and a speed in-situ survey in addition to the orientation of external columns, whereas internal columns orientation was determined using building design practices. The distribution of beams in plan is based on the in-situ survey. Figure 7.24 defines X and Y directions in plan; this coordinate system will be used as a reference in the following section.

Second, in-situ visual survey data allowed determining section dimensions of the external columns and beams at the first storey (see Figure 7.22); longitudinal and transversal reinforcement of some of the columns at the first storey are also known, as already highlighted above. Based on this knowledge, a simulated design procedure was carried out, aimed at determining dimensions of remaining beams and columns and the longitudinal and transversal reinforcement. To this end, a simplified structural model was employed (shear type model), (Verderame et al. 2010).

Hence, due the number of stories (only three) and the building practices at the time for this kind of structures, all column and beam section dimensions at upper levels were assumed equal to first level section dimensions, partly determined from the in-situ survey and partly from the simulated design procedure.

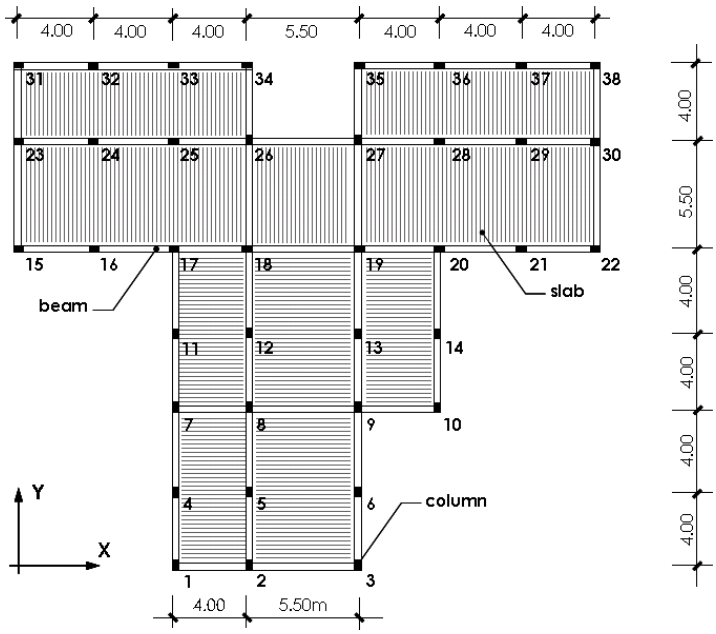

Figure 7.24. Dimensions in plan, columns orientation.

Column sections were considered equal to (300×500)mm; similarly, beam sections were assumed equal to (300×500)mm. Longitudinal reinforcement in columns at the first storey was composed of eight 12 mm bars placed along the 500 mm sides of the section; transversal reinforcement was composed of 6 mm stirrups 150 mm spaced, and stirrups are closed with a 90 degree hook.

It is worth to note that simulated design of longitudinal and transversal reinforcement was referred only to the first storey columns, since the collapse mechanism did not involve the remaining stories (see 7.7.1); this assumption is also confirmed considering other buildings collapsed because of a soft storey mechanism (Dolsek and Fajfar, 2001), similar to the present case study structure.

Based on Italian design practice, typical unidirectional joint-slabs were assumed, with 400 mm thick hollow bricks and 100 mm thick joists and a 40 mm thick layer of concrete on top. Slab way was assumed along the short directions of the wings and the web of the T-shaped plan (see Figure 7.22). Dead structural and non-structural loads were evaluated; live load Q_k was

given equal to 2 kN/m^2, according to code prescription.

Structural material properties were determined by means of steel and concrete used during the years of construction. Steel properties were evaluated from Italian deformed bars FeB44K; the medium value of the yielding strength f_{ym} was assumed equal to the nominal value of 440 MPa. The minimum value of the concrete strength, according to the code prescriptions in force when the structure was built, was given by f_{ck}=20 MPa. In this case, too, the medium value of the concrete compressive strength f_{cm} was assumed equal to the value f_{ck}=20 MPa.

According to Italian code prescriptions (DM 14/1/2008) Young modulus of concrete was assumed equal to E_c=27000 MPa. The assumptions made regarding concrete properties will not affect strictly the evaluation of stiffness and modal properties of the structure because the stiffness contribution of infills has a stronger impact on modal properties.

With regards to strength and stiffness infill properties, it was necessary to employ Italian Code (DM 14/1/2008) provisions, having determined the infill typology from photographic documentation. The structure has double layer brick infills, in the model an equivalent single layer infill was considered 200 (=120+80) mm thick.

Infill properties are characterized by several uncertainties and they affect linear and non-linear behavior of the structure. Therefore, the following two opposing parametric hypotheses regarding infill properties were proposed. The hypotheses assume maximum and minimum values for this typology by Italian Code (despite the possible overstrength due to mortar quality):

- *weak infill* hypothesis is characterized by a value of cracking shear stress (τ_o) equal to 0.30 MPa, and Young modulus (E_w) equal to 3600 MPa considering a ratio of 0.30 between shear modulus G_w and E_w.
- *strong infill* hypothesis is characterized by τ_o equal to 0.40 MPa, and E_w equal to 5600 MPa considering the same ratio of 0.30 between G_w and E_w.

Infill distribution was determined by photographic documentation (see Figure 7.20).

- **Linear model**

Linear model of the structure was build up according to the two different parametric hypotheses about infill stiffness properties (weak and strong). Beams and columns were modeled as frame elements, behavior of beam-column joints was assumed to be elastic and a rigid diaphragm constraint was imposed at the floor level. The infills were modeled by means of a three strut model that will be described in detail in the following.

An elastic shear stiffness (K) is assumed for the infill wall, consistent with the model proposed in (Fardis, 1997), according to equation (7.7), where Gw is the shear modulus of the infills, tw is the equivalent thickness, Lw and hw are, respectively, the clear length and the clear height of the infill panel. The 50% of the whole infill stiffness is assumed to be given by the contribution of the central strut (k_1), as shown in equation (7.8) and similarly to other authors (Crisafulli,1997). The remaining stiffness, given by the two off-diagonal struts, can be evaluated by the principle of virtual displacements (Chrysostomou et al., 2002). If an equal axial stiffness (k2 and k3) is assumed for the off-diagonal struts, than k(=k2=k3), depends on the infill stiffness K and on the axial stiffness of the central strut k_1 according equation (7.9).

Infills placed at the attic level, above the third level, were modeled as shell membrane elements, characterizing material with infill stiffness properties. A different model was adopted for these elements because of their low height and their non-rectangular shape, which would make not properly adequate a strut modeling.

$$K = \frac{G_w t_w L_w}{h_w} \tag{7.7}$$

$$k_1 = 0.50 \frac{K}{\cos^2 \theta} = 0.50 \frac{G_w t_w L_w}{h_w} \frac{1}{\cos^2 \theta} \tag{7.8}$$

$$k = (K - k_1 \cos^2 \theta) \Big/ \left[2(1-\alpha)^2 \cos^2 \theta \right] \tag{7.9}$$

According to the two infill properties (weak and strong), two different linear models were considered and their dynamic properties were evaluated.

Modal properties of the structures are summarized in Table 7-1; for each of the two models, the first mode has participant mass ratio essentially in X direction, showing a torsional shape in X-Y plan; the second mode is translational in Y direction; the third is a torsional mode. Differences between the first period (T) of the structure in the two infill properties hypotheses (weak and strong) provide an idea on how infill stiffness can influence structure global stiffness showing a difference between period values that is over 15%.

Table 7-1. Modal properties of the two structural models.

mode	strong infills				weak infills			
	T	UX	UY	RZ	T	UX	UY	RZ
	sec	[%]	sec	[%]	sec	[%]	sec	[%]
1	0.16	78	0	16	0.19	77	0	17
2	0.14	1	96	0	0.16	1	97	0
3	0.12	18	1	81	0.14	20	1	80

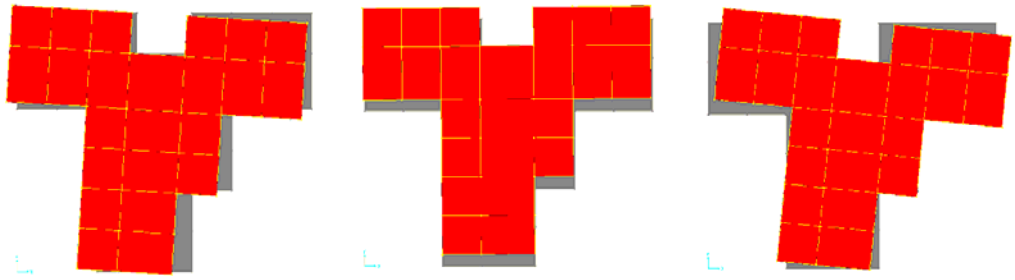

1st mode 2nd mode 3rd mode

Figure 7.25. Modal deformed shapes in X-Y plan.

In Figure 7.25, as an example, one of the models (*strong infills*) of the structure, made up by a user-friendly interface software (Computer and Structures, 2007), is represented; in particular deformed shapes in X-Y plan at the third level of the structure are reported.

- **Nonlinear element modeling and capacity models**

Modeling of structural and non-structural elements (infills) is based on the in-situ observation of damage suffered by the building, which highlights a brittle failure mode. Based on the damage survey, the following observations

can be carried out:

- damage is only concentrated at the first storey (soft storey mechanism); at upper levels the interstorey displacement demand did not even lead to the cracking of infill panels;
- no evidence of plastic rotation demand (that is, ductile failure mechanism) is present in columns at first storey, involved in the collapse mechanism;
- some columns, probably first causing the global collapse, point out the evidence of a brittle failure mechanism (shear failure);
- infills at first storey are completely failed or heavily damaged.

Hence, consistent with these considerations, the following modeling assumptions are made for the structural elements:

- beams and columns are modeled as elastic. Nevertheless, the possible overcoming of the yield limit and of the strength capacity for brittle failure mechanisms is verified through adequate capacity models, by means of a comparison carried out a posteriori between the strength demand obtained from the analysis and the strength demand given by the above mentioned capacity models;
- infills are represented by a non-linear three strut model. A non-linear modeling is needed not because of the damage suffered by the infills. Moreover, a three strut model, unlike a single strut model, allows to take into account the local interaction phenomena between the infill panel and the surrounding RC elements.

- **Nonlinear infill modeling**

Modeling of infills is aimed at analyzing the local interaction effects between the infill panel and the surrounding RC elements. To this end, two different modeling approaches can be adopted: the infill panel can be represented by non-linear shell elements and the panel-element interface by spring elements (Ellul and D'Ayala, 2008); the infill panel can be represented by strut macro-models (Crisafulli, 1997). Former models are characterized by a higher detail level, nevertheless latter models are widely spread, also due to the lower computational effort needed.

Herein a strut macro-model is adopted for infill panels. In particular, six struts, carrying load only in compression, are adopted to represent each panel. As a matter of fact, even if the single strut model is quite easy to be implemented, it is not able to represent the actual distribution of bending moments and of shear forces in frame members due to the local interaction with the infill panel, as already pointed out by many authors (Buonopane and White, 1999; Mosalam et al., 1997). Only the use of two more struts, right placed, besides the central one, allows to account for this interaction (Chrysostomou et al., 2002; El-Dakhakhni et al., 2003; Crisafulli, 1997). The central strut lies along the diagonal of the bay frame, from one corner to the opposite. The position of two remaining struts depends on the extension of the contact area along which the load transfer between the infill panel and the RC elements takes place, see Figure 7.26. The amount of this area depends on the stiffness and on the deflected shape of the frame members. The length of the contact area, according to several authors (Chrysostomou et al., 2002; El-Dakhakhni et al., 2003), can be expressed according to equation (7.10), in which λ'_h assumes the value in equation (7.11), where h_w is the infill height, L_w is the infill length in plan, t_w and E_w are the thickness and Young modulus of the infill, I_c and E_c represent RC columns' inertia and Young modulus, while $tg\theta$ is ratio between h_w and L_w.

$$z = \frac{\pi}{2 \cdot \lambda'_h} \cdot h_w = \alpha_c \cdot h_w \tag{7.10}$$

$$\lambda'_h = h_w \cdot \lambda_h = h_w \cdot \sqrt[4]{\frac{E_w \cdot t_w \cdot \mathrm{sen}(2\theta)}{4 \cdot E_c \cdot I_c \cdot h_w}} \tag{7.11}$$

In a similar way it is possible to evaluate the extension of the contact area between the infill panel and the adjacent beam; nevertheless, for the sake of simplicity it is assumed to be $\alpha_b = \alpha_c$ (Kaushik et al., 2008). Hence, the three struts are parallel to each other. The off-diagonal struts are placed at a distance equal to (z/2) from the

beam-column intersection.

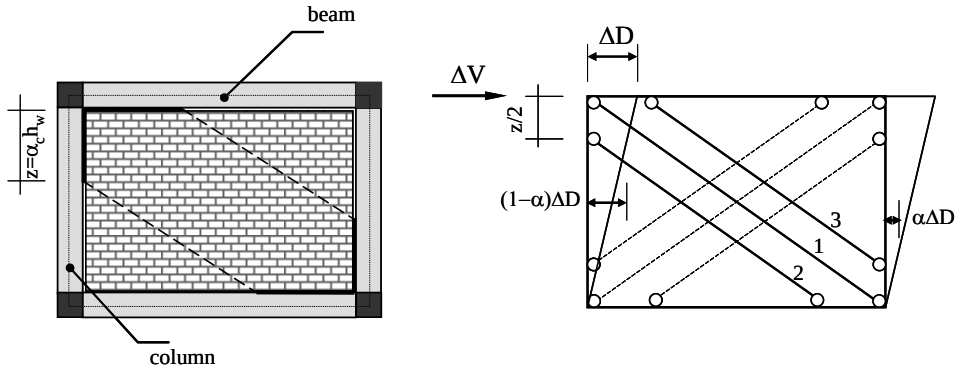

Figure 7.26. Three strut macro-model adopted for infill panels

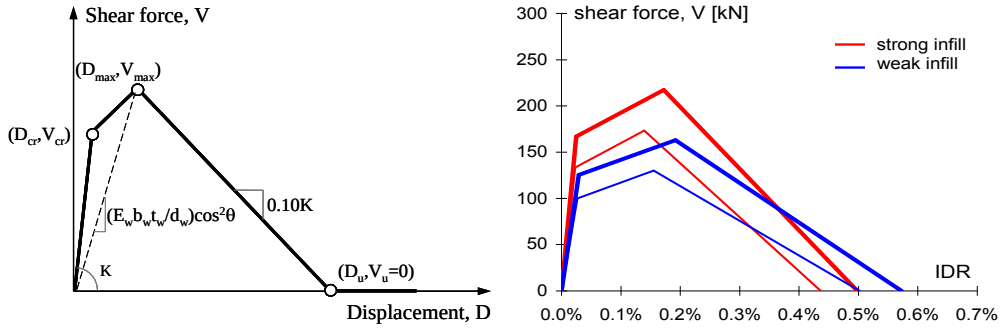

Figure 7.27. Shear force-displacement envelope proposed by [19] (a), specific shear force-IDR envelopes in structural model (b)

The adopted three-strut model has to reproduce the force-displacement response of the infill panel. To determine this curve, the model proposed in (Fardis, 1997) is adopted: the envelope curve is given by four different segments as shown in Figure 7.27: the initial shear behavior of the uncracked panel; the equivalent strut behavior of the cracked panel; the instability of the panel over its maximum strength; the final stage of the panel when the failure is achieved and the residual strength remains constant.

The main parameters of the model are: the initial stiffness of the uncracked wall, K, obtained according to equation (7.12), the secant stiffness, corresponding to the maximum infill strength, given by the axial stiffness of an equivalent strut, see equation (7.13), where t_w and E_w are the thickness and

Young modulus of the infill, tgθ is ratio between h_w and L_w, d_w is the diagonal length of the infill panel ($d_w = \sqrt{h_w^2 + L_w^2}$) and b_w was evaluated according to Mainstone's formula (Mainstone, 1971), see equation (7.14). Cracking load, V_{cr}, can be computed according to equation (7.15), where τ_o is the cracking shear stress; and maximum load, Vmax, is given by equation (7.16).

$$K = G_w t_w L_w / h_w \tag{7.12}$$

$$\frac{E_w b_w t_w}{d_w} \cos^2 \theta \tag{7.13}$$

$$b_w = \left[0.175 \cdot \left(\lambda_h \cdot h_w \right)^{0.4} \right] \cdot d_w \tag{7.14}$$

$$V_{cr} = \tau_o \cdot t_w \cdot L_w \tag{7.15}$$

$$V_{max} = 1.30 \cdot V_{cr} \tag{7.16}$$

It is assumed, consistent with other authors (Chrysostomou et al., 2002), that the central strut carries 50% of the whole load carried by the infill. Therefore, the axial load-axial displacement relationship of the central strut can be evaluated by the components of the lateral load-displacement relationship of the infill panel along the strut axis where ΔF_1 and $\Delta \delta_1$, see equations (7.17) and (7.18), are the incremental axial load and the incremental axial displacement, respectively, corresponding to 50% of the incremental lateral force ΔV and of the incremental lateral displacement ΔD of the infill panel, while k_1 is the axial stiffness of the central strut, see equation (7.19), and K is the lateral stiffness of the infill panel.

$$\Delta F_1 = 0.50 \frac{\Delta V}{\cos \theta} \tag{7.17}$$

$$\Delta \delta_1 = \Delta D \cos \theta \tag{7.18}$$

$$k_1 = \frac{\Delta F_1}{\Delta \delta_1} = 0.50 \frac{\Delta V}{\Delta D} \frac{1}{\cos^2 \theta} = 0.50 \frac{K}{\cos^2 \theta} \tag{7.19}$$

$$\Delta V = \left[k_1 \Delta\delta_1 + k(1-\alpha)(\Delta\delta_2 + \Delta\delta_3) \right] \cos\theta \tag{7.20}$$

Axial load-axial displacement relationships for off-diagonal struts are derived by assuming that the off-diagonal struts complement the central strut in obtaining a behavior equivalent to that of an infill panel.

The equilibrium equation between the shear in the infill panel and the forces in the struts is obtained using the principle of virtual displacements and assuming the same virtual displacement field as shown in Figure 7.26. The incremental shear in the infill panel ΔV is expressed as a function of the incremental forces in the three struts, see equation (7.20), where k is the axial stiffness of off-diagonal struts, evaluated by means of equation (7.9), while $\Delta\delta_2$ and $\Delta\delta_3$ are the incremental displacements corresponding to the incremental lateral displacement $\Delta\delta_1$ of the infill panel. From this equation, the incremental axial forces in the struts can be obtained according to expression in equations (7.21), (7.22)and (7.23), where ΔF_1, ΔF_2, and ΔF_3 are the incremental forces in the central, upper, and lower struts, respectively.

$$\Delta F_1 = k_1 \Delta\delta_1 = k_1 \Delta D \cos\theta \tag{7.21}$$

$$\Delta F_2 = k(1-\alpha)\Delta\delta_2 = k(1-\alpha)^2 \Delta D \cos\theta \tag{7.22}$$

$$\Delta F_3 = k(1-\alpha)\Delta\delta_3 = k(1-\alpha)^2 \Delta D \cos\theta \tag{7.23}$$

Equation (7.9) is used to calculate the stiffness of the off-diagonal struts, and equations (7.22) and (7.23) are employed for the evaluation of the incremental force in the off-diagonal struts, consistent with the load-displacement relationship assumed for the infill panel.

Finally, a Takeda hysteretic rule was assumed. It is worth noting that considering infill envelope characterized by very low IDR values as shown in Figure 7.27b, the hysteretic rule chosen does not strictly influence results.

- **Bending capacity model**

Bending behavior was evaluated *a posteriori* on analysis results, no plastic hinges were introduced in the model. In particular, it has to be verified if the bending demand exceeds or not the yield limit of the section. Of course, the

overcoming of this limit would not correspond to a ductile failure of the member, but it would mean that the basic hypotheses of the linear model are not satisfied. This verification is carried out only on columns and not on beams, since the collapse mechanism involved only columns at first storey. To this end, for each section the axial load-yielding moment relationship is evaluated and the yielding moment is evaluated step-by-step, depending on the axial load, and compared with the moment demand. The biaxial bending interaction between M_x and M_y is not taken into account.

- **Shear capacity model**

Shear behavior was evaluated *a posteriori* on analysis results, no shear plastic hinges were introduced in the model. Different models of shear capacity were evaluated considering the likely brittle failure shown by damage observation. The capacity model employed is the approach suggested by Eurocode 8 part 3 (CEN, 2005) that employs a different formulation as long as the shear span ratio of the column is above or below 2. If the shear span ratio (Lv/h) is higher than 2, shear strength is controlled by the stirrups. Shear strength is given by three contributions, respectively related to: axial load (only in compression), concrete resistance mechanisms and transversal reinforcement. Moreover, shear strength decreases as the displacement (that is, the ductility demand) increases. In particular, the cyclic shear resistance, V_R, decreases with the plastic part of ductility demand $\mu_{\Delta pl}$, expressed in terms of ductility factor $\mu_{\Delta pl} = \mu_{\Delta}-1$, (see Chapter 6).

Based on the shear capacity model proposed in EC8, it is possible to evaluate shear failure both in elastic (brittle failure, $\mu_{\Delta pl} = 0$) and in inelastic field (limited ductility failure, $\mu_{\Delta pl} > 0$). Herein, the shear capacity (V_{R1}) is calculated assuming $\mu_{\Delta pl} = 0$, consistent with the elastic modeling adopted for RC elements (beams and columns).

If the shear span ratio (L_V/h) is less or equal than 2, shear strength is controlled by web crushing along the diagonal of the column, which under cyclic loading may be calculated from the expression in (CEN, 2005), see again

Chapter 6.

- **Sliding shear failure**

In the case study structure sliding shear failure was considered, and the capacity model described in chapter 6 is adopted. The potential sliding surface corresponds to the casting separation between the top of the column and the beam-column joint, see Figure 7.23b. This surface highlights a poor treatment, similarly to what can be observed in other buildings in Pettino (Verderame et al., 2009). Therefore, the friction coefficient is given equal to 0.60, as proposed by ACI for untreated surfaces, see chapter 6.

Moreover, the value of clamping action contribution directly depends on the amount of an additional reinforcement area A_{sl} (ACI 318-05, 2005), which has to be effectively anchored in order to allow the development of a yield stress. In the case study structure such a proper anchorage detail was not present, or failed during the seismic event, see Figure 7.23; concrete cover crushed in all beam-column joints, thus limiting or even completely removing the upper anchorage of longitudinal reinforcement in columns. Hence, the contribution due to clamping action will not be taken into account in shear strength assessment.

Dowel action mechanism is directly linked to the amount of longitudinal reinforcement in columns. Moreover this reinforcement has to effectively resist a sliding shear movement. If longitudinal bars are placed in the opposite faces of the transverse section, as in the present case study building, this effectiveness depends on the restraining action on longitudinal bars given by transversal reinforcement near the sliding section. Specifically, stirrups placed in beam-column joint and placed at the top of the column. Transversal reinforcement has a low diameter and is closed with 90 degree hooks. Moreover, in corner columns, due to the absence of stirrups in joint area (see Figure 7.23b); only the restraining action of external concrete cover on longitudinal bars could permit the development of a dowel action mechanism. Therefore, the crushing of concrete cover previously discussed, strongly limits this contribution. In the following section, shear strength will be evaluated

both with and without the dowel action contribution (V_{R2}), according to equation (7.24). Sliding shear behavior was evaluated *a posteriori* on analysis results, no sliding shear plastic hinges were introduced in the model.

$$V_{R2} = \mu \cdot N + 0.25 \cdot A_{sl} \cdot f_y \quad (7.24)$$

7.7.3. Nonlinear dynamic analysis

Modeling issues and structural model described in above allow pursuing nonlinear dynamic analyses with the two structural models characterized by the two infill parametric hypotheses (*weak* and *strong*).

First of all, in the following, the input selected for the analyses is described, then analysis results are shown.

- **Seismic input choice**

The case study structure was very close to the epicenter (see section 7.4). Three accelerometric stations, whose epicentral distances were less than 6 km, registered the mainshock event, those stations where chosen also because of the vicinity to the case study structures, see Figure 7.28. In Table 7-2, station ID and geographic coordinates of each of the stations are reported. Table 7-2 reports record identifiers (ID), these ID later will be used to identify each accelerogram employed as input for analyses. Figure 7.28 shows the map of the site in which stations, the epicenter and the case study structure were reported. As it is possible to recognize from the map the closest station to the case study structure (42.376 lat. and 13.354 long.) was AQV (GX066 record), and AQG (CU104) and AQA (FA030) are approximately at the same distance from the structure. Since the principal aim is to find the main causes of the soft storey mechanism showed by the structure during the L'Aquila earthquake mainshock, the three records reported in Figure 7.28 have been assumed as input. Horizontal components of the chosen records were rotated considering building orientation in plan and orientation of each component registered to simulate as close as possible the effect of the real shaking on the structure. Each signal was filtered and corrected (Chioccarelli et al., 2009)

The selection procedure adopted in this paper is different from the

standard input selection procedure suggested by international codes and literature (Bommer and Acevedo, 2004), on the other hand it represents a key tool in providing realistic response for the analyses presented herein.

Table 7-2. Station IDs, record IDs and their localization

Station ID	Record ID	Latitude	Longitude
AQV	GX066	42.377	13.344
AQG	CU104	42.373	13.337
AQA	FA030	42.376	13.339

Elastic spectra of the input signal selected are provided in Figure 7.29 and compared with code elastic spectra. Elastic spectra of the horizontal components, rotated according to the axes previously assumed in Figure 7.24, are provided in Figure 7.29a. Elastic spectra of the vertical components are provided in Figure 7.29b.

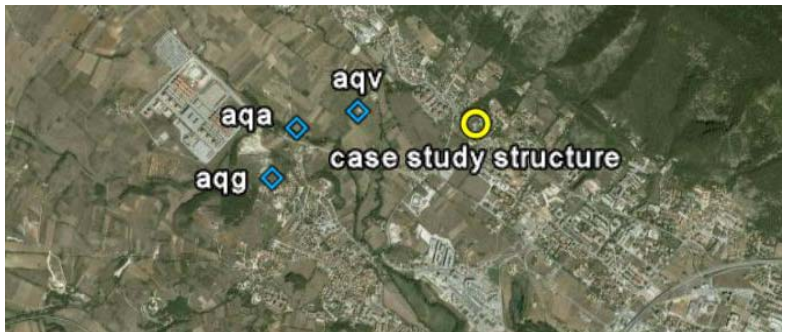

Figure 7.28. Map of the site, stations, epicenter and case study structure (Google Earth).

In Figure 7.29, horizontal and vertical Italian code spectra (CS. LL. PP., 2008) are reported respectively for two different limit states (near collapse SLC and life safety SLV) and for geographic coordinates of the case study structure (42.376 lat and 13.354 long). Different soil type spectra are considered, since it was not possible to determine specific soil type for the site. The accelerometric station closer to the structure (AQV) was characterized by B soil type (Ameri et al., 2009). According to the code, the vertical component elastic spectra do not present any difference because of soil type.

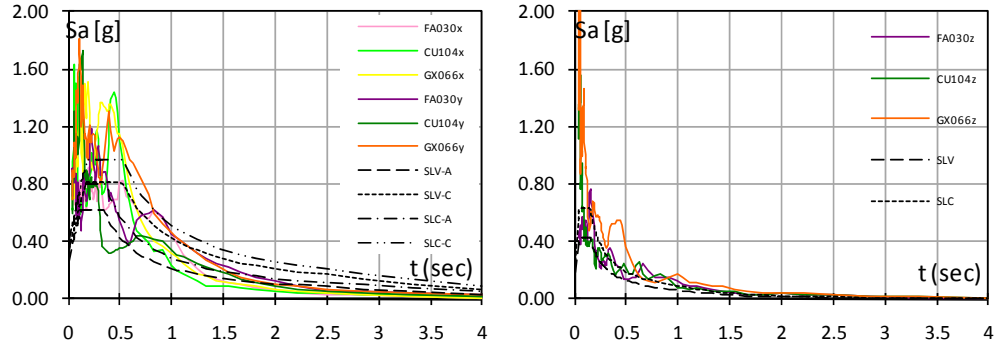

Figure 7.29. Elastic spectra for horizontal (a) and vertical (b) components of the record selected compared with target Italian code spectra for the site

Considering linear dynamic properties of each model (fundamental period) it is possible to predict roughly the expected response to each single record. For example horizontal components of the closest registered signal (GX066) in period range between 0.2 seconds and 0.25 seconds have spectral ordinates greatly higher than the horizontal components of the other two signals and it has the maximum vertical component in a wide range of periods. It is worth to note that other dedicated studies highlighted near source effect in the signals considered herein (for further details see Appendix C).

- **Results and discussion**

Results of nonlinear dynamic analyses are presented in the following. For the sake of brevity only the alignment assumed to be more representative of the behavior of the building is presented herein. In particular, the attention is focused on corner columns since, as highlighted in Figure 7.22, they were particularly damaged. Moreover, the lower axial load due to gravity loads on these columns, compared to remaining columns, leads to lower strength for flexure, shear and sliding shear mechanisms, since columns' section characteristics are the same, dimensions, longitudinal and transversal reinforcements. Furthermore, the higher distance from the centre of masses leads to higher seismic demand, both in terms of forces and displacement, compared to other columns, due to the torsional component of the plan deformation, similarly to what happens for the first modal shape (see Figure

7.25). Finally, the presence of adjacent infill panels increases the shear demand on these columns, due to local interaction effects.

Therefore, in the following the only results for column #3 at first storey are presented in Figure 7.30 to Figure 7.32 and discussed. In particular, for the three considered accelerograms, the demand at the top of the column is considered, since, based on analysis results, it is higher than the demand at the bottom. It is verified (i) if the yield limit is overcome and (ii) if a brittle failure due to shear or to sliding shear occurs. Interaction between axial load and bending moment or shear plays a relevant role for both verifications. To this end, it is sufficient to analyze the first three seconds of the analysis results.

After about 1.50 sec a severe variation in axial load is observed, compared to the gravity load value of 200 kN, up to 100% in compression and 150% in tension. Similarly, bending moment and shear increase too, compared to the almost null values due to gravity loads, but only with a positive or negative sign, respectively.

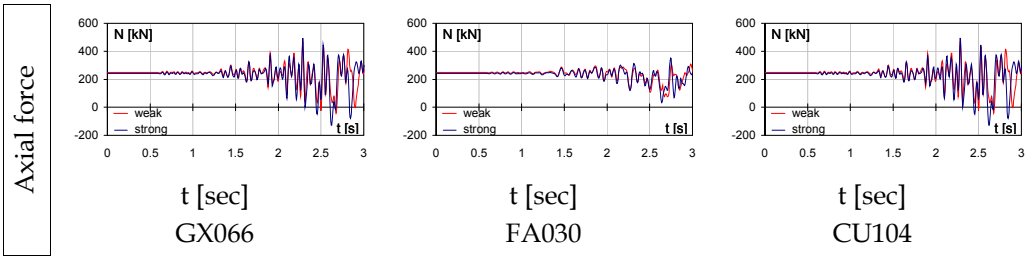

Figure 7.30. Analysis results for the top of column #3 (axial force).

The high variation in the axial load demand, in particular the variation leading to a compression decrease, contributes to the overcoming of the yield limit after 2.50 sec, for the three considered signals, as highlighted by the evolution of the ratio (M/M_y). As a matter of fact, the high decrease in axial load demand, compared with the gravity load demand, leads to a decrease in the yielding moment M_y, which finally equals the increasing moment demand, M. After that, the results reported in Figure 7.30 to Figure 7.32 are affected by the fact that the basic hypothesis standing behind the linear behavior of RC elements is not attended anymore. Nevertheless, the overcoming of the yield limit has not to be considered as a ductile failure.

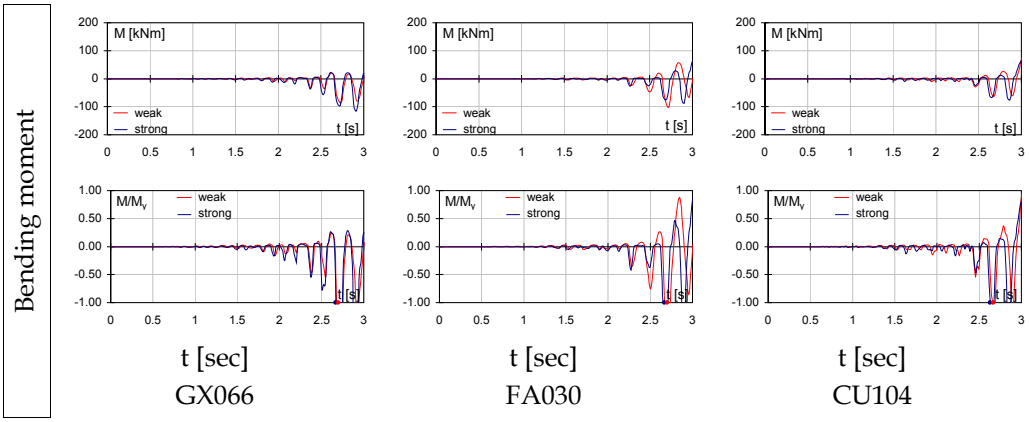

Figure 7.31. Analysis results for the top of column #3 (bending moment and demand over capacity ratios).

The increase in shear demand is also coupled with the decrease in axial load demand, nevertheless no shear failure takes place, at least during the first three seconds. In fact, the shear strength is made up of three contributions (see section 7.7.2), therefore it is not highly influenced by the variation in axial load.

On the contrary, the sliding shear strength highly depends on the axial load. If the sliding shear strength is considered as given by axial load and dowel action contribution, the sliding shear failure takes place, also in this case, almost at the same time of the section yielding. Only the FA030 accelerogram does not lead to a sliding shear failure during the first three seconds. Moreover, failure occurs for a shear demand about equal to 100 kN, which is the result of the local interaction with the adjacent infill panel.

If the dowel action is not considered, the sliding shear strength is proportional to the axial load. The failure occurs before than the previous case, when the dowel action mechanism is considered. This is true for all of the three signals, but above all for the GX066 signal, registered in the closest accelerometric station to the building (about 900 meters), which is probably the most representative one. Moreover, for this signal the vertical component is much severe than for the other signals, see Figure 7.29b. Nevertheless, it is worth to note that the shear demand leading to the failure, in this case, is quite low, even less than 50 kN, thus confirming a low value of the load given by the

interaction with the adjacent infill panel. Infill mechanical characteristics (*weak* or *strong*) do not seem to influence strictly the outcome of the verifications.

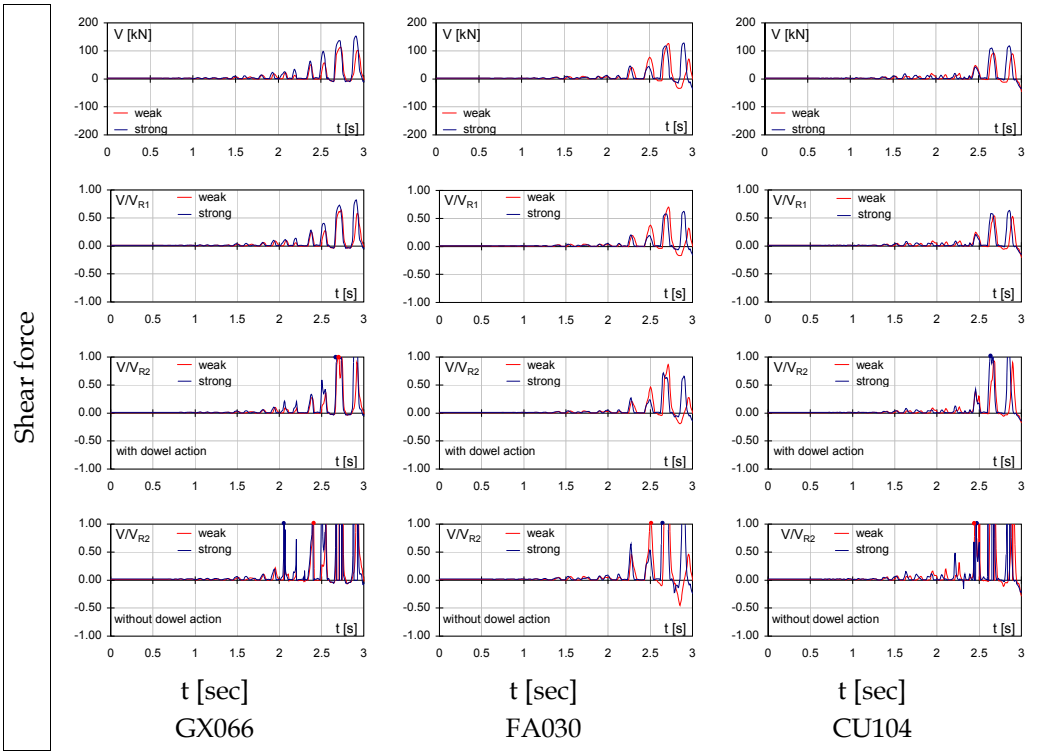

Figure 7.32. Analysis results for the top of column #3 (shear force and demand over capacity ratios for conventional shear V_{R1}, for sliding shear $V_{R2}$with and without dowel action).

At the bottom of column #3 the shear and bending moment demand is quite similar to the top of the column. In fact, the maximum values of demand are due, also in this case, to the local interaction with the adjacent infill, through the lower off-diagonal strut, (see Figure 7.26), even if for an opposite sign of the interstorey displacement. Therefore, from a theoretical standpoint, it is likely to foresee a similar outcome of the verifications: sliding shear failure, section yielding and absence of shear failure.

These considerations are confirmed by graphs reported in Figure 7.33, for GX066 signal. Nevertheless, the sliding shear failure, unlike the top of the column, takes place only if dowel action contribution is not considered.

The hypothesis of absence of dowel action to sliding shear capacity is likely for the top of the column because of the absence of stirrups in the beam-column joint and the crushing of the concrete cover; the same hypothesis becomes very conservative for the bottom of the column, because of the restrain action given by the foundation element. Thus the verifications are still carried out considering both the sliding shear capacity with and without dowel action contribution (Figure 7.32 and Figure 7.33), but the reliability of such hypothesis is different in for the top and the bottom of the columns.

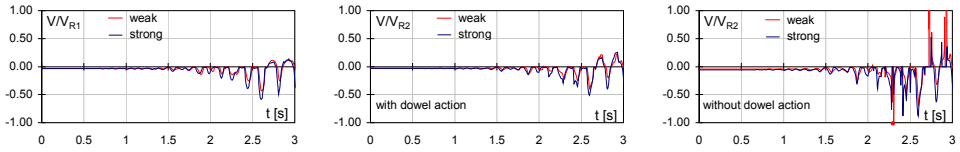

t [sec] t [sec] t [sec]

Figure 7.33. Analysis results for the bottom of column #3 (brittle demand over capacity ratios for GX066 signals.

If column #3 is considered as representative of the behavior of corner columns, it is possible to state that the mode of failure is certainly brittle; in particular it takes place due to a sliding shear mechanism at the top of the column, which has a lower strength compared to the bottom. These results seem to be confirmed by the damage observed during the in-situ survey (see Figure 7.22).

Finally, due to the brittle mode of failure, the interstorey displacement demand at the different levels is quite low, following a deformed shape similar to the first modal shape (see Figure 7.34), and in infills the only cracking displacement is overcome and the maximum strength is not attained.

In particular, referring to column #3, when the sliding shear failure takes place at the top of the column, without considering dowel action, the interstorey drift ratio (IDR) is equal to 0.01% and the adjacent infill is still in elastic field (no cracking is attained), while if the dowel action is considered the IDR value corresponding to failure is 0.1% and the adjacent infill is cracked. The deformed shape after failure cannot be determined, since no

shear hinge is included in the numerical model.

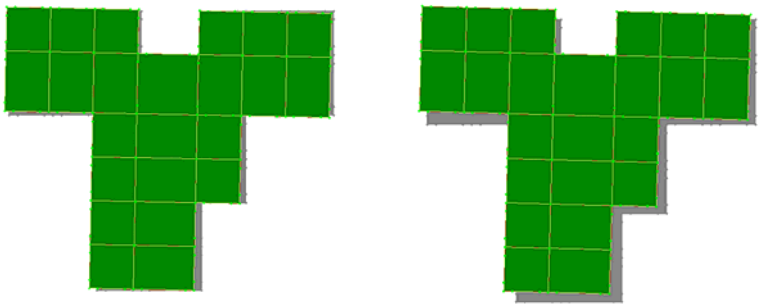

Figure 7.34. Plan deformed shape corresponding to the sliding shear failure, (a) without and (b) with dowel action contribution.

7.8 Conclusions

RC buildings in L'Aquila area do not represent the main part of the whole building stock that mainly comprises masonry buildings no higher than three storeys. Thanks to a detailed review of seismic codes in force in past decades, an analysis was made of the weaknesses that can be found in existing buildings. Damage recorded on RC structures after the L'Aquila mainshock event was then analyzed in the light of previous considerations about construction practices. Several general conclusions can be drawn about the performance of RC buildings:

- The main damage involved non-structural elements such as infill panels.
- Structural damage was found in columns, walls and beam-column joints, but most of the times it was caused by design procedures, consistently with the code prescriptions in force at the age of construction, not properly aimed at avoiding brittle failure mechanisms.
- Documented building collapses were essentially caused by irregularities in plan or elevation of the structural and non-structural complex.

One of the structural collapses was analitically studied and a back analysis of the collpasecauses was pursued. Numerical results confirmed the probable cause of failure indicated by damage observation. Analysis demonstrated that the approximation of linear modeling of RC members did

not affect the results as soon as the first element failure occurs (localized in the first few seconds of the signals). The main conclusions drawn from such numerical results can be summarized as follows:

- local interaction between infills and RC columns led to an increase in shear demand;
- axial force variation in RC columns, due to vertical component of the earthquake, produced changes in shear capacities more relevant for friction mechanism;
- no shear failure controlled by stirrups or by web crushing occurred;
- the most probable cause of the structural collapse can be addressed to a shear friction failure essentially determined by inadequate transversal reinforcement and improper treatment of casting surface.

The case study presents some peculiar details so the numericalresults cannot be easily genralized; on the other hand, it can help to focus on issues that play an important role when basic seismic design practice is not employed, as it was observed in many other cases documented during in field campaigns.

As a side consideration, it should be emphasized that seismic demand associated to the mainshock event exceeds the seismic demand characteristic of the T_R=475 years event determined on stiff soil; the latter can be considered as the main benchmark since it represents the seismic demand of the Life Safety Limit State for an ordinary building when designed according to the seismic code currently in force in Italy.

REFERENCES

ACI 318-05, 2005. Building code requirements for structural concrete (ACI 318-05) and commentary (ACI 318R-05). ACI committee 318 structural building code. American Concrete Institute.

Ameri G., Augliera P., Bindi D., D'Alema E., Ladina C., Lovati S., Luzi L., Marzorati S., Massa M., Pacor F., Puglia R., 2009. Strong-motion parameters of the Mw=6.3 Abruzzo (Central Italy) earthquake. http://esse4.mi.ingv.it/.

Bommer J.J, Acevedo A.B., 2004. The use of real earthquake accelerograms as input to dynamic analysis, *Journal of Earthquake Engineering*, **8** (Special Issue I), 43-91.

BS EN 1990, 2002. Eurocode – Basis of Structural Design.

Buonopane S.G., White R.N., 1999. Pseudodynamic testing of masonry-infilled reinforced concrete frame. *ASCE Journal of Structural Engineering*, **125**(6), pp. 578-589.

Chioccarelli E., De Luca F., Iervolino I., 2009. Preliminary study on L'Aquila earthquake ground motion records, V5.20. http://www.reluis.it/.

Chrysostomou C.Z., Gergely P., Abel J.F., 2002. A six-strut model for nonlinear dynamic analysis of steel infilled frames, *International Journal of Structural Stability and Dynamics* , **2**, 335-353.

Comité Européen de Normalisation, 2004. Eurocode 8 – Design of Structures for earthquake resistance – Part 1: General rules, seismic actions and rules for buildings. EN 1998-1, CEN, Brussels.

Comité Européen de Normalisation, 2005. Eurocode 8: design of structures for earthquake resistance – Part 3: assessment and retrofitting of buildings. European Standard EN 1998-3:2005. CEN, Brussels.

Crisafulli F.J., 1997. Seismic behaviour of reinforced concrete structures with masonry infills (Ph.D. Thesis). University of Canterbury. Christchurch, New Zealand.

CS. LL. PP. Circolare del Ministero dei Lavori Pubblici n. 65 del 10/4/1997, 1997 Istruzioni per l'applicazione delle "Norme tecniche per le costruzioni in zone sismiche" di cui al Decreto Ministeriale 16 gennaio 1996. G.U. n. 97 del 28/4/1997 (in Italian).

CS. LL. PP; DM 14 Gennaio 2008 Allegato A alle Norme Tecniche per le Costruzioni: Pericolosità Sismica. Gazzetta Ufficiale della Repubblica Italiana, 29, (in Italian).

CS. LL. PP. Circolare del Ministero dei Lavori Pubblici n. 617 del 2/2/2009, 2009 Istruzioni per l'applicazione delle "Nuove norme tecniche per le costruzioni" di cui al D.M. 14 gennaio 2008. G.U. n. 47 del 26/2/2009 (in Italian).

Decanini LD, De Sortis A, Goretti A, Liberatore L, Mollaioli F, Bazzurro L, 2004. Performance of reinforced concrete buildings during the 2002 Molise, Italy, earthquake. *Earthquake Spectra*, **20**(S1), S221–S255.

Decreto Ministeriale n. 40 del 3/3/1975, 1975. Approvazione delle norme tecniche per le costruzioni in zone sismiche. G.U. n. 93 dell'8/4/1975 (in Italian).

Decreto Ministeriale del 24/1/1986, 1986. Istruzioni relative alla normativa tecnica per le costruzioni in zona sismica. G.U. n. 108 del 12/5/1986 (in Italian).

Decreto Ministeriale del 16/1/1996, 1996. Norme tecniche per le costruzioni in zone sismiche. G.U. n. 29 del 5/2/1996 (in Italian).

Decreto Ministeriale del 14/1/2008, 2008. Approvazione delle nuove norme tecniche per le costruzioni. G.U. n. 29 del 4/2/2008 (in Italian).

Dolšek M, Fajfar P, 2001. Soft storey effects in uniformly infilled reinforced concrete frames, *Journal of Earthquake Engineering* , **5**(1), 1-12.

El-Dakhakhni W.W., Elgaaly M., Hamid A.A:, 2003. Three-strut model for concrete masonry-infilled steel frames. ASCE *Journal of Structural Engineering*, **129**(2), 177-185.

Hosseini M., 2005. Behavior of nonstructural elements in the 2003 Bam, Iran, earthquake. *Earthquake Spectra*, 21(S1), S439–S453.

Kaushik H.B., Rai D.C., Jain S.K., 2008. A rational approach to analytical modeling of masonry infills in reinforced concrete frame buildings. *Proceedings of The 14th World Conference on Earthquake Engineering,* October 12-17, Beijing, China.

Legge n. 1684 del 25/11/1962 (1962) Provvedimenti per l'edilizia, con particolari prescrizioni per le zone sismiche. G.U. n. 326 del 22/12/1962 (in Italian)

Liel A.B., Lynch K.P., 2009. Quick response report: Vulnerability of reinforced concrete frame buildings and their occupants in the 2009 L'Aquila, Italy earthquake. http://www.colorado.edu/hazards/research/qr/qr213.pdf.

Loh C.H., Tsai K.C., Chung L.L., Yeh C.H., 2003. Reconnaissance report on the 31 March 2002 earthquake on the East Coast of Taiwan. *Earthquake Spectra*, **19**(3), 531–556.

Mainstone R.J., 1971. On the stiffnesses and strengths of infilled frames, Proceedings of the Institution of Civil Engineering, Supplement IV, 57-90.

Mosalam K., White R.N., Gergely P., 1997. Seismic evaluation of frames with infill walls using pseudodynamic experiments. Rep. No. NCEER-97-0020.

Ordinanza del Presidente del Consiglio dei Ministri n. 3274 del 20/3/2003, 2003. Primi elementi in materia di criteri generali per la classificazione sismica del territorio nazionale e di normative tecniche per le costruzioni in zona sismica. G.U. n. 105 dell'8/5/2003 (in Italian).

Ordinanza del Presidente del Consiglio dei Ministri n. 3431 del 3/5/2005, 2005. Ulteriori modifiche ed integrazioni all'ordinanza del Presidente del Consiglio dei Ministri n. 3274 del 20 marzo 2003. G.U. n. 107 del 10/5/2005 (in Italian).

Paulay T., Priestley M.J.N., 1992. Seismic design of reinforced concrete and masonry buildings. Wiley, New York.

Regio Decreto Legge n. 573 del 29/4/1915, 1915. Che riguarda le norme tecniche ed igieniche da osservarsi per i lavori edilizi nelle località colpite dal terremoto del 13 gennaio 1915. G.U. n. 117 dell'11/5/1915 (in Italian).

Regio Decreto Legge n. 431 del 13/3/1927, 1927. Norme tecniche ed igieniche di edilizia per le località colpite dai terremoti. G.U. n. 82 dell'8/4/1927 (in Italian).

Regio Decreto Legge n. 682 del 3/4/1930, 1930. Nuove norme tecniche ed igieniche di edilizia per le località sismiche. G.U. n. 133 del 7/6/1930 (in Italian).

Regio Decreto Legge n. 640 del 25/3/1935, 1935. Nuovo testo delle norme tecniche di edilizia con speciali prescrizioni per le località colpite dai terremoti. G.U. n. 120 del 22/5/1935 (in Italian).

Regio Decreto Legge n. 2105 del 22/11/1937, 1937. Norme tecniche di edilizia con speciali prescrizioni per le località colpite dai terremoti. G.U. n. 298 del 27/12/1937 (in Italian).

Rossetto T., Peiris N., 2009. Observations of damage due to the Kashmir earthquake of October 8, 2005 and study of current seismic provisions for buildings in Pakistan. *Bulletin of Earthquake Engineering*, **7**(3), 681–699.

Stucchi et alii, 2007. DBMI04, il database delle osservazioni macrosismiche dei terremoti italiani utilizzate per la compilazione del catalogo parametrico CPTI04. http://emidius.mi.ingv.it/DBMI04/ Quaderni di Geofisica, Vol 49, pp.38 (in Italian).

Verderame G.M., Iervolino I., Ricci P., 2009. Report on the damages on buildings following the seismic event of 6th of April 2009 time 1.32 (UTC) – L'Aquila M=5.8, V1.20. http://www.reluis.it/.

Verderame G.M., Polese M., Mariniello C, Manfredi G., 2010. A simulated design procedure for the assessment of seismic capacity of existing reinforced concrete buildings. *Advances in Engineering Software*, **41**(2), 323-335.

Chapter 8

CONCLUSION AND PERSPECTIVES

Performance Based Earthquake Engineering (PBEE) represents the consolidated framework in which most of the research on seismic risk of the last years can be placed. Thus, it is in this framework that some specific issues regarding the whole process of control and assessment of seismic risk have been studied in this thesis.

The decoupling approach to PBEE of the Pacific Earthquake Engineering Center allows, in fact, to split the seismic risk problem in four main steps: hazard, demand prediction, modeling of damage states and failure and loss assessment. The research has focused on the first three aspects of the process.

8.1 Hazard and ground motion

Seismic hazard analysis has made in the recent years huge efforts allowing a more accurate representation of the ground motions (Cornell, 2004). The improvements in probabilistic seismic hazard analysis reflects on the accuracy of the whole process of PBEE. The specific issues considered in this research are the employment of advanced intensity measures for probabilistic seismic hazard analysis and the reliability of artificial, wavelet adjusted and linearly scaled records for input selection in nonlinear dynamic analysis according to actual code provisions.

The first topic, enjoying the results of previous researchers (Bozorgnia et al. 2010; Tothong, 2007), investigates inelastic displacement and equivalent number of cycles as advanced intensity measures for both peak and cyclic response. Two prediction equations for these two intensity measures are

estimated. The database considered is the ITalian ACcelerometric Archive, thus allowing a specific characterization for Italy. The prediction equations considered, obtained with a constant strength reduction factor approach, showed a standard deviation comparable to the one of ordinary prediction equations obtained for spectral acceleration. The advantage in the employment of such advanced intensity measures lies in a characterization of the hazard closer to the inelastic response of structures. In fact, inelastic displacement has shown to be a efficient, sufficient and robust to scaling intensity measure in the case of first mode dominated structures (Tothong, 2007). Associating inelastic displacement with a cyclic intensity measure can fulfill the lack of such an intensity measure for structures in which higher modes have a relevant weight on the response. Regarding the possible enhancements in probabilistic seismic hazard analysis, and given the supremacy in the actual code and research of peak response intensity measures, it can be important considering the correlation between these two intensity measure (inelastic displacement and equivalent number of cycles) to obtain a conditional hazard evaluation for a vector-valued inelastic intensity measures. Such tools are already available for intensity measures based on elastic response (Iervolino et al., 2010). Other than being employed for conditional hazard, such an inelastic vector valued intensity measure should be evaluated in term of properties, such as efficiency, sufficiency and robustness to scaling, following the path, to check such properties, already available in other studies (Tothong, 2007) and assessing if improvements respect to the inelastic displacement alone can be found (e.g. reliable employment for higher mode influenced structures).

The first straightforward employment of the prediction equations obtained in this study is the assessment of the reliability of simulated scenarios. Such prediction equations, in fact, can be useful to carry out a general validation of simulation techniques for synthetic accelerograms. The latter aspect will be fulfilled within the ReLUIS Project 2010-2013 (Task RS1), employing the response of the prediction equations as unbiased benchmark for the validation.

The latter perspective of such prediction equations, that still asks for further computational efforts, is the employment of the results for advanced expected damage maps for large scale risk assessment. In fact, given further development of the prediction equations, also for softening behaviors, each single degree of freedom shape can be directly linked to a specific structural behavior, materials and design approach. If a characterization of the building stock in such terms would be available, the response according to these advanced intensity measures can be mapped providing information not only regarding hazard but also regarding vulnerability aspects on a probabilistic basis. Such an approach could be compared to macro-seismic scales of damage (e.g. Grünthal G., 1998) and the approximations implicit in such approach could be assessed.

The second topic that regards hazard and ground motion focuses on code-based input selection and investigates the employment of modified accelerograms, such as artificial, wavelet adjusted and linearly scaled. The approach followed is a benchmarking procedure respect to unscaled real records to which the spectral constraint provided by codes (CEN, 2004; DM 14/1/2008) is applied. As it was shown in previous studies, spectral compatible unscaled real records are not an unbiased benchmark (PEER report 2009/01, 2009) in itself; on the other hand, they are, for sure, the actual code benchmark.

The results of the study presented in this research, given the statistical basis provided, thanks to employment of hypothesis tests, allow assessing that all the modified categories of record considered do not introduce any statistical significant "bias" in terms of peak response. On the other hand, a slight underestimation of the response is found for artificial records. The investigation regarding cyclic response found a statistical significance of the overestimation in term of cyclic response of artificial records respect to unscaled real records. The main conclusion is that, given the restraint on the elastic spectrum applied to the records selected for the analysis, according to current code provision, there is a satisfactory control of the peak response,

while if cyclic response is of any concern caution is needed when employing artificial records. The results of this study can be further developed respect to an unbiased benchmark, employing, for example, the inelastic spectra obtained thanks to the prediction equations above, and carrying out, hopefully, more robust conclusions regarding the employment of artificial records in nonlinear dynamic analyses.

8.2 Demand prediction

The aspect of demand prediction in the PBEE framework is related to the evaluation of dG(EDP|IM). So, once in hazard analysis it is assessed which one is the best intensity measure to be employed, demand prediction aspects are focused on the evaluation of engineering demand parameters by means of structural analysis procedures. Structural analysis methodologies are, indeed, the object of the study carried out in this thesis regarding demand prediction aspects. First the different analysis approaches (linear and non linear, static and dynamic) available in literature and codes are presented emphasizing pros and cons of each one (e.g. Krawinkler and Seneviratna, 1998; Chopra, 2007; Vamvatsikos and Cornell, 2002). Then, code provisions regarding analysis methodologies are critically reviewed, focusing the attention on the recent Italian seismic code (DM 14/1/2008; CS. LL. PP., 2009), in which some innovations and restrictions have been introduced respect to the more classical and consolidated approach provided in Eurocode (CEN, 2004).

In the second part of the research concerning demand prediction, specific aspects of the static pushover analysis are investigated. This analysis method, for its straightforward way in obtaining nonlinear response of structures, has become the routine analysis approach for existing buildings and it is employed by both researchers and practitioners. The study focuses on the piecewise linear fit aspects, providing an incremental dynamic analysis based methodology aimed at quantifying the error introduced by the fit and finally carries out an optimal fit for static pushover curves. The general conclusions regarding the optimal three points piecewise linear fit can represent a useful

methodological tool for other kind of studies, other than being an improvement of the actual static pushover procedure, allowing the control of the error introduced by the fit within 20%. In fact, once it is assessed that every capacity curve can be acceptably approximated with a three points' piecewise linear function, controlling the error introduced; it is possible to link such simplified fit shapes to specific collapse mechanisms. The coupling procedure of shape and hysteretic behavior of simplified single degree of freedom with specific collapse mechanisms of multiple degree of freedom systems can integrate the large scale mapping of vulnerability previously described as future perspective in section 8.1. If the single degree of freedom to multiple degree of freedom approximation is accepted, a weighted advanced hazard map can be produced on the basis of prediction equations evaluated for three points piecewise linear SDOF's backbones. The above perspectives, other than asking of an high computational effort, request for an accurate check of the possibility to indentify a specific shape and hysteretic behavior as representative of structural conditions of the building stock (age of construction, material, …). Regarding the latter aspect, it is helpful that the shape of a pushover curve can be linked to specific modes of failures. Thus, once it would be checked that a specific collapse mechanism is likely to be registered when a given material and design procedure (accounting also for old codes) are employed, it will be possible to categorize the whole building stock of a region with different three points piecewise linear SDOF's backbones and obtain a weighted mapping through advanced intensity measures such as the inelastic displacement and the equivalent number of cycles.

8.3 Modeling of damage states

Modeling of damage state phase in the PBEE involves the evaluation of capacity for structures, given the performance level (limit state) considered (Macgregor, 1997). Through the definition of capacities it is possible to evaluate damage measures (DM). This topic was investigated focusing the attention specifically on existing reinforced concrete buildings.

Reinforced concrete buildings, in fact, are characterized by specific weaknesses (Fardis, 2009), such as the high frequency of brittle failures given the absence of capacity design. Source of structural problems and causes of brittle failures can be the design approach employed at the time of construction, the lateral load resistant system that can be poor, the pernicious interaction, in most cases, with masonry infills.

The aspect of brittle failures in reinforced concrete building is investigated; firstly shear capacity analytical models suggested by codes and literature are considered, than such analytical approaches are compared with an experimental database and finally a practice-oriented approach is carried out for the quick control of shear-flexure hierarchy in existing reinforced concrete elements. Not only conventional shear mechanisms are considered but also type of non-conventional brittle failures in cast-in-place reinforced concrete frame structures are considered, such as the sliding shear failures (Paulay and Priestley, 1992).

The issue of brittle failures has a significant role in modeling of damage states for existing structures. Further considerations regarding this latter aspect are carried out thanks to the results of a reconnaissance campaign after the 2009 L'Aquila earthquake. Damage observation confirmed the significance of the issue regarding brittle failures. Damage observed on a specific collapsed reinforced concrete buildings allowed a detailed back analysis for the investigation of the likely causes of the soft storey mechanism registered. The strong vertical component and the local interaction with masonry infills have been singled out as the most likely causes of the brittle collapses that involved first storey columns and consequently triggered the progressive collapse of the whole building. The conclusions carried out for the case study structure found a confirmation in the recent American provisions for existing structures (ASCE/SEI 41-06, 2007).

The aspect of brittle failures in reinforced concrete structures needs further investigations. The aspect of sliding shear failures should be studied in specific experimental tests, in fact, experimental studies already available in

literature (e.g. Hofbeck et al., 1969) do not focus on the lack of detailing typical of existing structures.

It is evident that the present research considered only some specific issues that can be placed within the performance based earthquake engineering framework. On the other hand further enhancements are requested for more accurate and aware procedures (Cornell and Krawinkler, 2000) and additional experimental data are requested dealing with the multidisciplinary aspects involved in seismic risk control. The awareness that research studies can represent an enhancement and an advantage for communities and human beings lies at the core of the enthusiasm and the passion that researchers put in their job.

REFERENCES

American Society of Civil Engineers (ASCE), 2007. Seismic Rehabilitation of Existing Buildings, ASCE/SEI 41-06, Reston, Virginia.

Bozorgnia Y., Hachem M.M., Campbell K.W., 2010. Ground motion prediction equation ("attenuation relationship") for inelastic response spectra. *Earthquake Spectra* **26**(1), 1-23.

Chopra A.K., 2007. Dynamics of the Structures, Prentice Hall, Upper Saddle River, New Jersey, 3rd edition.

Comité Européen de Normalisation, 2004. Eurocode8, Design of Structures for earthquake resistance – Part1: General rules, seismic actions and rules for buildings. EN 1998-1, CEN, Brussels.

Cornell, C.A., 2004. Hazard, ground-motions and probabilistic assessment for PBSD, In Performance Based Seismic Design Concepts and Implementation, PEER Report 2004/05, Pacific Earthquake Engineering Research Center University of California Berkeley.

Cornell, A. and Krawinkler, H. , 2000. Progress and challenges in seismic performance assessment. PEER News, April 2000.

CS.LL.PP. Circolare 617, 2009. Istruzioni per l'applicazione delle Norme Tecniche per le Costruzioni, Gazzetta Ufficiale della Repubblica Italiana 47, 2/2/2009 (in Italian).

Decreto Ministeriale del 14 gennaio, 2008. Approvazione delle nuove norme tecniche per le costruzioni. G.U. n. 29 del 4/2/2008 (in Italian).

Fardis M.N., 2009. Seismic design, assessment and retrofitting of concrete buildings based on EN-Eurocode 8, Springer, August.

Grünthal G., 1998. Cahiers du Centre Européen de Géodynamique et deSéismologie: Volume 15 – European Macroseismic Scale 1998.

Hofbeck J.A., Ibrahim I.O. and Mattock A.H., 1969. Shear transfer in reinforced concrete. *ACI Journal*, **66**(13), February, 119-128.

Iervolino I., Giorgio M., Galasso C., Manfredi G., 2010. Conditional hazard maps for secondary intensity measures, *Bulletin of Seismological Society of America*, **100**(6), 3312-3319.

Krawinkler H., Seneviratna G.P.D.K., 1998. Pros and cons of a pushover analysis of seismic performance evaluation, *Engineering Structures*, **20**, 452-464.

Macgregor J.G., 1997. Reinforced Concrete Mechanics and Design. Prentice Hall Edition, New Jersey.

Paulay T., Priestley M.J.N., 1992. Seismic Design of Reinforced Concrete Structures and Masonry Buildings. Wiley, New York.

PEER ground motion selection and modification working group – Haselton C.B., editor, 2009. Evaluation of Ground Motion selection methods: prediction median interstory drift response of buildings. PEER report 2009/01 available at http://peer.berkeley.edu/publications/peer_reports/reports_2009.

Tothong P., Cornell C.A:, 2007. Probabilistic seismic demand analysis using advanced ground motion intensity measures, attenuation relationships, and near fault effects. *John A. Blume Earthquake Engineering Center, Department of Civil and Environmental Engineering, Stanford University*, CA 2007. Available at http://blume.stanford.edu/Blume/TRList.htm.

Vamvatsikos D. and Cornell C.A., 2002 Incremental Dynamic Analysis, *Earthquake Engineering and Structural Dynamics*, **31**, 491-514.

APPENDICES

Appendix A.

PREDICTION EQUATIONS' REGRESSION COEFFICIENTS

In this appendix the coefficients to be employed in the prediction equations in Chapter 2 are reported. Tables in the following shows the coefficients and the standard deviation values at each of the 20 period values considered. Data in Table A-1 refers to the prediction equation for elastic displacements; data in Table A-2 and Table A-3 refers to the prediction equation of inelastic displacements for EPH-k and EPH-p systems, respectively. Finally data in Table A-4 and Table A-5 refers to the prediction equation of equivalent number of cycles for EPH-k and EPH-p systems.

In Table A- the coefficients for elastic displacements, Sd_{el}, are 10, since, obviously there were no coefficients for the strength reduction factor. A soil type coefficient, s_1 is equal to 0 for all the periods.

In Table A-2 and Table A-3 the coefficients for inelastic displacements, Sd_i, are 13. A soil type coefficient, s_1, is equal to 0 for all the periods and the strength reduction factor coefficient, r_2, for Rs equal to 2, is equal to 0 for all the periods. In Table A-4 and Table A-5 the coefficients for the equivalent number of cycles, N_e, are 11. A soil type coefficient, s_1, is equal to 0 for all the periods and the strength reduction factor coefficient, r_2, for Rs equal to 2, is equal to 0 for all the periods.

For all the prediction equations considered the other coefficients and parameters have always the same values. In particular b_3 is equal to 0, R_{ref} is equal to 1, M_{ref} is equal to 5, and M_h is equal to 6.75.

Table A-1. Regression coefficients of the Sd_{el} prediction equation

T	a	b_1	b_2	c_1	c_2	h	s_2	s_3	s_4	s_5	σ_{TOT}
0.04	-0.649	-0.143	-0.077	-1.832	0.3112	7.152	0.1647	0.2405	-0.013	0.6079	0.3613
0.07	0.0515	-0.228	-0.081	-1.967	0.3504	7.6824	0.1538	0.237	-0.014	0.5214	0.3708
0.1	0.6081	-0.067	-0.059	-1.927	0.2812	8.0107	0.1669	0.2304	-0.052	0.5941	0.3794
0.15	1.1141	0.1287	-0.051	-1.784	0.1765	7.874	0.1617	0.2246	0.0504	0.7281	0.3836
0.2	1.3465	0.2158	-0.049	-1.678	0.1425	7.7236	0.1474	0.2275	0.02	0.5215	0.4008
0.25	1.3698	0.2439	-0.045	-1.583	0.1467	7.2679	0.1677	0.2352	0.0623	0.3842	0.3954
0.3	1.3626	0.2398	-0.046	-1.522	0.1694	6.9042	0.1856	0.2379	0.1206	0.282	0.3798
0.35	1.3825	0.2787	-0.046	-1.456	0.1627	6.5996	0.2091	0.2698	0.1861	0.21	0.3687
0.4	1.4409	0.3176	-0.049	-1.404	0.1515	6.2381	0.2172	0.2611	0.1644	0.1751	0.3567
0.45	1.4715	0.3782	-0.036	-1.358	0.1495	6.035	0.2158	0.2814	0.1809	0.1604	0.3553
0.5	1.521	0.4393	-0.033	-1.303	0.1275	5.6837	0.2055	0.2905	0.2078	0.1503	0.3517
0.6	1.5814	0.4742	-0.031	-1.268	0.135	5.7344	0.2119	0.306	0.3223	0.1167	0.3578
0.7	1.6501	0.5374	-0.029	-1.224	0.123	5.326	0.2094	0.3171	0.4636	0.1255	0.3576
0.8	1.6387	0.5243	-0.039	-1.192	0.1374	5.1411	0.2109	0.3143	0.5439	0.1147	0.3599
0.9	1.6512	0.5831	-0.033	-1.138	0.1274	4.8949	0.2061	0.3347	0.6604	0.1279	0.364
1	1.6303	0.5863	-0.038	-1.104	0.128	4.7499	0.2227	0.346	0.6966	0.1411	0.3651
1.25	1.5523	0.5716	-0.045	-1.041	0.1586	4.7853	0.2397	0.3719	0.7015	0.1677	0.3712
1.5	1.5524	0.5781	-0.044	-1.032	0.1766	4.7252	0.242	0.3747	0.6607	0.1784	0.38
1.75	1.5946	0.5904	-0.048	-1.035	0.1731	4.759	0.2485	0.3687	0.5921	0.1875	0.3838
2	1.6253	0.6253	-0.047	-1.014	0.1669	4.6828	0.2362	0.3613	0.544	0.1944	0.3776

Table A-2. Regression coefficients of the Sd_i prediction equation for EPH-k system.

T	a	b_1	b_2	c_1	c_2	h	s_2	s_3	s_4	s_5	r_4	r_6	r_8	σ_{TOT}
0.04	0.206	-0.068	-0.061	-1.772	0.326	10.793	0.161	0.240	0.130	0.524	0.304	0.382	0.421	0.400
0.07	0.179	0.017	-0.056	-1.531	0.314	9.004	0.177	0.257	0.163	0.486	0.287	0.388	0.442	0.401
0.1	0.258	0.003	-0.054	-1.487	0.344	8.083	0.174	0.282	0.225	0.459	0.217	0.313	0.363	0.391
0.15	0.452	0.018	-0.046	-1.457	0.361	7.676	0.204	0.306	0.250	0.478	0.121	0.192	0.235	0.381
0.2	0.720	0.078	-0.039	-1.464	0.344	7.618	0.205	0.301	0.282	0.390	0.070	0.120	0.149	0.376
0.25	0.919	0.160	-0.027	-1.451	0.323	7.720	0.210	0.308	0.314	0.321	0.045	0.082	0.109	0.377
0.3	1.027	0.185	-0.033	-1.429	0.306	7.611	0.223	0.317	0.329	0.280	0.028	0.060	0.078	0.377
0.35	1.183	0.266	-0.029	-1.406	0.273	7.471	0.231	0.321	0.368	0.241	0.020	0.042	0.059	0.375
0.4	1.275	0.334	-0.019	-1.375	0.258	7.203	0.234	0.321	0.389	0.218	0.010	0.026	0.034	0.372
0.45	1.309	0.365	-0.018	-1.334	0.243	6.951	0.226	0.323	0.407	0.206	0.006	0.015	0.020	0.373
0.5	1.385	0.423	-0.012	-1.309	0.226	6.773	0.227	0.323	0.440	0.196	-0.001	0.002	0.007	0.373
0.6	1.433	0.437	-0.018	-1.277	0.224	6.606	0.230	0.326	0.462	0.183	-0.012	-0.016	-0.015	0.373
0.7	1.509	0.473	-0.023	-1.243	0.207	6.404	0.225	0.324	0.504	0.171	-0.026	-0.033	-0.037	0.372
0.8	1.519	0.489	-0.027	-1.207	0.200	6.174	0.225	0.330	0.540	0.180	-0.025	-0.033	-0.041	0.373
0.9	1.521	0.497	-0.031	-1.181	0.200	5.901	0.230	0.336	0.587	0.182	-0.026	-0.043	-0.053	0.375
1	1.549	0.516	-0.034	-1.158	0.192	5.844	0.226	0.340	0.601	0.169	-0.028	-0.047	-0.060	0.378
1.25	1.575	0.534	-0.040	-1.125	0.192	5.571	0.231	0.350	0.598	0.185	-0.037	-0.057	-0.072	0.382
1.5	1.576	0.548	-0.043	-1.096	0.190	5.235	0.233	0.357	0.575	0.185	-0.036	-0.061	-0.074	0.386
1.75	1.586	0.579	-0.037	-1.077	0.194	5.064	0.227	0.343	0.548	0.179	-0.033	-0.058	-0.073	0.386
2	1.589	0.584	-0.040	-1.062	0.192	4.992	0.228	0.346	0.512	0.169	-0.038	-0.058	-0.076	0.388

Table A-3. Regression coefficients of the Sd_i prediction equation for EPH-p system.

T	a	b_1	b_2	c_1	c_2	h	s_2	s_3	s_4	s_5	r_4	r_6	r_8	σ_{TOT}
0.04	0.282	-0.084	-0.062	-1.784	0.337	10.564	0.165	0.242	0.132	0.507	0.210	0.254	0.276	0.381
0.07	0.341	0.048	-0.051	-1.554	0.303	9.146	0.181	0.265	0.175	0.497	0.237	0.299	0.329	0.388
0.1	0.390	0.051	-0.050	-1.485	0.320	8.271	0.182	0.281	0.234	0.471	0.211	0.277	0.304	0.385
0.15	0.534	0.085	-0.038	-1.435	0.334	7.675	0.206	0.302	0.249	0.461	0.141	0.202	0.229	0.378
0.2	0.738	0.117	-0.035	-1.440	0.332	7.545	0.209	0.297	0.299	0.362	0.100	0.146	0.167	0.378
0.25	0.913	0.183	-0.026	-1.425	0.317	7.537	0.212	0.306	0.341	0.292	0.071	0.109	0.130	0.379
0.3	1.025	0.229	-0.027	-1.399	0.299	7.330	0.224	0.321	0.375	0.251	0.055	0.091	0.105	0.383
0.35	1.150	0.282	-0.027	-1.382	0.276	7.167	0.227	0.328	0.412	0.215	0.048	0.072	0.085	0.380
0.4	1.224	0.326	-0.021	-1.362	0.272	6.937	0.231	0.332	0.437	0.198	0.033	0.052	0.060	0.378
0.45	1.264	0.359	-0.021	-1.325	0.257	6.672	0.226	0.333	0.453	0.189	0.024	0.038	0.044	0.379
0.5	1.317	0.392	-0.017	-1.310	0.252	6.584	0.227	0.333	0.477	0.182	0.016	0.024	0.033	0.380
0.6	1.376	0.418	-0.021	-1.277	0.247	6.412	0.227	0.334	0.501	0.184	-0.002	0.002	0.008	0.380
0.7	1.460	0.456	-0.023	-1.254	0.233	6.340	0.225	0.333	0.534	0.178	-0.015	-0.012	-0.013	0.382
0.8	1.486	0.475	-0.027	-1.227	0.225	6.144	0.228	0.340	0.570	0.192	-0.018	-0.020	-0.022	0.382
0.9	1.496	0.482	-0.031	-1.205	0.224	5.888	0.230	0.343	0.605	0.197	-0.025	-0.034	-0.036	0.384
1	1.521	0.499	-0.034	-1.186	0.216	5.810	0.230	0.344	0.615	0.187	-0.027	-0.037	-0.041	0.384
1.25	1.548	0.510	-0.041	-1.159	0.216	5.492	0.231	0.353	0.602	0.200	-0.039	-0.049	-0.056	0.388
1.5	1.549	0.523	-0.044	-1.131	0.216	5.198	0.231	0.356	0.567	0.201	-0.042	-0.058	-0.062	0.389
1.75	1.571	0.560	-0.036	-1.117	0.216	5.103	0.226	0.340	0.527	0.192	-0.039	-0.054	-0.061	0.391
2	1.579	0.566	-0.037	-1.106	0.215	5.074	0.223	0.341	0.491	0.181	-0.044	-0.055	-0.066	0.392

Table A-4. Regression coefficients of the N_e prediction equation for EPH-k system.

T	a	b_1	c_1	h	s_2	s_3	s_4	s_5	r_4	r_6	r_8	σ_{TOT}
0.04	0.366	0.053	0.385	4.780	0.039	0.047	0.089	0.022	0.389	0.529	0.605	0.184
0.07	0.235	0.053	0.410	5.236	0.036	0.059	0.071	0.088	0.357	0.492	0.567	0.177
0.1	0.243	0.041	0.377	5.343	0.035	0.061	0.075	0.147	0.311	0.433	0.506	0.169
0.15	0.261	0.031	0.345	5.036	0.024	0.047	0.060	0.109	0.274	0.382	0.452	0.159
0.2	0.249	0.019	0.321	4.738	0.037	0.040	0.064	0.043	0.261	0.371	0.440	0.150
0.25	0.248	0.018	0.312	4.549	0.046	0.042	0.066	0.011	0.257	0.368	0.433	0.152
0.3	0.214	0.009	0.316	4.490	0.044	0.042	0.076	0.000	0.258	0.368	0.436	0.150
0.35	0.205	0.000	0.312	4.436	0.039	0.039	0.062	0.016	0.248	0.357	0.425	0.153
0.4	0.198	0.000	0.308	4.354	0.035	0.044	0.087	0.016	0.246	0.355	0.426	0.150
0.45	0.218	0.005	0.299	4.166	0.036	0.036	0.120	0.009	0.242	0.353	0.426	0.154
0.5	0.201	0.006	0.305	4.118	0.040	0.040	0.118	0.010	0.242	0.357	0.429	0.154
0.6	0.187	-0.002	0.305	4.087	0.028	0.034	0.154	-0.003	0.238	0.353	0.425	0.153
0.7	0.184	-0.005	0.300	4.022	0.033	0.038	0.160	-0.001	0.236	0.349	0.420	0.154
0.8	0.205	-0.003	0.285	3.900	0.036	0.043	0.154	-0.013	0.233	0.346	0.418	0.154
0.9	0.192	-0.009	0.286	3.886	0.038	0.045	0.149	-0.006	0.229	0.344	0.416	0.151
1	0.178	-0.013	0.286	3.874	0.042	0.038	0.140	-0.002	0.235	0.349	0.421	0.148
1.25	0.182	-0.022	0.269	3.746	0.034	0.030	0.096	-0.024	0.227	0.342	0.417	0.148
1.5	0.173	-0.023	0.268	3.543	0.042	0.030	0.080	-0.015	0.221	0.337	0.407	0.153
1.75	0.187	-0.023	0.247	3.354	0.049	0.039	0.080	-0.006	0.223	0.334	0.398	0.158
2	0.220	-0.018	0.222	3.366	0.050	0.041	0.107	0.011	0.219	0.326	0.400	0.171

Table A-5. Regression coefficients of the N_e prediction equation for EPH-p system.

T	a	b_1	c_1	h	s_2	s_3	s_4	s_5	r_4	r_6	r_8	σ_{TOT}
0.04	0.627	0.054	0.419	4.367	0.039	0.040	0.079	0.028	0.258	0.410	0.520	0.191
0.07	0.391	0.069	0.521	5.432	0.043	0.053	0.104	0.065	0.209	0.320	0.405	0.193
0.1	0.331	0.065	0.513	6.013	0.043	0.066	0.139	0.060	0.170	0.254	0.325	0.186
0.15	0.309	0.057	0.475	5.857	0.046	0.063	0.122	0.027	0.152	0.209	0.264	0.172
0.2	0.302	0.043	0.433	5.422	0.055	0.063	0.125	-0.013	0.146	0.199	0.244	0.162
0.25	0.290	0.037	0.417	5.136	0.059	0.069	0.137	-0.018	0.144	0.194	0.231	0.163
0.3	0.272	0.027	0.408	4.933	0.054	0.063	0.122	-0.019	0.146	0.188	0.225	0.162
0.35	0.275	0.022	0.394	4.738	0.053	0.059	0.129	-0.005	0.133	0.175	0.210	0.161
0.4	0.274	0.019	0.383	4.621	0.045	0.054	0.154	-0.005	0.132	0.176	0.210	0.159
0.45	0.287	0.020	0.371	4.406	0.043	0.044	0.179	-0.010	0.132	0.172	0.206	0.160
0.5	0.277	0.019	0.371	4.366	0.045	0.045	0.174	-0.008	0.131	0.173	0.203	0.158
0.6	0.274	0.010	0.358	4.234	0.039	0.037	0.174	-0.023	0.130	0.168	0.194	0.158
0.7	0.278	0.008	0.346	4.175	0.038	0.036	0.171	-0.019	0.125	0.159	0.186	0.159
0.8	0.286	0.008	0.335	4.091	0.037	0.039	0.147	-0.028	0.122	0.157	0.183	0.156
0.9	0.277	0.004	0.332	4.053	0.041	0.040	0.134	-0.025	0.122	0.155	0.179	0.150
1	0.268	-0.002	0.330	3.997	0.040	0.034	0.115	-0.020	0.116	0.150	0.173	0.149
1.25	0.247	-0.014	0.318	3.799	0.038	0.026	0.075	-0.032	0.113	0.147	0.173	0.146
1.5	0.209	-0.026	0.321	3.732	0.038	0.024	0.070	-0.028	0.113	0.150	0.176	0.146
1.75	0.178	-0.038	0.321	3.741	0.037	0.022	0.074	-0.023	0.111	0.152	0.179	0.146
2	0.154	-0.047	0.318	3.882	0.035	0.017	0.089	-0.012	0.115	0.158	0.191	0.151

Appendix B.

SPECTRAL COMPATIBLE GROUND MOTIONS: REAL RECORDS

In this appendix data regarding real records selected and employed in Chapter 3 are reported. Tables in the following shows the sets of real records selected.

Table B-1 to Table B-4 collect, for the URR class, records no. and event no. according to European Strong Motion Database. Table B-5 to Table B-12 collect the same information for SF5 and SF12 classes, respectively (in these two tables the scaling factor (SF) applied to each single record is also reported). In the tables, x and y represent the two horizontal components of the record, according to the definition by European Strong Motion Database.

Table B-1. Information according to ESD for URR records, set I.

Set	Waveform no.	Earthquake no.	Earthquake Name	Date	M_w	Fault Mechanism	R_e (km)
I	365y	175	Lazio Abruzzo	07/05/1984	5.9	normal	5
	4674x	1635	South Iceland	17/06/2000	6.5	strike slip	5
	4675y	1635	South Iceland	17/06/2000	6.5	strike slip	13
	4675x	1635	South Iceland	17/06/2000	6.5	strike slip	13
	6326y	2142	South Iceland (aftershock)	21/06/2000	6.4	strike slip	14
	6332x	2142	South Iceland (aftershock)	21/06/2000	6.4	strike slip	6
	6335x	2142	South Iceland (aftershock)	21/06/2000	6.4	strike slip	15

Table B-2. Information according to ESD for URR records, set II.

Set	Waveform no.	Earthquake no.	Earthquake Name	Date	M_w	Fault Mechanism	R_e (km)
II	182y	87	Tabas	16/09/1978	7.3	oblique	12
	242x	115	Valnerina	19/09/1979	5.8	normal	5
	242y	115	Valnerina	19/09/1979	5.8	normal	5
	1231x	472	Izmit	17/08/1999	7.6	strike slip	9
	1231y	472	Izmit	17/08/1999	7.6	strike slip	9
	3802x	1226	SE of Tirana	09/01/1988	5.9	thrust	7
	7142y	2309	Bingol	01/05/2003	6.3	strike slip	14

Table B-3. Information according to ESD for URR records, set III.

Set	Waveform no.	Earthquake no.	Earthquake Name	Date	M_w	Fault Mechanism	R_e (km)
III	234x	108	Montenegro (aftershock)	24/05/1979	6.2	thrust	30
	287x	146	Campano Lucano	23/11/1980	6.9	normal	23
	287y	146	Campano Lucano	23/11/1980	6.9	normal	23
	290x	146	Campano Lucano	23/11/1980	6.9	normal	32
	665x	286	Umbria Marche	26/09/1997	6	normal	21
	6500x	497	Duzce 1	12/11/1999	7.2	oblique	23
	7156x	2313	Firuzabad	20/06/1994	5.9	strike slip	21

Table B-4. Information according to ESD for URR records, set IV.

Set	Waveform no.	Earthquake no.	Earthquake Name	Date	M_w	Fault Mechanism	R_e (km)
IV	55x	34	Friuli	06/05/1976	6.5	thrust	23
	198x	93	Montenegro	15/04/1979	6.9	thrust	21
	198y	93	Montenegro	15/04/1979	6.9	thrust	21
	4678x	1635	South Iceland	17/06/2000	6.5	strike slip	32
	6342x	2142	South Iceland (aftershock)	21/06/2000	6.4	strike slip	20
	6342y	2142	South Iceland (aftershock)	21/06/2000	6.4	strike slip	20
	7187x	2322	Avej	22/06/2002	6.5	thrust	28

Table B-5. Information according to ESD and SF factors for SF5 records, set I.

Set	Waveform no.	Earthquake no.	Earthquake Name	Date	M_w	Fault Mechanism	R_e (km)	SF
I	234y	108	Montenegro (aftershock)	24/05/1979	6.2	thrust	30	2.499
	292x	146	Campano Lucano	23/11/1980	6.9	normal	25	3.206
	292y	146	Campano Lucano	23/11/1980	6.9	normal	25	3.207
	368x	175	Lazio Abruzzo	07/05/1984	5.9	normal	22	3.000
	410x	189	Golbasi	05/05/1986	6	oblique	29	4.918
	5272x	1338	Mt. Vatnafjoll	25/05/1987	6	oblique	24	5.848
	6262y	1635	South Iceland	17/06/2000	6.5	strike slip	31	2.848

Table B-6. Information according to ESD and SF factors for SF5 records, set II.

Set	Waveform no.	Earthquake no.	Earthquake Name	Date	M_w	Fault Mechanism	R_e (km)	SF
II	182y	87	Tabas	16/09/1978	7.3	oblique	12	0.499
	182x	87	Tabas	16/09/1978	7.3	oblique	12	0.568
	471y	227	Vrancea	30/05/1990	6.9	thrust	6	8.037
	1243x	473	Izmit (aftershock	13/09/1999	5.8	oblique	15	2.640
	4674	1635	South Iceland	17/06/2000	6.5	strike slip	5	0.604
	4675x	1635	South Iceland	17/06/2000	6.5	strike slip	13	1.459
	7142y	2309	Bingol	01/05/2003	6.3	strike slip	14	0.646

Table B-7. Information according to ESD and SF factors for SF5 records, set III.

Set	Waveform no.	Earthquake no.	Earthquake Name	Date	M_w	Fault Mechanism	R_e (km)	SF
III	182y	87	Tabas	16/09/1978	7.3	oblique	12	0.499
	182x	87	Tabas	16/09/1978	7.3	oblique	12	0.568
	471y	227	Vrancea	30/05/1990	6.9	thrust	6	8.037
	1243x	473	Izmit (aftershock	13/09/1999	5.8	oblique	15	2.640
	4674	1635	South Iceland	17/06/2000	6.5	strike slip	5	0.604
	4675x	1635	South Iceland	17/06/2000	6.5	strike slip	13	1.459
	7142y	2309	Bingol	01/05/2003	6.3	strike slip	14	0.646

Table B-8. Information according to ESD and SF factors for SF5 records, set IV.

Set	Waveform no.	Earthquake no.	Earthquake Name	Date	M_w	Fault Mechanism	R_e (km)	SF
IV	473y	228	Vrancea	31/05/1990	6.3	thrust	7	21.82
	3802x	1226	SE of Tirana	09/01/1988	5.9	thrust	7	1.693
	6326y	2142	South Iceland	21/06/2000	6.4	strike slip	14	1.649
	6332x	2142	South Iceland	21/06/2000	6.4	strike slip	6	0.363
	6335y	2142	South Iceland	21/06/2000	6.4	strike slip	15	1.664
	6335x	2142	South Iceland	21/06/2000	6.4	strike slip	15	1.510
	6349y	2142	South Iceland	21/06/2000	6.4	strike slip	5	0.229

Table B-9. Information according to ESD and SF factors for SF12 records, set I.

Set	Waveform no.	Earthquake no.	Earthquake Name	Date	M_w	Fault Mechanism	R_e (km)	SF
I	169x	80	Calabria	11/03/1978	5.2	normal	10	2.539
	382y	176	Lazio Abruzzo	11/05/1984	5.5	normal	16	12.81
	383x	176	Lazio Abruzzo	11/05/1984	5.5	normal	14	9.502
	5078x	1464	Mt. Hengill Area	04/06/1998	5.4	strike slip	18	14.22
	5085x	1464	Mt. Hengill Area	04/06/1998	5.4	strike slip	15	15.71
	5086x	1464	Mt. Hengill Area	04/06/1998	5.4	strike slip	15	8.396
	5090x	1464	Mt. Hengill Area	04/06/1998	5.4	strike slip	18	6.128

Table B-10. Information according to ESD and SF factors for SF12 records, set II.

Set	Waveform no.	Earthquake no.	Earthquake Name	Date	M_w	Fault Mechanism	R_e (km)	SF
II	95y	52	Friuli (aftershock)	17/06/1976	5.2	oblique	26	21.30
	95x	52	Friuli (aftershock)	17/06/1976	5.2	oblique	26	19.03
	642y	292	Umbria Marche	14/10/1997	5.6	normal	23	3.049
	1891y	651	Kranidia	25/10/1984	5.5	?	23	7.382
	1893y	652	Near SW coast of Peloponnes	10/12/1987	5.2	?	30	11.38
	5089y	1464	Mt. Hengill Area	04/06/1998	5.4	strike slip	23	11.92
	5895y	1932	Arnissa	09/07/1984	5.2	normal	30	17.54

Table B-11. Information according to ESD and SF factors for SF12 records, set III.

Set	Waveform no.	Earthquake no.	Earthquake Name	Date	M_w	Fault Mechanism	R_e (km)	SF
III	847x	363	Umbria Marche	26/03/1998	5.4	oblique	41	8.620
	1884y	229	Filippias	16/06/1990	5.5	thrust	43	16.71
	1899x	657	Gulf of Kiparissiakos	07/09/1985	5.4	oblique	37	9.182
	1994x	645	Skydra-Edessa	18/02/1986	5.3	?	31	18.97
	4560y	1387	Bovec	12/04/1998	5.6	strike slip	38	19.42
	5087x	1464	Mt. Hengill Area	04/06/1998	5.4	strike slip	32	28.14
	7089x	2290	Pasinler	10/07/2001	5.4	strike slip	32	9.833

Table B-12. Information according to ESD and SF factors for SF12 records, set IV.

Set	Waveform no.	Earthquake no.	Earthquake Name	Date	M_w	Fault Mechanism	R_e (km)	SF
IV[6]	410x	189	Golbasi	05/05/1986	6	oblique	29	5.918
	471y	227	Vrancea	30/05/1990	6.9	thrust	6	8.737
	473y	228	Vrancea	31/05/1990	6.3	thrust	7	19.32
	1243x	473	Izmit (aftershock)	13/09/1999	5.8	oblique	15	3.237
	5272x	1338	Mt. Vatnafjoll	25/05/1987	6	oblique	24	10.85
	6761y	2222	Vrancea	30/08/1986	7.2	thrust	49	1.439
	410x	189	Golbasi	05/05/1986	6	oblique	29	5.918

[6] "Manually" selected and scaled.

Appendix C.
L'AQUILA EARTHQUAKE

In this appendix data and observations on L'Aquila earthquake are collected; in particular regarding the mainshock event. Most of this material is the result of a merge and summary of two reports (Chioccarelli et al., 2009; Iervolino et al., 2010), available on line and written right after the earthquake.

The core of this appendix is a comparison of the mainshock data with the hazard data according to the recent Italian seismic code (DM 14/1/2008).

In Table C-1, data regarding the stations of the Accelerometric National Network (RAN) that registered the mainshock of L'Aquila earthquake (M_w 6.3, date 2009/04/06 1.32 am – UTC) within a fault distance of 30km are reported. Asterisks on the EC8 soil classification means that the station was characterized only on the basis of geological information (data updated at May 2001, according to Ameri et al, 2009). In Table C-2 and Table C-3 the peak parameters values and integral parameters values on the registered signals are shown, respectively. Registered signals have been processed with a baseline correction and a Butterworth bandpass filter (order 4, $freqency_1$=0.1Hz, $frequency_2$=25Hz); x component corresponds to East-West registration (EW), y component to North-South (NS) and z components to Up-Down (UD). Peak parameters evaluated are the Peak Ground Acceleration (PGA), the Peak Ground Velocity (PGV) and the Peak Ground Displacement (PGD); while integral paramentes are the Arias Intensity (I_A), see equation (A.1), the so called Cosenza and Manfredi index (I_D), see equation (A.2) and the significant duration (Sd), estimated between 5% and 95% of the I_A released.

$$I_A = \frac{\pi}{2 \cdot g} \int_0^{t_E} a^2(t)\, dt \tag{A.1}$$

$$I_D = \frac{2 \cdot g}{\pi} \frac{I_A}{PGA \cdot PGV} \tag{A.2}$$

Table C-1. Stations' information and localization.

Record Identifier	Station Id	Latitude	Longitude	Station Na	Altitude (m)	Soil Type
GX066	AQV	42.38	13.34	L'AQUILA - V. ATERNO - CENTRO VALLE	692	B
FA030	AQG	42.37	13.34	L'AQUILA - V. ATERNO - COLLE GRILLI	721	A*
CU104	AQA	42.38	13.34	L'AQUILA - V. ATERNO - F. ATERNO	693	B*
AM043	AQK	42.34	13.40	L'AQUILA - V. ATERNO - AQUIL PARK IN	726	B*
EF021	GSA	42.42	13.52	GRAN SASSO (LAB. INFN ASSERGI)	1,062	A*
TK003	CLN	42.09	13.52	CELANO	803	A*
BI016	AVZ	42.03	13.43	AVEZZANO	746	B*
CR008	ORC	41.95	13.64	ORTUCCHIO (NUOVA)	732	A*
BY048	MTR	42.52	13.24	MONTEREALE	975	A*
GE1463	GSG	42.46	13.55	GRAN SASSO (LAB. INFN GALLERIA)	1,200	A*
BX007	FMG	42.27	13.12	FIAMIGNANO	1,071	A*
DF006	ANT	42.42	13.08	ANTRODOCO	568	B*
BY003	CSO	42.10	13.08	CARSOLI	653	A*

Table C-2. PGA, PGV and PGD values of the registered components (x = East-West; y = North-South; z=Up-Down).

Record Identifier	Station Id	PGA_X	PGV_X	PGD_X	PGA_Y	PGV_Y	PGD_Y	PGA_Z	PGV_Z	PGD_Z	Epicentral Distance
		[cm/s²]	[cm/s]	[cm]	[cm/s²]	[cm/s]	[cm]	[cm/s²]	[cm/s]	[cm]	[km]
GX066	AQV	613.8	36.7	8.4	586.2	40.5	4.1	411.7	13.4	2.5	4.8
FA030	AQG	408.2	33.6	7.9	426.1	35.9	3.9	211.4	9.1	1.9	4.3
CU104	AQA	386.8	30.5	6.4	442.0	24.5	3.9	373.2	9.4	1.9	5.8
AM043	AQK	335.5	30.3	7.8	333.6	38.5	11.8	343.8	15.0	4.9	5.6
EF021	GSA	150.6	9.7	3.0	146.6	7.4	2.2	110.3	5.5	1.5	18
TK003	CLN	79.2	4.6	2.6	87.1	6.7	1.9	44.1	5.7	1.9	31.6
BI016	AVZ	60.6	10.5	4.6	69.6	10.6	4.4	25.7	3.6	1.3	34.9
CR008	ORC	67.1	6.1	1.3	39.9	3.7	0.9	29.7	3.8	0.6	49.4
BY048	MTR	42.4	3.3	1.0	59.6	3.1	0.7	22.9	3.2	0.8	22.4
GE1463	GSG	20.1	3.5	1.6	29.2	3.1	1.8	19.4	3.0	1.8	22.6
BX007	FMG	23.7	2.5	1.2	26.0	1.7	0.6	18.5	1.5	0.4	19.3
DF006	ANT	19.6	1.9	0.4	25.8	2.2	0.5	11.5	1.1	0.2	23.1
BY003	CSO	17.3	2.2	1.0	17.1	1.4	0.6	14.8	2.0	0.7	33

Table C-3. I_A, I_D and Sd values for the registered components(x = East-West; y = North-South; z=Up-Down).

Record Identifier	Station Id	$I_{A,X}$	$I_{D,X}$	Sd_X	$I_{A,Y}$	$I_{D,Y}$	Sd_Y	$I_{A,Z}$	$I_{D,Z}$	Sd_Z	Epicentral Distance
		[cm/s]	[/]	[s]	[cm/s]	[/]	[s]	[cm/s]	[/]	[s]	[km]
GX066	AQV	283.0	7.8	7.6	199.7	5.3	7.7	89.6	10.1	6.1	4.8
FA030	AQG	129.6	5.9	8.0	129.8	5.3	8.5	31.4	10.2	8.3	4.3
CU104	AQA	158.9	8.4	7.4	172.6	10.0	7.6	52.9	9.4	6.7	5.8
AM043	AQK	100.3	6.2	12.2	119.8	5.8	11.3	111.4	13.5	10.5	5.6
EF021	GSA	40.0	17.1	8.4	43.7	25.1	8.8	13.5	14.0	9.5	18
TK003	CLN	3.7	6.3	6.6	3.9	4.1	7.7	1.7	4.2	8.3	31.6
BI016	AVZ	7.8	7.7	20.9	9.8	8.3	18.3	2.4	16.3	17.9	34.9
CR008	ORC	4.1	6.2	9.8	2.5	10.8	13.7	0.9	4.8	13.3	49.4
BY048	MTR	3.4	15.1	15.1	5.8	19.7	11.4	1.3	11.3	19.4	22.4
GE1463	GSG	0.6	5.5	11.6	0.9	6.2	9.5	0.6	6.5	14.4	22.6
BX007	FMG	1.2	12.5	18.6	1.0	14.7	23.0	0.8	18.3	21.6	19.3
DF006	ANT	0.9	14.2	24.6	1.8	19.1	21.2	0.3	15.3	22.4	23.1
BY003	CSO	0.8	13.1	24.4	0.6	14.5	24.6	0.5	10.3	20.6	33

In Figure C.1a, the thirteen stations considered are localized with the epicenter, the rupture surface and some remarkable towns where a concentration of damage was registered after the mainshock. Figure C.1b shows macroseismic intensity data registered in three hundred towns in the area struck by the earthquake (according to QUEST - Quick Earthquake Survey Team, http://www.ingv.it/); data are grouped in 10km bins and the mean of each bin is shown (that is why values plotted are not integers). Data in Figure C.1b emphasize the step registered in the macroseismic intensity when comparing data within and beyond 20km.

Data from Table C-2 and Table C-3 emphasize the significant differences between characteristics of the signals registered within 15km from the fault and the others, that is why the following comparisons with code spectra are provided separately for the group of thirteen records all registered within 30km. The above observations suggest that signals closest to the fault could have been characterized by *near-source* effects. Moreover, given the lack of reliability regarding soil classification of most of the stations (only AQV characterization is based on Vs30 data), all the signals are compared with code

spectra evaluated for soil class A and C (EC8 classification), only aimed at a simulation of the lower upper bound of soil amplification on the basis of the most frequent soil classes of the area, (that is why D soil class was not considered). Figure C.2 shows the two groups in which the thirteen stations have been divided.

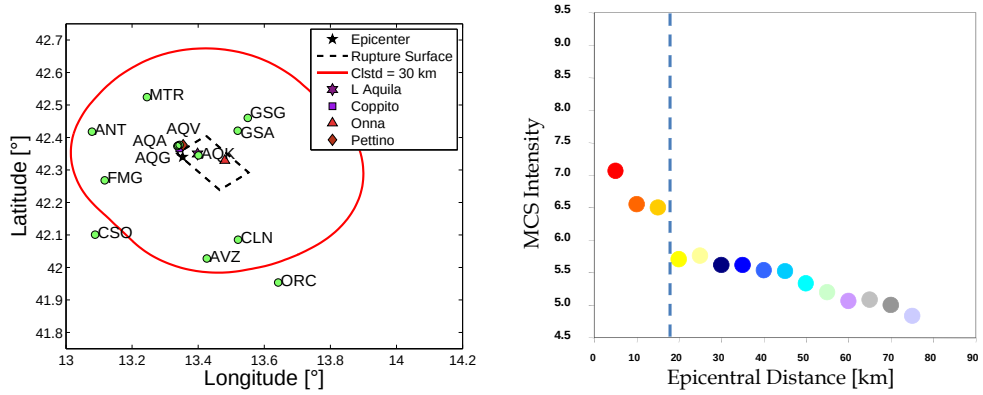

Figure C.1. Sites map, stations' and epicenter's localizations (a); macroseismic intensity attenuation with the epicentral distance (b).

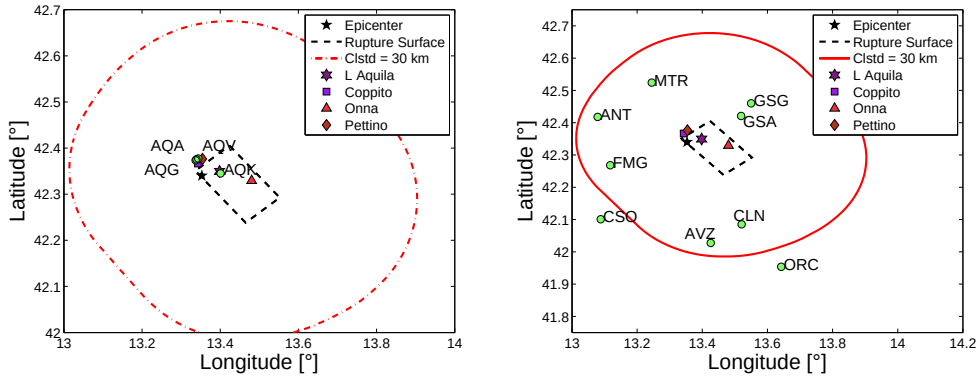

Figure C.2. Stations' localization within 15km (a) and beyond 15km (b).

Figure C.3 to Figure C.5 show the comparison of acceleration, velocity and displacement spectra for soil classes A and C with the two groups of signals. It is to be noted that the geometric mean of the horizontal components was evaluated. The differences between the two groups are evident. As side consideration it is to be noted the low frequency content of the horizontal

components in AQK station, clearly highlighted in Figure C.4a and justified by the pulse-like characteristics of this signals that are shown in Iervolino et al., (2010).

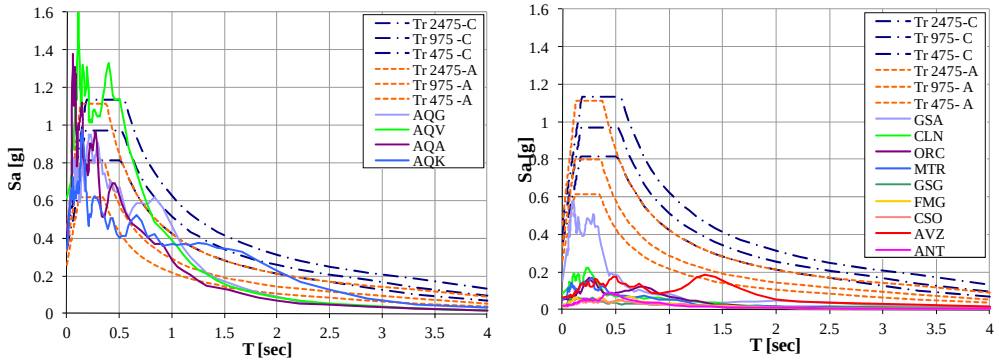

Figure C.3. Comparison of Italian code acceleration spectra for soil classes A and C with the spectra of the geometrical mean of the horizontal components of the signals registered within 15km (a) and beyond 15km (b).

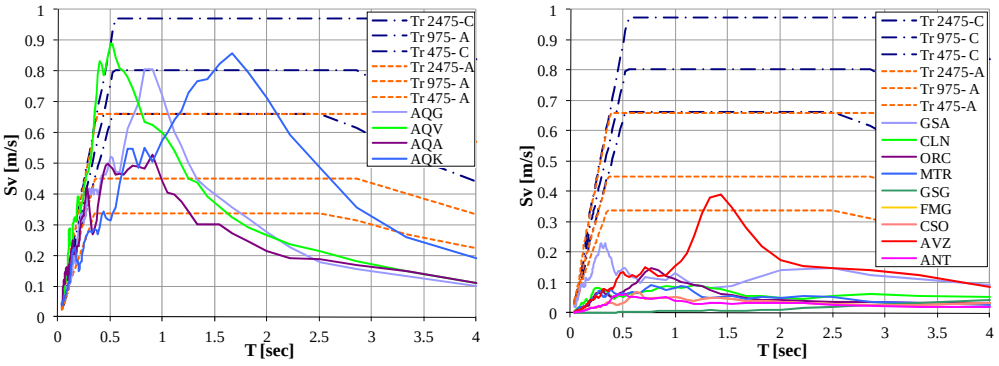

Figure C.4. Comparison of Italian code velocity spectra for soil classes A and C with the spectra of the geometrical mean of the horizontal components of the signals registered within 15km (a) and beyond 15km (b).

Spectra of the vertical components are compared in Figure C.6 to Figure C.8; in this case no soil class differences are made since the Italian code does not provide any difference for soil amplification in the case of the vertical components. The four closest stations, belonging to the first group, are characterized by significantly higher value of accelerations, velocities and

displacements than ones provided by the code.

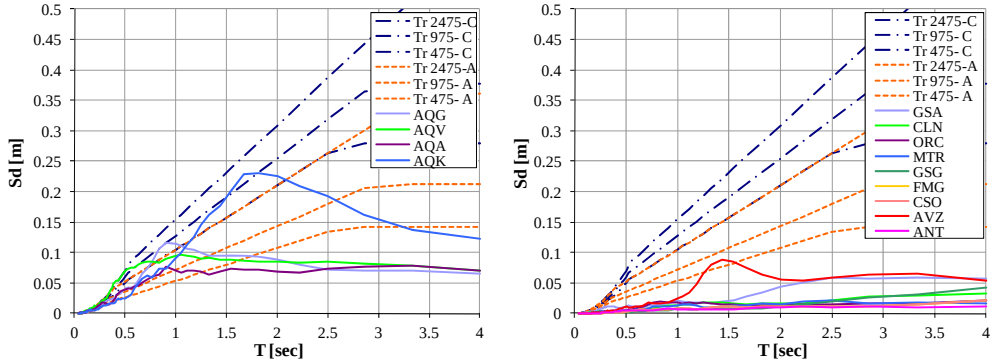

Figure C.5. Comparison of Italian code displacement spectra for soil classes A and C with the spectra of the geometrical mean of the horizontal components of the signals registered within 15km (a) and beyond 15km (b).

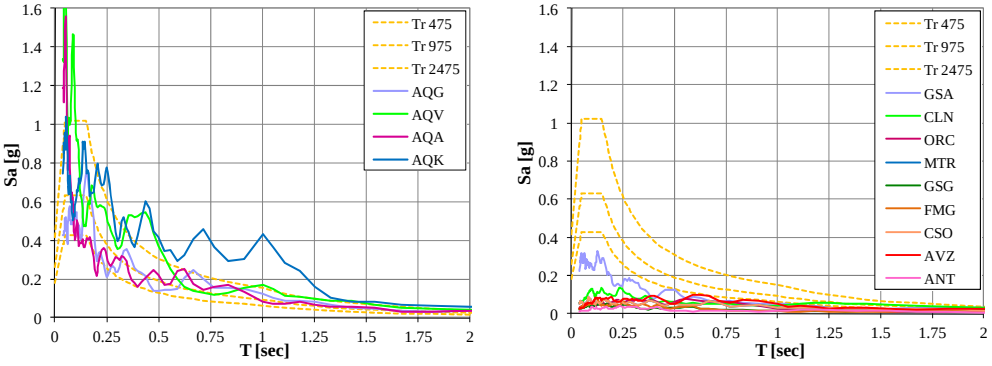

Figure C.6. Comparison of Italian code acceleration spectra (vertical) with the spectra of the vertical components of the signals registered within 15km (a) and beyond 15km (b).

The latter effect is a peculiar characteristic of L'Aquila earthquake and it can be addressed as the most likely cause of brittle collapses observed in the area close to the epicenter (see Chapter 7).

In Figure C.9, the last comparison with code spectra, provided only for the first group of signals, regards Housner intensities. H10 and H50 have been computed on the velocity spectra according to the Italian code and on the velocity spectra of the signals. H_{10} is the integral of the velocity spectrum

between 0.1 and 0.5 seconds, while H_{50} is the same integral evaluated between 0.2 and 2.0 seconds. Housner intensities of the registered signals are comprised in the range of return periods (Tr) between 475 and 2475 years evaluated for code spectra. Changing the range of the integration, so switching from H_{10} to H_{50}, it is evident the differences of the four signals. AQK stations, in fact, is characterized by the highest H_{50} because of the low frequency content already highlighted above.

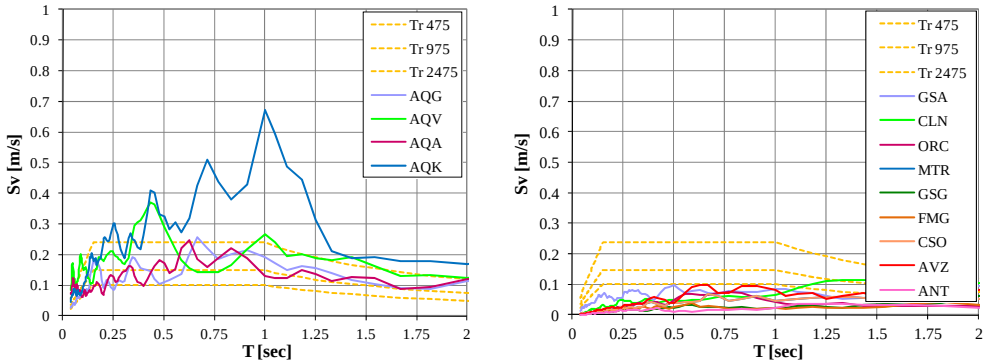

Figure C.7. Comparison of Italian code velocity spectra (vertical) with the spectra of the vertical components of the signals registered within 15km (a) and beyond 15km (b).

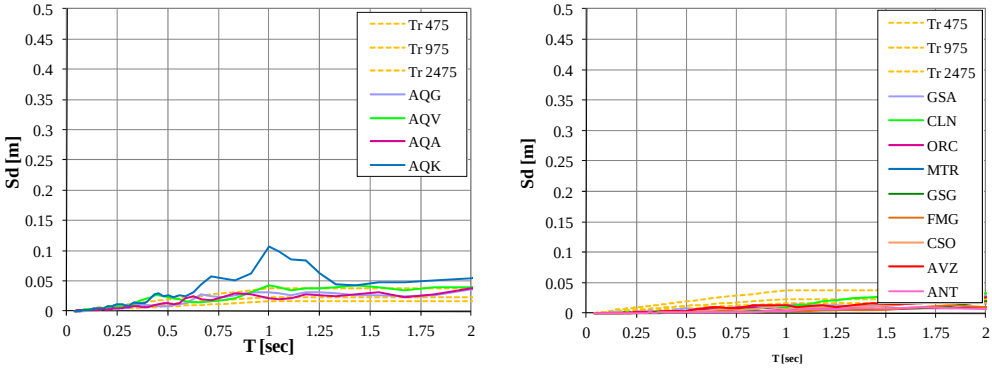

Figure C.8. Comparison of Italian code displacement spectra (vertical) with the spectra of the vertical components of the signals registered within 15km (a) and beyond 15km (b).

The aspects regarding soil classes of the closest four stations have not

been emphasized given the uncertainties in the classification. On the other hand, three of them belongs to soil class B and only AQG station is classified as A, so the direct comparison of the three stations AQK, AQA and AQV should be not affected by different effects of soil amplification. It should be noted that the latter assumption takes for granted that soil classification according to Italian code is exhaustive, obviously changing the approach to the problem and emphasizing the geotechnical point of view this assumption can be considered not reliable at all.

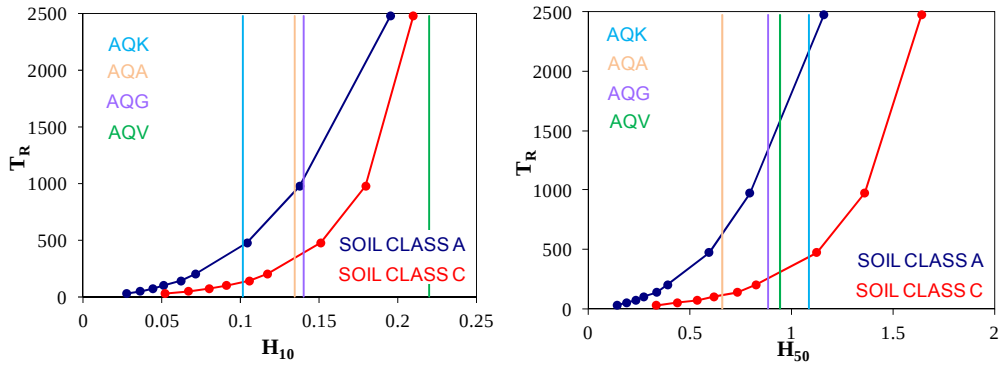

Figure C.9. Housner intensities, H10 and H50 evaluated on code spectra at different return periods Tr for soil classes A and C compared with H10 and H50 of the geometrical mean of the horizontal components for the signals registered within 15km.

A further comparison is provided in Figure C.10 to Figure C.15 between spectra of the four records close to the epicenter and the 16°, 50° and 84° percentiles of the UHS spectra on firm soil (A) according to the Istituto Nazionale di Geofisica e Vulcanologia (INGV) data, available on line at the address http://esse1.mi.ingv.it/index.html. These data are evaluated for Tr equal respectively to 475 and 2500 years. In Figure C.10 to Figure C.15 is also provided, in panels (b) the same comparison accounting for C soil amplification by means of coefficient S_S (CS.LL. PP., 2008), see equation (A.3).

$$S_S = 1.0 \le 1.7 - 0.6 \cdot \frac{a_g}{g} \cdot F_0 \le 1.5 \qquad \text{(A.3)}$$

The comparisons of the spectra for the two soil types highlight that the soil amplification becomes non significant for Tr equal to 2500 years, since S_S parameters in such cases tends to become equal to one.

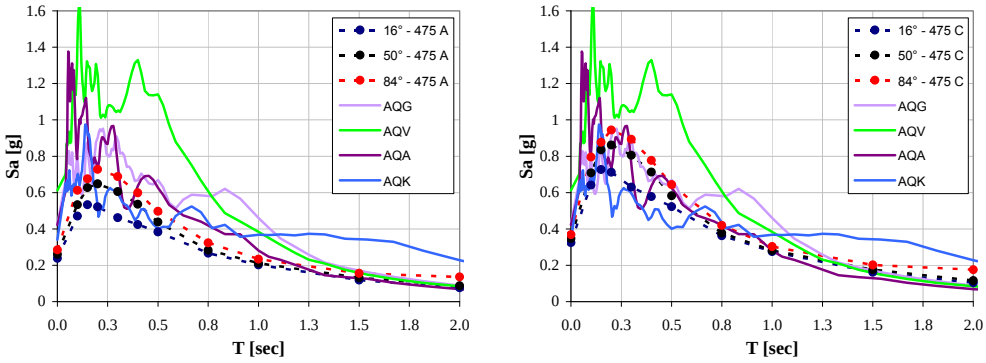

Figure C.10. Comparison of spectra of the four signals registered within 15km and UHS acceleration spectra evaluated for three different percentiles (16°, 50° and 84°) on A soil class (a) and C soil class (b) for Tr equal to 475 years.

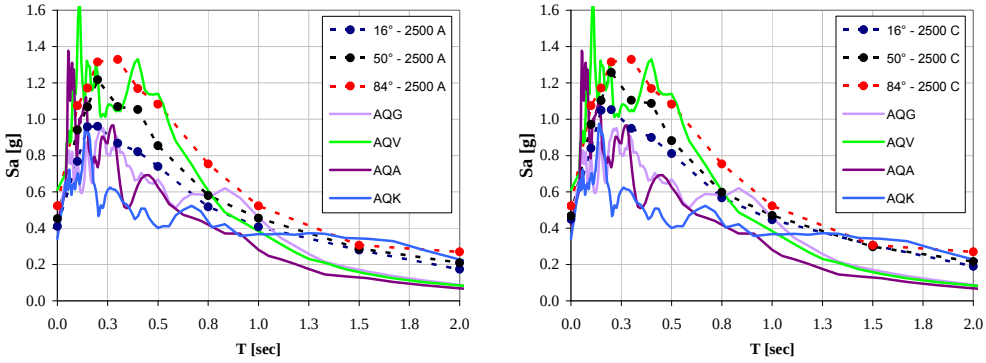

Figure C.11. Comparison of spectra of the four signals registered within 15km and UHS acceleration spectra evaluated for three different percentiles (16°, 50° and 84°) on A soil class (a) and C soil class (b) for Tr equal to 2500 years.

The comparisons provided above are not meant at all for the evaluation of the effective return period of L'Aquila earthquake; in this sense there is no basis to compare probabilistic seismic hazard analysis results with a single event. On the other hand such comparisons can help in the analysis of the structural and nonstructural damage observed, since design spectra according

to Codes represent a benchmark.

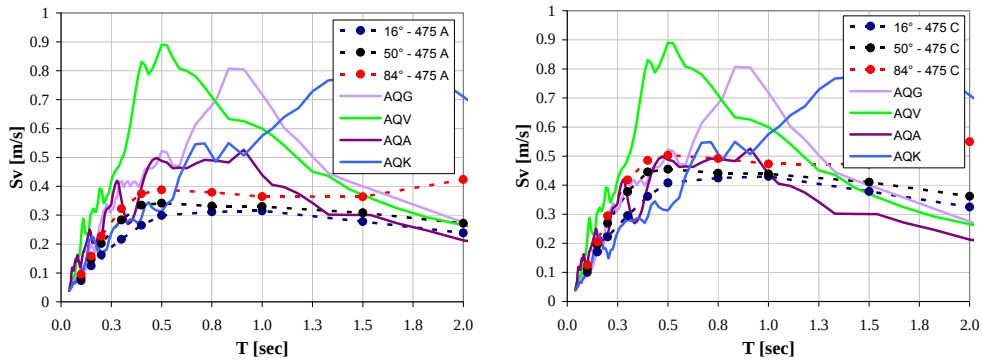

Figure C.12. Comparison of spectra of the four signals registered within 15km and UHS velocity spectra evaluated for three different percentiles (16°, 50° and 84°) on A soil class (a) and C soil class (b) for Tr equal to 475 years.

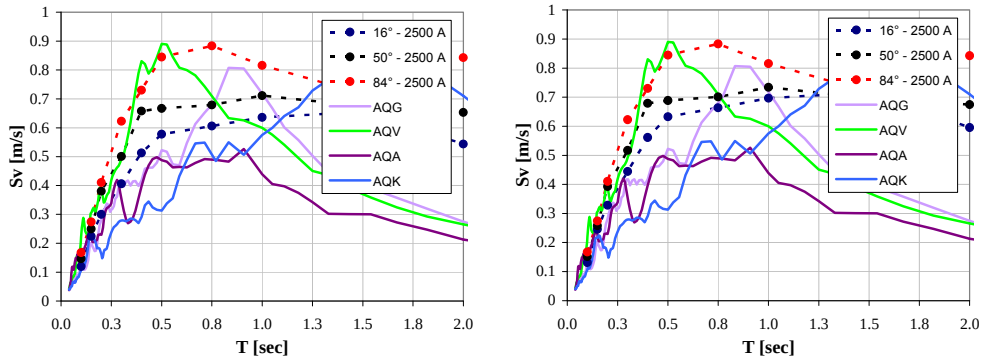

Figure C.13. Comparison of spectra of the four signals registered within 15km and UHS velocity spectra evaluated for three different percentiles (16°, 50° and 84°) on A soil class (a) and C soil class (b) for Tr equal to 2500 years.

The comparisons above allowed highlighting some peculiar characteristics of L'Aquila earthquake. Firstly it has been shown that the spectra of the vertical components of the signals registered within the epicenter are significantly higher than the spectra provided by Codes and secondly that the low frequency content of some signals could have been caused by directivity effects. This two observations can be intersected with structural damage observed and provide additional recommendations or emphasize

specific structural weaknesses of a building stock typical of an area.

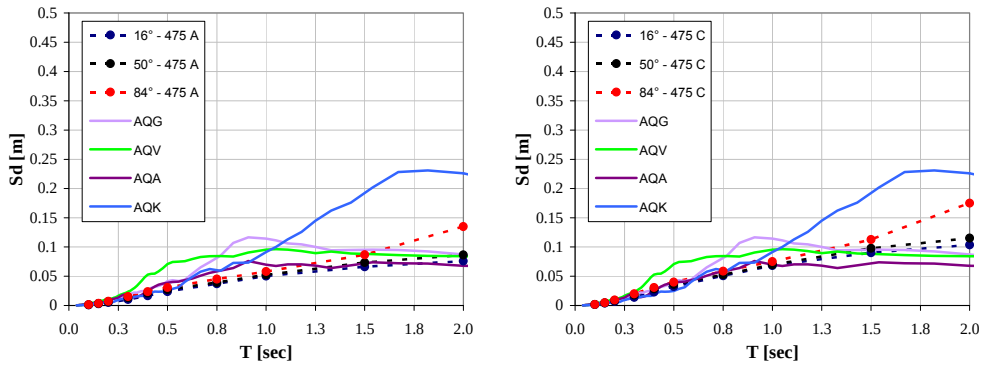

Figure C.14. Comparison of spectra of the four signals registered within 15km and UHS displacement spectra evaluated for three different percentiles (16°, 50° and 84°) on A soil class (a) and C soil class (b) for Tr equal to 475 years.

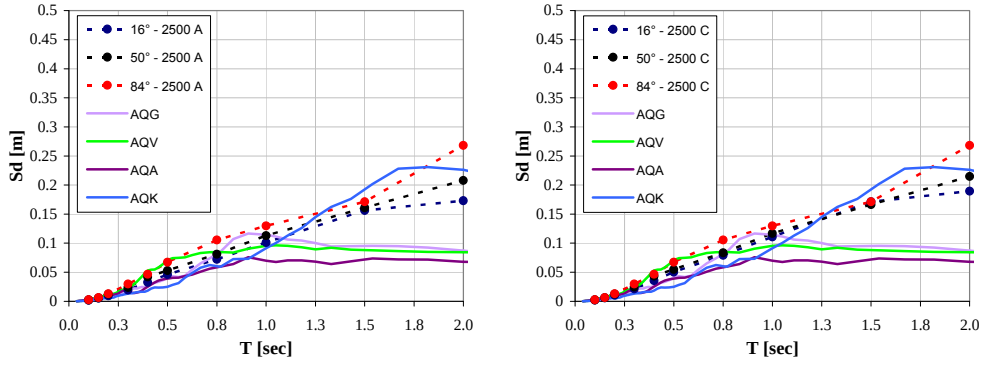

Figure C.15. Comparison of spectra of the four signals registered within 15km and UHS displacement spectra evaluated for three different percentiles (16°, 50° and 84°) on A soil class (a) and C soil class (b) for Tr equal to 2500 years.

APPENDIX C REFERENCES

Ameri G., Augliera P., Bindi D., D'Alema E., Ladina C., Lovati S., Luzi L., Marzorati S., Massa M., Pacor F., Puglia R., 2009. Strong-motion parameters of the Mw=6.3 Abruzzo (Central Italy) earthquake. http://esse4.mi.ingv.it/.

Chioccarelli E., De Luca F., Iervolino I., 2009. Preliminary study of L'Aquila earthquake ground motion records V5.21; available at http://www.reluis.it.

Decreto Ministeriale del 14 gennaio, 2008. Approvazione delle nuove norme tecniche per le costruzioni. G.U. n. 29 del 4/2/2008 (in Italian).

Iervolino I., De Luca F., Chioccarelli E., Dolce M., 2010. L'azione sismica registrata durante il mainshock del 6 aprile 2009 a l'aquila e le prescrizioni del DM 14/01/2008 V.1, available at http://www.reluis.it, (in Italian).